UNDERSTANDING PLASMID TRANSFER IN BACTERIAL BIOFILMS

Ho Yu Liu

100373622

70,363 words

A thesis submitted in fulfilment of the requirements of the University of East Anglia for the degree of Doctor of Philosophy

Quadram Institute Bioscience

Norwich Medical School, University of East Anglia

September 2025

ABSTRACT

Antimicrobial resistance remains an enormous challenge, with the horizontal transfer of resistance genes between species a major contributor to the evolution of resistance. Most bacteria exist in polymicrobial biofilm communities, and biofilms have been suggested to encourage plasmid persistence and promote horizontal gene transfer. However, much current knowledge is based on experiments conducted using planktonic bacteria that are not representative of real-world bacterial communities. It remains unclear which environmental drivers impact horizontal gene transfer within polymicrobial biofilms, or which genes are involved in plasmid acquisition.

In this study, a multispecies biofilm conjugation model was developed to monitor the movement of pHYCTX14, a clinically relevant conjugative plasmid, between *Escherichia coli* and *Salmonella enterica* serovar Typhimurium. Using this model, the impact of a range of chemicals, including food preservatives and antimicrobials, on the rate of plasmid movement was investigated. The results indicated that the chemicals tested had very different impacts on conjugation efficiency, with the lowest conjugation efficiency obtained for experiments conducted under stress from sodium nitrite, and the highest obtained for experiments conducted under stress from copper sulphate.

Using a massively parallel transposon mutagenesis approach, TraDIS-*Xpress,* genes involved in the acquisition of pHYCTX14 in *E. coli* and *S.* Typhimurium were also identified. Key genes identified to be involved in plasmid acceptance included those associated with energy production, bacterial membrane structure, efflux and RNA polymerase recycling.

This work describes the development of a multispecies biofilm conjugation model to explore how external stress factors can influence the rate of plasmid movement within biofilms, and the use of TraDIS-*Xpress* to investigate the genes involved in host plasmid acceptance.

These experiments have laid the groundwork for further investigations into the evolution of antimicrobial resistance within multispecies biofilms and into developing a detailed insight into the host-plasmid interplay.

Keywords: Biofilms, antimicrobial resistance, plasmids, horizontal gene transfer, conjugation, TraDIS-*Xpress*

書中自有黃金屋,

書中自有顏如玉,

萬般皆下品,

惟有讀書高。

ACKNOWLEDGEMENTS

First, I would like to start by thanking my primary supervisor, Prof. Mark Webber, or as I sometimes like to call him, '*professor*' or 'the supreme prof.' Thank you for giving me the chance to begin this PhD, and an even bigger thank you for pushing me across the finish line – a line I often wasn't sure I would get to. Your door was always open to me to voice and express whatever concerns I had, whether they were related to science or not, and the guidance, encouragement, as well as unwavering support you have given me through the ups and downs of the past few years, is something that I will forever be grateful for. Thank you for all the opportunities you have given me; it has been a privilege and honour to learn from, and work alongside you. I guess if I tried to list everything that I could thank you for, then this acknowledgements section would be the length of the results chapters themselves, so I will finish by thanking you for always believing in me, even when I didn't believe in myself. I hope that one day, I can take what I have learnt from you and give other young scientists the experience and mentorship you have given me. You truly are the best. Thank you for all you have done and continue to do for me.

I also extend my thanks to the rest of my supervisory team, Dr. Gemma Langridge, my secondary supervisor, and Dr. Eleftheria Trampari, for all the help and advice I have received over the past four years. I have really enjoyed our scientific discussions both during and outside of the review meetings. It was comforting to know that I was always welcome to seek advice from you both whenever I required it.

To all the members of the Webber group, past and present: Maria, Heather, Iliana, Leanne, Yasir, Keith, Caroline, Josh, Haider, Sarah, Sam, Emma, Gregory, Ryan, Will, James, Yuming, Tristan, Stuart – thank you for being the best group anyone could ask for. From lunches on the sofas to pub golf and even post Microsoc karaoke, it's been wonderful to work with and to learn from you all over the past few years. A special mention must go to Heather, Maria and Iliana, my desk neighbours who have been there for me during some of the very tough times of this PhD. Sometimes, even from hundreds of miles

away, with an average message reply rate of three business weeks (love you Maria). Thank you for always reminding me to ‘do better, be better’.

To Oleksii and Gab, the two, once strangers, I started this journey with. What a journey it has been! I’m so thankful that I met you both and that we have been able to go through the past four years together. It’s definitely been a rollercoaster of a ride from the very first day, but I hope that we have many more garden barbecues, random dinners and maybe (?) even roller-skating adventures together. May we forever be the (Future) ‘Asian’ Dr gang.

To the rest of my friends I have made in Norwich and at QIB: particularly Agata, Claire, Alice, Steven, Lizzi, Steph, and Marnie, thank you for making the office such a lovely space to work in. To the Rhizo+ team, Alice and Steven, putting together our little business idea will always be one of my favourite memories. And to everyone else at QIB, particularly the QSF 2021 – 2022 committee, comms, sequencing, media teams and the Binfies, thank you for making my time here so positive and for all the help over the past few years.

給我親愛的父母 (To my parents)：感謝您們這些年來給予女兒的支持。這四年的路走得不容易，但是每次回家能夠吃到您們煮的菜，煲的湯，都會覺得這一切都是值得的。女兒今天能夠拿到的博士學位少不了您們這麼多年的栽培和鼓勵，所以這個成就也是屬於您們的。

Thank you for all the support that you have given me over the years. The past four years have not been easy, but being able to eat the home-cooked food and soup you made me every time I travelled home made everything feel worthwhile. Your encouragement and care have been a big part of my journey to getting a PhD; therefore, this achievement also belongs to you both.

To the rest of my family, especially my 弟弟 (brother), 姐姐 (sister), 大姨 (Auntie Ying), 大姨丈 (Uncle Choi), 雯雯表姐 (Jackie) and 細表姐 (Rachel): thank you for always being only one text or phone call away, and to my dearest 細佬表哥 (Nigel): I wish you were here to celebrate this with me, but I know you’ve been watching me through every step of this journey and you’re

probably holding a mini party for me up there. I hope I have done you proud <3.

To all my other friends from near and far: thank you for putting up with me and for providing a distraction from the PhD when I most needed it.

And finally, to myself. It's been four years of craziness, good times, bad times, and everything in between. I have been challenged in more ways than one, but through this experience, I have also matured both as a scientist and as an individual. A wise person once said to me, 'I hope that one day you see yourself the way other people see you.' I don't know if I have achieved this over the past few years, but it is something that I will continue to remind myself of in the future.

Thank you to everyone who has been a part of this incredibly fulfilling and rewarding journey. I will always look back fondly on this chapter of my life – onto the next adventure!

PUBLICATIONS

Liu, H.Y., Prentice, E.L., & Webber, M.A. Mechanisms of antimicrobial resistance in biofilms. npj Antimicrob Resist 2, 27 (2024). https://doi.org/10.1038/s44259-024-00046-3

Zhang, Y., Lin, Y., Ruan, Y., Yang, J., Holden, E.R., Felgate, H., Solsona, M., **Liu, H.Y.,** Liang, G., Jiang, H., Webber, M.A., Zhuo, C. Pivotal plasmids drive the global spread of CTX-M-27 in *Escherichia coli*. Infection (2025). https://doi.org/10.1007/s15010-025-02664-z

Liu, H.Y., Trampari, E., Langridge, G.C., & Webber, M.A. Investigating the impact of food preservatives on conjugation efficiency in multispecies biofilm communities – *in preparation.*

Liu, H.Y., Muhammad, Y., Holden, E.H., Sims, L., Trampari, E., Langridge, G.C., & Webber, M.A. Identifying essential genes for plasmid acceptance in Gram-negative bacteria – *in preparation.*

CONFERENCE ATTENDANCE

Microbial Genomics Early Career Researcher Symposium 2025 (Norwich, UK) – oral presentation (Best oral presentation, second place)

Biofilms 11 conference 2025 (Cardiff, UK) – flash oral presentation and poster presentation

ESCMID Global 2025 (Vienna, Austria) – oral presentation

Centre for Microbial Interactions Annual Conference 2025 (Norwich, UK) – poster presentation (People's choice poster award, second place)

British Society for Antimicrobial Chemotherapy Antimicrobial Resistance Mechanisms workshop 2024 (Birmingham, UK) – oral presentation

Microbiology Society Annual Conference 2024 (Edinburgh, UK) – poster presentation

Microbes in Norwich Symposium 2024 (Norwich, UK) – Poster presentation

Antibiotic discovery acceleration (ABX) meeting 2023 (Norwich, UK) – poster presentation

Microbiology Society Annual Conference 2023 (Birmingham, UK) – poster presentation

Microbes in Norwich Symposium 2023 (Norwich, UK) – poster presentation

TABLE OF CONTENTS

LIST OF FIGURES

LIST OF TABLES

LIST OF ABBREVIATIONS

ACT	Artemis comparison tool
AI-2	Autoinducer-2
AMR	Antimicrobial resistance
ARG-ANNOT	Antibiotic Resistance Gene-ANNOTation
ATP	Adenosine triphosphate
BLAST	Basic Local Alignment Search Tool
bp	base pair
BRIG	BLAST ring image generator
CARD	Comprehensive Antibiotic Resistance Database
c-di-GMP	Cyclic diguanylate monophosphate
CF	Cystic fibrosis
CFU	Colomy forming units
CT	Cycle threshold
DGC	Diguanylate cyclase
ECOFF	Epidemiological cut-off
EDTA	Ethylenediaminetetraacetic acid
EPS	Extracellular polymeric substances
ESBL(s)	Extended spectrum beta-lactamase(s)
EUCAST	European Committee for Antimicrobial Susceptibility Testing
G-DOC	Gene doctoring
HGT	Horizontal gene transfer
HMW	High molecular weight
IPTG	Isopropyl beta-D-1-thiogalactopyranoside
IRIDA	Integrated Rapid Infectious Disease Analysis
IS	Insertion sequence
kbp	Kilobase pairs
LB	Lysogeny broth
logFC	Log fold-change
LPS	Lipopolysaccharide
MDR	Multidrug resistant
MFS	Major facilitator superfamily
MGE	Mobile genetic element
MH	Mueller Hinton
MIC	Minimum inhibitory concentration
MLST	Multilocus sequence type
NalR	Nalidixic acid resistant
NCBI	National Centre of Biotechnology Information
NET	Neutrophil extracellular trap

OD	Optical density
OMV	Outer membrane vesicle
ONT	Oxford Nanopore Technology
oriT	Origin of transfer
PBS	Phosphate-buffered saline
PDE	Phosphodiesterase
RifR	Rifampicin resistant
RNAP	RNA polymerase
RND	Resistance-nodulation-division
RT	Reverse transcription
SaPI	*S. aureus* pathogenicity islands
SDS	Sodium dodecyl sulphate
SNP	Single nucleotide polymorphism
SPI(s)	*Salmonella* pathogenicity island(s)
ST	Sequence type
SWI/ SNF	Switch/ sucrose non-fermentable
T4SS	Type IV secretion system
T6SS	Type VI secretion system
TA	Toxin-antitoxin
TBE	Tris/ Borate/ EDTA
TCA	Tricarboxylic acid
Tm	Melting temperature
TraDIS-*Xpress*	Transposon directed insertion-site sequencing with expression
Tris-EDTA	TE
UPEC	Uropathogenic *E. coli*
VFDB	Virulence Factor Database
w/o	Without
WGS	Whole genome sequencing
X-Gal	5-Bromo-4-chloro-3-indoyl beta-D-galactopyranoside
XLD	Xylose lysin deoxycholate
YT	Yeast extract tryptone medium

CHAPTER 1:
INTRODUCTION

“Nothing in life is to be feared, it is only to be understood.

Now is the time to understand more, so that we may fear less”

< Maria Salomea Skłodowska-Curie >

The majority of this literature review has previously been published in npj Antimicrobial Resistance: Liu, H.Y., Prentice, E.L., & Webber, M.A. Mechanisms of antimicrobial resistance in biofilms. *npj Antimicrob Resist* **2**, 27 (2024). https://doi.org/10.1038/s44259-024-00046-3 (Liu et al., 2024). The version presented here has been updated with various more recent examples and references from those published.

Statement of contributions to the literature review: Ho Yu Liu designed the overall structure of the paper and took a lead role both in writing and deciding the final contents of the manuscript. Emma Prentice and Mark Webber contributed ideas to the manuscript and assisted with proofreading the paper.

1.1 INTRODUCTION

In nature, most bacteria exist in biofilms, aggregated communities of microorganisms that are encased in a self-produced matrix. Cells in a biofilm exhibit a distinct lifestyle from those in a planktonic state, with strains showing major differences in gene and protein expression when grown as biofilms compared to their planktonic equivalents (Sauer et al., 2022). The biofilm mode of life is one of the most abundant and robust lifestyles found on earth, and biofilms can be found in seawater, groundwater, soil, and ocean sediment, where they drive the bio-geochemical cycle of many elements in these environments (Flemming et al., 2016, Berne et al., 2018). Owing to the protective characteristics of the matrix (Flemming and Wingender, 2010) and changes in cell physiology that lead to the formation of metabolically dormant cells (Flemming et al., 2016, Trampari et al., 2021), biofilms are generally highly tolerant of different chemical and physical stressors in the environment (Halan et al., 2012, Hobley et al., 2015).

Despite many beneficial uses in industry, biofilms can also pose threats to human health, facilitating the contamination of drinking water (Wingender and Flemming, 2011) and medical devices, including indwelling implants, contributing to persistent infections that are challenging to eradicate (del Pozo and Patel, 2007, Flemming et al., 2016).

Biofilm infections are particularly problematic as effective treatment is often highly challenging due to the intrinsic resistance to antimicrobials and the innate host immune response (del Pozo and Patel, 2007). Biofilms are important contributors to many bacterial infections (Khatoon et al., 2018) and are common causes of chronic infections where prolonged presence of the biofilm induces an adaptive inflammatory response without the biofilm being cleared by the immune system (Yang et al., 2011, Burmølle et al., 2014, Vestby et al., 2020). These infections can occur in a range of locations, including in chronic wounds, heart valves and the lungs, as well as on medical implants, including catheters and prosthetic devices (Høiby et al., 2010, Khatoon et al., 2018). The impacts of biofilm infections vary but can be very severe. For example, biofilms in the cystic fibrosis (CF) lung underpin chronic infection and are the major reason life expectancy for sufferers is limited to 35-50 years (Guillaume et al., 2022). Chronic wounds caused by biofilms are also a major cause of morbidity, with nearly $300 billion estimated to be spent per year on the management of biofilm wound infections (Cámara et al., 2022).

1.2 THE BIOFILM LIFE CYCLE

The unique properties of cells in a biofilm promotes infection and plays a key role in the intrinsic antibiotic-resistant properties of bacteria. Biofilm formation is an intricate process that involves the production of extracellular components such as adhesins and multiple changes to cell physiology (Tolker-Nielsen, 2015). The specific processes associated with the development of a biofilm and the biofilm structure can vary based on the species and strains of bacteria, as well as on the surrounding environmental conditions (Tolker-Nielsen, 2015). For example, *Pseudomonas aeruginosa* biofilms form mushroom-shaped microcolonies in flow chambers when a glucose medium is used, but when citrate is used as the carbon source, 'flat' biofilms are formed (Klausen et al., 2003). *Staphylococcus aureus* can employ distinct mechanisms for successful biofilm formation depending on the environment. These biofilm archetypes include: the polysaccharide biofilm, which is dependent on the expression of poly-N-acetylglucosamine and polysaccharide intercellular adhesin; the protein/ extracellular (eDNA) biofilm, which uses surface proteins to mediate

cell-to-cell contact and incorporate eDNA from lysed cells into the biofilm matrix; the fibrin biofilm, in which fibrin acquired via coagulase-mediated activation of plasminogen, is used as a scaffold to support the biofilm; and the amyloid biofilm, which uses phenol-soluble molecules to promote both biofilm dispersal and accumulation (Zapotoczna et al., 2016). The programme of biofilm matrix formation used depends on strains and conditions.

Interactions between the host and bacteria strongly impacts biofilm formation during infection. For example, *S. aureus* biofilms grown for < 24 hours on human plasma-conditioned surfaces, subjected to shear flow in a chemically defined medium to mimic human infection, were significantly more susceptible to rifampicin and vancomycin than biofilms grown on polystyrene in a bacteriological medium (Zapotoczna et al., 2015).

Although the mechanisms of biofilm formation are complex, there are some generically important events, and the lifecycle can be described broadly in five main steps: initial attachment, irreversible attachment, micro-colony formation, biofilm maturation and dispersion (Sauer et al., 2022) **(Figure 1.1)**.

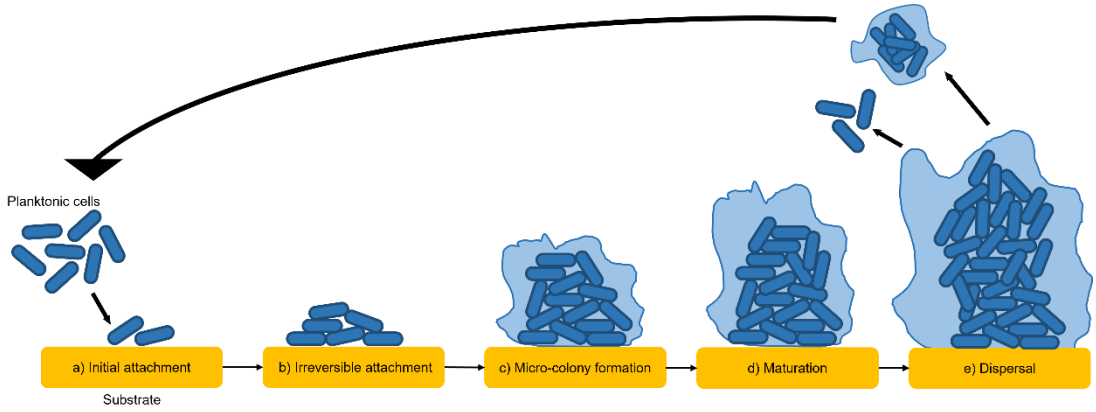

Figure 1.1 - The lifecycle of a surface attached biofilm showing **a)** the initial attachment of cells to a substrate, **b)** irreversible attachment of cells, **c)** micro-colony formation, **d)** biofilm maturation, and **e)** dispersal of cells or aggregates that move on to colonise other substrates.

The formation of a biofilm commences with the adhesion of free-living planktonic cells to a biotic or abiotic surface (Flemming et al., 2016, Bjarnsholt, 2013) (**Figure 1.1a**). Cells can attach to a diverse range of surfaces, including water pipes, indwelling medical devices (e.g. catheters (Donlan, 2002, Muhammad et al., 2020)), as well as living tissues (Donlan, 2001) (e.g. epithelial cells in the gut and urinary tract (Vigil et al., 2012, Xicohtencatl-Cortes et al., 2019)). Traditional models of biofilm formation have described how single cells initiate binding to a surface, where this initial attachment is reversible and followed by committed irreversible attachment (Berne et al., 2018, Muhammad et al., 2020) (**Figure 1.1b**). We now know, initial seeding is often from clumps of cells that represent aggregates of bacteria that can form *in vivo*, for example, in a mucus layer, or are themselves groups that have been lost from an existing biofilm (Kragh et al., 2016).

During chronic infections, bacteria often attach to each other to form self-contained aggregates that are not associated with substratum (Kragh et al., 2023, Fazli et al., 2009). It has been suggested that self-contained aggregates may allow bacterial communities to colonise new niches under unfavourable conditions as they are more resilient to stress than free-floating planktonic cells (Kragh et al., 2016). Furthermore, biofilms can also begin formation via indirect attachment of bacteria to surfaces through attachment to host proteins that coat these surfaces (Kwiecinski et al., 2016). For example, in infections involving indwelling medical catheters, host fibrin and fibrinogen have been found to promote the attachment of *S. aureus* to the catheters, contributing to biofilm formation (Vanassche et al., 2013). It has been found that the *S. aureus* fibrinogen-binding clumping factor A (ClfA), which binds fibrinogen and fibrin, was key for *coa*-dependent *S. aureus* biofilm formation on plasma-coated surfaces, overall demonstrating an important role for the host in biofilm formation during infection (Zapotoczna et al., 2015). Recent work has exploited this process to treat staphylococcal biofilm device-related infections under biomimetic conditions, where *S. aureus* biofilms exposed to fibrinolytic agents were effectively dispersed, with dispersed cells being killed when antistaphylococcal antimicrobials were added in combination (Hogan et al., 2018).

Once adhesion of cells has been established (**Figure 1.1b**), the biofilm begins to form microcolonies and enter the maturation step (**Figure 1.1c and 1.1d**) in response to signals such as an increase in intracellular cyclic diguanylate monophosphate (c-di-GMP), a secondary messenger molecule (Otto, 2013) that plays a major role in the regulation of biofilm formation (Mhatre et al., 2020). c-di-GMP is synthesised by diguanylate cyclases (DGCs) and broken down by phosphodiesterases (PDEs), and high levels of c-di-GMP reduce motility, promoting a sessile lifestyle. In *Burkholderia cenocepacia,* for example, the protein RpfR has both DGC and PDE activity, and mutations in *rpfR* that reduce the activity of the PDE domain to prevent c-di-GMP breakdown results in larger aggregates, increased matrix and biofilm mass production (Mhatre et al., 2020).

During the maturation process, cells expand to form micro-colonies (Donlan, 2001), and the extracellular matrix is secreted (Lister and Horswill, 2014) (**Figure 1.1c and 1.1d**). The matrix can make up over 90% of the mass of a biofilm (Flemming and Wingender, 2010) and comprises an agglomeration of various biopolymers, collectively known as extracellular polymeric substances (EPS) (Flemming and Wingender, 2010). Common biopolymers of the matrix include polysaccharides, lipids, proteins, and eDNA (Flemming and Wingender, 2010, Flemming et al., 2016). However, the EPS found in a biofilm matrix can vary vastly depending on a range of factors, including which microorganisms are present, nutrient availability, and the environmental temperature (Flemming et al., 2016, Flemming and Wingender, 2010).

Once the biofilm has matured, cells can detach from the surface and move on to colonise new substrates (Rumbaugh and Sauer, 2020) (**Figure 1.1e**). The process of cell dispersal is complex (Rumbaugh and Sauer, 2020), and so far, seeding, erosion and sloughing have been identified as mechanisms of cell dispersal in biofilms (Kaplan, 2010). Seeding, also known as central hollowing, is an active process of cell dispersal (Kaplan, 2010), in which large quantities of cells or micro-colonies are released promptly from the biofilm, resulting in the formation of hollow cavities within the biofilm (Kaplan, 2010, Rumbaugh and Sauer, 2020). This is often initiated by cells in the biofilm in reaction to

environmental changes, for example, stress from lack of nutrients or the presence of antimicrobials (Muhammad et al., 2020). In contrast to seeding, sloughing, where substantial fragments detach abruptly from the biofilm (Kaplan, 2010), and erosion, where smaller fragments detach from the biofilm over time (Kaplan, 2010, Rumbaugh and Sauer, 2020), occur passively as a result of external forces (Rumbaugh and Sauer, 2020), like mechanical processes such as toothbrushing and shear flow (Fleming and Rumbaugh, 2017). Recent research has investigated the ability of enzymes, such as glycoside hydrolases, that can break down glycosidic bonds between sugars within the EPS of the biofilm matrix, to induce biofilm dispersal. Both *in vitro* monospecies and multispecies biofilm models comprised of *P. aeruginosa* and/or *S. aureus* have been used to explore whether these enzymes could be used to treat patients with chronic wound infections (Redman et al., 2020, Redman et al., 2021).

1.3 MECHANISMS OF ANTIMICROBIAL RESISTANCE IN BIOFILMS

Some of the fundamental properties of a biofilm described above (metabolic dormancy, protection from EPS) result in intrinsic tolerance to antimicrobials (Olsen, 2015). In addition to this intrinsic tolerance, various features can also facilitate the evolution of antibiotic resistance within and between species of bacteria in a biofilm (Bowler et al., 2020).

1.3.1 The biofilm matrix

The matrix is a structurally robust layer that acts as a protective barrier for the cells in a biofilm and is a characteristic hallmark of biofilm formation (Hobley et al., 2015, Flemming and Wingender, 2010). The success of the biofilm lifestyle has largely been attributed to the matrix, and various components of the matrix can have protective properties against a range of environmental stress factors, including antibiotics (Hobley et al., 2015). The biofilm matrix can hinder antibiotic absorption into the biofilm (Olsen, 2015) (**Figure 1.2**).

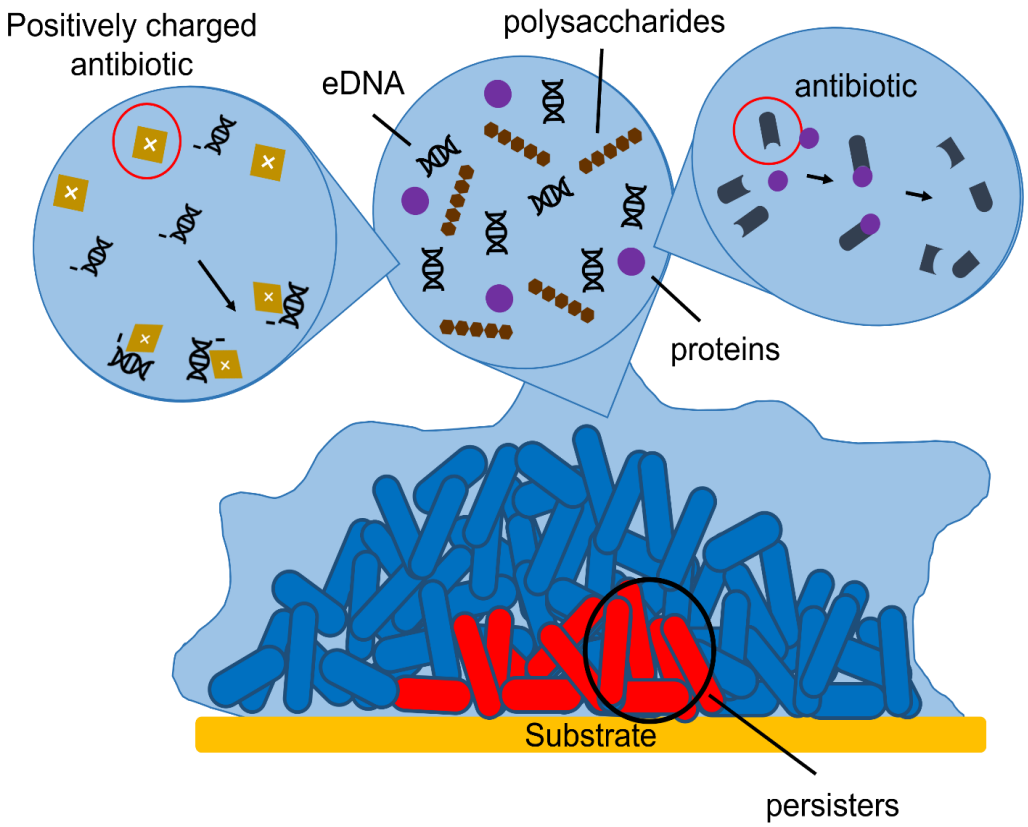

Figure 1.2 - Components of the matrix that can hinder the absorption of antibiotics into the biofilm. Positively charged antibiotics (such as aminoglycosides) can bind to negatively charged eDNA found in the matrix, reducing antibiotic penetration, polysaccharides can present a permeability barrier, and secreted enzymes can break down antibiotics resulting in a reduced concentration of antibiotics reaching the bacteria cells (Redman et al., 2021, Burmeister, 2015).

Some antibiotics form complexes with components of the matrix or are broken down by enzymes, resulting in a reduced concentration of antibiotics reaching the bacterial cells as a consequence (Goel et al., 2021). Other antibiotics, such as positively charged aminoglycosides, can bind to negatively charged biopolymers like eDNA (Goel et al., 2021) in the matrix, slowing down antibiotic penetration (Olsen, 2015). During chronic infections, polymorphonuclear leukocytes can be recruited to biofilms before undergoing bacteria-induced necrosis, releasing host eDNA, and studies have shown that in the CF lung, eDNA produced by *P. aeruginosa*, together with the host eDNA, can form a physical shield to protect the biofilm from tobramycin and host immune cells (Alhede et al., 2020). Similarly, *P. aeruginosa* biofilms can also be protected by host neutrophil extracellular trap (NET) formation. In ocular *P. aeruginosa*

biofilms, it has been found that when host neutrophils formed a layer around the biofilm, they were unable to penetrate the biofilm but instead, induced NET formation, creating a barrier which inhibited the spread of the bacteria into the brain. However, whilst this may have prevented the infection from spreading into the brain, NET formation also hindered the access of antibiotics such as tobramycin into the biofilm, leading to ocular biofilms that were resistant killing by both antibiotics and neutrophils, increasing the severity of the infection in the eye (Thanabalasuriar et al., 2019).

In addition to access to a biofilm, the number of target cells present within a biofilm can impact susceptibility to drugs. It has long been known that the density of a target population can impact susceptibility to some antibiotics, a phenomenon known as the inoculum effect (Brook, 1989). For example, the efficacy of various beta-lactam antibiotics is lower against high-density populations of *Haemophilus influenzae* and *S. aureus* (Dingle Tanis et al., 2022, Brook, 1989). Relatively few studies have explored the importance of the inoculum effect against biofilms; however, research using *P. aeruginosa* biofilms has shown that various beta-lactams, including tobramycin, ceftazidime and imipenem, all demonstrate an inoculum effect against biofilms under laboratory conditions (Lichtenberg et al., 2022, Hengzhuang et al., 2013).

Apart from impeding the access of antibiotics into biofilms (Goel et al., 2021), eDNA found in the matrix also plays an integral role in maintaining the structure of these aggregated microbial communities (Trampari et al., 2021, Okshevsky et al., 2015). Although once thought to be unimportant and only released from lysed cells, it has now been acknowledged that eDNA is often essential for the formation and preservation of the biofilm structure (Jakubovics et al., 2013, Whitchurch et al., 2002). eDNA can be produced in considerable amounts through an active process that is linked to outer membrane-derived vesicles in some species of bacteria, including *P. aeruginosa* (Whitchurch et al., 2002, Hynen et al., 2021), where the presence of DNase can prevent the formation of biofilms, as well as disperse those that have already formed (Whitchurch et al., 2002). This effect of DNase on biofilms

has also been observed in other species, including *Escherichia coli* and *Micrococcus luteus,* where NucB, a DNase*,* was able to disintegrate established biofilms of both species (Jakubovics et al., 2013). In addition to DNase, cellulase has recently been suggested to promote the clearing of biofilms in species such as *E. coli* and *P. aeruginosa,* as it breaks down cellulose, an exopolysaccharide present in the biofilm matrix of various species that provides structural protection (Lim et al., 2019, Kamali et al., 2021).

The matrix also functions as a reservoir, holding an array of active biomolecules within the biofilm (Flemming and Wingender, 2010, Karygianni et al., 2020). Enzymes found in the matrix can break down complex sugars into fermentable polysaccharides that can be used as a nutrient source (Karygianni et al., 2020), as well as introduce changes to the structure of the matrix to maintain or change the properties of the biofilm (Flemming et al., 2023). Other proteins in the matrix include amyloids such as curli, which can be important for dictating biofilm structure (Misra et al., 2023). Additional biomolecules in the matrix can be derived from the contents of cells that have been lysed (Flemming and Wingender, 2010), and these cells can release DNA that may become a source of genes for horizontal gene transfer (HGT) (Flemming and Wingender, 2010).

Cells in a biofilm are immobilised and held together closely, allowing for high levels of cell-to-cell interactions making the biofilm an excellent environment for HGT (Flemming and Wingender, 2010, Karygianni et al., 2020) and, therefore, the transfer of antimicrobial resistance (AMR) genes through various routes, including conjugation via conjugative plasmids, as well as integrative and conjugative elements (Lécuyer et al., 2018), and transduction via bacteriophage (Solheim et al., 2013), facilitating the role of biofilms as resistance gene reservoirs (Uruén et al., 2021). Recently, it has also been suggested that outer membrane vesicles (OMVs) may promote the HGT of AMR genes in biofilms of bacterial species, including *P. aeruginosa* (Johnston et al., 2023).

1.3.2 Horizontal gene transfer

HGT is a major contributor to the AMR crisis (Baker et al., 2018). The emergence and transmission of AMR genes from non-pathogenic to pathogenic bacteria, as well as between different strains and species of pathogenic bacteria, has been fuelled by HGT through the movement of mobile genetic elements (MGEs) carrying genes that confer resistance to most clinically important antibiotics (Von Wintersdorff et al., 2016). Genetic material can be transferred between bacteria by HGT, which was traditionally described as consisting of three main mechanisms (**Figure 1.3**): transformation, where DNA from the surrounding environment is taken up by the bacteria; transduction, where the movement of genetic material is facilitated by bacteriophage (Burmeister, 2015); and conjugation, where genes are moved between cells via a process that requires direct contact between the donor and recipient cell through structures such as pili that are found on the cell surface (Burmeister, 2015, Von Wintersdorff et al., 2016). All three mechanisms are relevant in biofilms. However, conjugation is often regarded as the most important mechanism for the transfer of AMR genes, particularly in multidrug-resistant (MDR) Gram-negative pathogens, where clinically relevant AMR genes, such as *bla*$_{\text{CTX-M-15}}$, an extended-spectrum beta-lactamase (ESBL), in bacteria are often carried by conjugative MGEs, including plasmids (Von Wintersdorff et al., 2016). The spread of these genes between bacterial cells have been strongly associated with conjugation of AMR encoding plasmids (Hennequin et al., 2012).

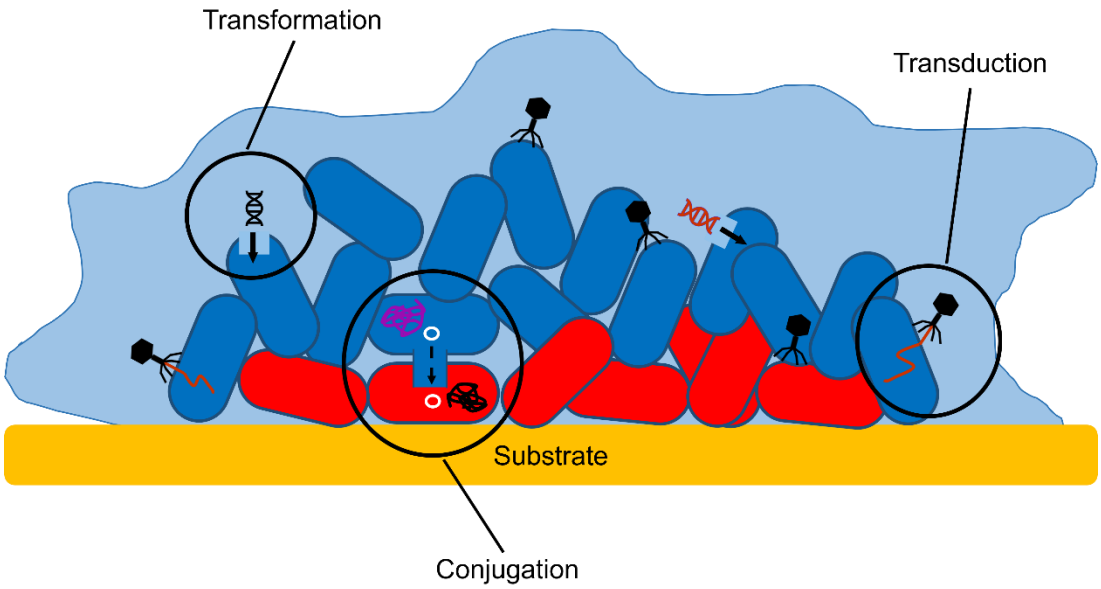

Figure 1.3 - The three main mechanisms of HGT. Transformation, the taking up of DNA from the environment into the bacterial cell; transduction, the insertion of DNA (red) into the bacteria by bacteriophage; and conjugation, the transfer of genes on a plasmid (white) from a donor to a recipient cell through direct contact via pili (Von Wintersdorff et al., 2016) (Burmeister, 2015). The bacterial chromosomes are shown in pink, or black and the plasmid is shown in white.

A number of recent studies have proposed other mechanisms of HGT, including lateral transduction and OMV-mediated transfer (Humphrey et al., 2021, Johnston et al., 2023).

Lateral transduction is described as the mobilisation of large sections of the bacterial genome by temperate bacteriophage (Chee et al., 2023), and thus far, this mechanism has largely been described in *S. aureus* and *Salmonella* (Bowring et al., 2022). In *S. aureus*, it has been found that many *S. aureus* pathogenicity islands (SaPIs), large mobile gene clusters encoding various accessory proteins and virulence factors (Chee et al., 2023), neighbour prophage integration sites, allowing these gene clusters to be transferred via lateral transduction (Humphrey et al., 2021). In *Salmonella*, *Salmonella* pathogenicity islands (SPIs), such as SPI-2, can also be found downstream of prophage attachment sites and be transferred via lateral transduction (Humphrey et al., 2021).

OMVs are nanostructures formed and released from the outer membrane of Gram-negative bacteria (Avila-Calderón et al., 2021) that have various functions, for instance, in cytotoxin and virulence factor transfer as well as in nutrient acquisition (Jan, 2017). More recently, OMVs have also been suggested as a mechanism of HGT (Michaelis and Grohmann, 2023), and studies have reported that OMVs may mediate the HGT of plasmids in various species. In *P. aeruginosa,* for example, it was found that OMVs were able to transform pBBR1MCS-5, a plasmid encoding for gentamicin resistance, into recipient *P. aeruginosa* cells. Additionally, OMVs obtained from biofilm populations of *P. aeruginosa* were able to transform the plasmid more efficiently compared to those obtained from planktonic populations (Johnston et al., 2023).

The *bla*$_{\text{NDM-1}}$ gene, encoding carbapenem resistance, and *bla*$_{\text{CTX-M}}$ genes, encoding extended-spectrum beta-lactamases (ESBLs) (Moremi et al., 2021), conferring resistance to cephalosporins, are important examples of AMR genes that have been transferred widely between various pathogenic Gram-negative bacteria (Baker et al., 2018, Von Wintersdorff et al., 2016). These can often be readily transferred in biofilms. For example, the movement of *bla*$_{\text{CTX-M-15}}$ through a population of *Klebsiella pneumoniae*, causing an outbreak in France, was attributed to the efficient transfer of a plasmid within biofilms (Hennequin et al., 2012).

Although very high concentrations of antibiotics are often needed to kill cells within a biofilm, they have been shown to be highly sensitive to sub-inhibitory concentrations of drugs, which can rapidly select for mutants with resistance mutations (Trampari et al., 2021). Evolution of AMR occurs due to both the acquisition of point mutations as well as HGT, and adaptation may result in changes to other phenotypic traits of the bacteria, including the ability to form biofilms (Trampari et al., 2021). For example, *Salmonella* biofilms were shown to rapidly evolve resistance when exposed to sub-lethal concentrations of either ciprofloxacin, cefotaxime or azithromycin. Whilst resistance emerged rapidly, mutants were significantly less able to form a biofilm, demonstrating tradeoffs in adaptation (Trampari et al., 2021). In addition to antimicrobials,

studies have shown that biofilm evolution can also be driven by non-antibiotic antimicrobials, including toxic metals such as copper (Koechler et al., 2015), and these toxic metals have been proposed to promote the spread of resistance in biofilms through HGT (Koechler et al., 2015).

Compared to cells in the planktonic state, HGT occurs much more frequently between cells in a biofilm community (Madsen et al., 2012), and it has been identified that the rate of conjugation can be increased by up to 16000-fold in *S. aureus* biofilms compared to their planktonic equivalents (Ciofu et al., 2022). The transfer of a plasmid encoding $bla_{\text{NDM-1}}$ between strains of *K. pneumoniae* has also been found to be elevated in biofilm cells (Element et al., 2023). There are several reasons proposed for this, including the close proximity of cells within a biofilm that allows for efficient intercellular communication (Flemming and Wingender, 2010), and the large reservoir of diverse DNA and AMR genes present within a polymicrobial biofilm (Uruén et al., 2021). The importance of HGT for the transmission of AMR genes in biofilms has been demonstrated in oral biofilms, where mutated mosaic *pbp2x* genes were transferred between different *Streptococcus* spp, resulting in penicillin resistance (Chi et al., 2007). This has also been demonstrated in lake water biofilm communities, where pKJK5, a conjugative plasmid encoding resistance to trimethoprim, was transferred between species of bacteria forming biofilms on microplastics (Arias-Andres et al., 2018). Furthermore, the transfer of AMR genes via HGT in biofilms has also been studied in *Campylobacter jejuni*, where the HGT of a chromosomally encoded AMR gene was found to be increased by up to 17.5-fold in biofilms when compared to the planktonic cells. It was also found that mutants that had gained the AMR gene in the plasmid were actively dispersed from the biofilm into the supernatant, indicating that biofilms also facilitate the spread of AMR into the wider population (Ma et al., 2021).

The formation of biofilms has also been found to facilitate plasmid persistence (Røder et al., 2021, Ciofu et al., 2022) in the absence of selection, with examples where plasmid maintenance was found to be much higher in biofilm populations relative to planktonic counterparts (Metzger et al., 2022). Persister cells, which are common in biofilms, can act as plasmid reservoirs where host

cells survive antibiotic challenge (Bakkeren et al., 2019). This has been demonstrated for *Salmonella enterica serovar* Typhimurium in mice, where persisters harbouring AMR plasmids can survive antibiotic treatment before then being able to efficiently spread AMR through conjugation to other bacteria, such as *E. coli*, in the gut microbiota (Bakkeren et al., 2019). Additionally, using an evolution model, a study investigating the transfer of an MDR IncP-1 plasmid, pB10, in *Acinetobacter baumannii*, found that biofilm populations were able to maintain the plasmid at higher rates in comparison to their planktonic counterparts under no selection. Although plasmid persistence improved over time in the planktonic population, this was coupled with the loss of transfer genes, suggesting that, in general the biofilm mode of life may aid the HGT of plasmids encoding AMR genes in bacteria (Metzger et al., 2022).

The ability to maintain AMR plasmids, in combination with the elevated levels of HGT in biofilms, has been suggested as an important mechanism contributing to the evolution and spread of resistance in pathogenic microbes (Ciofu et al., 2022), a major cause for concern given the role biofilms play in persistent, chronic infections (Uruén et al., 2021).

Away from the clinical environment, many food-associated biofilms are multispecies and demonstrate higher resistance to disinfectants compared to monospecies biofilms (Yuan et al., 2022, Galié et al., 2018). The intrinsic ability of biofilms to tolerate biocides leads to persistent contamination of environments in the food chain, encouraging plasmid stability and HGT (Van Houdt and Michiels, 2010, Rossi et al., 2014). This can be exacerbated by other stresses in the food processing environment, such as high salt concentrations and low temperatures, which can alter conjugation rates and thereby influence the spread of resistance through the HGT of plasmids carrying AMR genes, resulting in reservoirs of AMR biofilms in the food chain, which can cause contamination of products (Zarzecka et al., 2022). Various studies have investigated the link between the food chain and the dissemination of AMR, for example, in India, where 3% of the samples collected from a range of locations in a food market were found to be capable of causing enteric disease, with most being resistant to common antimicrobials

used to treat these infections (Das et al., 2025). Similarly, in China, the transmission of AMR genes between the environment, humans and food products was observed within the city of Dengfeng in Henan Province. A high load of AMR genes were detected in bacterial samples taken from food, where MGEs were found to play a key role in shaping the resistome found on food produce (Feng et al., 2025).

Overall, this has serious clinical implications for the spread of AMR into humans in a One Health context (Brown et al., 2024), and the clinical implications of AMR transfer within the food chain, including food-producing environments, should be studied further.

1.3.3 Tolerance and persistence

The ability to survive antibiotic exposure can be conferred by the carriage of a specific gene or mutation, which renders a target cell resistant to an antibiotic. However, physiological changes to a cell's metabolism can also be important in determining survival in the presence of an antimicrobial.

Within a biofilm, there are cells present at various phases of the growth cycle, with metabolically active cells generally being found at the surface of the biofilm (Percival et al., 2011) and dormant, slow-growing cells, as well as metabolically inactive cells, including 'persister' cells (Wood et al., 2013), largely being found in the deeper layers (del Pozo and Patel, 2007, Olsen, 2015). Slow-growing cells often display 'tolerance' to stress, including antibiotics. Tolerance is characterised by an ability to survive temporary exposure to concentrations of antibiotics that would typically be fatal (Brauner et al., 2016). This is a distinct phenotype from persistence, which is usually exhibited by a smaller subpopulation of persister cells which have entered a distinct dormant state where growth is fully arrested (Balaban et al., 2019).

Persister cells undergo a phenotypic, rather than genetic, change into a state of metabolic inactivity (Wood et al., 2013, Conlon et al., 2015). These cells are commonly described as having restricted synthesis of macromolecules (Trampari et al., 2021), arrested growth (Olsen, 2015), and an ability to tolerate a wide range of antimicrobials, particularly those that are bactericidal (Conlon et al., 2015). Many antimicrobials target cells that are actively growing and replicating (del Pozo and Patel, 2007), and the presence of persisters may interfere with the action of antimicrobials as the cellular processes they target are no longer crucial for the survival of these cells (Trampari et al., 2021). Persister cells contribute considerably to the chronic nature of biofilm infections as the site of infection can be repopulated by persisters after the cells sensitive to antimicrobials are eliminated and treatment is ceased (Olsen, 2015, del Pozo and Patel, 2007) (**Figure 1.4**). Regular treatment using antibiotics has been shown to lead to an increase in infections comprising resistant strains of bacteria due to the selection of resistance *in vivo,* and studies have proposed that the reservoir of persistent cells contributes to this (Kolář et al., 2001).

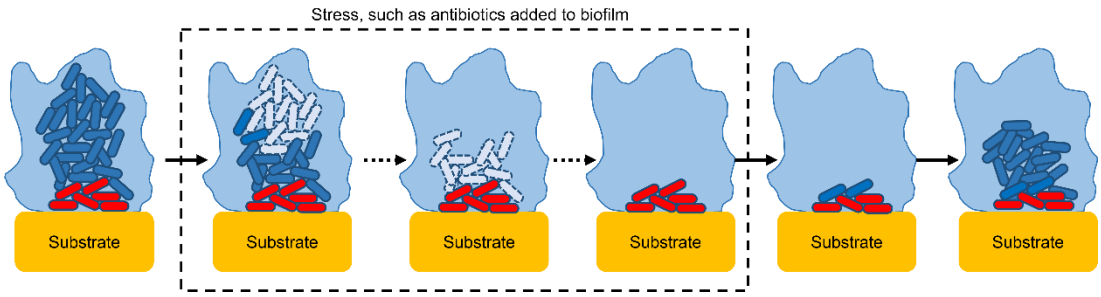

Figure 1.4 - The repopulation of a biofilm infection by persisters (red) after actively growing biofilm cells are killed by stress such as antibiotics.

The exact mechanisms of persister formation are not fully understood, and relatively few species have been studied (Percival et al., 2011). However, the generation of large quantities of persisters in biofilms has been connected with a number of toxin-antitoxin (TA) systems (Olsen, 2015), and certain stress conditions have been shown to increase the rate of persister cell formation (Goel et al., 2021, Alhede et al., 2020).

The *E. coli hipAB* TA system is a well-studied system associated with the formation of persisters (Conlon, 2014). In the *hipAB* TA system, the HipA toxic

protein phosphorylates Glu-tRNA synthetase, which suppresses protein synthesis in the cell (Shan et al., 2017, Conlon, 2014); this can be neutralised by the antitoxin HipB, via the formation of a complex, which inhibits HipA transcription (Wen et al., 2014). Stress from various stimuli in the environment, such as DNA damage, antimicrobials, and starvation (Olsen, 2015, Wen et al., 2014), has been shown to lead to stress-related expression of toxins in TA systems (Shan et al., 2017), resulting in protein synthesis suppression, and this has been suggested to result in elevated levels of persisters (Wen et al., 2014).

Although tolerance, persistence and resistance are distinctly different bacterial states, they are not mutually exclusive and are often interconnected. For instance, persisters can promote the selection of resistant strains of pathogenic bacteria due to their association with chronic, recurrent infections that require the prolonged use of antimicrobial treatment (Windels et al., 2019, Fisher et al., 2017), and tolerance has been suggested to increase the rate of which resistant bacterial strains are evolved (Levin-Reisman et al., 2017). Therefore, given the role that they play in the development of AMR in bacteria, it is important to understand and study resistance in conjunction with tolerance and persistence in order to address AMR as a whole (Trastoy et al., 2018).

1.4 INTERACTIONS BETWEEN CELLS WITHIN A BIOFILM AND ANTIMICROBIAL RESISTANCE

Most biofilms found in nature are polymicrobial (Yang et al., 2011), including biofilms associated with infections in humans, for example, in the CF lung and the oral cavity or in chronic wounds (Elias and Banin, 2012). Despite this, most research in the past has been conducted using monospecies planktonic cultures that do not accurately reflect real-world bacterial communities (Trampari et al., 2021, Bottery et al., 2022). More recent studies have developed tools to investigate the complexity of multispecies biofilms.

Cells in a biofilm are held within close proximity of each other by EPS in the matrix, enabling strong cell-to-cell interactions to occur between them (Flemming and Wingender, 2010). These interactions are critical and govern

the spatial organisation of strains to induce cooperation or competition in biofilms (Varposhti et al., 2014). Studies have found that bacterial species can both compete and cooperate, depending on the resources available to cells in the surrounding environment, although environments with less diverse resources appear to facilitate cooperation (Solowiej-Wedderburn et al., 2025).

Various interspecies interactions in polymicrobial communities have been shown to modify antibiotic efficacy, resulting in other members of the community being less susceptible to treatments during polymicrobial infections (Bottery et al., 2022). The closed environment provided by the biofilm matrix also helps to promote intercellular signalling through mechanisms such as quorum sensing as well as establish synergistic cooperation between the cells (Flemming et al., 2016).

Synergy has been shown to occur during the formation of multispecies biofilms when stress factors, such as the addition of biocides or removal of nutrients, have been implemented in the environment (Wicaksono et al., 2022), and previous studies have suggested that biofilm formation and resistance to antimicrobials can be promoted by synergistic interactions in multispecies biofilms (Burmølle et al., 2006). An example is where *Streptococcus* spp. in the oral cavity interacts synergistically with *Candida albicans* in a multispecies biofilm. *C. albicans* can increase biofilm formation in streptococci, and in turn, the streptococci can increase the invasive characteristics of the fungi (Marsh and Zaura, 2017). Synergistic interactions between species in polymicrobial biofilms have also been described in bacteria isolated from food contact surfaces in the food processing environment, where high levels of synergy have been found to occur in biofilms comprised of bacteria such as *Bacillus licheniformis*, *Microbacterium lacticum, Calidifontibacter indicus* and *Stenotrophomonas rhizophila*, that are commonly found in dairy products (Sadiq et al., 2023).

Stress within a biofilm can come from limited space, nutrient availability, the presence of metabolic waste products, or from external sources such as biocides and antimicrobials. The adaptive nature of cells in response to stress can promote interactions between species in the form of competition and

cooperation, which can lead to the formation of persister cells and lower susceptibility to antimicrobials within the biofilm (Flemming et al., 2016, Olsen, 2015, Fisher et al., 2017).

1.4.1 Quorum sensing

Quorum sensing is the regulation of gene expression in response to changes in the density of a bacterial community (Sadiq et al., 2017). Quorum sensing allows cells in a biofilm to coordinate behaviours (Brackman and Coenye, 2015), and is mediated through the production and detection of bacterial chemical signal molecules known as autoinducers (Elias and Banin, 2012). Quorum sensing can be responsible for the regulation of various bacterial processes, including the expression of virulence factors (Pena et al., 2019). It has been demonstrated that quorum sensing plays a role in infections caused by *P. aeruginosa*, for example, in the CF lung, where mRNA transcripts for *lasR* and *lasI* (genes involved in *P. aeruginosa* quorum sensing) have been found in mucus samples obtained from CF patients. A decline in virulence is observed in *P. aeruginosa* when there is a deficiency in components involved in quorum sensing (Smith and Iglewski, 2003). Quorum sensing also controls biofilm formation (Pena et al., 2019), and studies have shown that suppressing quorum sensing in bacteria can impede biofilm formation (Zhou et al., 2020).

As well as being important in coordinating community behaviour within biofilms, quorum sensing has also been shown to impact the antibiotic susceptibility of biofilms. Quorum sensing can elevate bacterial resistance to various stressors, including oxidative, heavy metal and thermal stress, stress from the immune system, and stress from antibiotics such as tobramycin (García-Contreras et al., 2015). Previous studies have found a strong correlation between quorum sensing, AMR, and biofilm formation in clinical *P. aeruginosa* isolates (Hemmati et al., 2024), and the potential of combining antibiotic therapy with quorum sensing inhibitors when treating *P. aeruginosa* and *S. aureus* biofilms has also been investigated in the past (Brackman et al., 2011). In *P. aeruginosa* and *S. aureus* biofilm wound models, the use of quorum sensing inhibitors resulted in increased susceptibility of the biofilm to the antibiotics tested. This was also observed in *Caenorhabditis elegans* and *Galleria*

mellonella models, where a significantly larger number of infected *C. elegans* and *G. mellonella* survived when treated with both quorum sensing inhibitors and antibiotics compared to those that were only treated with antibiotics (Brackman et al., 2011). These studies show that quorum sensing plays a role in the resistance of bacteria to various antimicrobials, and treating biofilm infections with a combination of quorum sensing inhibitors and antibiotics may lead to higher treatment success rates in the future (Brackman et al., 2011).

A number of quorum sensing pathways, distinguished by the type of autoinducer involved, have been identified (Elias and Banin, 2012), and it has been found that some pathways, such as the autoinducer-2 (AI-2) pathway, found broadly across both Gram-positive and Gram-negative species of bacteria, can mediate interspecies communication (Pereira et al., 2013, Elias and Banin, 2012). This system plays a key part in the establishment of multispecies biofilms (Li and Tian, 2012), for example, in biofilms comprising of *H. influenzae* and *Moraxella catarrhalis* in rodent otitis media infections. Although AI-2 could not be produced by *M. catarrhalis*, AI-2 is produced by *H. influenzae,* which influences *M. catarrhalis* to produce more biomass, with biofilms becoming consequently less antibiotic susceptible (Pereira et al., 2013).

1.4.2 Competition between bacterial species within a biofilm

Bacteria occupying a similar niche can interact with each other in various ways, which can result in synergy or antagonism. Whilst some species are indifferent to the presence of others, many can impact others in a way which results in competition between them (Elias and Banin, 2012). Mechanisms of competition in biofilms can be split broadly into two groups: exploitative competition, an indirect mechanism where a species of bacteria hinders another species' access to nutrients or resources; and interference competition, where the survival of a species is directly affected by mechanisms such as the secretion of growth inhibitors such as antibiotics by its competition (Rendueles et al., 2015), as well as by the production of molecules that can prevent the attachment and colonisation of new species in the biofilm (Russel et al., 2017, Rendueles and Ghigo, 2012). These competitive interactions are

essential for the evolution and shaping of multispecies biofilms (Elias and Banin, 2012), and studies have suggested that competitive interactions can increase tolerance to antimicrobials in multispecies biofilms (Parijs and Steenackers, 2018).

Cells within a biofilm can protect themselves from the stress of competitors passively rather than antagonistically. In *S.* Typhimurium, the presence of competing strains and species can result in increased biofilm production and antibiotic tolerance. It has been demonstrated that in the presence of *E. coli,* a genetically distinct *S*. Typhimurium strain upregulated genes involved in biofilm formation, efflux, invasion of host cells, and antibiotic tolerance (Lories et al., 2020). Genes upregulated in the presence of competition included *aadA*, which encodes an aminoglycoside adenylyltransferase involved in resistance to aminoglycosides, such as streptomycin and spectinomycin (Stern et al., 2018). Additionally, *tolC*, encoding the outer membrane component of the AcrAB-TolC efflux pump, was also upregulated in mixed species biofilms, suggesting that increased efflux of antimicrobials, including quinolones, chloramphenicol, and tetracyclines, may occur in mixed species biofilms (Lories et al., 2020). The efflux of antimicrobials by efflux pumps can lead to sub-inhibitory intracellular concentrations of drugs, which can promote the selection of AMR strains of bacteria (Lorusso et al., 2022).

A number of competition quenching strategies, such as reducing cell density to decrease overall competition, inactivating the type VI secretion system (T6SS) of competing strains, as well as inhibiting the general RpoS stress response, have been found to reduce the antibiotic tolerance of *S.* Typhimurium SL1344 in a mixed species biofilms consisting of two *S.* Typhimurium strains (SL1344 and ATCC 14028) and *E. coli* (MG1655), suggesting that with further exploration, it may be possible to use competition quenching strategies alongside traditional antibiotics to improve treatment outcomes of polymicrobial biofilm infections (Lories et al., 2024).

1.4.3 Cooperation between bacterial species within a biofilm

Whilst competition can be antagonistic, there are also many examples of cooperation within a biofilm, where cells can behave collectively, providing them access to the benefits from behaviours which would not be possible for individual cells on their own (Nadell et al., 2016).

Some species of bacteria are capable of cooperating via coaggregation (Elias and Banin, 2012), a process that requires highly specific interactions between pairs of bacteria (Foster and Kolenbrander, 2004), and is essential for the formation of multispecies biofilms (Rickard et al., 2003). Coaggregation allows different species to attach to one another to stabilise the biofilm and protect all species involved (Klayman et al., 2009). An early example of bacterial coaggregation arose from investigations into dental plaque obtained from the human oral cavity (Rickard et al., 2003). Biofilms in the oral cavity can develop sequentially, where species of bacteria such as *Streptococcus mutans* and *Streptococcus gordonii* can colonise the surface of teeth first, altering the environmental conditions that then allow a succession of other bacterial species to colonise the surface (Elias and Banin, 2012). Coaggregation using curli, produced by many Gram-negative species, is important in the gastrointestinal tract, and cross-seeding of curli subunits between species of the gut microbiota increases surface attachment of cells and facilitates biofilm formation (Zhou et al., 2012). For example, it was demonstrated that curli expression was associated with enhanced biofilm formation and tolerance to common biocides in a range of Shiga toxin-producing *E. coli* strains (Wang et al., 2012). Additionally, in *E. coli* and *S.* Typhimurium strains lacking EPS expression, a significant increase in tolerance to biocides was observed when these strains formed a mixed-species biofilm with an EPS-producing companion, compared to when grown in a monoculture. This demonstrates how, in mixed communities, common goods can be exploited by individual strains, and this can affect antimicrobial susceptibility (Wang et al., 2013, Wang et al., 2012).

A study investigated the interactions between isolates of *E. coli*, *P. aeruginosa*, and *Enterobacter cloacae* from water sources, and the ability of chlorine to

eradicate monospecies and multispecies biofilms formed by these species. It was found that a chlorine concentration of 50-300-fold higher was required for the eradication of the multispecies biofilms compared to the monospecies biofilms (Schwering et al., 2013). Enhanced tolerance to disinfectants has also been found in *Listeria monocytogenes* and *Lactobacillus plantarum* multispecies biofilms (Van der Veen and Abee, 2011). A study also found that when grown as monospecies biofilms, *P. aeruginosa, Pseudomonas protegens,* and *K. pneumoniae* were more susceptible to sodium dodecyl sulphate (SDS) and tobramycin (Kelvin Lee et al., 2016), whereas multispecies biofilms were resistant to both agents. *P. aeruginosa* encodes a secreted SDS hydrolase (SdsA1), which can degrade and metabolise SDS within the biofilm. Additionally, *P. protegens* produces aminoglycoside-modifying enzymes that break down tobramycin and offer a community benefit. When the three species were grown as monocultures and exposed to tobramycin, only *P. protegens* survived, showing the importance of different roles within a multispecies biofilm, and how the importance of knowing which species are present, as a species may enjoy resistance to an antimicrobial without possessing a specific resistance mechanism itself. Species common in CF patients have been found to have higher biomass and less susceptibility to a variety of antibiotics, including tobramycin, ciprofloxacin, cefotaxime, and chloramphenicol, when grown in a multispecies biofilm with *P. aeruginosa* (Lopes et al., 2012).

1.5 THE MOLECULAR BASIS OF PLASMID TRANSFER AND ACCEPTANCE

The transfer of a plasmid between two cells is a contact-dependent process (Virolle et al., 2020), where the plasmid to be transferred is linearised at the origin of transfer (*oriT*) and transferred across a pilus extending from the donor cell to the recipient cell via the formation of a mating junction (Low et al., 2022, Virolle et al., 2020, Waksman, 2025). The genes encoding transfer machinery, such as *tra* and *trb* genes in IncF plasmids found in Gram-negative bacteria, required for plasmid transfer, are generally carried on conjugative plasmids, although the expression of these genes, in addition to the linearisation of the plasmid via the relaxosome, is regulated by the donor cell (Virolle et al., 2020).

After linearisation, the plasmid (referred to as the T-strand) is translocated through the bacterial membrane across the pilus to the recipient cell using the conjugative type IV secretion system (T4SS), where the plasmid is then recircularised. However, the molecular basis of plasmid recircularisation remains unknown (Waksman, 2025).

Whilst the donor cell is responsible for the expression of genes that physically translocate the plasmid, it is known that the recipient is also important for successful conjugation (Allard et al., 2023). In addition to the role of the host cell in regulating a plasmid after it enters the cell (Ruiz-Masó et al., 2017), host cells can prevent the acceptance of plasmids through various defence mechanisms. An example of this is restriction modification systems, a widespread defence system, that can act as a barrier for the uptake of conjugative plasmids by cleaving double-stranded DNA encoding unmodified recognition sequences. Recently, it has been found that some plasmids encode anti-restriction genes that result in resistance against a range of these systems (Dimitriu et al., 2024). In addition to restriction modification, CRISPR-Cas systems have also been found to hinder the uptake of plasmids into host cells in species such as *Enterococcus faecalis* (Upreti et al., 2024). Some studies have also suggested that restriction-modification systems and CRISPR-Cas systems can work together to prevent the conjugation of plasmids into bacteria in species such as *K. pneumoniae* (Yang et al., 2024).

1.6 CONCLUSIONS

The majority of bacteria exist within biofilms (Costerton et al., 1987), a context where various phenotypic characteristics contribute to the elevated levels of tolerance to antimicrobials observed compared to their planktonic equivalents (Olsen, 2015, Trampari et al., 2021). The high levels of cell-to-cell interactions in biofilms make these communities an excellent environment for the evolution of AMR through HGT (Uruén et al., 2021, Flemming and Wingender, 2010).

Given that most biofilms, including those that are associated with the majority of infections in humans, are polymicrobial (Trampari et al., 2021, Yang et al., 2011, Khatoon et al., 2018), it is important to recognise that bacteria may

behave differently when in a multispecies community (Bottery et al., 2022) and investigate the evolution of AMR in bacteria in a biofilm context (Trampari et al., 2021).

Furthermore, although it is well established that HGT plays a crucial role in the spread of bacterial AMR, the direct correlation between the use of antimicrobials and the impact on the rate of HGT is poorly understood (Liu et al., 2021), and there remains a lack of understanding of the mechanisms and factors driving plasmid movement in multispecies biofilms (Trampari et al., 2021, Bottery et al., 2022). Interspecies interactions in polymicrobial communities can modify antibiotic efficacy, resulting in members of the community being less susceptible to treatments during polymicrobial infections (Bottery et al., 2022).

In the future, developing models to study and understand AMR using models of mixed community biofilms will be needed to better understand how bacteria survive and how AMR evolves in this crucial context. How environmental stresses can exacerbate and influence rates of HGT in biofilms should be explored. It would also be useful to build on current research and further investigate the genes that are important for biofilm formation, in addition to those that drive HGT of resistance genes in biofilms, as this knowledge will be required in the development of future strategies to treat and manage biofilm infections, as well as control the spread of AMR in bacterial populations within the One Health framework.

1.7 PROJECT HYPOTHESIS

I. The movement of plasmids between bacterial species within a multispecies biofilm community will be influenced by environmental stress factors.
II. The core host genome plays a significant role in plasmid acceptance.

1.8 PROJECT AIMS

I. Develop a multispecies biofilm model that can be used to measure plasmid movement between bacterial species.

II. Use the multispecies biofilm conjugation model to investigate how different stressors impact conjugation efficiency in a multispecies biofilm community.

III. Explore the important genes for plasmid acceptance in *E. coli* and *S.* Typhimurium using TraDIS-*Xpress.*

CHAPTER 2:
MATERIALS AND METHODS

“You are only as good as your controls”

< Mark Alexander Webber >

2.1 BACTERIA USED IN THIS STUDY

For this study, an *E. coli* isolate was required to establish a multispecies biofilm model with *S.* Typhimurium 14028S, to conduct investigations within a real-world context. Ten *E. coli* isolates were initially chosen from a panel of isolates isolated from various food sources (Janecko et al., 2023) (**APPENDIX I**). These isolates were selected as they represented common sequence types (STs) found in the study and did not encode AMR genes either via plasmids or in the genome, according to the genomic data gathered during the study. Isolates in the initial panel of strains that carried IncF plasmids were also omitted. After initial testing of the ten *E. coli* (**Chapter 4**), EC18LG-0005-1 was selected to be used in the biofilm model as it was found to co-exist well with *S*. Typhimurium 14028S (Jarvik et al., 2010) in a biofilm context, and belonged to ST10, the most common lineage of *E. coli* found in the Enterobase collection of genomes, which includes isolates from infection and other sources, belonging to this species (Zong et al., 2018).

Mutants and transconjugants derived from EC18LG-0005-1 and *S.* Typhimurium 14028S were used in the biofilm conjugation experiments. The plasmid used for conjugation (pHYCTX14) was obtained from EC-HY-3, a clinical *E. coli* isolate previously isolated from faecal samples of healthy volunteers returning to the United Kingdom from South East Asia (Bevan et al., 2021) (**Table 2.1**). The plasmid was selected for this study as it belonged to plasmid incompatibility type F, the most common plasmid type isolated from both humans and animals (Rozwandowicz et al., 2018), and encoded *bla*$_{\text{CTX-M-14}}$, one of the most widely disseminated ESBLs worldwide (Valverde et al., 2009). Other bacterial isolates, as well as mutants and transconjugants arising from this study, are listed in **APPENDIX II**.

E. coli BW25113 was used as a control strain where required (**Table 2.1**), and its corresponding transposon mutant library (Yasir et al., 2020), as well as the *S.* Typhimurium 14028S transposon mutant library (Holden et al., 2022), were used for TraDIS-*Xpress* experiments.

Table 2.1 - List of bacteria used in this study

Name	Source	Genomic mutations conferring AMR			Plasmid(s)		Antibiotic selection
		Animo acid substitution	Gene of substitution	AMR	Incompatibility type	Resistance gene(s)	
S. Typhimurium 14028S	ATCC	-	-	-	IncFIB(S)	-	-
S. Typhimurium 14028S NalR	Made in House	Ser83Phe	*gyrA*	Nalidixic acid	IncFIB(S)	-	100 µg/mL nalidixic acid
E. coli EC18LG-0005-1	(Janecko et al., 2023)	-	-	-	-	-	-
E. coli EC18LG-0005-1 RifR pHYCTX14	Made in House	Glu513Leu	*rpoB*	Rifampicin	IncFII	$bla_{\text{CTX-M-14}}$	100 µg/mL rifampicin 8 µg/mL cefotaxime
BW25113	(Grenier et al., 2014)	-	-	-	-	-	-
EC-HY-3	(Bevan et al., 2021)	-	-	-	IncFII	$bla_{\text{CTX-M-14}}$	8 µg/mL cefotaxime

2.2 GENERAL BACTERIAL GROWTH CONDITIONS

Unless otherwise stated, bacterial strains were cultured in Lysogeny Broth (LB) or LB agar and incubated at 37 °C for 18 – 24 hours. Broth cultures were also subjected to shaking at 180 – 250 rpm.

For differentiation between *E. coli* and *S.* Typhimurium species, molten LB agar was supplemented with 40 µg/mL X-Gal (5-Bromo-4-chloro-3-indolyl beta-D-galactopyranoside) (XGAL001, Formedium Limited) and 1 mM IPTG (Isopropyl beta-D-1-thiogalactopyranoside) (IPTG005, Formedium Limited) for blue/white screening. Xylose lysine deoxycholate (XLD) agar (CM0469, Oxoid) and Brilliance *Salmonella* agar (CM1092 and SR0194, Oxoid) were also used as selective agar for the two species.

2.3 CALCULATING COLONY FORMING UNITS OF BACTERIA

Colony forming units (CFU) is a common unit of measurement used to estimate the number of viable bacterial cells within a sample (Bhuyan et al., 2023).

Unless otherwise stated, the CFU of bacterial samples were estimated by serially diluting the bacterial cultures in phosphate-buffered saline (PBS) to an appropriate concentration and inoculating into an even lawn onto agar plates and incubated overnight. The appropriate concentration the cells were diluted to was determined by recovering a lawn of between 30 and 300 single colonies on an agar plate.

Colonies on the plates were recorded using a combination of manual counting and openCFU (Geissmann, 2013), an automated colony counting software, and the CFU was calculated using the following formula:

$$CFU = \frac{Number\ of\ colonies\ recorded}{Volume\ inoculated\ (mL)\ \mathrm{x}\ dilution\ factor}$$

2.4 MOLECULAR BIOLOGY TECHNIQUES

2.4.1 Polymerase chain reaction

To check for the presence and absence of expected genes or DNA sequences, 10 µL PCR reactions consisting of 5 µL GoTaq® G2 Green Master Mix (M7822, Promega), 4 µL molecular-grade water (W4502, Sigma) and 0.5 µL of forward and reverse primers (10 µM) were used. Template DNA was added by picking single bacterial colonies off agar plates using toothpicks and resuspending the cells in the reaction mixture.

To prepare amplicons for sequencing or for the construction of recombinant plasmids, GoTaq® G2 Green Master Mix was replaced with NEBNext® Ultra™ II Q5® Master Mix (M0544S, NEB), with relative concentrations of the primers and polymerase remaining the same as above. 0.5 µL – 1 µL of bacterial DNA was added to each PCR reaction, and the volume of molecular-grade water was adjusted to maintain the final reaction volume. PCR reactions were ran in an Applied Biosystems™ Veriti™ 96-well Thermal Cycler (4375786, Fisher Scientific) following the settings in **Table 2.2**.

Table 2.2 – PCR programme

Stage	**1**	**2 - cycles (~25 – 35)**			**3**	**4**
Step	Initial denature-tion	De-natura-tion	Anneal-ing	Amplifi-cation	Final amplification	Hold
Temp-erature	95 °C	95 °C	60 – 63 °C*	72 °C	72 °C	4 °C
Duration	3 minutes	30 seconds	30 seconds	30 seconds** or 1 minute*** per 1 kb of amplified product	7 minutes	∞

*Depending on the melting temperature (Tm) of the primers used

** NEBNext® Ultra™ II Q5® Master Mix polymerase

***GoTaq® G2 Green Master Mix polymerase

2.4.2 Agarose gel electrophoresis

Agarose gel electrophoresis was used to visualise the products of the PCR reactions and determine their size. Unless otherwise stated, 1% agarose gel was prepared using 1x Tris/ Borate/ EDTA (TBE) buffer (B52, Thermofisher), and 5 µL Midori Green Advance DNA stain (MG04, Nippon Genetics Europe) was added per 50 mL agarose gel used. To run the PCR products on the gel, gel loading dye (B7025S, NEB) was added to the DNA according to the manufacturer's instructions. Loading dye was omitted if the products were amplified using GoTaq® G2 Green Master Mix as the dye is already present in this master mix. 5 µL of reaction was loaded into each well, and the gel was run in 1 x TBE buffer at 120V for 20 – 30 minutes. 5 µL of 1 kb DNA ladder (N3232S, NEB) was included in each run to allow the size of the bands to be estimated.

2.4.3 Genomic DNA extraction

DNA was extracted from bacterial isolates for sequencing and as a template for PCR reactions.

2.4.3.1 Low molecular weight DNA extraction

Overnight cultures of selected strains were prepared, and 300 – 1000 µL of each strain was subjected to centrifugation at 16,000 x *g* for five minutes. The supernatant was discarded, and the pellets were resuspended in 100 µL lysing buffer (100 µL 0.5 mg/mL lysozyme (L6876, Sigma) and 50 µL 20 mg/mL RNase A (12091021, Invitrogen) in 10 mL Tris-EDTA (ethylenediaminetetraacetic acid) (TE) buffer), transferred to clean microcentrifuge tubes and incubated at 37 ºC, 1600 rpm. After 25 minutes, 10 µL lysing additive (600 µL 10% SDS, 60 µL 20 mg/mL proteinase K (P8107S, NEB), and 60 µL 20 mg/mL RNase A in 528 µL TE buffer) was added per sample, then incubated for a further 15 minutes at 65 ºC, 1600 rpm. To isolate the DNA, 50 µL DNA-binding magnetic beads (KAPA Pure Beads 07983298001, Roche) was added to each sample, mixed well and incubated for five minutes at room temperature before placing on a magnetic rack for two

to five minutes. Once the supernatant was clear, it was discarded, and the beads were washed three times with 100 µL freshly prepared 80% ethanol. After the third wash, the beads were left to dry at room temperature until the remaining ethanol had evaporated. To elute the DNA, the samples were removed from the magnetic rack, and the beads were resuspended in 50 µL 10 mM Tris-HCl or molecular-grade water. After incubating at room temperature for five minutes, the samples were returned to the magnetic rack until the supernatant was clear. The supernatant was then collected and stored at – 20 °C for further use.

2.4.3.2 High molecular weight DNA extraction

For the extraction of high molecular weight (HMW) DNA, DNA was extracted from 100 – 500 µL of overnight bacterial cultures using the Zymo Quick-DNA HMW MagBead Kit (D6060, Zymo Research) following the manufacturer's instructions, replacing 100 mg/mL lysozyme with 5 mg/mL lysozyme for the microbial lysis step.

2.4.3.3 DNA quantification

To quantify the DNA extracted, the Qubit dsDNA High Sensitivity (Q32854, ThermoFisher Scientific) or Broad Range (Q32853, ThermoFisher Scientific) kits were used, following the manufacturer's instructions.

2.4.4 DNA sequencing

2.4.4.1 Illumina NextSeq short-read sequencing

DNA was normalised to 5 ng/µL using 10 mM Tris-HCl, and short-read whole genome sequencing (WGS) was performed using the Illumina Nextseq 500 or Nextseq 2000 by the Quadram Institute sequencing team following the flex library protocols described in **APPENDIX III**.

2.4.4.2 Oxford Nanopore Technology long-read sequencing

Long-read DNA sequencing was performed using R9 or R10 flow cells in an Oxford Nanopore Technology (ONT) minION or promethION sequencer by the

Quadram Institute sequencing team following the protocol described in **APPENDIX IV**.

2.4.5 Isolation of large (> 20 kilobase pairs (kbp)) plasmids

Overnight cultures of strains carrying the relevant plasmids were supplemented with appropriate antibiotics to ensure plasmid carriage. The ZymoPURE II Plasmid Midiprep Kit (D4201, Zymo Research) was used to isolate plasmid DNA from 50 mL of overnight culture following steps one to six, then the centrifugation protocol as provided by the manufacturer.

To confirm that the plasmid of the correct size was isolated, a sample of the elution was visualised on the Agilent 4200 TapeStation system (G2991BA, Agilent), using the Genomic DNA ScreenTape (5067-5365, Agilent) and the corresponding reagents (5067-5366, Agilent), following the manufacturer's instructions.

2.4.6 Electrocompetent cells and transformation

To prepare electrocompetent cells, 500 µL of overnight culture was inoculated into 50 mL 2x Yeast extract tryptone medium (YT) broth. Cells were grown at 37 °C, 250 rpm until an optical density at 600 nm (OD_{600}) of 0.2 – 0.3, corresponding to mid-logarithmic growth phase. The cells were transferred to a sterile 50 mL tube and subjected to centrifugation at 4 °C, 3000 x *g* for ten minutes. The supernatant was discarded, and the pellet was washed twice, in 12.5 mL and 25 mL ice-cold sterile 10% glycerol, respectively. For the washing steps, the pellet was first resuspended in 1 mL 10% glycerol before topping up with 10% glycerol to the required volume and subjected to centrifugation following the same conditions as previously stated. After the second washing step, the pellet was resuspended in 1 mL 10% glycerol, and the suspension was transferred into a microcentrifuge tube and subjected to centrifugation for 1 minute at maximum speed. The supernatant was discarded, and the pellet was resuspended in the appropriate amount of 10% glycerol required for transformation (50 µL cells per electroporation) before aliquots of 50 µL were made in microcentrifuge tubes and stored on ice until use.

For transformation, 2 µL of DNA to be transformed was added to the 50 µL aliquot of cells, and electroporation was completed in ice-cold 2 mm electrode gap cuvettes (E6-0060, Geneflow), using the Gene Pulser Xcell electroporator (1652660, Bio-Rad) set at 2.5 kV, 200 Ω, 25 µF. After electroporation, cells were immediately recovered in 1 mL SOC outgrowth medium (B9020S, NEB), transferred to a sterile microcentrifuge tube and incubated at 37 °C, 600 rpm for one hour. After incubation, cells were subjected to centrifugation at maximum speed for one minute, and the pellet was resuspended in 100 µL supernatant before inoculating onto LB agar supplemented with the appropriate antibiotics to select for successful transformants. A negative control of cells with no transformed DNA and a positive control transformed with pUC19 (supplied with C2987I, NEB) was included for each experiment. Cells transformed with pUC19 were recovered on LB agar supplemented with 100 µg/mL carbenicillin.

2.4.7 Constructing single gene deletion mutants

To construct single gene deletion mutants, the Gene Doctoring (G-DOC) (Lee et al., 2009) method, utilising λ-Red recombination, was used.

In general, this technique requires the cloning of homologous regions upstream and downstream of the target gene that have been amplified by PCR into pDOC-K, which is then transformed via electroporation into the recipient strain carrying the pACBSCE helper plasmid. λ-Red and I-SceI expression on pACBSCE is then induced using arabinose. I-SceI cleaves pDOC-K, and the recombination of the resulting linear DNA fragment with the homologous regions on the chromosome is mediated via the λ-Red proteins, replacing the target gene with the kanamycin-resistant cassette. I-SceI also cleaves pACBSCE, leading to the loss of both plasmids from the recipient strain. Recombinants are selected for on agar supplemented with kanamycin and sucrose, as only cells that have lost the *sacB* gene, indicating loss of pDOC-K, and therefore successful recombination, are able to grow on this type of media (Lee et al., 2009) (**Figure 2.1**).

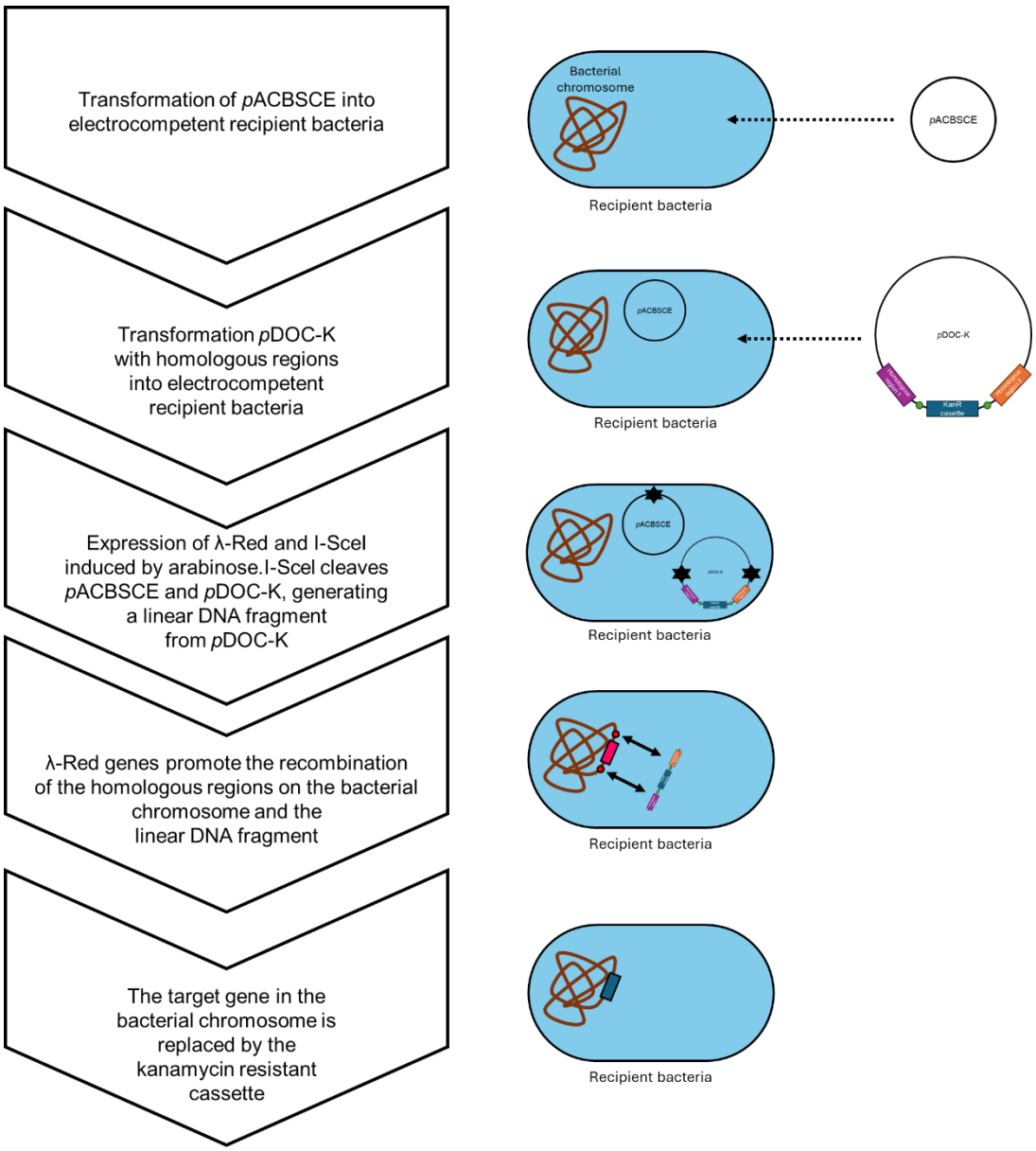

Figure 2.1 – Construction of single gene deletion mutants using the gene doctoring technique. Figure adapted from (Lee et al., 2009)

2.4.7.1 Plasmids

Overnight cultures of strains carrying pACBSCE and pDOC-K were supplemented with 30 µg/mL chloramphenicol and 50 µg/mL kanamycin, respectively, to ensure plasmid carriage. DNA was isolated using the NucleoSpin® Plasmid Mini Kit for plasmid DNA (740588.250, Macherey-Nagel) following the manufacturer's instructions and agarose gel electrophoresis (2.3.2) was used to visualise extracted DNA and confirm plasmids were successfully isolated.

2.4.7.2 Designing homologous regions

Homologous regions were designed by selecting 270 base pairs (bp) upstream and downstream of the target gene, adding an overlap of 30 bp into the target gene adjacent to the selected regions. Two endonucleases from multiple cloning sites one (for homologous region one) and two (for homologous region two), on pDOC-K, were selected, ensuring that at least six bp separated the two endonucleases on the plasmid, and their sequences were added to either end of the regions. Finally, six random bases were added to either end to give the sequences for the homologous regions (**Figure 2.2**).

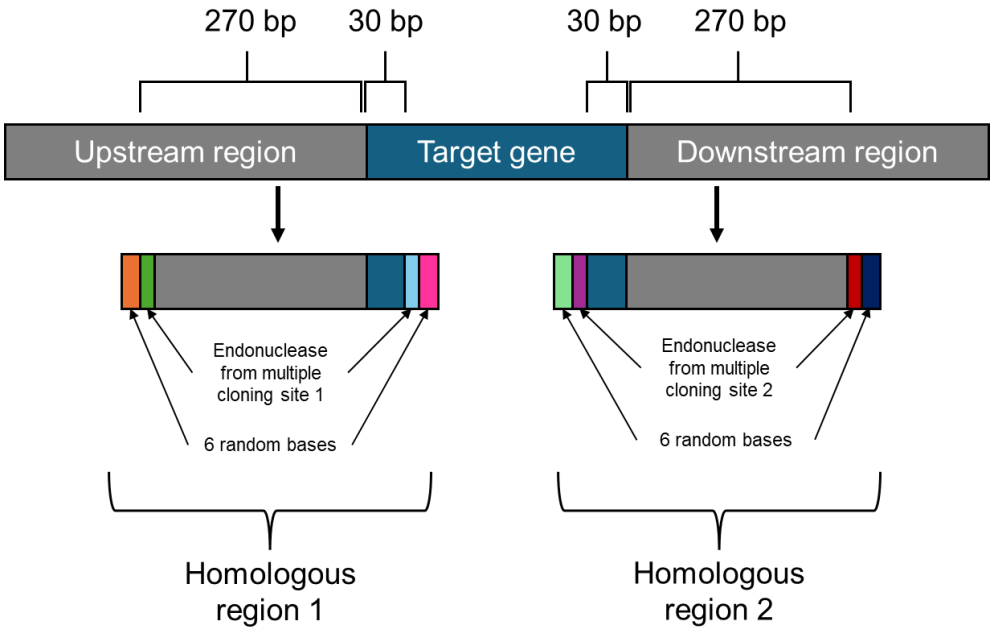

Figure 2.2 – The design of homologous regions for target genes for the construction of single gene deletion mutants.

2.4.7.3 Amplification of products to insert into pDOC-K

Homologous regions were amplified using PCR. The size of the products were confirmed via agarose gel electrophoresis. The PCR products were cleaned and purified using the NucleoSpin® Gel and PCR Clean-up Mini kit (740609.250, Macherey-Nagel), following the protocol for PCR clean-up as provided by the manufacturer. PCR products were stored at – 20 °C until further use.

2.4.7.4 Restriction digests

Restriction digests for the amplified homologous regions were performed as double digests in 50 µL reactions consisting of 5 µL rCutSmart™ Buffer (B6004S, NEB), 1 µL of each restriction enzyme (NEB), 1-2 µL DNA and molecular-grade water adjusted to maintain the final reaction volume. For pDOC-K, double digests were performed in 10 µL reactions consisting of 5 µL vector DNA, 1 µL rCutSmart™ Buffer, 1 µL of each restriction enzyme and molecular-grade water to 10 µL. Plasmid digests were incubated at 37 °C overnight, and other digests were incubated at 37 °C for one hour. Digested products were visualised via gel electrophoresis to confirm their size and cleaned using the NucleoSpin® Gel and PCR Clean-up Mini kit before ligation.

2.4.7.5 Ligations and transformation into chemically competent *E. coli*

Digested vectors and inserts were ligated in reactions consisting of 0.5 – 1 µL digested vector, 3 µL digested insert, 1 µL T4 DNA ligase (M0202S, NEB), 1 µL T4 DNA ligase reaction buffer (B0202S, NEB) and molecular-grade water to a final reaction volume of 10 µL. Ligations were incubated at 16 °C overnight.

Ligated plasmids were transformed via heat-shock into chemically competent NEB® 5-alpha Competent *E. coli* (High Efficiency) cells (C2987I, NEB). 10 µL ligation was mixed with 50 µL *E. coli* cells, then left on ice for ten minutes before transferring to a heat block at 42 °C for two minutes, then back onto ice for a further two minutes. To recover the cells, 1 mL SOC outgrowth medium

(B9020S, NEB) or LB broth was added to the reaction and incubated for two hours at 37 °C. After incubation, cells were subjected to centrifugation at maximum speed, then the pellet was resuspended in 100 µL supernatant before inoculating onto LB agar plates supplemented with appropriate antibiotics for selection. A negative control of the digested vector with no insert was included in every experiment.

2.4.8 Reverse Transcription -qPCR

The expression of genes of interest under certain conditions was determined using Reverse transcription (RT)-qPCR.

2.4.8.1 Primer design

Primers for RT-qPCR were designed using Primer 3 (version 4.1.0) (Kõressaar et al., 2018, Koressaar and Remm, 2007, Untergasser et al., 2012), and parameters were set to those described in **Table 2.3**, with all other settings left as default.

Table 2.3 – Parameters used in Primer 3 (version 4.1.0)

Parameter	Minimum	Optimum	Maximum
Primer size (bp)	58	60	62
Primer Tm (°C)	50	60	65
Primer GC content (%)	50	55	60
Product size range (bp)	700-200		

Primer pairs returned by the software were checked for self-dimers and heterodimers using the Integrated DNA Technologies OligoAnalyzer™ Tool (IDT, 2025) and the primer pair with the lowest self-dimer and heterodimer risk (highest ΔG value above -6) was selected.

2.4.8.2 Primer validation

To validate the primers against target genes of interest, the Luna® Universal One-Step RT-qPCR Kit (E3005S, NEB) was used. The reaction master mixes were set up following the relative volumes of each component as suggested by the manufacturer, adjusting them for 10 µL (half) reactions, and the Luna® WarmStart® RT Enzyme Mix was replaced with molecular-grade water. DNA was diluted to 1 ng/µL and then serially diluted 1:2 to 0.03 ng/µL using molecular-grade water. In a 96-well plate, 8 µL master mix and 2 µL DNA were added to the appropriate wells (**Figure 2.3**); DNA was replaced with molecular-grade water for the no DNA control. The plate was sealed, and reactions were ran in an Applied Biosystem 7500 RT-qPCR machine (4351105, ThermoFisher Scientific), following the programme detailed in **Table 2.4**.

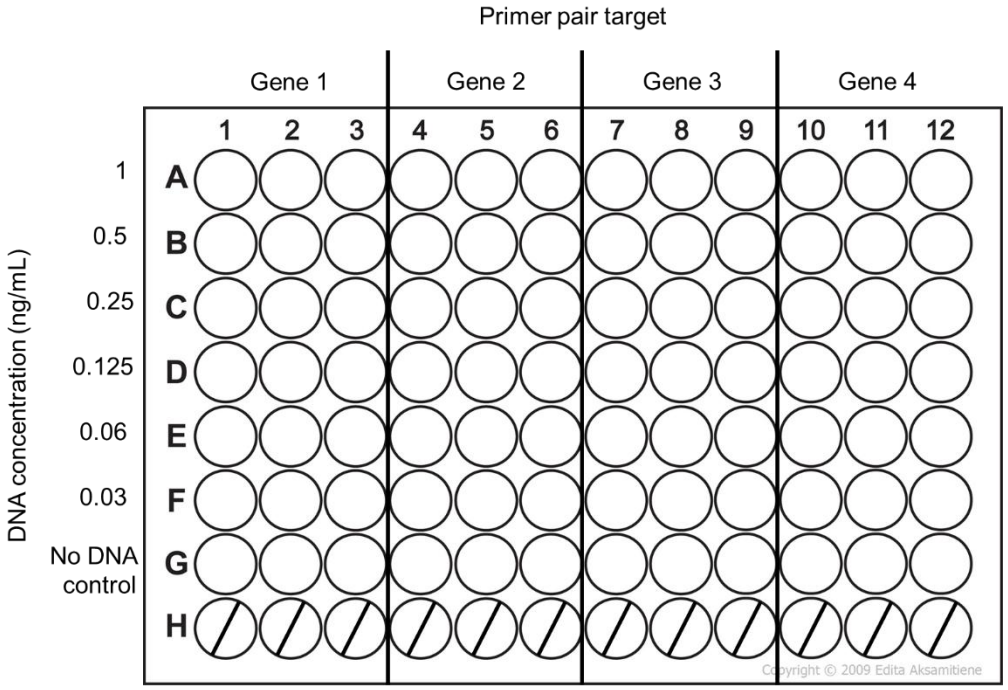

Figure 2.3 – 96-well plate set up for RT-qPCR primer validation

Table 2.4 - RT-qPCR programme

Stage	**1**	**2**	**3 – cycles (~ 40 - 45)**		**4**
Step	Reverse Transcription	Initial denature	Denature	Extension	Melt curve
Temp	55 °C	55 °C	95 °C	60 °C	60 – 95 °C**
Time	10 minutes	1 minute	10 seconds	60 seconds*	Various**

* For the Applied Biosystem RT-qPCR machine

** Following the settings given by the machine

2.5 PLASMIDS

Table 2.5 – List of plasmids used in this study

Plasmid	**Source**
pHYCTX14	(Bevan et al., 2021)
pUC19	Supplied with C2987I, NEB
pACBSCE	(Lee et al., 2009)
pDOC-K	(Lee et al., 2009)

2.6 PRIMERS

Primers were designed in SnapGene (Snapgene, 2025) and synthesised by Merck.

Table 2.6 – List of primers arising from this study

Name		Primer sequence	Role
invA	fwd	TCATTGACGTTGCGCGCCAGC	Amplification of *invA* in *S.* Typhimurium
	rev	GGGAACTCTGCCGGGATTCCC	
lacY	fwd	CAGCACCAGATAAGCGCCCTGG	Amplification of *lacY* in *E. coli*
	rev	GCTGTGCACTCATCCTCGCCG	
bla$_{\text{CTX-M-14}}$	fwd	CTTTATGCGCAGACGAGTGCGGTG	Amplification of *bla*$_{\text{CTX-M-14}}$ in pHYCTX14
	rev	GCTGCCGGTCTTATCACCCACAG	
pHYCTX14 ctrl	fwd	TGTTCAAGTTTGATTCCTTGGGCTCTTCAGAATAC	Amplification of pHYCTX14 backbone
	rev	AGCGGTGTGGTGTTACTCGGT	
pHYCTX14 + *bla*$_{\text{CTX-M-14}}$	fwd	ACACACGTGGAATTTAGGGAATACTGATGTAACACGGATTGACCGTATTGGGAGTTTGAGATGGTGACAA	Amplification of *bla*$_{\text{CTX-M-14}}$ and part of the pHYCTX14 backbone on either side of *bla*$_{\text{CTX-M-14}}$
	rev	GGAAGATACGTGATCTGATCCTTCAACTCAGCAAAAGTTCGATTTATTCAACAAAACCAGTTACAGCCCT	

Table 2.6 cont.

acrB homologous region 1	fwd	GACTTAAAGCTTCGCCGCGTGGC	Amplification of homologous regions adjacent to *acrB* in *E. coli* for insertion into pDOC-K to create the Δ*acrB* deletion mutant
	rev	TTAAGCCCTAGGAATCGGGCGATCG	
acrB homologous region 2	fwd	TACGGCCTCGAGGAGCACAGC	
	rev	CCGTACGCTAGCGGATTGCTCTGAA	
tolC homologous region 1	fwd	TCTAAGGAATTCTTCTCGTGCAATAATTTCTACATCGTTTTTGCCA	Amplification of homologous regions adjacent to *tolC* in *E. coli* for insertion into pDOC-K to create the Δ*tolC* deletion mutant
	rev	TACCGGCCTAGGGCCGATAAGAATGG	
tolC homologous region 2	fwd	TATTGCCTCGAGAGTAACGGTCATAACCCTTTCC	
	rev	GTCGCAGCTAGCATCACTCTTTTCACAGC	
galU homologous region 1	fwd	AGTCCGGAATTCTGCGATGCCTGG	Amplification of homologous regions adjacent to *galU* in *E. coli* for insertion into pDOC-K to create the Δ*galU* deletion mutant
	rev	GCTAGACCTAGGTTTTTTGACTTTCGTATTAATGGCAGCC	
galU homologous region 2	fwd	GTCATTCTCGAGCTTGAAGAAGAGATGGGCATTAAGA	
	rev	GGATCGGCTAGCATATAGCTACGTTGACGAAAAC	

Table 2.6 cont.

hldD homologous region 1	fwd	AGTCCGGAATTCTTCCGCACGAGC	Amplification of homologous regions adjacent to *hldD* in *E. coli* for insertion into pDOC-K to create the Δ*hldD* deletion mutant
	rev	GCTAGACCTAGGAAAGCCCGCGC	
hldD homologous region 2	fwd	GCATTACTCGAGTCGAGCGGTATCAAGGC	
	rev	ATTAGCGCTAGCAGCGCCCCG	
rapA homologous region 1	fwd	GTCATTGAATTCCGAACACTATCTGACCCGCC	Amplification of homologous regions adjacent to *rapA* in *E. coli* for insertion into pDOC-K to create the Δ*rapA* deletion mutant
	rev	GCTAGACCTAGGGATCCAGCGTTGACCA	
rapA homologous region 2	fwd	GTCATTCTCGAGCTGCGTTTGATCGTTGTAACG	
	rev	GCTAGAGCTAGCACTGGCGTTTTAACTCCC	
waaB homologous region 1	fwd	GCGTAAGAATTCAACAAAAAAACTTGCCCAACACAATTATAATGCA	Amplification of homologous regions adjacent to *waaB* in *E. coli* for insertion into pDOC-K to create the Δ*waaB* deletion mutant
	rev	AGCATACCTAGGAACAGCTTCGCCAATAAAGG	
waaB homologous region 2	fwd	CATTGCCTCGAGATTATTTCTGTTATTTCCCGGAGGAAATAATG	
	rev	CTGCAAGCTAGCAATATATCTTAATTCTTGTTTTATATTGCCTGGCCA	

Table 2.6 cont.

waaC homologous region 1	fwd	CCGTAAGAATTCGCCTGTAAAGCCATTGTCACT	Amplification of homologous regions adjacent to *waaC* in *E. coli* for insertion into pDOC-K to create the Δ*waaC* deletion mutant
	rev	GGCTCACCTAGGCGACGATGTTTTAACG	
waaC homologous region 2	fwd	CCGCACCTCGAGGAAACGGTATTTAATAAAATCAATTCCT	
	rev	ATTGTCGCTAGCGTGATAGTGCCAGGA	
waaJ homologous region 1	fwd	CCGTAAGAATTCGACTCTACTTGAAGCCTTGTCGT	Amplification of homologous regions adjacent to *waaJ* in *E. coli* for insertion into pDOC-K to create the Δ*waaJ* deletion mutant
	rev	CATACGCCTAGGCTCAGTCTCCTGGAAAAAAAC	
waaJ homologous region 2	fwd	GGCAGGCTCGAGTTGTATTTTATAAAAAAGCTAAAGCATTAATACT	
	rev	ATTGCAGCTAGCGAATCGACACCATAGG	
bla$_{\text{CTX-M-14}}$ (RT-qPCR)	fwd	TCAGCCTGTCGAGATCAAGC	Amplification of *bla*$_{\text{CTX-M-14}}$ in pHYCTX14 to measure gene expression using RT-qPCR
	rev	TCAGTTCTGCCAGCGTCATT	
traM (RT-qPCR)	fwd	AGTCTCTCAGTCCTCATGTCTC	Amplification of *traM* in pHYCTX14 to measure gene expression using RT-qPCR
	rev	ACCTTTCCATCTCAGCCGAC	

Table 2.6 cont.

gyrB (RT-qPCR)	fwd	GGACCCGAAATTCTCCTCCC	Amplification of *gyrB* in *E. coli* to measure gene expression using RT-qPCR
	rev	TGCCAGCAGTTCGTTCATCT	

2.7 ANTIMICROBIAL SUSCEPTIBILITY TESTING

Antimicrobial susceptibility testing was used to determine the minimum inhibitory concentration (MIC) of various antimicrobials against bacterial strains. The MIC of a drug is defined as the lowest concentration required to inhibit visible growth of a microorganism *in vitro* (Kadeřábková et al., 2024). Unless otherwise stated, MIC was determined using the microbroth or agar dilution methods, with Mueller Hinton (MH) broth or agar, as indicated by the European Committee for Antimicrobial Susceptibility Testing (EUCAST) guidelines (EUCAST, 2022).

2.7.1 Microbroth dilution method

Overnight cultures of the relevant strains and stock solutions of required antimicrobials, at double the maximum concentration required for the assay, were prepared. In a 96-well plate, 100 µL broth was added to columns two to 12, before adding 100 µL antimicrobial stock solution to columns one and two, then serially diluted 1:2 from columns two to 11. Drug was omitted from the final column. Overnight cultures (~ 10^9 cells) were first diluted 1:100, then diluted a further 1:20 in LB broth, and 100 µL was added to all appropriate wells in the plate. The plate was sealed using a gas-permeable membrane and incubated at 37 °C. After 18 - 24 hours, the plate was removed and visually observed for bacterial growth. The minimum concentration of antimicrobial where no bacterial growth was observed was recorded as the MIC. Three biological replicates were performed for each bacterial isolate, and a drug-sensitive control strain was included for each antimicrobial tested.

2.7.2 Agar dilution method

The agar dilution method was also used to determine the MIC of antimicrobials against bacterial strains.

Overnight cultures were diluted 1:10,000 before 5 µL spots were inoculated onto agar plates supplemented with antimicrobials at doubling dilutions using a 96-well pin replicator. Plates were incubated at 37 °C for 18 – 24 hours, then observed for colonies. The lowest concentration of antimicrobial that inhibited

bacterial growth was recorded as the MIC. Start and stop plates with no drug were included as controls, and two biological replicates were performed for each isolate. A drug-sensitive control strain was also included for each antimicrobial tested.

2.8 MUTANT SELECTION

To select for antibiotic-resistant mutants, 10 mL overnight cultures were prepared, then subjected to centrifugation at 2000 x *g* at 20 °C for ten minutes. After discarding the supernatant, the pellets were resuspended in 1 mL MH broth before inoculating 100 µL into an even lawn onto MH agar plates supplemented with appropriate antibiotics at a range of concentrations. After incubating overnight, colonies were recovered from the plates, grown in broth supplemented with relevant antibiotics and stored for further analyses to confirm the phenotype and genotype of the selected colonies, via antimicrobial susceptibility testing and sequencing, respectively.

2.9 TESTING PLASMID STABILITY

The stability of pHYCTX14 within bacterial strains was tested, as plasmid persistence was required in the absence of selective pressure.

Overnight cultures of bacterial strains carrying the plasmid were prepared. Each day, 5 µL of culture was passaged into 5 mL fresh broth and incubated at 37 °C overnight. After seven days, a small sample of culture was streaked onto agar supplemented with 8 µg/mL cefotaxime for plasmid selection to confirm whether the plasmid remained within the bacterial population. Furthermore, cells were diluted 1:10,000,000 and 40 µL was inoculated into an even lawn onto agar plates with and without cefotaxime. After incubation, the CFU was calculated to give an indicator of the proportion of cells that kept or lost the plasmid after seven days.

2.10 GROWTH CURVES

The differences between the growth rates of bacteria under different conditions were measured over 18 hours.

Stock solutions of the chemicals to be used were prepared in LB without (w/o) NaCl broth. Chemicals were added to a 96-well plate and diluted to double the required concentration using LB w/o NaCl to a final volume of 100 µL in each well. Overnight cultures were diluted 1:10,000 in LB w/o NaCl broth, and 100 µL was added to the wells. Using the BioTek LogPhase 600 Microbiology Reader (Agilent), absorbance in each well at 600 nm was measured every 20 minutes for 18 hours. Four biological replicates were performed for each concentration of chemical tested alongside a bacterial control with no additional chemicals. A broth control to test for sterility was also included in each 96-well plate.

2.11 BIOFILM ASSAYS

2.11.1 Biofilm competition assay

To obtain an indication of how well various *E. coli* isolates and *S.* Typhimurium 14028S could co-exist together within a biofilm, the two species were grown in competition with each other using an adapted version of the biofilm evolution model developed previously (Trampari et al., 2021).

Overnight cultures of the two species of bacteria were prepared, and 50 µL of both species was inoculated into 5 mL LB broth w/o NaCl in glass universal tubes. A sterile 5 mm glass bead (18406, Sigma) or 6 mm stainless steel bead (6 mm, AISI 316, Simply Bearings Ltd) was added to the universals using sterile tweezers to be used as the substrate for biofilm formation, and the cultures were incubated horizontally at 37 °C, 100 rpm, for approximately 48 hours to encourage biofilm formation. After 48 hours, beads were removed from the universals using sterile tweezers, washed in 10 mL PBS to remove planktonic cells and placed into microcentrifuge tubes containing 1 mL PBS. Each bead was then vortexed vigorously for 30 seconds to displace biofilm cells into the PBS. Cells were then diluted 1:10,000, and 100 µL was

inoculated into an even lawn onto LB agar plates supplemented with X-Gal and IPTG to differentiate the two species via blue/white screening. After incubating the plates at 37 °C overnight, the number of blue (*E. coli*) and white (*S.* Typhimurium) colonies were recorded, and the CFU of each strain at the end of the experiment was used to indicate how well they could co-exist together in a biofilm. Four biological replicates were carried out per pair of bacterial isolates, and monospecies biofilm controls for both species were also included.

2.11.2 Biofilm productivity assay

A biofilm productivity assay was used to determine whether plasmid carriage and/or selection for specific single nucleotide polymorphisms (SNPs), conferring resistance to antibiotics, affected biofilm formation in *S.* Typhimurium 14028S or the *E. coli* food isolates.

Adapting the previous protocol (2.9.1), monospecies biofilms were grown in 5 mL LB w/o NaCl broth and ten sterile steel beads were used as the substrate for biofilm formation. The biofilm cells were recovered in 3 mL PBS and diluted before plating onto LB agar plates. After incubation, the number of colonies on the plates were recorded to calculate the CFU. Three biological replicates were carried out for each strain, and the relevant wild-type strains were also included as controls.

2.12 CONJUGATION ASSAYS

2.12.1 Conjugation on filter discs

Conjugation assays on filter discs were used to transfer pHYCTX14 into strains of interest (**Figure 2.4**).

Overnight cultures of the donor and recipient strain were prepared, and 1 mL was subjected to centrifugation for three minutes at 13,000 x *g*. The pellets were resuspended in 50 µL LB broth after removing the supernatant. A nylon membrane filter disc, 0.45 µM/25 mm (Z290815, Sigma), was sterilised in the Stratagene UV Stratalinker® 1800 at 1200µ joules x 100 and placed onto an

LB agar plate. After mixing, the donor/ recipient suspension was pipetted onto the filter, then incubated at 37 °C for three hours. A filter control (filter on LB agar with no bacteria added) was also included. After incubation, the filter was transferred into 1 mL LB broth and vortexed vigorously to recover the cells. To select for transconjugants, 100 µL of cells were inoculated into an even lawn onto LB agar supplemented with antibiotic to select for the recipient strain, as well as 8 µg/mL cefotaxime to select for the plasmid. For the controls, cells were diluted 1:10,000 and 100 µL was inoculated onto LB agar and LB agar supplemented with antibiotics to select for the donor and the recipient strain, respectively. The donor and recipient strains were also inoculated onto LB and various selective media as controls. Colonies yielded on LB agar supplemented with antibiotics to select for transconjugants were randomly selected for PCR to confirm that they were the expected species and carried the plasmid. Confirmed transconjugants were stored for further use.

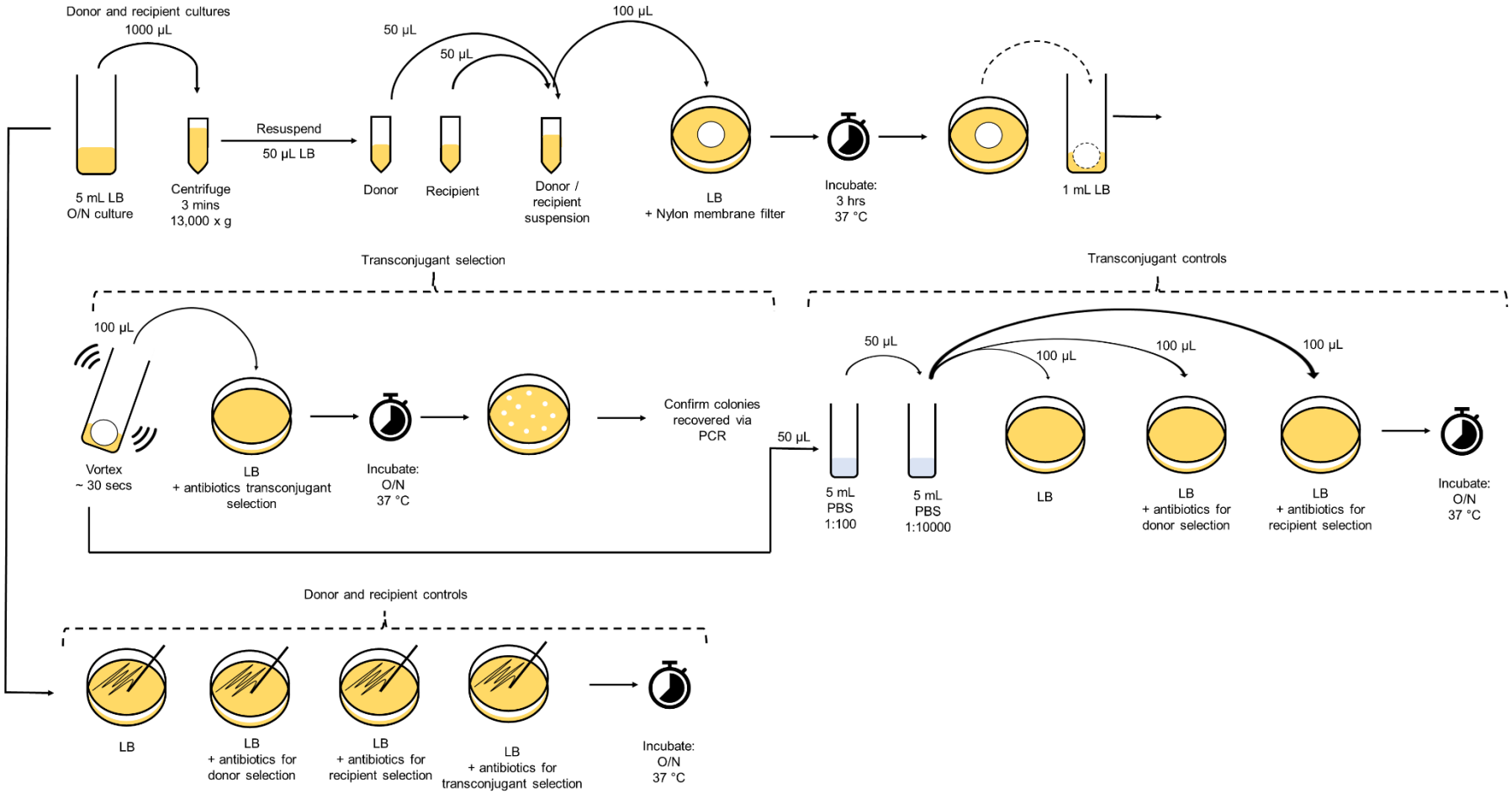

Figure 2.4 – Conjugation assays on filter discs

2.12.2 Conjugation in a multispecies biofilm model

The model used for the biofilm competition assays (2.9.1) was adapted to conjugate plasmids between two species within a biofilm context (**Figure 2.5**).

The model was set up with the donor and recipient strain as previously described, with ten steel beads as substrate for biofilm formation. Where a stressor was added to the model to investigate its impact on conjugation efficiency, a stock solution of the chemical was prepared as detailed previously (2.10), and the desired amount was added to the universal before incubation. After incubating, biofilm cells were recovered in 3 mL LB w/o NaCl and incubated at 4 °C for 120 minutes to resuscitate cells and restore cefotaxime resistance phenotype. For transconjugant selection, 100 µL of biofilm cells recovered were inoculated into an even lawn onto LB agar supplemented with antibiotics to select for the recipient strain, as well as 2 µg/mL cefotaxime to select for the plasmid. For the controls, the cells were serially diluted 1:10,000, and 5 µL of each dilution was spotted onto LB agar, LB supplemented with antibiotics to select for the donor and the recipient strain, respectively, and LB supplemented with X-Gal and IPTG. A time-zero measurement was also taken at the beginning of the experiment to determine whether even numbers of donor and recipient cells were initially inoculated into the model. A 50 µL sample from universal tubes inoculated with both the donor and recipient strains was taken and diluted 1:10,000 before 50 µL was inoculated into an even lawn on LB agar, supplemented with X-Gal and IPTG for blue/white screening.

Four biological replicates were carried out per pair of bacterial isolates, and two monospecies biofilm controls for both species were also included. The monospecies controls were grown under no stress and recovered using the same method as the multispecies biofilms. Cells were serially diluted 1:10,000, and 5 µL of each dilution was spotted onto LB and the various selective media as controls. Colonies yielded on LB agar supplemented with antibiotics to select transconjugants were randomly selected for PCR to confirm that they were the expected species and carried the plasmid. Colonies were also

inoculated onto XLD and Brilliance *Salmonella* agar to check for the expected phenotype.

The number of colonies recovered on the plates were recorded to calculate CFU, which was then used to calculate conjugation efficiency using the following formulas:

To calculate the ratio of donor cells per recipient cell available at time zero:

$$Ratio\ of\ donor\ cells\ per\ recipient\ cell = \frac{\left(\frac{Donor\ CFU\ at\ time\ zero}{Recipient\ CFU\ at\ time\ zero}\right)}{1}$$

To calculate the normalised transconjugant CFU:

$$Normalised\ transconjugant\ CFU = \left(\frac{1}{Ratio\ of\ donor\ cells\ per\ recipient\ cell}\right) \text{x}\ transconjugant\ CFU$$

To calculate the normalised conjugation efficiency:

$$Normalised\ conjugation\ efficiency = \frac{Normalised\ transonjugant\ CFU}{Recipient\ and\ transconjugant\ CFU}$$

.

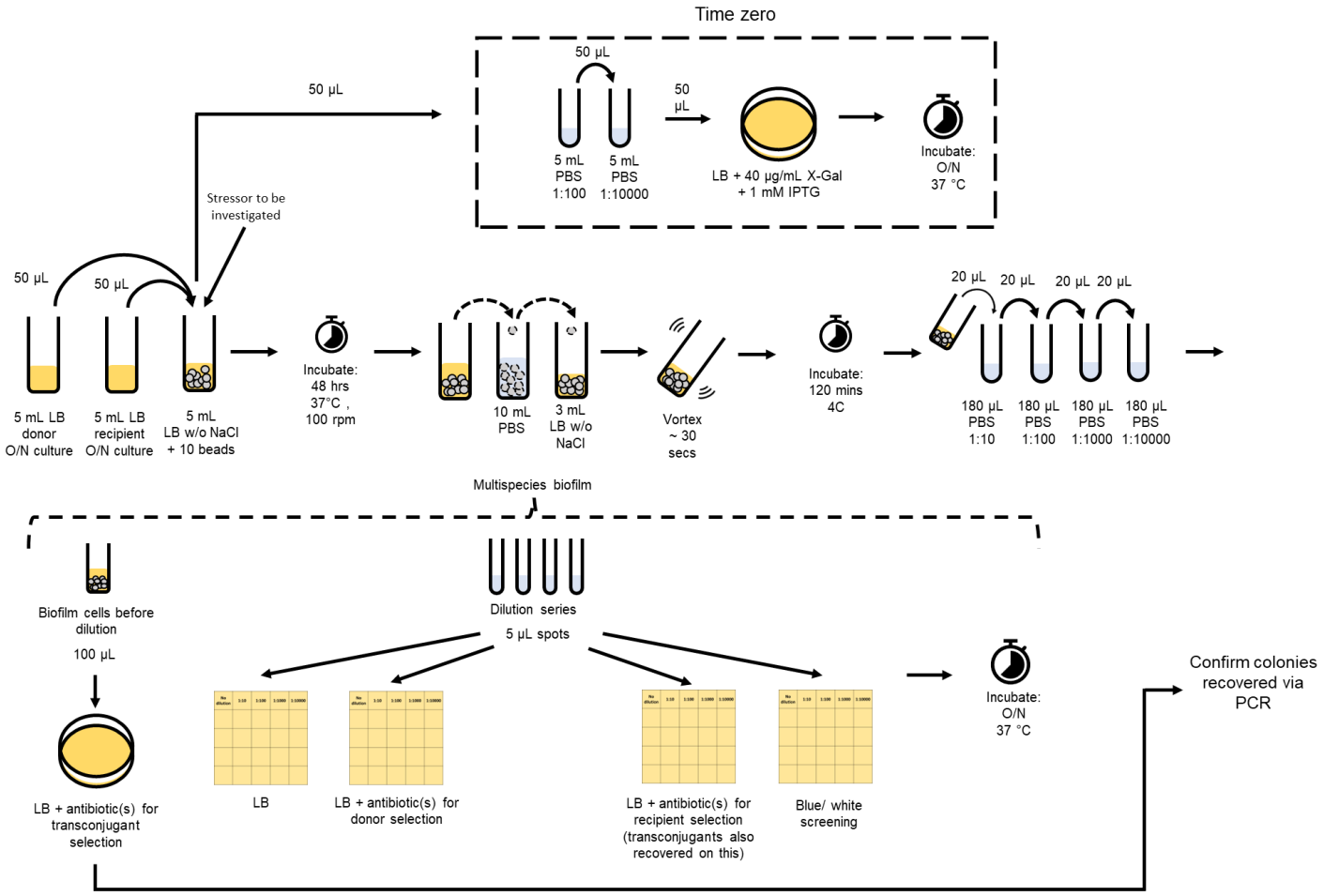

Figure 2.5 – The multispecies biofilm conjugation model

2.13 TRADIS

To investigate important genes for plasmid acceptance in *E. coli* and *Salmonella* using Transposon Directed Insertion-site sequencing with expression (TraDIS-*X*press), pHYCTX14 was conjugated into an *E. coli* BW25113 transposon mutant library (Yasir et al., 2020) and an *S.* Typhimurium transposon mutant library (Holden et al., 2022).

2.13.1 Conjugating pHYCTX14 into transposon mutant libraries

A 15 mL overnight culture of the donor strain was prepared. For the mutant library (the recipient), a 15 µL aliquot (approximately 10^7 mutants) of glycerol stock was inoculated into 15 mL LB broth and incubated for one hour at 37 °C. Both cultures were subjected to centrifugation in 1 mL aliquots at 13,000 x *g* in sterile microcentrifuge tubes, and pellets were resuspended in 50 µL LB broth after discarding the supernatant. The aliquots of donor and recipient strains were mixed and pipetted onto sterile nylon membrane filters. After incubation, the cells on the filters were recovered in LB broth. Filters were split into sets of three, and each set was placed into 3 mL broth. The cells recovered from the filters were inoculated onto bioassay plates (CLS431111, Sigma) supplemented with 50 µg/mL kanamycin and 8 µg/mL cefotaxime, and incubated overnight at 37 °C. The following day, colonies from the plates were directly resuspended in LB broth. An appropriate volume of 100% glycerol was added to give a final concentration of 20 – 25% glycerol, and 1 mL aliquots were made in cryovials for storage at -80 °C for *E. coli*, and -20 °C for *S.* Typhimurium.

2.13.2 Exposure of transposon mutant libraries to cefotaxime

As a control, the mutant libraries were exposed to cefotaxime to identify the baseline of genes that were important for survival to the antibiotic rather than for acceptance of the plasmid.

The protocol detailed above was followed, with the absence of the donor strain, and cells were recovered on bioassay plates supplemented with 50 µg/mL kanamycin and cefotaxime at a range of concentrations up to 8 µg/mL.

2.13.3 Genomic DNA extraction for library preparation and sequencing

The Zymo Quick DNA miniprep kit (D3024, Zymo Research) was used to extract DNA from the mutant libraries. The bacterial sample for DNA extraction was prepared by adding 170 µL DNA elution buffer (included in the kit) to 30 µL glycerol stock, and then the protocol for biological fluids and cells was followed according to the manufacturer's instructions.

The DNA was quantified using Qubit and normalised to 12 ng/µL using molecular-grade water for library preparation and sequencing following the protocol detailed in (Holden et al., 2022).

2.13.4 Data analysis

FastQ files generated from sequencing were aligned to reference genomes and analysed using QuaTraDIS (version 1.3.3), using BWA (version 0.719 - r1273). QuaTraDIS was built on previous TraDIS analysis tools, BioTraDIS (Barquist et al., 2016) and AlbaTraDIS (Page et al., 2019). Sequences arising from the *E. coli* BW25113 mutant library were aligned to CP009273 (Grenier et al., 2014), and *S.* Typhimurium sequences were aligned to CP001363 for *S.* Typhimurium ATCC 14028S (Jarvik et al., 2010).

QuaTraDIS was used to align the sequencing reads that contained the transposon tag sequence to the corresponding reference genome to create plot files. The mapping quality cutoff score (m) was set to zero, and all other parameters were left as default. Plot files created were further analysed in QuaTraDIS using the comparison pipeline to determine significant differences between insertion frequencies between the control and test conditions for each gene. Genes with a *q*-value (*p*-value corrected for false discovery rate) < 0.01 were recorded as being significantly different between the control and test conditions. The plot files were visualised in Artemis (version 18.2.0) (Carver et

al., 2012) to analyse the differences in transposon insertion frequencies manually, and these results were compared to those from the comparison pipeline to generate a list of genes for further experiments.

2.13.4.1 Pathway enrichment analysis

The list of genes recorded as important, or essential, for plasmid acceptance in the comparison pipeline, indicated by a *q*-value <0.01 and a negative log fold-change (logFC), were analysed using ShinyGo (version 0.82) (Ge et al., 2020), a pathway enrichment tool, to identify the main pathways the genes are involved in. For the gene list generated from the *E. coli* mutant library, the species was set to *Escherichia coli* str. K-12 substr. MG1655 (STRING. 511145.*Escherichia*) for the analysis, and for *S.* Typhimurium, the species was set to *Salmonella enterica* subsp. enterica serovar Typhimurium (STRING. 90371.*Salmonella*). All parameters in the tool were left as default.

2.14 BIOINFORMATIC METHODS

Sequencing data obtained during the project was stored on the Quadram Institute Bioscience Integrated Rapid Infectious Disease Analysis (IRIDA) platform (version 19.09.2) (Matthews et al., 2018) and Galaxy interface (version 23.0) (Afgan et al., 2018).

2.14.1 Galaxy interface

2.14.1.1 Quality control of sequencing reads

Read quality reports

Sequencing reads generated were analysed with FastQC (version 0.72+galaxy1) (Andrews., 2024) to generate read quality reports and check that sequences were of suitable quality for genome assembly.

Taxonomic profiling of reads

To ensure that the sequencing reads were not contaminated, a taxonomic profile of the reads was obtained using Kraken2 (version 2.1.1+galaxy1) (Wood and Salzberg, 2014) and Bracken (version 2.8) (Lu et al., 2017).

The fastq.gz files were processed using fastp (version 0.23.2+galaxy0) (Chen et al., 2018). Qualified quality Phred was set at 20, and all other parameters were kept as default. To assign taxonomic labels to the sequences, output files from fastp were ran in Kraken2. The confidence interval was set to 0.1, and all other parameters were left as default. Sequences were queried against the k2_nt_20230502 bacterial database.

Using the report output from Kraken, Bracken was used to estimate the abundance of the bacterial species found in the sequences. The kmer distribution was set to k2_nt_20230502, and all other settings were left as default.

2.14.1.2 Genome assemblies and annotations

Short-read genome assembly

For short-read DNA assemblies, reads generated from Illumina sequencing were assembled using Shovill (version 1.1.0+galaxy0) (Seemann, 2017).

Hybrid genome assembly

To obtain polished hybrid genome assemblies, long-read DNA sequences generated from ONT sequencing were first assembled and then polished using the short-read sequences. An overview of the workflow used is illustrated in **Figure 2.6**. All parameters for these tools were left as default unless otherwise specified.

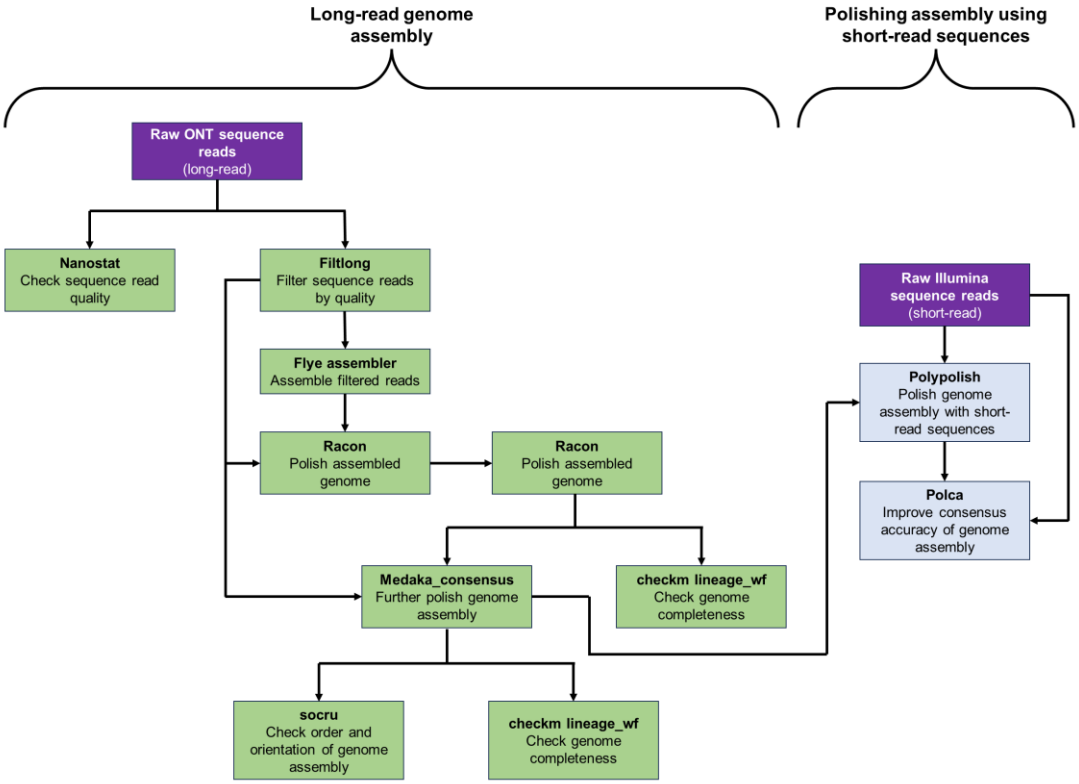

Figure 2.6 – Overview of the workflow used to assemble hybrid bacterial genomes in the Galaxy interface

Long-read genome assembly

The quality of the raw sequencing reads were checked in Nanostat (version 0.1.0) (De Coster et al., 2018) and filtered by quality using Filtlong (version 0.2.0) (Wick, 2017). The parameters used for Filtlong were:

- Input: Raw nanopore fastq file
- Output threshold:
    - Min. length = 1000
    - Min. mean quality = 50

Filtered reads were assembled using Flye assembler (version 2.5) (Lin et al., 2016, Kolmogorov et al., 2019) using the following parameters:

- Input: Filtered fastq from Filtlong
- Mode: nanopore raw
- Estimated genome size = 4.8m
- Reduced coverage for initial contig assembly: 50

The assembled genome was then polished twice using Racon (version 1.3.1.1) (Vaser et al., 2017), using the prebuilt in-house Racon_polishing_2_rounds workflow. Parameters in the workflow were set to:

- Input: filtered nanopore reads from Filtlong
- Produce an overlaps file in Map with minimap2 (version 2.12) (Li, 2018, Li and Durbin, 2009, Li and Durbin, 2010):
    - Reference: Scaffold file from Flye assembly
    - Single or paired-end reads: single
    - Fastq dataset: Raw nanopore reads
    - Output format: BAM/SAM
- Target sequence: Scaffold assembly from Flye assembler

The output polished assembly from Racon was checked for completeness using checkm lineage_wf (version 1.0.11) (Parks et al., 2015) and then further

polished using medaka_consensus (version 0.11.5) (Nanoporetech, 2018) using the parameters detailed below:

- Basecalled data: Filtered reads
- Draft assemblies: Output from Racon
- Model: r941_min_high_g303

Completeness of the polished genome was checked using checkm lineage_wf, then the order and orientation of the genome assembly was calculated using socru (version 2.2.4) (Page and Langridge, 2019).

Polishing the long-read genome assembly using short-read sequences

The assembly obtained from the previous step was polished using Polypolish (version 0.5.0) (Wick and Holt, 2022) using the following parameters:

- Assembly: FASTA output from medaka_consensus
- Input reads type or collection: paired end/paired collection
    - Forward reads (R1): forward reads from Illumina sequencing
    - Reverse reads (R2): reverse reads from Illumina sequencing

Finally, polka (version 4.0.9) (Zimin and Salzberg, 2020) was used to improve the consensus accuracy in genome assemblies. Parameters were set to:

- Long read assembly: Output from Polypolish
- Input reads type or collection: Paired end/ paired collection
    - Forward reads (R1): forward reads from Illumina sequencing
    - Reverse reads (R2): reverse reads from Illumina sequencing

Genome annotations

Assembled genomes were annotated using Bakta (version 1.6.1+galaxy0) (Schwengers et al., 2021) and the Bakta database V5.1_2024-01-19.

2.14.1.3 Multilocus sequence typing

The ST of bacterial isolates were determined using multilocus sequence typing (MLST) (Version 2.16.1) (Seemann, 2016b) using the default programme parameters. Where the tool was unable to call the full allelic profile of a genome, and therefore unable to provide the ST of an isolate, the locus combination given by the tool was manually queried against the MLST (Achtman) scheme in PubMLST (Jolley et al., 2018) to obtain the ST.

2.14.1.4 Screening of contigs for antimicrobial and virulence genes

Assembled contigs were screened for antimicrobial and virulence genes using ABRicate (version 0.9.7) (Seemann, 2016a), against the following databases: National Centre of Biotechnology Information (NCBI) AMRFinderPlus (Feldgarden et al., 2019); Comprehensive Antibiotic Resistance Database (CARD) (Jia et al., 2017); ResFinder (Zankari et al., 2012); Antibiotic Resistance Gene-ANNOTation (ARG-ANNOT) (Gupta et al., 2014); Virulence Factor Database (VFDB) (Chen et al., 2016); PlasmidFinder (Carattoli et al., 2014); EcOH (Ingle et al., 2016); and MEGARes 2.0 (Doster et al., 2019).

2.14.1.5 Calling for single nucleotide polymorphisms

Snippy

Snippy4 (version 4.4.3+galaxy2) (Seemann, 2015) was used to identify SNPs between short-read sequence data from bacterial isolates of interest and reference genomes previously published or obtained via hybrid genome assembly.

Mapping and manual confirmation of single nucleotide polymorphisms

To manually confirm SNPs, short-read sequence reads were mapped against the corresponding unannotated reference genome using Bowtie2 (version 2.3.4.3+galaxy0) (Langmead and Salzberg, 2012, Langmead et al., 2009). The BAM file obtained from mapping was read against the annotated reference genome in Artemis, and where SNP marks were observed through

all the sequencing reads, the amino acid substitution was verified via manual curation of the gene sequence.

2.14.2 IRIDA pipelines

A range of pipelines were available in the IRIDA platform for the assembly and annotation of short-read DNA sequences.

Genome assemblies using the IRIDA Assembly and Annotation pipeline (last accessed in 2022) were completed using Quast (version 5.0.2) (Gurevich et al., 2013) to check sequence read quality and Shovill (version 1.0.4) for genome assembly. MLST (version 2.16.1) was used to determine the ST of bacterial isolates, and screening of antimicrobial and virulence genes was completed using ABRicate 0.8.

2.14.3 Plasmid characterisation

2.14.3.1 Plasmid incompatibility type

To verify the incompatibility type of a plasmid, the plasmid sequence was submitted to PlasmidFinder 2.1 (Carattoli et al., 2014). Incompatibility type was predicted against the Enterobacteriales database, and parameters were left as default.

2.14.3.2 Comparison of plasmid sequences

Artemis comparison tool

Artemis comparison tool (ACT) (Carver et al., 2005) was used to compare the sequences of pHYCTX14 and other reported plasmids to identify areas of similarities and differences between the sequences.

To obtain the ACT crunch file required in ACT, a Basic Local Alignment Search Tool (BLAST) database of pHYCTX14 was made using NCBI BLAST+ makeblastdb (version 2.10.1 + galaxy0) (Altschul et al., 1997, Camacho et al., 2009, Cock et al., 2015). The crunch comparison file was then created by performing a BLASTn of the plasmid sequences of interest (the nucleotide

query sequences) against the BLAST database using NCBI BLAST+ blastn (version 2.10.1 + galaxy0). Results were visualised using ACT in Artemis.

BLAST ring image generator

BLAST ring image generator (BRIG) (Alikhan et al., 2011) was used to illustrate the similarities and differences between multiple plasmid sequences within one figure.

Manual curation of a plasmid map

To manually curate the pHYCTX14 plasmid map, the nucleotide and protein sequence of each feature on the plasmid was extracted from the plasmid sequence. The sequences were queried against the NCBI (Sayers et al., 2024) and Uniprot (Consortium, 2022) databases using BLASTn and BLASTp. The best matches from both databases were compared and analysed, and a fully annotated map of pHYCTX14 was created in SnapGene (Snapgene, 2025). The *oriT* on the plasmid was estimated using OriTfinder2 (Li et al., 2018b), with all parameters left as default.

Estimating plasmid copy number

Plasmid copy number was estimated by dividing the average read depth of the plasmid contig from chromosomal contigs.

2.15 DATA VISUALISATION AND STATISTICAL ANALYSES

Unless otherwise stated, data visualisation and statistical analyses were performed in GraphPad Prism (version 10.4.1) (Prism, 2024). Analyses performed are described in detail in the relevant chapters. Some statistical analyses were done in consultation with the Quadram Institute's in-house statistician, George Savva, and these are described in detail in **Chapter 6**.

CHAPTER 3:
SELECTING A CANDIDATE PLASMID TO BE USED IN THE MULTISPECIES BIOFILM MODEL

“Science is about exploring, and the only way to uncover the secrets of the universe is to go and look”

< Brian Edward Cox >

3.1 INTRODUCTION

MGEs are widely recognised for the role that they play in the spread of AMR via HGT in bacterial populations (Dimitriu, 2022). Many types of MGEs, including bacteriophages, transposons, insertion sequences (IS) and plasmids, contribute to the spread of AMR (Tokuda and Shintani, 2024). However, the conjugation of plasmids encoding AMR genes has been recognised as one of the major mechanisms that has led to the rapid and global dissemination of MDR bacteria (Fursova et al., 2022). Conjugative plasmids can also act as vectors for the mobilisation of non-intercellularly transferable MGEs carrying AMR genes, such as transposons (Rozwandowicz et al., 2018, Tokuda and Shintani, 2024), into bacterial cells where they can then integrate into the bacterial chromosome or other plasmids (Yao et al., 2022).

For this study, a conjugative plasmid encoding a clinically relevant AMR gene was required to monitor the movement of plasmids within a multispecies biofilm community. Therefore, the first step was to select and characterise a candidate plasmid for this project.

3.2 AIMS AND OBJECTIVES

- Screen a collection of isolates for mobilisable plasmids encoding resistance genes of interest to select a suitable candidate for this study.
- Fully characterise the candidate plasmid.

3.3 RESULTS

3.3.1 Analysis of different strains carrying clinically relevant resistance genes on mobile genetic elements

To identify potential plasmids that could be used to model the impact of different stresses on plasmid movement, a large collection of strains available within the group was initially screened (**Chapter 2**) for clinically relevant AMR genes such as *bla* genes, encoding beta-lactam resistance (Lee et al., 2015), and *ant*, *aac* or *aph* genes, encoding resistance against aminoglycosides (Kallová et al., 1997).

These isolates represented various Gram-negative species collected from past studies that were characterised for AMR. Based on previous analyses of their AMR profiles, it was considered likely that they would carry relevant resistance genes on common plasmid types.

3.3.1.1 Isolates carrying *bla*$_{\text{CTX-M}}$

A collection of 15 clinical isolates acquired as part of a study investigating the carriage of plasmids encoding *bla*$_{\text{CTX-M}}$ in faecal samples of healthy volunteers returning to the United Kingdom from South Asia was investigated (Bevan et al., 2021). These isolates were previously annotated as being *E. coli* and identified to carry variations of the *bla*$_{\text{CTX-M}}$ gene, although no sequence data was available, and it was unclear whether the genes were chromosomally integrated or carried on a plasmid.

To gain more genomic information for further characterisation, these isolates were recovered from glycerol stocks, and DNA was sequenced using ONT technology. Of the 15 isolates, six were successfully revived and sequenced. However, due to contamination introduced during the sequencing run, high-quality sequence data and long-read genome assemblies were only obtained for two isolates.

The MLST and AMR profiles of these isolates were confirmed, and the genomes were analysed in Artemis (Carver et al., 2012) to identify plasmid contigs within transfer machinery (*tra* genes). The nucleotide sequences of the contigs encoding *bla*$_{\text{CTX-M}}$ were extracted and compared to isolates in the NCBI database (Sayers et al., 2024) using BLASTn (Camacho et al., 2009) to confirm whether the sequences were similar to previously reported bacterial chromosomal or plasmid sequences, and to predict whether the AMR genes were chromosomally integrated or encoded on plasmids**.** Where relevant, contig sequences were also submitted to PlasmidFinder 2.1 (Carattoli et al., 2014) to predict the plasmid incompatibility type (**Table 3.1**).

3.3.1.2 Isolates from Nigeria

A separate collection of bacterial isolates obtained in a study investigating the prevalence of MDR in clinical Gram-negative pathogens in Nigeria (Ogbolu et al., 2011) was also analysed for genes of interest. Short-read sequence data was available for these isolates, and their genomes had also been annotated previously. However, as the genome assembly and annotation tools had received updates since the study was first conducted, the sequences of these isolates were reassembled and annotated using the pipeline available on the IRIDA platform (Matthews et al., 2018).

Several isolates in this collection were found to carry *bla*$_{NDM}$, *bla*$_{CTX-M}$, and *ant* genes that confer resistance to clinically relevant antibiotics. Analysis of the annotated genomes and results from BLASTn suggested that these genes were carried on mobile plasmids and could be valuable candidates for future experiments. As before, contig sequences were submitted to PlasmidFinder 2.1 to identify the plasmid incompatibility type (**Table 3.1**).

Table 3.1 – Bacterial isolates carrying resistance genes of interest

Name	Source	Organism	AMR gene of interest	Location of the AMR gene (Chromosome /plasmid)	Incompatibility type	Transfer machinery	Top 5 matches in BLASTn
EC-HY-3	(Bevan et al., 2021)	*E. coli*	$bla_{\text{CTX-M-14}}$	Plasmid	IncFII	*traI*, *traD*	• *Shigella sonnei* plasmid pEG430-2, strain EG0430 • *Klebsiella pneumoniae* isolate INF310-sc-2280104 genome assembly, plasmid: 5 • *Escherichia coli* isolate MINF_1A-sc-2280431 genome assembly, plasmid: 3 • *Escherichia coli* isolate MSB1_3B-sc-2280406 genome assembly, plasmid: 3 • *Escherichia coli* isolate MSB1_9I-sc-2280417 genome assembly, plasmid: 3

Table 3.1 cont.

EC-HY-4	(Bevan et al., 2021)	*E. coli*	$bla_{CTX\text{-}M\text{-}15}$	Chromosome	N/A	Tn3 family transposase Tn2	• *Escherichia coli* strain CVM N17EC1164 chromosome, complete genome • *Escherichia coli* isolate 2-101 chromosome, complete genome • *Escherichia coli* 042 chromosome, complete genome • *Escherichia coli* strain A1_181 chromosome, complete genome • *Escherichia coli* strain K71-77 chromosome, complete genome

Table 3.1 cont.

ECS6	Nigeria	*Acinetobacter*	*bla*$_{NDM-1}$	Chromosome/ plasmid	Unknown	Mob proteins & family transposase ISAba125	• *Acinetobacter baumannii* strain VB473 chromosome, complete genome • *Acinetobacter schindleri* strain HZE23-1 plasmid pHZE23-1-1, complete sequence • *Acinetobacter defluvii* strain WCHA30 chromosome, complete genome • *Acinetobacter towneri* strain G295 plasmid pNDM-GJ02, complete sequence • *Acinetobacter baumannii* genome assembly *Acinetobacter baumannii* CHI-32, plasmid: pNDM-32

Table 3.1 cont.

ECS6	Nigeria	*Klebsiella*	*bla*$_{CTX-M-15}$	Plasmid	Unknown	Tn3 family transposase Tn2	• *Klebsiella quasipneumoniae* strain dm978b plasmid p_dm978b_NDM1, complete sequence • *Klebsiella pneumoniae* strain dm883b plasmid p_dm883b_NDM1, complete sequence • *Klebsiella pneumoniae* strain dm803b plasmid p_dm803b_NDM5, complete sequence • *Klebsiella pneumoniae* strain dm749b plasmid p_dm749b_NDM5, complete sequence • *Escherichia coli* strain dm655 plasmid p_dm655_NDM5, complete sequence

Table 3.1 cont.

ECS7	Nigeria	*E. coli*	$bla_{CTX\text{-}M\text{-}15}$	Plasmid	Unknown	IS1380 family transposase ISEcp1, Tn3 family transposase Tn2	• *Escherichia coli* plasmid p2, complete sequence • *Escherichia coli* plasmid p1, complete sequence • *Klebsiella pneumoniae* isolate Kpn2166 genome assembly, plasmid: pCTX-M15_Kpn2166 • *Escherichia coli strain* WCHEC96200 plasmid pCTXM15_000200, complete sequence • *Escherichia coli* strain WCHEC000837 plasmid pCTXM15_000837, complete sequence

Table 3.1 cont.

ECS14	Nigeria	*Acinetobacter*	*ant(2")-Ia*	Plasmid	Unknown	IS6 family transposase IS15DII	• *Acinetobacter baumannii* strain J9 plasmid pJ9-1, complete sequence • *Klebsiella oxytoca strain* FDAARGOS_500 plasmid unnamed1, complete sequence • *Acinetobacter baumannii* strain FDAARGOS_533 plasmid unnamed2, complete sequence • *Acinetobacter baumannii* strain A297(RUH875) plasmid pA297-1 (pRAY*), complete sequence • *Acinetobacter baumannii* strain Nord4-2 plasmid pR32_3, complete sequence

Table 3.1 cont.

PID_0159_DO9	Nigeria	*Acinetobacter*	*ant(2")-Ia*	Plasmid	Unknown	None observed	• *Acinetobacter baumannii* strain Nord4-2 plasmid pR32_3, complete sequence • Uncultured prokaryote from Rat gut metagenome metamobilome, plasmid pRGRH0627 • *Acinetobacter baumannii* strain ACN21 plasmid unnamed6, complete sequence • *Acinetobacter baumannii* LAC-4 plasmid pABLAC2, complete sequence • *Acinetobacter baumannii* strain MC23 plasmid pMC23.3, complete sequence

3.3.2 Selecting and characterising a candidate plasmid

Information on the location and mobility of relevant AMR genes encoded by the isolates collected during previous studies was collated (**Table 3.1**) and evaluated to select a suitable candidate to be used in a multispecies biofilm model.

Given that this study planned to focus on Gram-negative bacterial species, the increasing clinical prevalence of beta-lactamase-producing Gram-negative bacteria harbouring genes such as *bla*$_{\text{CTX-M,}}$ *bla*$_{\text{TEM}}$ or *bla*$_{\text{SHV}}$, that encode ESBLs (El Aila et al., 2023), or *bla*$_{\text{NDM}}$, which confers resistance to carbapenems, a class of antibiotics often reserved to treat severe infections caused by ESBL-producing bacteria (Acman et al., 2022), isolates encoding these genes on MGEs were of particular interest. Therefore, those encoding *ant* genes, conferring resistance to aminoglycosides, were omitted from consideration.

Of the isolates in **Table 3.1**, four were found to encode variations of *bla*$_{\text{CTX-M,}}$ and one was found to encode *bla*$_{\text{NDM-1}}$. As initial experiments in this study aimed to measure the movement of plasmids between bacterial species in a multispecies biofilm, chromosomally integrated genes were excluded, and the plasmid encoding *bla*$_{\text{CTX-M-14}}$ in EC-HY-3 was chosen as the candidate for this study. This plasmid was selected as it encoded a clinically important resistance gene and represented a common plasmid incompatibility type harboured by *Enterobacteriaceae* (Villa et al., 2010). Additionally, in the initial analyses, *tra* genes were identified in the contig sequence, suggesting that the plasmid can be conjugated between bacterial cells.

The complete plasmid sequence was obtained from the annotated hybrid genome assembly of EC-HY-3 for further characterisation and to confirm its suitability for this project.

3.3.2.1 The chosen plasmid is unique, although related to other formerly reported plasmids

The plasmid sequence was compared to those in the NCBI database using BLASTn to identify whether it had been reported previously. It was found that the plasmid is unique, although it shared a large percentage identity (>99%) with some previously described plasmids.

Various tools were then used to compare the sequence of the candidate plasmid, referred to as pHYCTX14 in this study, to those that were closely related to assess their similarities and differences.

Artemis Comparison Tool

Using ACT (Carver et al., 2005), the relationship between pHYCTX14 and plasmid p143-3 from *S. enterica* strain 143 (Accession number: CP091565.1), the most closely related plasmid (percentage identity = 99.77% across 92% of the plasmid) in the database, was visualised (**Figure 3.1**).

As expected, comparison of the two plasmids revealed that they were largely similar (**Figure 3.1a**), with both plasmids containing a unique region not found in the other plasmid sequence. In p143-3, the unique region contained a range of hypothetical proteins (**Figure 3.1b**), and in pHYCTX14, the unique region encoded *bla*$_{\text{CTX-M-14}}$ alongside two unannotated genes (**Figure 3.1c**) (the unannotated genes were further investigated in **3.3.2.2**).

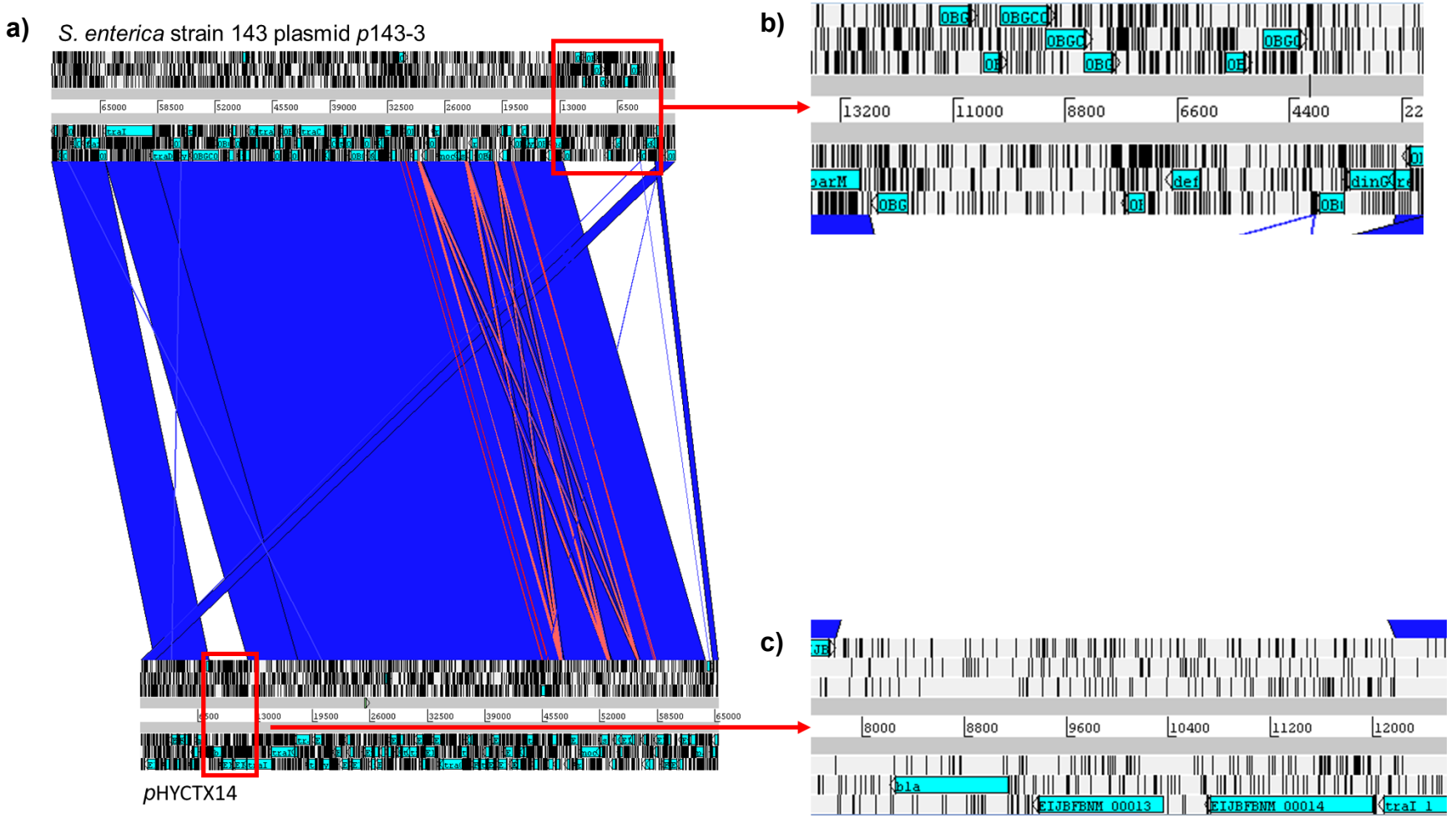

Figure 3.1 – a) Comparison of p143-3 and pHYCTX14 plasmid sequences visualised in ACT, showing **b)** the region only encoded on p143-3 and **c)** the region only encoded on pHYCTX14. Red bands represent forward matches and blue bands represent reverse matches between the two DNA sequences.

BLAST Ring Image Generator

To compare pHYCTX14 against a larger range of other similar plasmids, the differences between the sequences of the five closest matches (percentage identity >99%) from the NCBI database and pHYCTX14 were analysed and illustrated using BRIG (Alikhan et al., 2011) (**Figure 3.2**).

The image generated by BRIG confirmed that pHYCTX14 was distinct, although closely related to formerly reported plasmids. Similarly to p143-3, the major variation between pHYCTX14 and the four additional plasmids included in this analysis was the region between approximately 50000 bp and 55000 bp in pHYCTX14, where *bla*$_{\text{CTX-M-14}}$ is encoded.

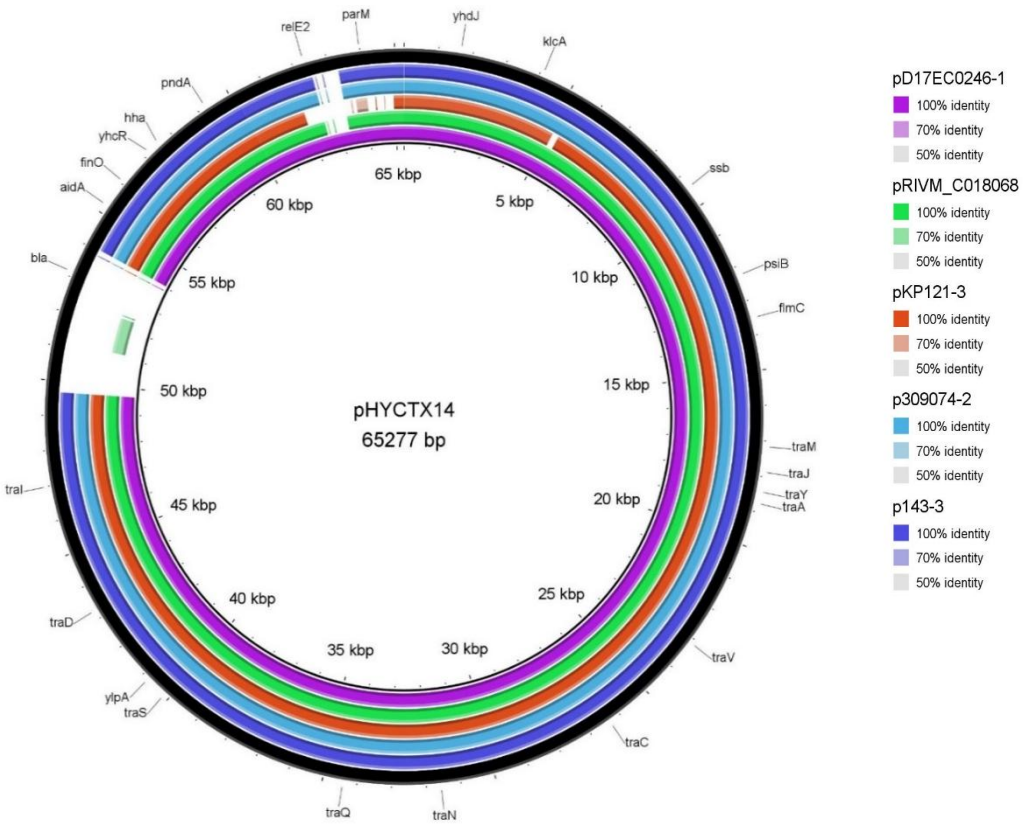

Figure 3.2 - BRIG diagram illustrating the differences between the pHYCTX14 sequence (outer black ring) and the sequences of five closely related plasmids formerly reported to the NCBI database.

3.3.2.2 Curating the pHYCTX14 plasmid map

As there was a large number of features that were unannotated in the plasmid sequence of pHYCTX14, a fully annotated map of the plasmid was manually curated to develop a better understanding of the plasmid structure.

Each coding sequence in the plasmid was extracted and compared against the NCBI and Uniprot (Consortium, 2022) databases. The best matches from these databases were compared and analysed to determine the best annotation for the selected feature. The location of the *oriT* on the plasmid was estimated using oriTfinder2 (Li et al., 2018b). The features were manually annotated using SnapGene (Snapgene, 2025) to create the plasmid map (**Figure 3.3**). A list of all the features in pHYCTX14, as well as their location and size, is given in **Table 3.2**.

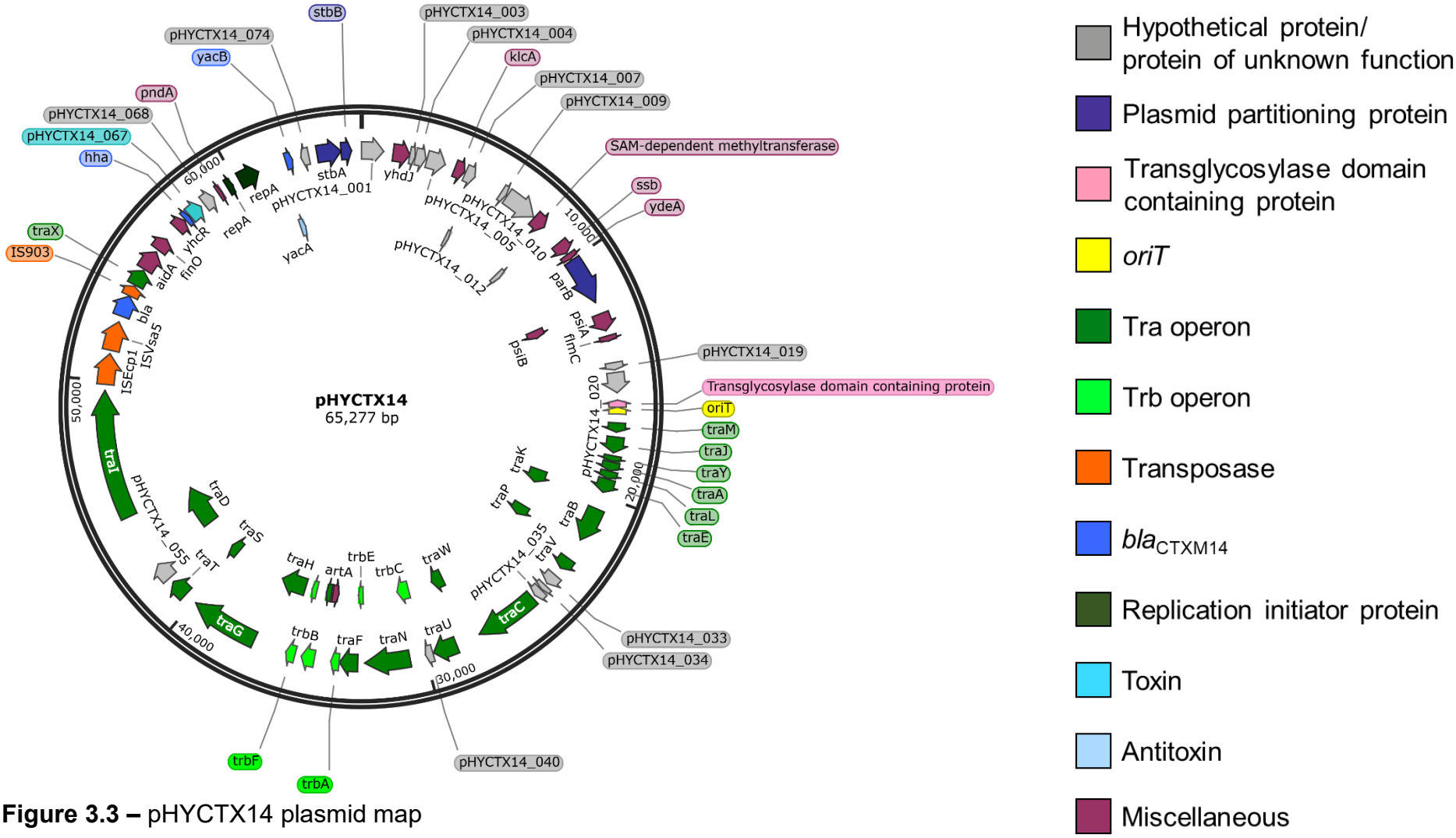

Figure 3.3 – pHYCTX14 plasmid map

Table 3.2 – Features found on pHYCTX14

Feature name	Location	Size (bp)
pHYCTX14_001	20-922	903
yhdJ	1307-1990	684
pHYCTX14_003	1991-2212	222
pHYCTX14_004	2226-2660	435
pHYCTX14_005	2705-3475	771
klcA	3888-4313	426
pHYCTX14_007	4360-4782	423
pHYCTX14_008	4779-4970	192
pHYCTX14_009	6013-6243	231
pHYCTX14_010	6295-7656	1362
SAM-dependent methyltransferase	7703-8266	564
pHYCTX14_012	8266-8532	267
ssb	9127-9654	528
ydeA	9712-9945	234
parB	10006-11970	1965
psiB	12039-12473	435
psiA	12470-13189	720
flmC	13411-13623	213
pHYCTX14_019	14524-14820	297
pHYCTX14_020	14931-15752	822
Transglycosylase domain containing protein	16049-16338	510
oriT	16339-16617	278
traM	16972-17355	384
traJ	17547-18194	648
traY	18314-18541	228
traA	18575-18937	363
traL	18952-19263	312
traE	19285-19851	567
traK	19838-20566	729
traB	20566-21993	1428
traP	21983-22573	591
trbD	22512-22880	369
traV	22877-23392	516
pHYCTX14_033	23741-24217	477
pHYCTX14_034	24316-24534	219
pHYCTX14_035	24562-24909	348
traC	25035-27665	2631
trbL	27662-28048	387
traW	28045-28677	633
traU	28674-29666	993
pHYCTX14_040	29696-30001	306
trbC	30010-30648	639
traN	30645-32495	1851
trbE	32522-32779	258

Table 3.2 cont.

traF	32772-33515	744
trbA	33529-33870	342
artA	33851-34186	336
traQ	34267-34551	285
trbB	34538-35083	546
trbJ	35073-35360	288
trbF	35338-35733	396
traH	35720-37093	1374
traG	37090-39915	2826
traS	39912-40421	510
traT	40435-41166	732
pHYCTX14_055	41369-42106	738
traD	42157-44355	2199
traI	44355-49625	5271
ISEcp1	49864-51126	1263
ISVsa5	51261-52469	1209
bla	52714-53589	876
IS903	53604-54036	433
traX	54090-54773	684
aidA	54832-55692	861
finO	55795-56355	561
yhcR	56941-57402	462
hha	57448-57657	210
pHYCTX14_067	57695-58285	591
pHYCTX14_068	58440-58913	474
pndA	59160-59309	150
repA	59593-59841	249
repA	60153-61010	858
yacA	61923-62192	270
yacB	62189-62470	282
pHYCTX14_074	62816-63151	336
stbA	63489-64469	981
stbB	64472-64894	423

pHYCTX14 encodes conjugative machinery

An *oriT* and genes from both the Tra and the Trb operons, which are involved in the expression of the conjugative T4SS required for conjugation to occur (Waksman, 2025), were found on pHYCTX14. The plasmid carried 23 of the 24 *tra* genes typically found on type F plasmids (Virolle et al., 2020), and eight of the eleven core *trb* genes (Li et al., 1999) (**Table 3.2**). *traR*, *trbG*, *trbI* and *trbH* were not found in the plasmid sequence.

Genes required for plasmid stability and vertical transfer of plasmids in host cells are encoded on pHYCTX14

In order to persist within a population of bacterial cells, plasmids often encode a range of mechanisms, such as plasmid partitioning (Baxter and Funnell, 2014) and TA systems (Rawlings, 1999).

pHYCTX14 was found to encode several genes associated with plasmid stability, including *stbA* and *stbB* of the StbABC operon, which is involved in plasmid partitioning (Quèbre et al., 2022), as well as *parB*, a gene typically expressed alongside *parA* and *parS* as part of the ParABS system, also involved in plasmid segregation (Broedersz et al., 2014). In addition to this, pHYCTX14 encoded the type II TA system, YacAB (Tu et al., 2020).

A truncated IS903 is located next to *bla*$_{\text{CT-X-M-14}}$

Many *bla*$_{\text{CTX-M}}$ genes encoded on plasmids are located adjacent to small transposable elements known as IS (Eckert et al., 2005, Touchon and Rocha, 2007). The *bla*$_{\text{CT-X-M-14}}$ gene in pHYCTX14 was flanked by two complete IS, ISEcp1 and ISVsa5. Observations from the annotated plasmid sequence revealed that the gene was also neighboured by an incomplete IS903, which was verified by aligning the IS903 amino acid sequence in pHYCTX14 with a complete *E. coli* IS903 amino acid sequence (Accession number: CDN96694) using BLASTp (Camacho et al., 2009) (**Figure 3.4**).

Figure 3.4 – Graphical summary of the pHYCTX14 IS903 amino acid sequence alignment with a complete *E. coli* IS903 amino acid sequence obtained from BLASTp (Camacho et al., 2009). The red line shows an alignment score of >=200.

pHYCTX14 is a low-copy-number plasmid

The plasmid copy number of pHYCTX14 was estimated to be one to two copies per cell by dividing the average read depth of the plasmid contig from chromosomal contigs.

3.4 DISCUSSION

Several isolates collected during previous studies were found to carry clinically important resistance genes, including *bla*$_{\text{CTX-M,}}$ *bla*$_{\text{NDM}}$ and *ant*, that were potentially encoded on MGEs and could be used to monitor the movement of AMR genes within a multispecies biofilm.

From the initial screening, EC-HY-3 was identified to encode *bla*$_{\text{CTX-M-14,}}$ and analysis of the contig encoding this gene suggested that the gene was carried on an incompatibility type FII conjugative plasmid. IncF plasmids are regularly involved in the dissemination of AMR between bacteria of the *Enterobacteriaceae* family (Muthuirulandi Sethuvel et al., 2019), and *bla*$_{\text{CTX-M}}$ genes, such as CTX-M-14, encode ESBLs (El Aila et al., 2023). ESBLs confer resistance to a wide range of beta-lactam antibiotics, including first-, second-, and third-generation cephalosporins (Husna et al., 2023). Clinically, ESBL encoding bacteria have caused major challenges for the treatment of Gram-negative bacterial infections (El Aila et al., 2023), and *bla*$_{\text{CTX-M-14}}$, as well as *bla*$_{\text{CTX-M-15,}}$ are considered the most widespread variants of *bla*$_{\text{CTX-M}}$ worldwide (Woodford et al., 2011).

Detailed characterisation of the full plasmid sequence identified the presence of *oriT,* as well as 23 genes from the Tra operon and eight genes from the Trb

operon on pHYCTX14. The Tra and Trb operons are involved in the expression of the T4SS and conjugative pili, which are required for successful plasmid conjugation between donor and recipient cells (Waksman, 2025). Notably, *traR*, *trbG*, *trbI* and *trbH* were not encoded on the plasmid.

The absence of *traR* from the Tra operon, in addition to *trbG*, *trbI* and *trbH* in the *trb* operon, was not expected to affect the ability of pHYCTX14 to conjugate between bacterial cells during this study, as research has shown that the absence of these genes does not inhibit conjugation of type F plasmids (Maneewannakul and Ippen-Ihler, 1993, Karczmarczyk et al., 2014, Maneewannakul et al., 1992, Li et al., 2015). Investigations into mutant pOX38 plasmids with *traR*, *trbI* or *trbH* deletions revealed that deletion of these genes does not impact the rate of conjugation, and the plasmids were able to conjugate with the same efficiency as the wild-type plasmid (Maneewannakul and Ippen-Ihler, 1993, Maneewannakul et al., 1992). pCA08, an IncF plasmid which does not encode *trbG*, has also been found to be mobile (Li et al., 2015), and other previously characterised conjugative type F plasmids, such as pEQ011, also encode incomplete Trb operons (Karczmarczyk et al., 2014).

The morphological structure of conjugative pili encoded on plasmids can be split into two phenotypes: short rigid pili, produced by P-type T4SS, that promotes conjugation on surface-associated bacterial populations; and long flexible pili, produced by F-type T4SS, that promotes conjugation in both surface and liquid bacterial communities (Virolle et al., 2020, Lawley et al., 2003). As pHYCTX14 is an IncFII plasmid, encoding the F-type T4SS, the presence of transconjugants in the planktonic phase of the biofilm conjugation model was also briefly investigated (**Chapter 6**).

Comparing pHYCTX14 with plasmids reported to the NCBI database determined that the plasmid shared a backbone with those previously observed and would be a suitable candidate for future experiments, as it was relevant to circulating plasmids found in Gram-negative species of bacteria, such as *K. pneumoniae* and *S. enterica,* described in past studies. A unique region was found between approximately positions 50000 and 55000 in the pHYCTX14 sequence, corresponding to the location where *bla*$_{\text{CTX-M-14}}$ and

ISEcp1, ISVsa5 and IS903 are encoded. It is likely that an ancestor of pHYCTX14 gained a transposon carrying *bla*$_{\text{CTX-M-14}}$. A detailed comparison of pHYCTX14 with the closely related plasmid p143-3 suggested that some genes, between approximately positions 2300 and 12860, were either lost by pHYCTX14 or gained by the ancestor of p143-3. Interestingly, the IS903 flanking *bla*$_{\text{CTX-M-14}}$ appeared to be truncated. Previous studies have shown that *bla*$_{\text{CTX-M-14}}$ is often flanked with ISEcp1 upstream and IS903 downstream (Liao et al., 2015), where ISEcp1 is associated with in the transposition and expression of *bla*$_{\text{CTX-M}}$ genes (Zhang et al., 2025a), and IS903 is suggested to play a role with the overall structure and integrity of the resistance cassette, with the truncation or loss of IS903 often associated with changes to the overall structure of the cassette (Zhao and Hu, 2013). There is limited research on whether changes to the structure and stability of the resistance cassette as a result of a truncated IS903 impacts the mobility of the cassette via transposition. Therefore, the ability of *bla*$_{\text{CTX-M-14}}$ to mobilise from pHYCTX14 into the bacterial chromosome could not be concluded solely from the characterisation of the plasmid sequence, and additional tests were designed to determine whether the resistance gene had mobilised into the bacterial chromosome during the conjugation experiments in this study (**Chapter 4**).

The ability of the candidate plasmid to maintain itself within the bacterial population in the absence of selective pressure was an important consideration for this project. Plasmid profiling of pHYCTX14 indicated that the *yacA* and *yacB* from the YacAB type II TA system (Tu et al., 2020), as well as *stbA* and *stbB* from the StbABC partitioning system (Quèbre et al., 2022), were encoded on the plasmid.

Plasmid partitioning systems are particularly important for the persistence of low-copy plasmids in bacteria as they ensure that plasmids are segregated evenly into daughter cells during bacterial replication (Baxter and Funnell, 2014, Guynet et al., 2011). Research has shown that the loss of *stbC* from StbABC from the plasmid pR388 did not significantly impact plasmid persistence (Guynet et al., 2011). Therefore, the absence of *stbC* in pHYCTX14 was unlikely to affect its stability.

TA systems, also known as plasmid addiction systems, promote plasmid persistence by encoding a stable toxin (*yacB* encoded on pHYCTX14) and an unstable antitoxin (*yacA* encoded on pHYCTX14) (McVicker and Tang, 2016, Van Melderen, 2010). If the plasmid is not inherited by daughter cells during bacterial replication, the antitoxin will be rapidly degraded, and the toxin will kill the cells through a process known as post-segregational killing (Van Melderen, 2010). To confirm that pHYCTX14 could be maintained without antibiotic selection during the experiments in this study, the stability of the plasmid in relevant bacterial isolates was tested before proceeding with further investigations (**Chapter 4**).

3.5 CONCLUSIONS

In this chapter, pHYCTX14, an IncFII plasmid encoding *bla*$_{\text{CTX-M-14}}$, was selected as the candidate plasmid to be used in this study. Comprehensive characterisation of the plasmid demonstrated that it would be suitable for the experiments planned and could be used to monitor the impact of various stressors on the rate of plasmid movement in a multispecies biofilm within a real-world context.

Chapter 4 describes the development of a biofilm bead model to establish multispecies biofilm communities using a selection of *E. coli* food isolates and *S.* Typhimurium 14028S, as well as the conjugation of pHYCTX14 into the relevant isolates to build the strain bank required for this project.

CHAPTER 4: ESTABLISHING A MULTISPECIES BIOFILM COMMUNITY AND BUILDING THE STRAIN BANK

“Science could predict that the universe must have had a beginning”

< Stephen William Hawking >

4.1 INTRODUCTION

Polymicrobial biofilm communities are common contributors to many bacterial infections, and these infections are often challenging to eradicate due to the intrinsically resistant nature of biofilms to antimicrobials (Liu et al., 2024). Biofilms have also been found to encourage plasmid persistence and promote HGT (Uruén et al., 2021). Despite this, the understanding of antimicrobial resistance within the scientific community has mainly been built from experiments conducted using bacteria in the planktonic state, which is not reflective of the biofilm lifestyle that most bacteria exhibit (Trampari et al., 2021), and the factors that drive movement of plasmids within polymicrobial biofilm communities remains to be investigated (Liu et al., 2024).

In **Chapter 3**, the candidate plasmid pHYCTX14 was selected for this study. To monitor the movement of this plasmid within a multispecies biofilm, a multispecies community consisting of bacterial strains that could stably co-exist within a biofilm was needed, and *E. coli* and *S.* Typhimurium were chosen as the candidate species to establish the model biofilm community for this project.

Salmonella is a common pathogen transmitted through the consumption of contaminated food products (He et al., 2023) and is one of the leading causes of gastroenteritis in humans worldwide (Ehuwa et al., 2021, Zweifel and Stephan, 2012). Aside from being a prevalent cause of disease in humans, *Salmonella* also populates the gut of various animals, including birds, dogs and reptiles (Ehuwa et al., 2021), where *E. coli* is also a common inhabitant (Sørum and Sunde, 2001, Silva et al., 2012). Many commensal *E. coli* in food animals have been shown to harbour a range of AMR genes, acting as a reservoir of MDR bacteria. These genes can be disseminated to other, potentially pathogenic, strains and species of bacteria, such as *Salmonella*, leading to the spread of MDR bacteria to humans through the food chain (Szmolka and Nagy, 2013). This is especially concerning given the key role *Salmonella* plays in human gastrointestinal infections (Majowicz et al., 2010).

Studies have shown the mobilisation of MGEs, including plasmids encoding AMR genes, for example, *bla*$_{\text{CTX-M-27}}$ and *bla*$_{\text{CTX-M-64,}}$ between *E. coli* and *Salmonella* in food-producing animals (Zhao et al., 2021, Zhao et al., 2020), as well as the ability for the two species to form mixed-species biofilms (Wang et al., 2013, Lin et al., 2022b). IncFII plasmids encoding *bla*$_{\text{CTX-M-14}}$ have also been suggested to be widespread amongst healthy farm animals in countries such as China (Szmolka and Nagy, 2013). Considering these factors, *E. coli* and *Salmonella* were suitable candidates for this study, given the intended use of pHYCTX14 (**Chapter 3**) to monitor the rate of plasmid movement within a multispecies biofilm in this project.

Previously, both closed and open biofilm models have been used to study plasmids. Examples of closed biofilm models include those that are conducted in polystyrene plates where biofilms form on the base and sides of the wells, that have been used to investigate the movement of plasmids in *Klebsiella pneumoniae* biofilms (Element et al., 2023), as well as the impact of plasmid carriage on biofilm formation (García-Bayona L Auid et al., 2024, Gama et al., 2020). Open biofilm models, such as those conducted in microfluidic devices, have also previously been used to study the real-time movement of plasmids between different species of bacteria, such as *Pseudomonas putida* and *E. coli* (Li et al., 2018a), as well as between bacterial communities from activated sludge (Qiu et al., 2018). Studies have also used flow cells to investigate plasmid persistence in biofilms formed by *P. putida* (Røder et al., 2021).

This chapter describes the development of a bead-based multispecies biofilm conjugation model to study plasmid transfer among strains. A selection of *E. coli* food isolates were grown in competition with *S*. Typhimurium 14028S to establish stable multispecies biofilm communities under different growth conditions, and pHYCTX14 was conjugated into relevant strains to build the strain bank required for this project.

4.2 AIMS AND OBJECTIVES

- Select a panel of *E. coli* food isolates from a previous study to grow in competition with *S.* Typhimurium 14028S in a biofilm context.
- Establish a multispecies biofilm community using *E. coli* and *S.* Typhimurium 14028S.
- Select for rifampicin and nalidixic acid resistant *E. coli* and *S.* Typhimurium strains.
- Conjugate pHYCTX14 into rifampicin and nalidixic acid resistant strains to build the strain bank.
- Conduct relevant tests to ensure pHYCTX14 could be stably maintained within bacterial populations without antibiotic selection.
- Investigate whether SNPs in *rpoB* or *gyrA*, as well as carriage of pHYCTX14, impact biofilm formation in the *E. coli* or *S.* Typhimurium strains.

4.3 RESULTS

4.3.1 Selecting a panel of *E. coli* food isolates

Ten *E. coli* food isolates (**APPENDIX I**) were selected from a panel of various isolates isolated from a range of food sources (Janecko et al., 2023) to be grown in competition with *S.* Typhimurium 14028S within a biofilm context. The ten isolates chosen represented prevalent STs found in the study and were selected based on the criteria that they did not encode transferable AMR genes and did not carry IncF plasmids. Additionally, blue colonies were recovered when these isolates were inoculated onto LB agar supplemented with X-Gal and IPTG, indicating expression of *lacZ* and synthesis of the β-galactosidase enzyme. This suggested that the selected *E. coli* were suitable for the proposed multispecies biofilm model, as *S.* Typhimurium 14028S does not encode *lacZ* and therefore, the two species could be easily differentiated using blue/white screening (**Figure 4.1**).

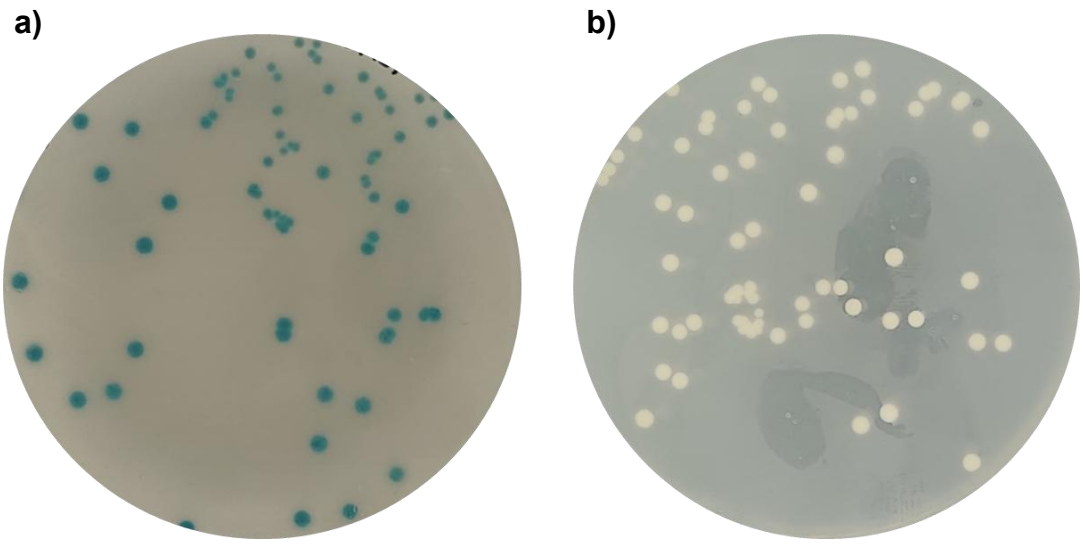

Figure 4.1 – Representative plates of **a)** *E. coli* and **b)** *S.* Typhimurium 14028S inoculated onto LB agar supplemented with X-Gal and IPTG.

4.3.2 Initial *E. coli* and *S.* Typhimurium competition assays

An adapted version of the biofilm evolution model (Trampari et al., 2021) was used to grow the ten *E. coli* food isolates obtained from the food survey in competition with *S.* Typhimurium 14028S to see whether any pairs of *E. coli* and *Salmonella* could co-exist in a mixed-species biofilm. The biofilms were initially grown using glass beads as substrate at 37 °C, and blue/white screening was used to estimate the CFU/bead of the *E. coli* and *Salmonella* biofilms recovered.

Scatter graphs of the CFU were plotted for each pair of *E. coli* and *Salmonella* (**Figure 4.2**). Three *E. coli* isolates, EC18LG-0005-1, EC18PR-0008-3 and EC18PK-0020-1, were observed to co-exist best with *S.* Typhimurium 14028S. No significant difference was found between the CFU/bead of EC18LG-0005-1 and *Salmonella* (Welch's *t*-test, $p = 0.071$) and for EC18PR-0008-3 and *Salmonella* (Welch's *t*-test, $p = 0.959$) when recovered from a mixed species biofilm. A significant difference was found between the CFU/bead of EC18PK-0020-1 and *Salmonella* recovered from the biofilm (Welch's *t*-test, $p = 0.034$). As more variation was observed between the CFU/ bead recovered from the other seven *E. coli* isolates and *S.* Typhimurium when grown in co-culture, these were omitted from further experiments.

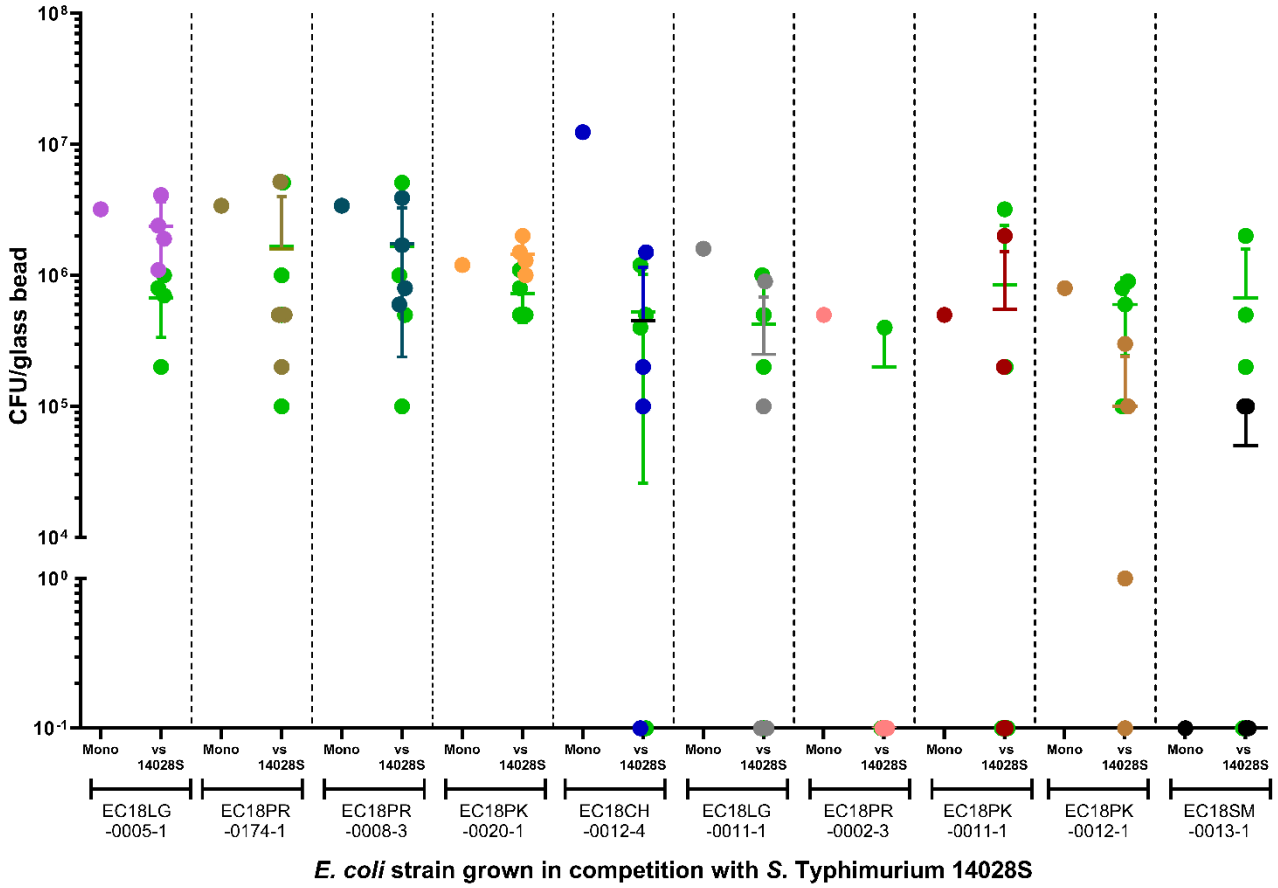

Figure 4.2 - CFU of *E. coli* and *S.* Typhimurium 14028S biofilm cells recovered from glass beads as monospecies (mono) or mixed species (vs 14028S) biofilms. Data points represent individual replicates. Green data points represent *S.* Typhimurium 14028S, and different *E. coli* isolates were given unique colours in a sequential order as indicated by the brackets. Horizontal lines show the mean, and error bars denote one standard deviation above and below the mean. For data points where zero was recorded, a pseudocount of 0.1 was plotted. The limit of detection was <1 CFU/ bead.

4.3.3 The selected multispecies biofilm communities are maintained under different conditions

Although the *p*-value calculated indicated a significant difference between the CFU of EC18PK-0020-1 and *S.* Typhimurium recovered from a mixed species biofilm, further investigations using EC18PK-0020-1, alongside EC18LG-0005-1, EC18PR-0008-3, were still conducted as the scatter graph (**Figure 4.2**) indicated that the CFU/bead recorded for the two species were still similar.

To test the stability of the three *E. coli* and *S.* Typhimurium biofilm communities under different growth conditions, the competition assays were repeated at 37 °C and 21 °C, using both glass and steel beads as substrates for biofilm formation.

4.3.3.1 *E. coli* and *S.* Typhimurium multispecies biofilms grown at 37 °C on glass and steel beads

Similar to the previous results obtained, *S*. Typhimurium co-existed well with EC18LG-0005-1, EC18PR-0008-3 in a biofilm at 37 °C, with no significant difference found between the CFU/ bead obtained on both glass (**Figure 4.3a**) (Welch's *t*-test, EC18LG-0005-1 $p = 0.226$ and EC18PR-0008-3 $p = 0.158$), and steel (**Figure 4.3b**) (Welch's *t*-test, EC18LG-0005-1 $p = 0.077$ and EC18PR-0008-3 $p = 0.408$). For EC18PK-0020-1, a significant difference was found between the CFU/bead of the two species recovered on glass beads (**Figure 4.3a)** (Welch's *t*-test, $p = 0.002$), but no significant difference was found when steel beads (**Figure 4.3b**) were used as the substrate for biofilm formation (Welch's *t*-test, $p = 0.292$).

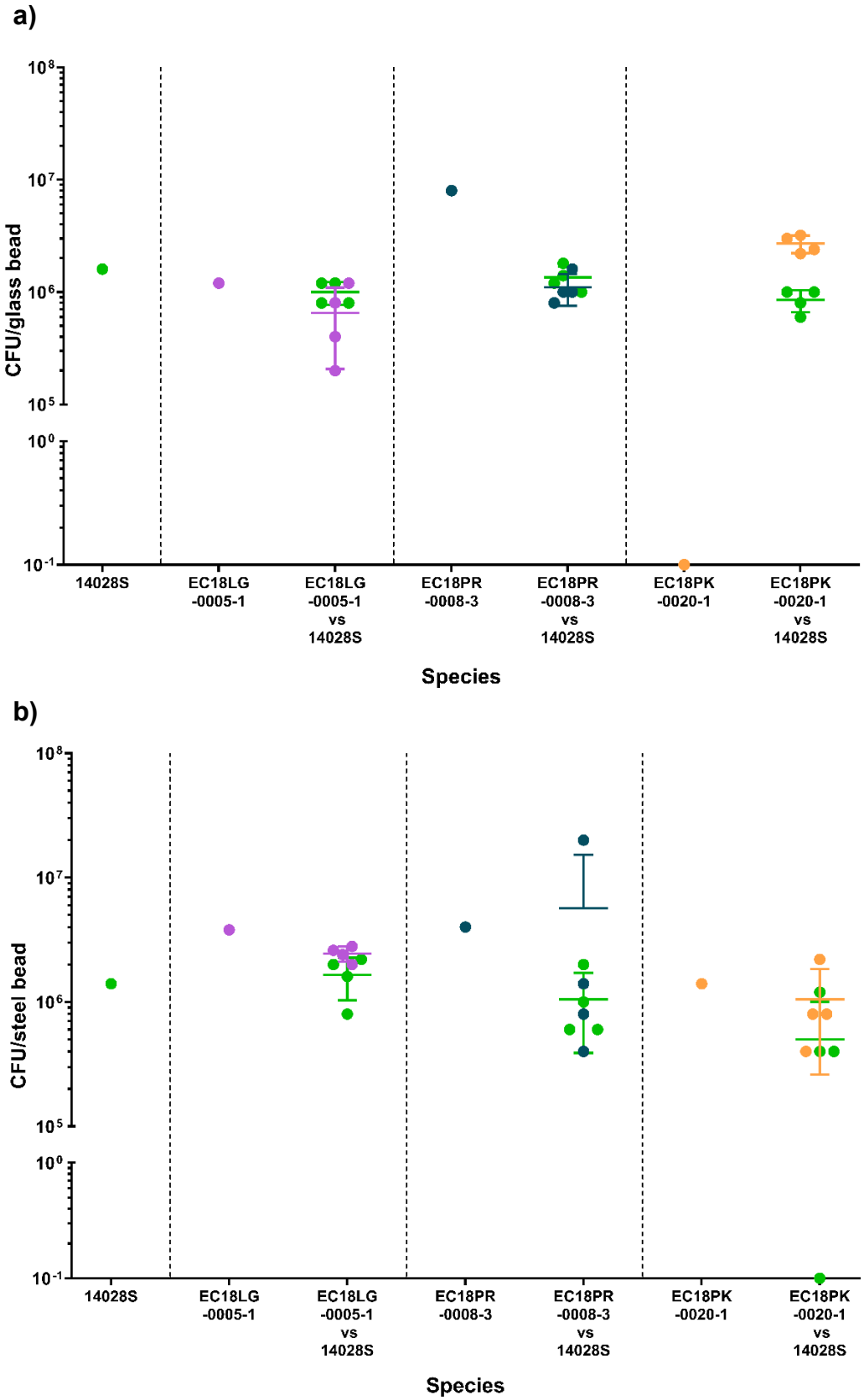

Figure 4.3 - CFU of *E. coli* and *S.* Typhimurium 14028S biofilm cells grown at 37 °C recovered from **a)** glass beads or **b)** steel beads as monospecies or mixed species (vs 14028S) biofilms. Data points represent individual replicates. Green data points represent *S.* Typhimurium 14028S, and the different *E. coli* isolates were given unique colours as indicated in the figure. Horizontal lines show the mean, and error bars denote one standard deviation above and below the mean. For data points where zero was recorded, a pseudocount of 0.1 was plotted. The limit of detection was <1 CFU/ bead.

4.3.3.2 *E. coli* and *S.* Typhimurium multispecies biofilms grown at 21 °C on glass and steel beads

When grown at 21 ºC, all three *E. coli* isolates co-existed well with *S.* Typhimurium 14028S in a biofilm community on both glass (**Figure 4.4a**) and steel beads (**Figure 4.4b**). No significant differences were observed between the CFU recorded for *S.* Typhimurium 14028S and EC18LG-0005-1, EC18PR-0008-3, as well as EC18PK-0020-1 on both materials (Welch's *t*-test, $p = 0.178$, $p = 0.090$ and $p = >0.999$ (glass beads) and $p = 0.844$, $p = 0.465$ and $p = 0.341$ (steel beads), respectively).

As no statistically significant differences were observed between the CFU of *E. coli* and *S.* Typhimurium obtained at both 21 °C and 37 °C on the steel beads, and subsequent experiments planned to use steel beads due to its relevance to the food production environment (Awad et al., 2018), both temperatures were suitable for future biofilm experiments. 37 °C was chosen as the initial temperature for downstream experiments as it represents the optimal growth temperature for both species.

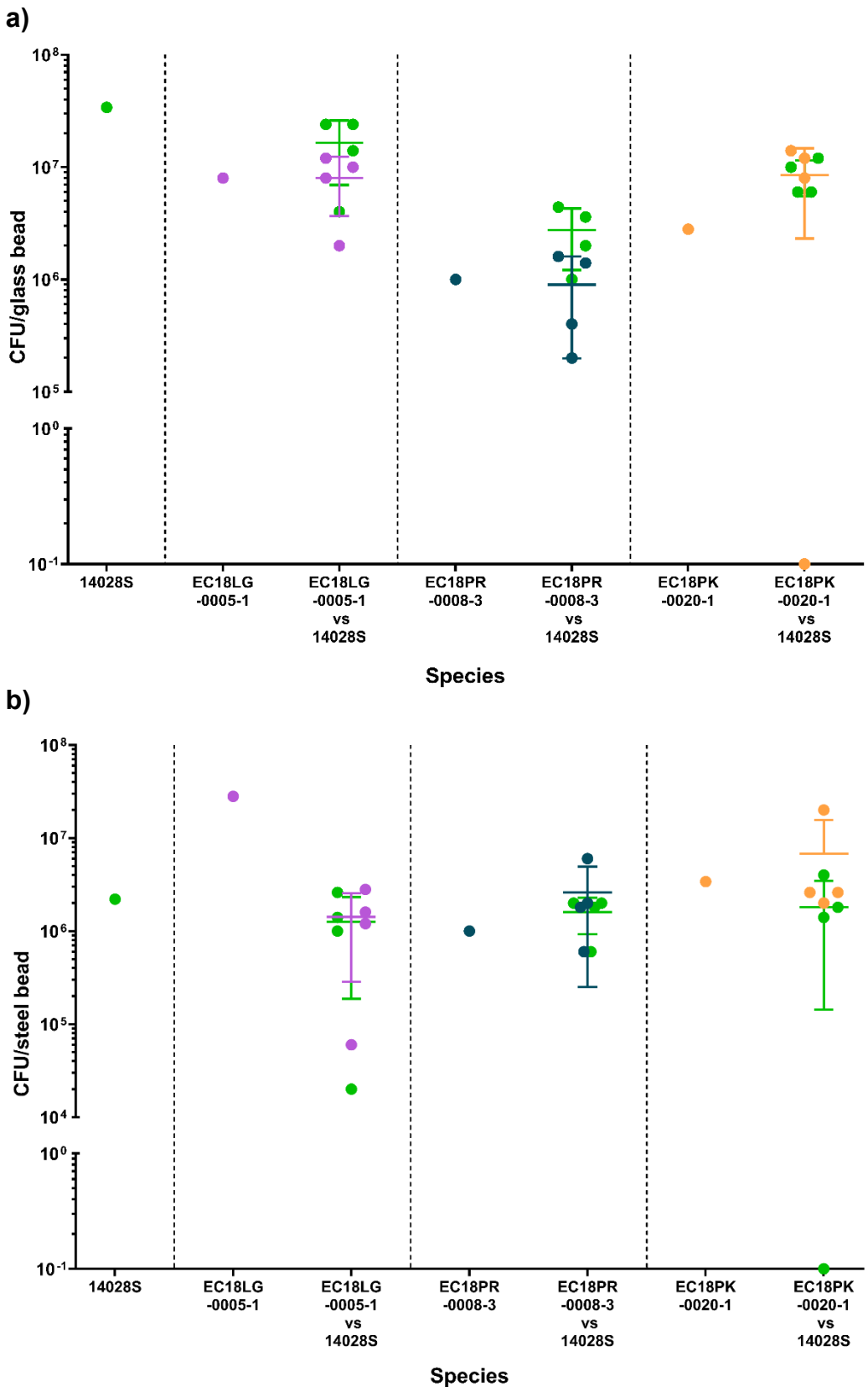

Figure 4.4 - CFU of *E. coli* and *S.* Typhimurium 14028S biofilm cells grown at 21 °C recovered from **a)** glass beads or **b)** steel beads as monospecies or mixed species (vs 14028S) biofilms. Data points represent individual replicates. Green data points represent *S.* Typhimurium 14028S, and the different *E. coli* isolates were given unique colours as indicated in the figure Horizontal lines show the mean, and error bars denote one standard deviation above and below the mean. For data points where zero was recorded, a pseudocount of 0.1 was plotted. The limit of detection was <1 CFU/ bead.

4.3.4 Selected strains were transformable with pUC19

As it was important in downstream experiments for the selected strains to accept external DNA, pUC19, a small cloning plasmid (Schweizer, 1991), was transformed into EC18LG-0005-1, EC18PR-0008-3, and EC18PK-0020-1 via electroporation. Transformants were successfully recovered on LB agar supplemented with 100 µg/mL carbenicillin, demonstrating the ability of these strains to accept foreign plasmids.

4.3.5 Obtaining hybrid genome assemblies of EC18LG-0005-1, EC18PR-0008-3, and EC18PK-0020-1

HMW DNA of the *E. coli* food isolates were extracted, and long-read sequencing was performed using ONT. Hybrid genomes of these isolates were assembled using the long-read sequence reads and the short-read sequencing data previously obtained as part of the food survey (Janecko et al., 2023).

4.3.6 Building the strain bank

4.3.6.1 *S.* Typhimurium 14028S and selected *E. coli* food isolates do not exhibit rifampicin or nalidixic acid resistance

The ability to track donor and recipient strains was required to monitor the movement of pHYCTX14 between *E. coli* and *Salmonella* during this study, and traditionally, this is achieved by selecting resistant mutants to antibiotics, which can then be used to discriminate the strains. To determine which antibiotics may be viable, the baseline MIC of different antibiotics against *S.* Typhimurium 14028S, EC18LG-0005-1, EC18PR-0008-3, and EC18PK-0020-1 were investigated. Rifampicin and nalidixic acid were chosen, as single point mutations in *rpoB* and *gyrA* could confer high-level resistance to these drugs, respectively.

Using the microbroth dilution method**,** the MIC of rifampicin and nalidixic acid was determined in the relevant strains to identify if there was any existing resistance to these antibiotics.

The results obtained (**Table 4.1**) were compared to the epidemiological cut-off (ECOFF) value for *E. coli* stated by EUCAST (EUCAST, 2022), where possible, to determine whether the strains showed sensitivity to the antibiotics they were tested against. For nalidixic acid, the ECOFF value was 8 µg/mL; therefore, all isolates were sensitive to this antibiotic. No ECOFF value was available for rifampicin. However, as the concentration of rifampicin to be used for selection in subsequent experiments would be considerably higher than the MIC obtained, it was determined that both rifampicin and nalidixic acid could be used as markers for selection in future experiments.

Table 4.1 - MIC of rifampicin and nalidixic acid for EC18LG-0005-1, EC18PR-0008-3, EC18PK-0020-1 and *S.* Typhimurium 14028S.

Strain	MIC of antibiotic (µg/mL)	
	Rifampicin	**Nalidixic acid**
S. Typhimurium 14028S	8	8
EC18LG-0005-1	8	4
EC18PR-0008-3	8	8
EC18PK-0020-1	16	4

4.3.6.2 Rifampicin and nalidixic acid resistant *S.* Typhimurium and *E. coli* were selected for

To select for mutants resistant to rifampicin or nalidixic acid, bacterial cultures were exposed to either of these antibiotics at a range of concentrations.

Colonies yielded after exposure to rifampicin at 512 and 256 µg/mL, or nalidixic acid at 32 µg/mL, were recovered and characterised phenotypically by testing their MIC against rifampicin or nalidixic acid using the microbroth dilution method. All mutant colonies demonstrated an MIC of 256 µg/mL or above to rifampicin or nalidixic acid. After confirming that the recovered colonies exhibited the expected phenotype, the mutants were sequenced using an Illumina instrument, and the genomes were checked for SNPs in the expected targets, *rpoB* and *gyrA*, that would indicate resistance against rifampicin and

nalidixic acid, respectively (**Table 2.1 and APPENDIX II**). An error was identified in the sequence data of EC18PR-0008-3, and it was not possible to call for SNPs in the mutants recovered for this isolate; therefore, it was dismissed from further experiments.

4.3.6.3 pHYCTX14 was conjugated into strains to be used in the biofilm conjugation model

pHYCTX14 was moved into the rifampicin resistant (RifR) and nalidixic acid resistant (NalR) versions of *S.* Typhimurium 14028S, EC18LG-0005-1, and EC18PK-0020-1 via conjugation on filter discs.

A range of primers (**Table 4.2**) were designed for PCR to cross-check the species of the colonies recovered from LB plates supplemented with antibiotics for transconjugant selection, as well as check for plasmid presence or absence (**Figure 4.5**). The recovered transconjugant colonies were also streaked onto XLD and Brilliance *Salmonella* agar to check their phenotype (**Figure 4.6**). These checks were particularly important as they allowed any issues with strain contamination to be identified and rectified promptly. Colonies that presented both the correct phenotype on the selective agar and the correct genotype when visualised using gel electrophoresis were also sequenced using Illumina technology.

Table 4.2 – List of primers to cross-check the species of the colonies recovered from LB plates supplemented with antibiotics for transconjugant selection, as well as check for plasmid presence or absence.

Name	Role
invA	Amplification of *invA* in *S.* Typhimurium
lacY	Amplification of *lacY* in *E. coli*
bla$_{\text{CTX-M-14}}$	Amplification of *bla*$_{\text{CTX-M-14}}$ in pHYCTX14
pHYCTX14 backbone	Amplification of pHYCTX14 backbone
bla$_{\text{CTX-M-14}}$ + pHYCTX14 backbone	Amplification of *bla*$_{\text{CTX-M-14}}$ and part of the pHYCTX14 backbone on either side of *bla*$_{\text{CTX-M-14}}$

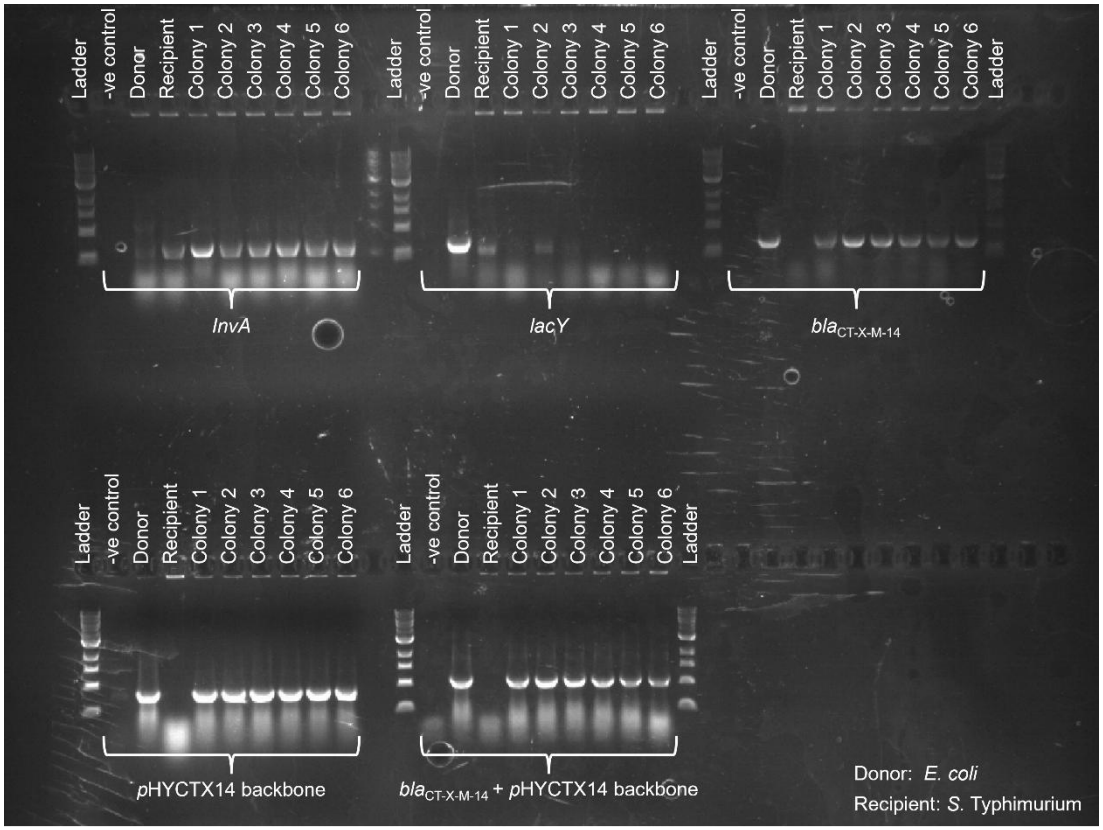

Figure 4.5 – Agarose gel electrophoresis of PCR products obtained from colonies recovered on LB plates supplemented with antibiotics for transconjugant selection from the conjugation of pHYCTX14 using *E. coli* as the donor strain and *S.* Typhimurium 14028S as the recipient strain. Bands show the size of the product obtained relative to the ladder (1kb) for the primers used in the reaction (indicated by the square brackets under the bands).

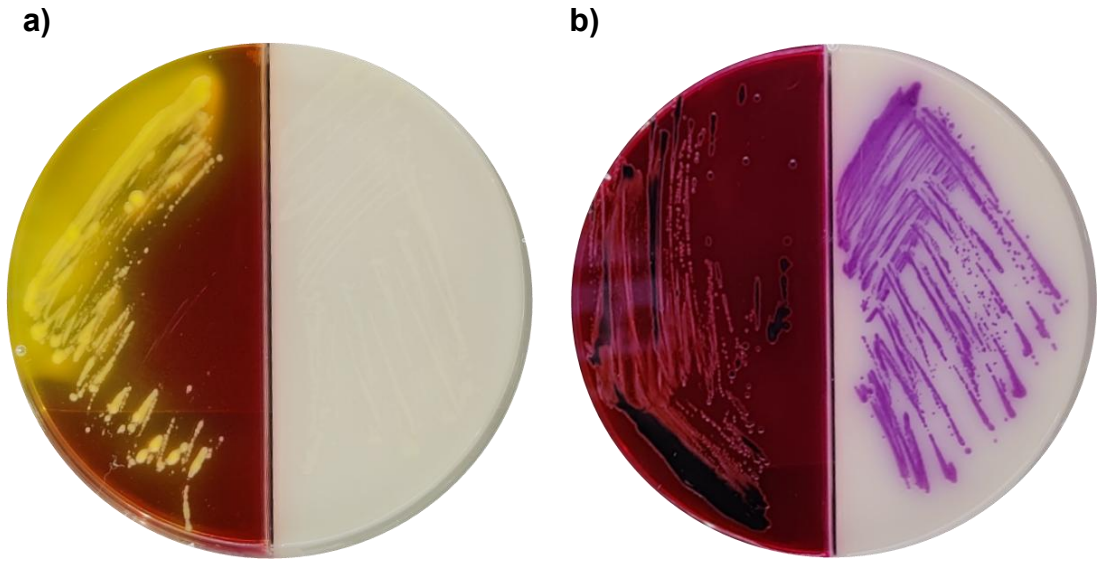

Figure 4.6 - Representative plates of **a)** *E. coli* and **b)** *S.* Typhimurium 14028S inoculated onto XLD (red) and Brilliance *Salmonella* (white) agar.

4.3.6.4 pHYCTX14 can be maintained within the bacterial population without antibiotic selection

As it was important for the plasmid to be maintained in the population without antibiotic selection in later experiments, the stability of pHYCTX14 within bacterial strains in the absence of selective pressure was tested.

Cultures of strains carrying the plasmid were passaged into fresh LB broth over seven days, and streaking on agar supplemented with cefotaxime confirmed that the plasmid remained within the bacterial population. The proportion of cells that kept or lost the plasmid after seven days was also estimated by calculating the CFU of cells recovered on agar plates with and without cefotaxime (**Figure 4.7**). For the majority of strains, the CFU of cells recovered on LB supplemented with 8 µg/mL cefotaxime was ≤ 10-fold lower than the CFU recovered on LB agar after a seven-day passage, with the exception being EC18PK-0020-1 NalR pHYCTX14, where the CFU recovered on LB supplemented with 8 µg/mL cefotaxime was approximately 100-fold lower than the CFU recovered on LB agar. Overall, the results suggested that under no antibiotic selection, most bacterial cells in the population maintain the plasmid, with a low level of plasmid loss.

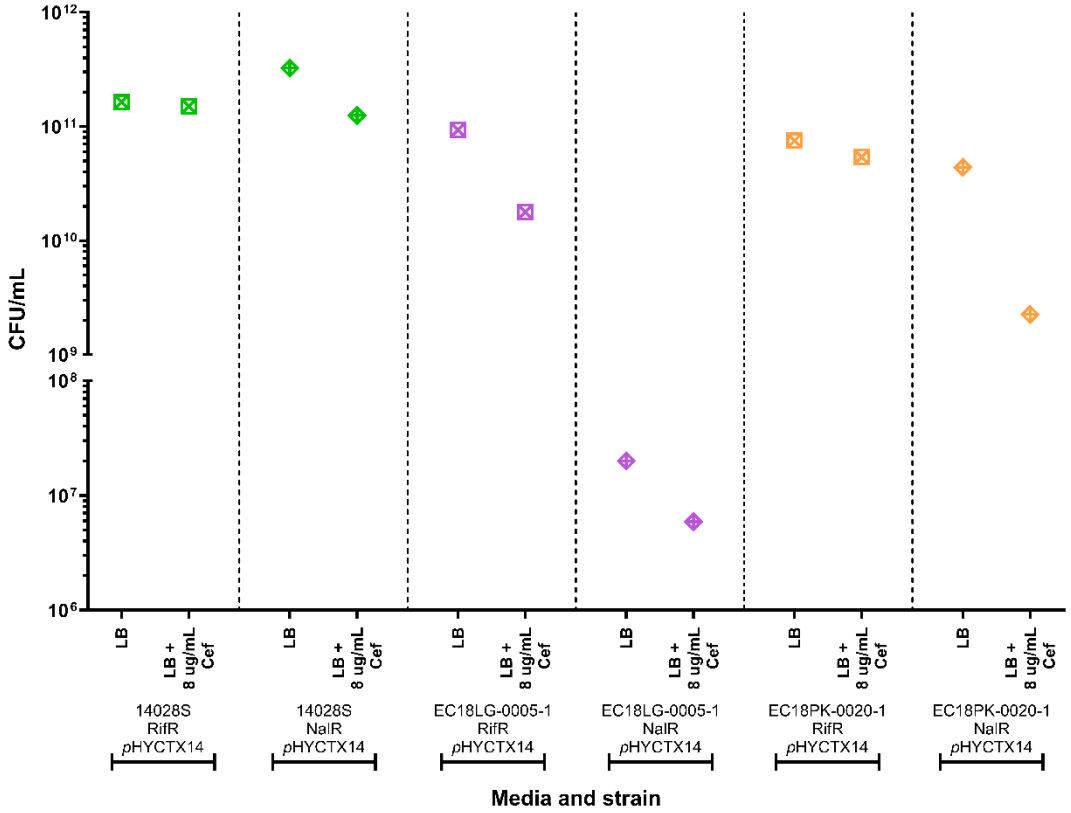

Figure 4.7 - CFU of *E. coli* and *S.* Typhimurium strains carrying pHYCTX14 recovered on LB agar and LB agar supplemented with 8 µg/mL cefotaxime after passaging in LB broth without cefotaxime selection for seven days. Points represent individual replicates. The limit of detection was <1 CFU/ mL.

4.3.6.5 Mutations in *gyrA* appear to impact biofilm formation in EC18LG-0005-1

To identify whether carriage of pHYCTX14, or the presence of SNPs in *rpoB* or *gyrA*, would affect the ability of the bacterial strains to form biofilms, the panel of strains were grown as biofilms on steel beads at 37 ºC, and the CFU recovered from the beads on LB agar was used as an indicator of how well the strain was able to form biofilm.

The results indicated that for *S.* Typhimurium 14028S (**Figure 4.8a**) and EC18PK-0020-1 (**Figure 4.8b**), SNPs in *rpoB* and *gyrA*, conferring resistance to rifampicin and nalidixic acid, respectively, had no significant impact on biofilm formation compared to the wild-type strains. Similarly, carriage of pHYCTX14 did not significantly impact biofilm formation in either strain (**APPENDIX V**). In EC18LG-0005-1, however (**Figure 4.8c**), the SNP in *gyrA* resulted in a significant decrease in biofilm formation compared to the wild-type strain (Welch's *t*-test $p = 0.029$ and $p = 0.034$ for EC18LG-0005-1 NalR and EC18LG-0005-1 NalR pHYCTX14, respectively). It was concluded that pHYCTX14 did not cause the deficit in biofilm, as the presence of the plasmid did not have a significant effect on biofilm formation in any other strains, including EC18LG-0005-1 RifR pHYCTX14 (**APPENDIX V**).

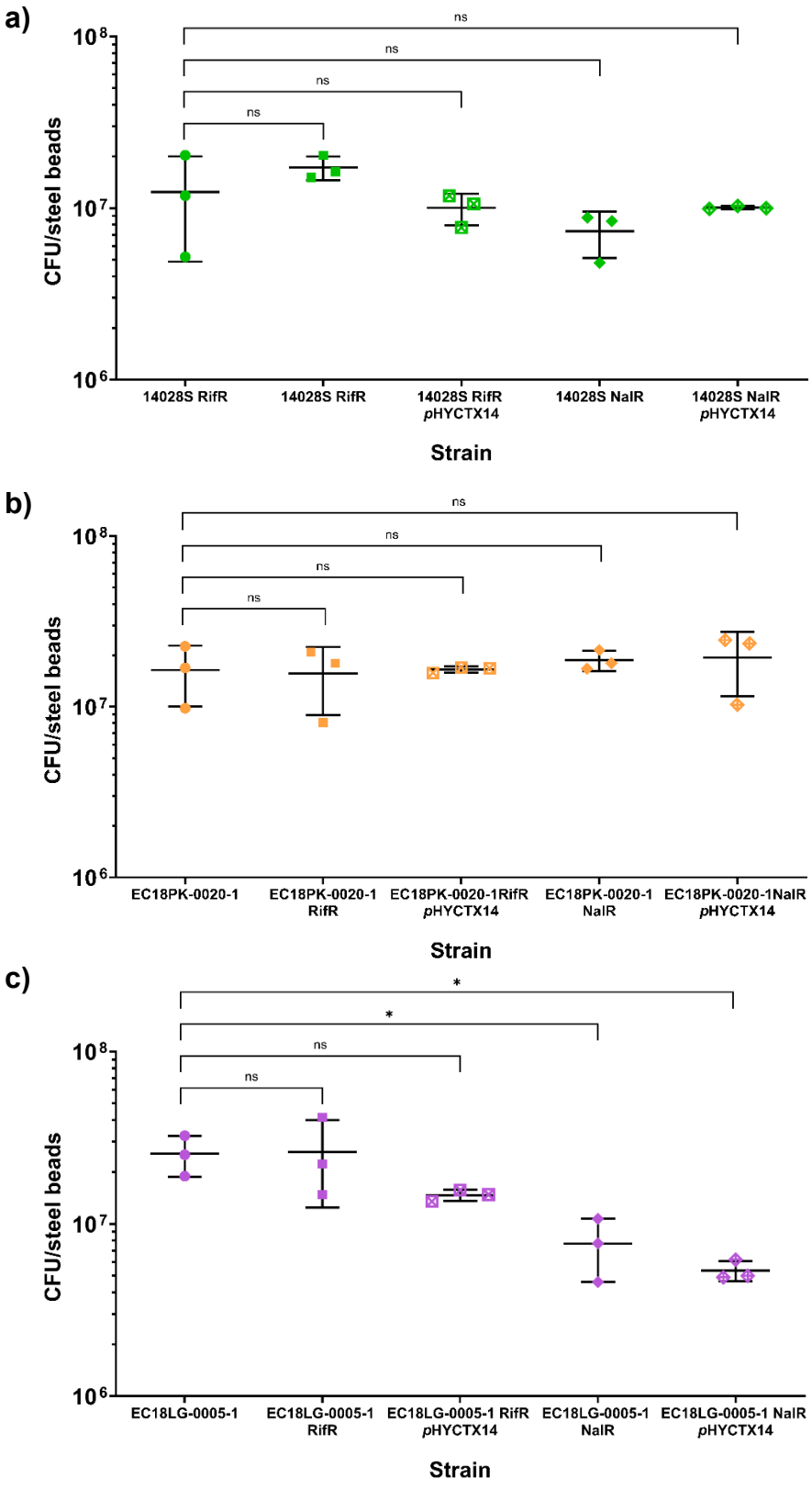

Figure 4.8 - The CFU/steel beads of **a)** *S.* Typhimurium 14028S **b)** EC18PK-0020-1 and **c)** EC18LG-0005-1 RifR or NalR strains with and without pHYCTX14 carriage compared to the wildtype. Data points represent individual replicates. Horizontal lines show the mean, and error bars denote one standard deviation above and below the mean. A significant difference ($p \leq 0.05$) is represented by an asterisk (*) and no significance is represented by 'ns'. The limit of detection was <1 CFU/ beads.

4.4 DISCUSSION

The results from the competition assays indicated that the *E. coli* food isolates EC18LG-0005-1 and EC18PR-0008-3 were able to co-exist with *S.* Typhimurium 14028S, as mixed-species biofilms under all the conditions tested. Interestingly, when EC18PK-0020-1 was grown in co-culture with *S.* Typhimurium 14028S, statistical analyses indicated that the two species maintained more equal populations when steel was used as the substrate for biofilm formation compared to glass. As grade 316 steel is commonly used in the food production environment (Awad et al., 2018), further experiments in this study planned to use steel beads and therefore, the outcomes from the competition assays suggested that the three pairs of *E. coli* and *S.* Typhimurium 14028S could be used to build model communities that would be used to monitor the impact of stress on the rate of HGT in multispecies biofilms. Furthermore, all three *E. coli* isolates were successfully transformed with pUC19 via electroporation. Although pUC19 is a small cloning vector (Schweizer, 1991), and not representative of the larger, conjugative plasmid pHYCTX14, that would be used to monitor HGT within a biofilm in this study, successful recovery of transformants suggested that these *E. coli* do not actively target and cleave plasmid DNA, or silence transcription of genes expressed on plasmids through mechanisms such as restriction modification systems (Rodic et al., 2017), or histone-like nucleoid structuring proteins (Singh et al., 2014).

When testing the stability of pHYCTX14 in the *S.* Typhimurium 14028S and the *E. coli* strains, the results indicated a small decrease in the population of bacterial cells carrying the plasmid after seven days. However, as investigations into the effects of various stressors on conjugation efficiency were planned to be carried out over a 48-hour period, this was unlikely to impact experiments going forward.

The negative impact of the SNP in *gyrA* on biofilm formation in EC18LG-0005-1 was an unexpected observation, as this was not seen in the results for *S.* Typhimurium 14028S or EC18PK-0020-1. Previous studies have shown that in *S.* Typhimurium biofilms, the acquisition of point mutations conferring

resistance to antibiotics, including ciprofloxacin, can lead to a trade-off in biofilm formation (Trampari et al., 2021). However, the results from this study were not specific to *E. coli*.

In *E. coli,* previous research on the relationship between *gyrA* point mutations and biofilm formation in uropathogenic E. coli (UPEC) revealed a higher prevalence of *gyrA* mutations in UPEC that formed biofilms compared to non-biofilm-forming UPEC (Sultan et al., 2021). However, in *Salmonella* Typhi, mutants containing multiple SNPs in *gyrA* appeared to form less biofilm compared to a fluoroquinolone-sensitive wild-type strain (Musanna et al., 2024). Overall, these studies suggest that the impact of SNPs on biofilm formation may differ between different species and even different strains of bacteria within a species, and it may be interesting to investigate whether SNPs in *gyrA*, conferring resistance to quinolone antibiotics, also negatively impact biofilm formation in other strains of *E. coli* or Gram-negative bacteria in the future.

Whilst 37 °C was chosen as the initial temperature to establish the biofilm conjugation model, as it represented the optimal growth temperature for both *E. coli* and *S.* Typhimurium under laboratory conditions, it is not representative of the temperatures used in the food industry, where perishable products such as meat is stored at 0 - 1 °C (Eze et al., 2024). The temperatures of animals where the two species commonly co-exist are also typically higher, for example, in chickens, where body temperature is 41 - 42 °C (Troxell et al., 2015). However, low temperatures do not allow experiments to be completed within a reasonable time frame, so once the concept of plasmid conjugation within the multispecies biofilm is established at 37 °C, the biofilm conjugation model can be adapted to measure conjugation efficiency at different temperatures found in real-world environmental conditions.

4.5 CONCLUSIONS

This chapter describes the successful establishment of multispecies biofilm communities that can be used to measure the rate of conjugation using *E. coli* and *S.* Typhimurium. There remains the limitation that only one *Salmonella*

strain was used as a candidate for this study. Due to time constraints, it was not possible to test multiple *Salmonella* isolates in competition with the panel of *E. coli,* so *S*. Typhimurium 14028S was chosen as a test. This strain of *S.* Typhimurium is well characterised (Jarvik et al., 2010) and is also commonly used to study biofilm evolution dynamics (Trampari et al., 2021), making it a suitable reference strain for this project. In addition, a transposon mutant library, previously generated in this strain of *S*. Typhimurium (Holden et al., 2022), was planned to be used for downstream experiments to investigate the genes involved in *S.* Typhimurium plasmid acquisition.

Chapter 5 describes the steps taken to optimise the multispecies biofilm model to allow plasmid movement between *E. coli* and *S.* Typhimurium in a biofilm to be measured.

CHAPTER 5:
OPTIMISATION OF THE MULTISPECIES BIOFILM COMMUNITY TO MONITOR PLASMID MOVEMENT

“Everything is theoretically impossible, until it is done”

< Robert Anson Heinlein >

5.1 INTRODUCTION

In **Chapter 4**, multispecies biofilm communities were established using *S.* Typhimurium 14028S and *E. coli* food isolates. The candidate plasmid, pHYCTX14, was conjugated into marked versions of these isolates to build the strain bank used in this study.

In past studies, bead-based biofilm models have been used to investigate the evolution of biofilms in various bacterial species, including *B. cenocepacia* (Ellis et al., 2015), and *Bacillus thuringiensis* (Lin et al., 2022a), where plastic beads were used as the substrate for biofilm formation to study long-term bacterial biofilm adaptation. Glass bead-based biofilm models have also been used to explore the evolution of AMR in *S.* Typhimurium biofilms exposed to different antimicrobials (Trampari et al., 2021), as well as in the long-term adaptation and evolution of multispecies bacterial biofilm communities, such as those comprised of *Lactococcus lactis* and *Leuconostoc mesenteroides* that are often used as starter cultures for dairy products (Henriksen et al., 2022). Plasmid transfer in intraspecies biofilms has also been studied using various bead-based models. For example, calcium alginate beads have been used to investigate how gel structure impacts plasmid transfer between strains of *P. putida* (Mater et al., 1999), and glass beads have also been used as substrate for biofilm formation within flow reactors, to research the movement of the RP1 plasmid between in two marine *Vibrio* strains under flow conditions (Angles et al., 1993).

This chapter describes the steps taken to optimise the multispecies biofilm community to allow plasmid movement between the two species in a biofilm to be measured using a steel bead-based biofilm evolution model.

5.2 AIMS AND OBJECTIVES

- Optimise the multispecies biofilm model to be able to measure conjugation efficiency within a biofilm context.

5.3 RESULTS

Preliminary attempts to conjugate pHYCTX14 between *E. coli* and *S.* Typhimurium in a biofilm context demonstrated that various optimisations were needed to be able to measure a baseline plasmid transfer rate between the two species, before stress factors could be introduced into the biofilm conjugation model.

5.3.1 The number of cells recovered from the biofilm can be increased by using more beads

Initially, one steel bead was used as the substrate for biofilm formation in the biofilm conjugation model. However, this resulted in a low rate of biofilm recovery for both donor and recipient strains in the multispecies biofilm, and it was not possible to detect any transconjugants. To investigate whether increasing the number of beads used in the model would increase the recovered CFU, EC18LG-0005-1, EC18PK-0020-1 and *S.* Typhimurium 14028S were grown as monoculture biofilms at 37 °C on one, three, five, eight and ten steel beads.

For all three isolates, increasing the number of beads increased the CFU recovered, with at least ten times more cells recovered when ten beads were used, compared to when one bead was used as the substrate for biofilm formation (**Figure 5.1**). It was hypothesised that, in addition to increasing the biofilm CFU recovered, introducing more beads into the model would also result in more contact between the donor and recipient species of bacteria, increasing the chances of plasmid conjugation between the two species, as the beads are agitated during the incubation period. It was possible that when a single bead was being used in the biofilm conjugation model, the donor and recipient bacteria were forming separate microcolonies on the bead, and there was not enough contact between the donor and recipient bacteria for successful conjugation.

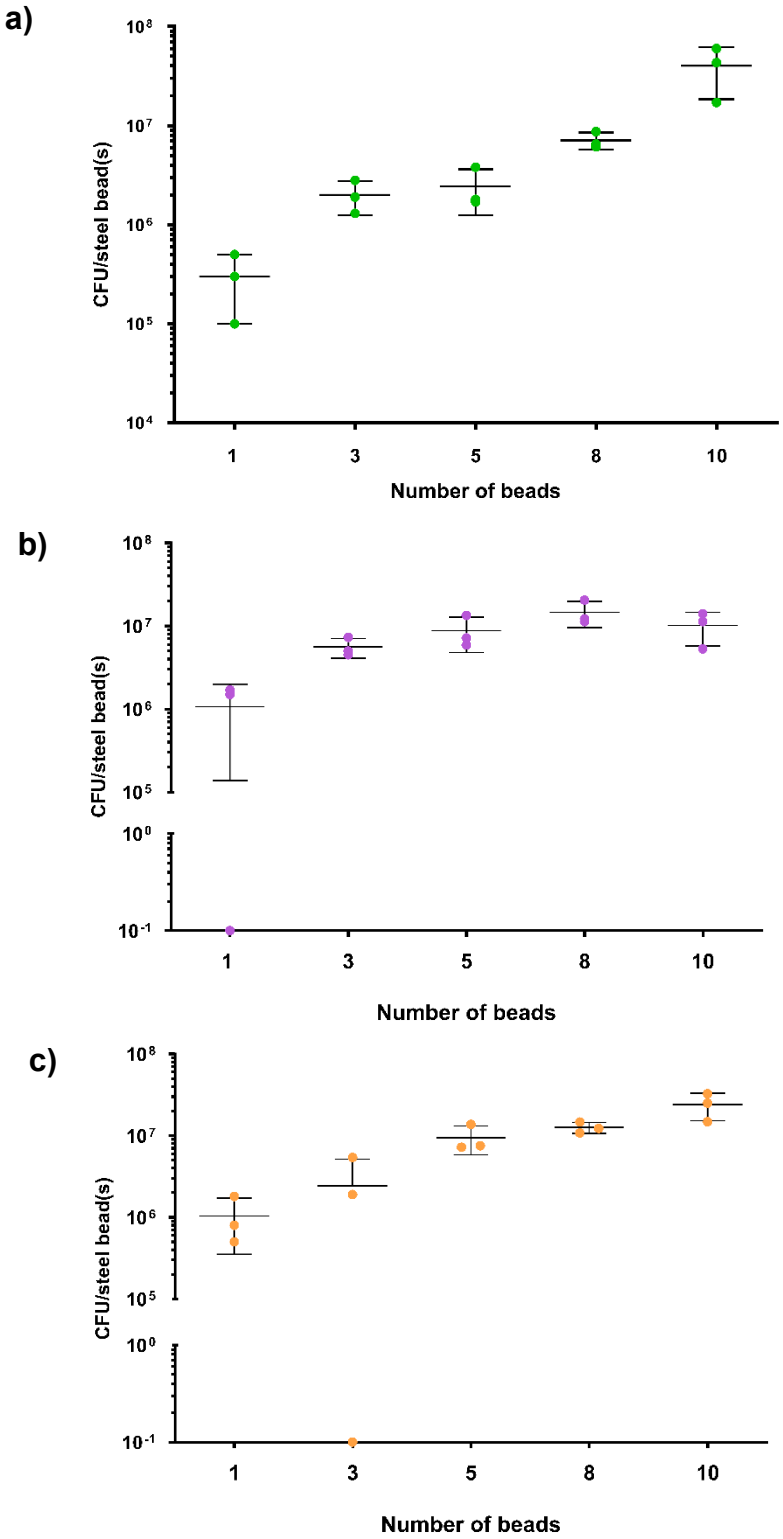

Figure 5.1 - CFU recovered from biofilms grown on one, three, five, eight or ten steel beads for **a)** *S.* Typhimurium 14028S, **b)** EC18LG-0005-1 and **c)** EC18PK-0010-1. Data points represent individual replicates. Horizontal lines show the mean, and error bars denote one standard deviation above and below the mean. For data points where zero was recorded, a pseudocount of 0.1 was plotted. The limit of detection was <1 CFU/ beads.

5.3.2 Recovery of EC18LG-0005-1 RifR pHYCTX14 biofilm cells needed to be optimised

After increasing the number of beads used in the biofilm conjugation model to ten beads, EC18LG-0005-1 RifR pHYCTX14 and *S.* Typhimurium 14028S NalR were chosen as the donor and recipient strains, respectively, for the conjugation of pHYCTX14 at 37 °C between two species using the biofilm conjugation model.

To investigate whether a sub-inhibitory concentration of cefotaxime would select for higher numbers of transconjugants in the recipient strain of bacteria, two biofilm conjugation models, one with no stressor and one supplemented with 0.125 µg/mL of cefotaxime, were set up in parallel. This concentration of cefotaxime represented ¼ of the *S.* Typhimurium 14028S NalR MIC to this antibiotic and was chosen to exert stress on the recipient strain without causing detrimental impacts on fitness. The expected growth of colonies recovered on selective agar from the multispecies biofilm conjugation model, as well as the monospecies controls, is illustrated in **Table 5.1** to help interpret the pattern of colonies on selective agar plates in the following figures.

Table 5.1 - Expected growth of colonies recovered on selective agar from the multispecies biofilm conjugation model and the monospecies controls. '+' denotes growth expected and '-' denotes no growth expected.

		Drug LB agar was supplemented with			
		No drug	100 µg/mL rifampicin and 8 µg/mL cefotaxime	100 µg/mL nalidixic acid	100 µg/mL nalidixic acid and 8 µg/mL cefotaxime
Expected growth	Donor	+	+	-	-
	Recipient	+	-	+	-
	Transconjugants	+	+	+	+

For both models, no colonies were recovered from the agar plates supplemented with 100 µg/mL nalidixic acid and 8 µg/mL cefotaxime, (selecting for transconjugants), and it was also not possible to recover the donor strain from the multispecies biofilm on LB agar that had been supplemented with 100 µg/mL rifampicin and 8 µg/mL cefotaxime, after recovery from the steel beads (**Figure 5.2**).

The presence of EC18LG-0005-1 RifR pHYCTX14 in the multispecies biofilm was confirmed as blue colonies were present on the LB agar plates supplemented with 40 µg/mL X-Gal and 1 mM IPTG for blue/white screening, and recovered at similar rates to the recipient strain, *S.* Typhimurium 14028S NalR (**Figure 5.3**), suggesting that the *E. coli* was not outcompeted by the *Salmonella* strain in the experiment.

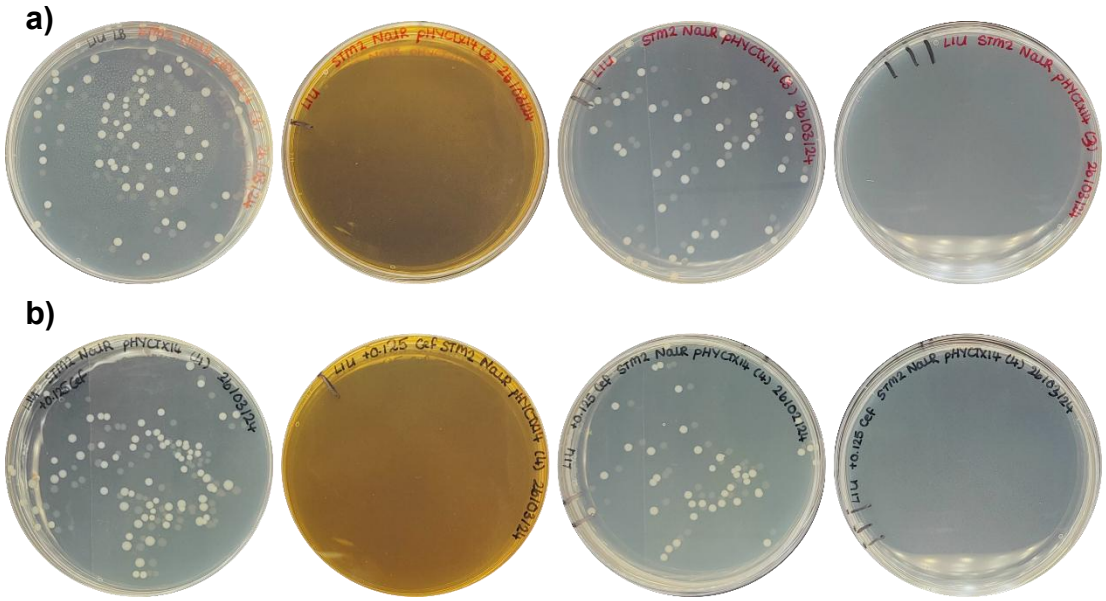

Figure 5.2 - Representative colonies recovered on LB agar supplemented with no drug (no selection), 100 µg/mL rifampicin and 8 µg/mL cefotaxime (donor selection), 100 µg/mL nalidixic acid (recipient selection), and 100 µg/mL nalidixic acid and 8 µg/mL cefotaxime (transconjugant selection) (in order from left to right) from the conjugation of pHYCTX14 from EC18LG-0005-1 RifR pHYCTX14 to *S.* Typhimurium 14028S NalR on steel beads in **a)** LB w/o NaCl and **b)** LB w/o NaCl supplemented with 0.125 µg/mL cefotaxime.

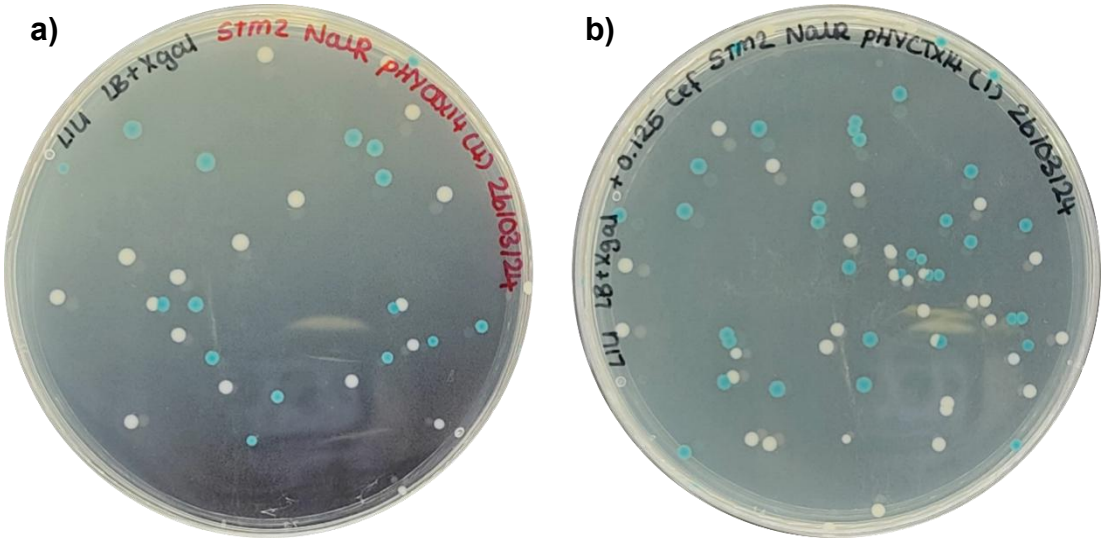

Figure 5.3 - Representative colonies recovered on LB agar supplemented with X-Gal (40 µg/mL), and IPTG (1 mM) from the conjugation of pHYCTX14 from EC18LG-0005-1 RifR pHYCTX14 to *S.* Typhimurium 14028S NalR on steel beads in **a)** LB w/o NaCl and **b)** LB w/o NaCl supplemented with 0.125 µg/mL cefotaxime. Blue colonies represent *E. coli* and white colonies represent *Salmonella.*

Surprisingly, bacteria were not recovered on LB agar supplemented with 100 µg/mL rifampicin and 8 µg/mL cefotaxime from an *E. coli* monospecies control, although colonies were recovered on drug-free agar (**Figure 5.4**).

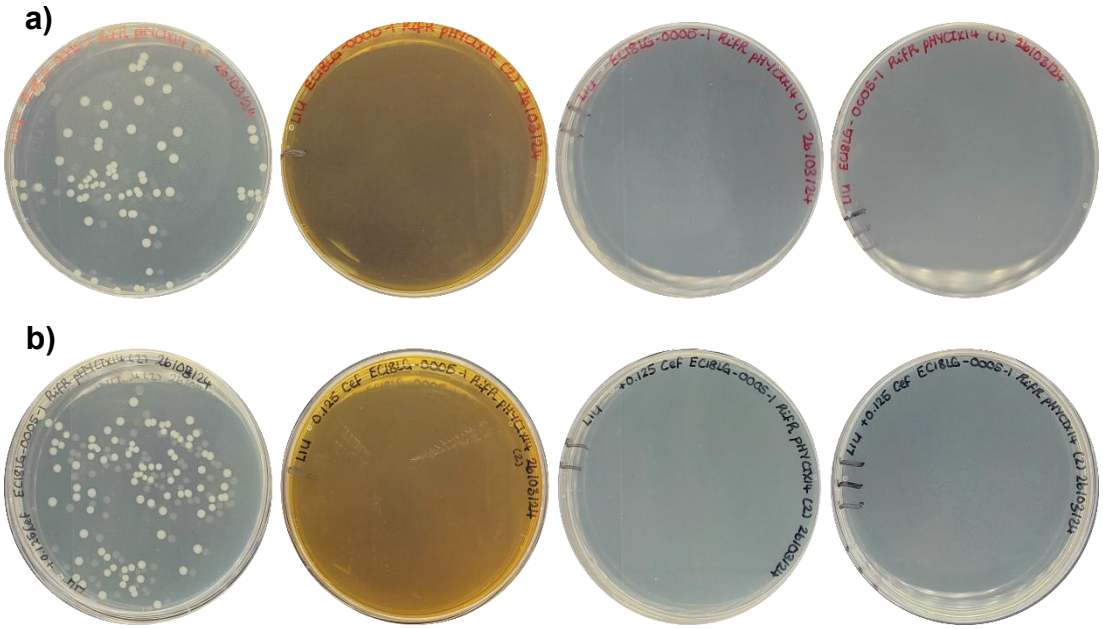

Figure 5.4- Representative colonies recovered on LB agar supplemented with no drug (no selection), 100 µg/mL rifampicin and 8 µg/mL cefotaxime (donor selection), 100 µg/mL nalidixic acid (recipient selection), and 100 µg/mL nalidixic acid and 8 µg/mL (transconjugant selection) (in order from left to right) from a monospecies EC18LG-0005-1 RifR pHYCTX14 biofilm control grown on steel beads in **a)** LB w/o NaCl and **b)** LB w/o NaCl supplemented with 0.125 µg/mL cefotaxime.

After further attempts to conjugate pHYCTX14 between EC18LG-0005-1 RifR pHYCTX14 and *S*. Typhimurium 14028S NalR, it was confirmed that after growing on steel beads, the *E. coli* was surviving but could not be recovered on LB agar supplemented with 100 µg/mL rifampicin and 8 µg/mL cefotaxime, and the model would require further optimisation before plasmid movement could be monitored.

A series of variables, including the concentration of antibiotics the cells were inoculated on after recovery from the biofilm model, as well as the time and temperature for cell recovery, were tested to identify why the donor and transconjugants could not be recovered from the model (**Figure 5.5**).

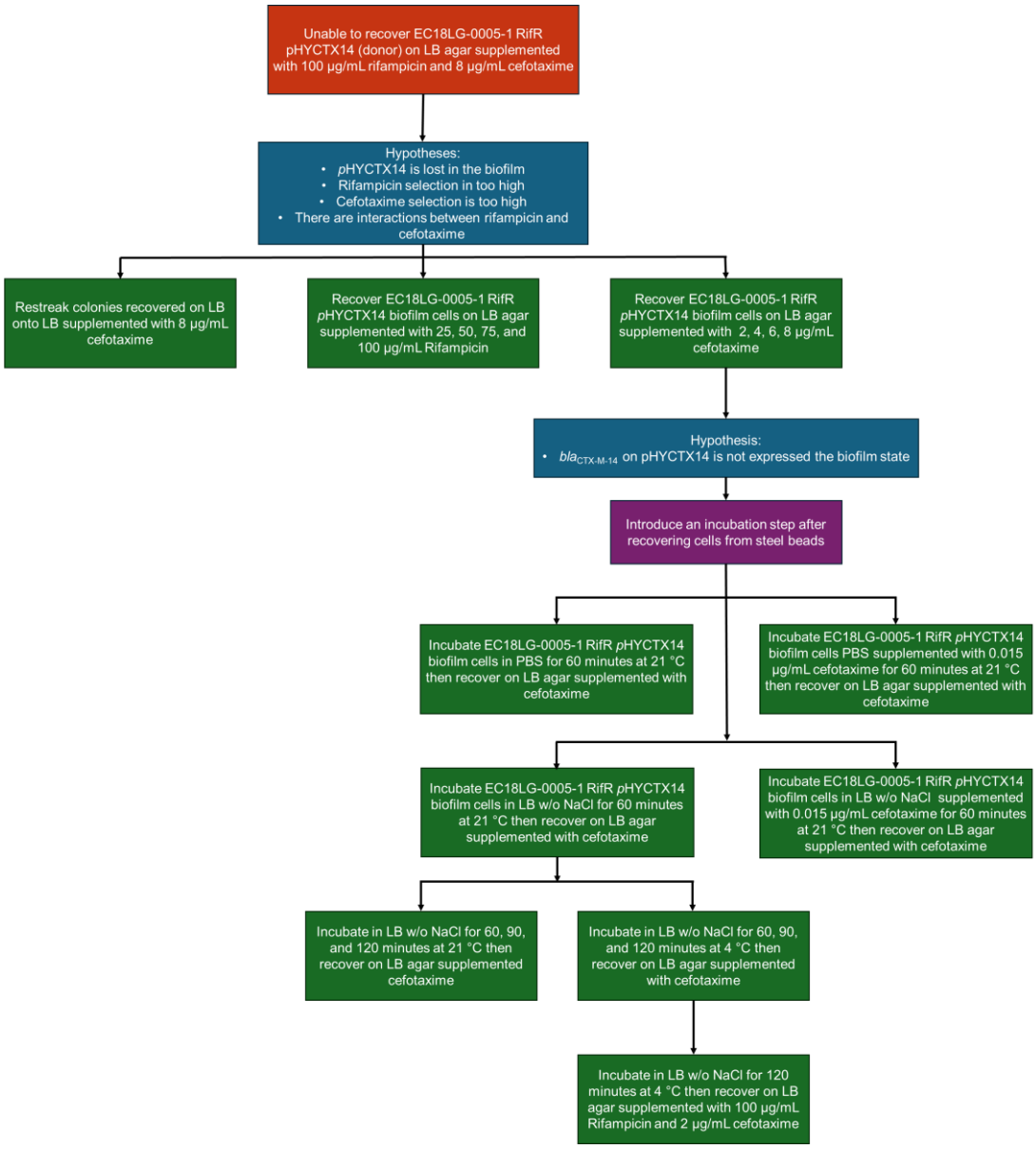

Figure 5.5 – Overview of the steps taken to optimise selection of the donor strain, EC18LG-0005-1 RifR pHYCTX14, after recovery from the multispecies biofilm conjugation model.

5.3.2.1 The plasmid is not lost from EC18LG-0005-1 RifR pHYCTX14 after growing as a biofilm

After recovering EC18LG-0005-1 RifR pHYCTX14 biofilm cells on drug-free LB agar, colonies were randomly selected and streaked onto LB agar supplemented with 8 µg/mL cefotaxime to investigate whether pHYCTX14, encoding *bla*$_{\text{CTX-M-14}}$, was lost from the bacterial population when grown as a biofilm.

Bacterial growth on the agar plates supplemented with cefotaxime was observed, which suggested that the plasmid was not lost, and subsequent PCR reactions confirmed that the *bla*$_{\text{CTX-M-14}}$ gene remained encoded on the plasmid and had not mobilised into the bacterial chromosome.

5.3.2.2 Recovery of EC18LG-0005-1 RifR pHYCTX14 biofilm cells on lower concentrations of rifampicin and cefotaxime

To investigate whether there were interactions between rifampicin or cefotaxime, or if the concentrations of the two antibiotics were too high for the recovery of the donor strain from the biofilm conjugation model, EC18LG-0005-1 RifR pHYCTX14 biofilm cells were inoculated separately on LB agar supplemented with rifampicin or cefotaxime at a range of concentrations after growing on steel beads.

The concentration of rifampicin did not impact the ability to recover EC18LG-0005-1 RifR pHYCTX14 from the biofilm conjugation model

EC18LG-0005-1 RifR pHYCTX14 biofilm cells were recovered from steel beads and inoculated onto LB agar supplemented with 25, 50, 75 and 100 µg/mL rifampicin. Bacterial growth on all concentrations of rifampicin tested (**Figure 5.6a**) indicated that the concentration of the antibiotic (100 µg/mL) initially used to select for the donor cells after recovery from the biofilm conjugation model did not impact the fitness of the strain.

For cefotaxime, EC18LG-0005-1 RifR pHYCTX14 biofilm cells were inoculated on LB agar supplemented with 2, 4, 6, and 8 µg/mL antibiotic, and it was identified that the strain could not grow even on lower concentrations of cefotaxime after biofilm cells were recovered from the steel beads (**Figure 5.6b**).

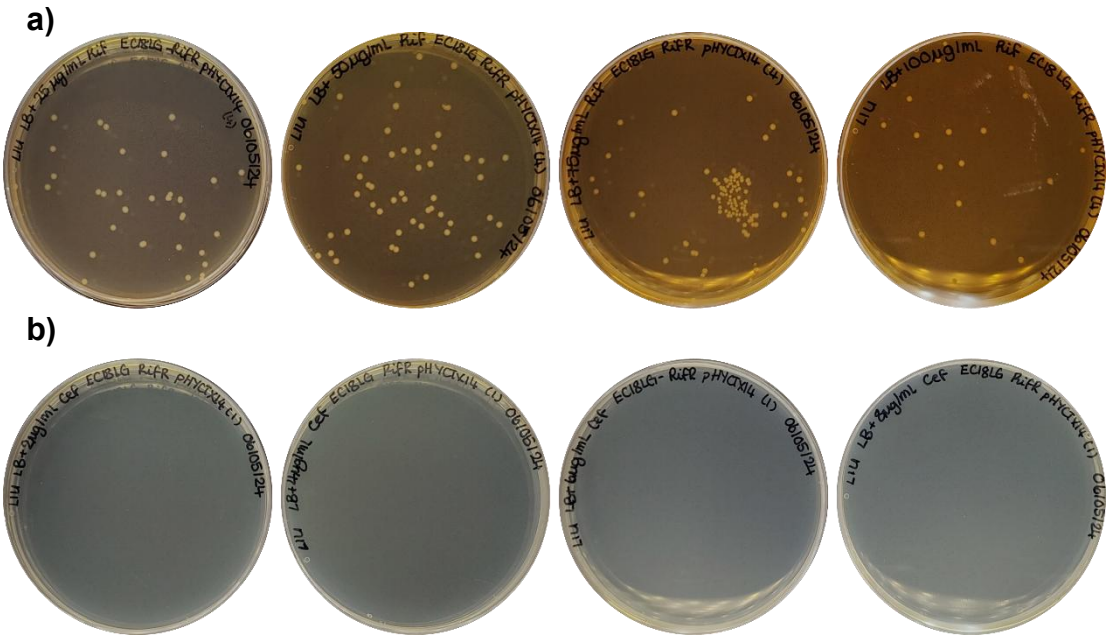

Figure 5.6 - Representative colonies of EC18LG-0005-1 RifR pHYCTX14 biofilm grown on steel beads recovered on **a)** LB agar supplemented with 25, 50, 75 and 100 µg/mL rifampicin (in order from left to right) and **b)** LB agar supplemented with 2, 4, 6, and 8 µg/mL cefotaxime (in order from left to right).

5.3.2.3 Introducing the incubation step

Previously, it was confirmed that pHYCTX14 was not lost from the bacterial population, although EC18LG-0005-1 RifR pHYCTX14 could not be grown on LB agar supplemented with cefotaxime after cells were recovered from the biofilm conjugation model. Therefore, it was hypothesised that *bla*$_{\text{CTX-M-14}}$ was not actively expressed when cells were grown in a biofilm. An incubation step was introduced between the recovery of biofilm cells on the steel beads and inoculating onto agar plates supplemented with cefotaxime, to test whether changing the cells from a biofilm to a planktonic state would increase expression of *bla*$_{\text{CTX-M-14}}$.

Incubating biofilm cells in PBS did not increase EC18LG-0005-1 RifR pHYCTX14 recovery

EC18LG-0005-1 RifR pHYCTX14 biofilm cells were recovered from the steel beads and incubated in PBS for 60 minutes at 21 °C, before inoculating onto LB agar supplemented with cefotaxime at the same concentrations as previously stated. In parallel, biofilm cells were also incubated in PBS supplemented with 0.015 µg/mL cefotaxime to investigate whether a subinhibitory concentration of the antibiotic would induce the expression of *bla*$_{\text{CTX-M-14}}$. For both experiments, no colonies were recovered across all four concentrations of cefotaxime tested (**Figure 5.7**).

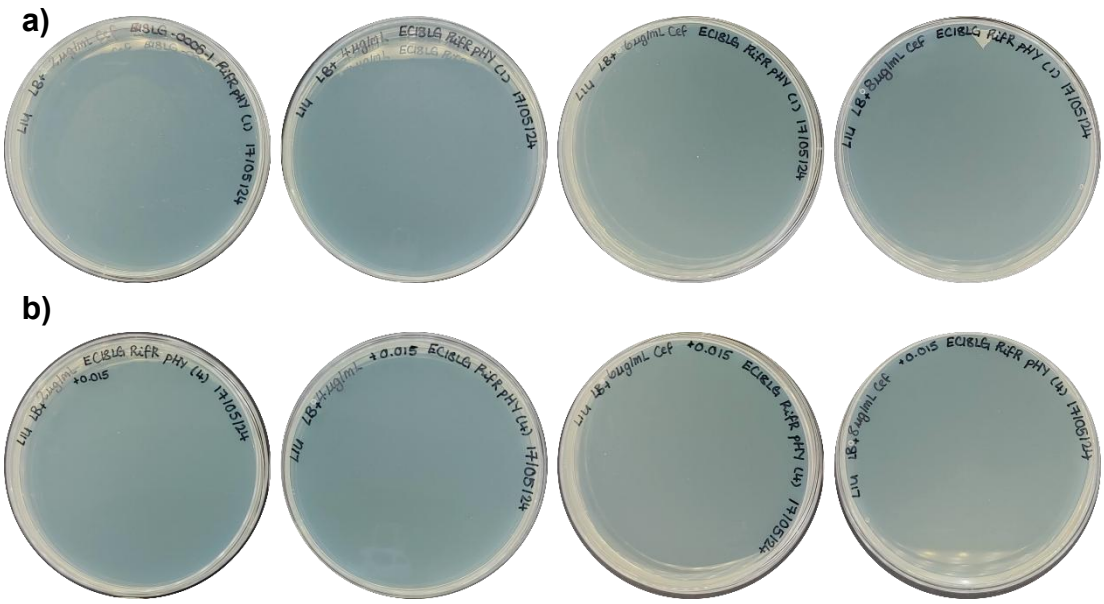

Figure 5.7 - Representative colonies of EC18LG-0005-1 RifR pHYCTX14 biofilm grown on steel beads recovered after incubation for 60 minutes at 21 °C in **a)** PBS and **b)** PBS supplemented with 0.015 µg/mL cefotaxime. Bacteria were inoculated on LB agar supplemented with 2, 4, 6, and 8 µg/mL cefotaxime (in order from left to right).

Incubating biofilm cells in LB w/o NaCl appeared to increase recovery of EC18LG-0005-1 RifR pHYCTX14

To investigate whether incubating the cells in a medium with nutrition to stimulate growth would increase the expression of *bla*$_{\text{CTX-M-14}}$ in the biofilm cells, and allow EC18LG-0005-1 RifR pHYCTX14 to be recovered on LB agar supplemented with cefotaxime, biofilm cells were incubated in LB w/o NaCl for 60 minutes at 21 °C, before inoculating onto LB agar supplemented with cefotaxime. As before, cells were also incubated in LB w/o NaCl supplemented with 0.015 µg/mL cefotaxime.

Colonies were recovered on LB agar plates supplemented with 2 µg/mL cefotaxime after incubating in LB w/o NaCl (**Figure 5.8a**), suggesting that incubating the biofilm cells in nutrient-rich media increased expression of *bla*$_{\text{CTX-M-14}}$. Supplementing the media with a sub-inhibitory concentration of cefotaxime for incubation did not increase the number of colonies recovered on the agar plates (**Figure 5.8b**).

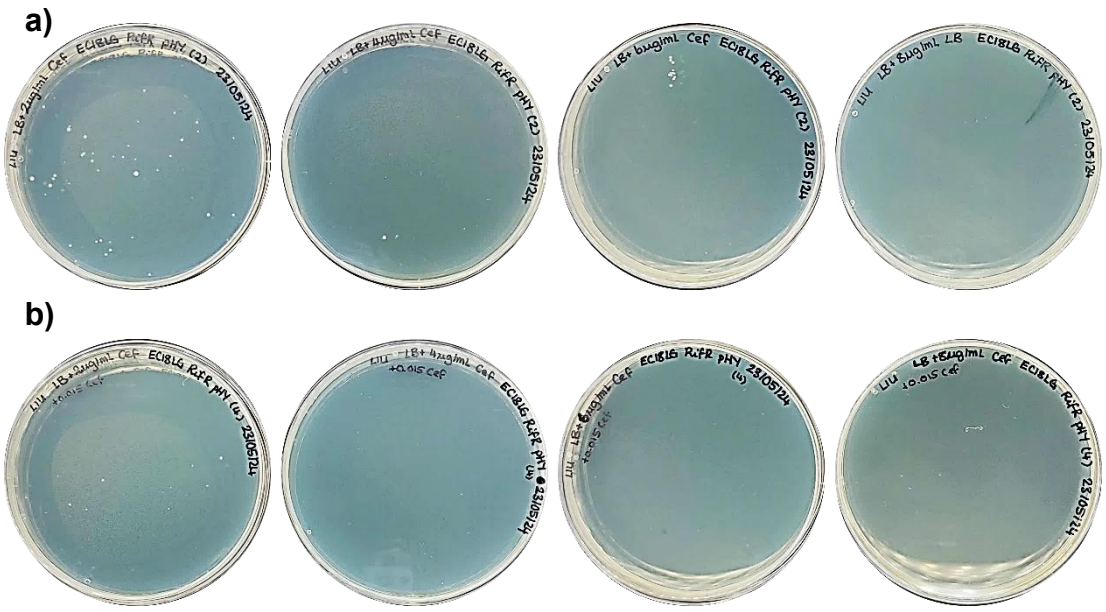

Figure 5.8 - Representative colonies of EC18LG-0005-1 RifR pHYCTX14 biofilm grown on steel beads recovered after incubation for 60 minutes at 21 °C in **a)** LB w/o NaCl and **b)** LB w/o NaCl supplemented with 0.015 µg/mL cefotaxime. Bacteria were inoculated on LB agar supplemented with 2, 4, 6, and 8 µg/mL cefotaxime (in order from left to right).

Incubating EC18LG-0005-1 RifR pHYCTX14 biofilm cells in LB w/o NaCl for 120 minutes at 4°C provided efficient recovery

To explore whether the number of colonies recovered on LB agar supplemented with cefotaxime could be improved by increasing the incubation period, experiments were repeated with incubation at 21 °C in LB w/o NaCl for 60, 90 and 120 minutes. In parallel, biofilm cells were also incubated at 4 °C to investigate whether using a lower incubation temperature, to avoid the potential impact of cells replicating during a longer incubation period, would decrease the number of colonies recovered.

The CFU of EC18LG-0005-1 RifR pHYCTX14 recovered from the steel beads were plotted in a scatter graph to compare the conditions tested (**Figure 5.9**). The results indicated that incubating the cells for longer periods increased the number of colonies that grew on LB agar supplemented with 2 µg/mL cefotaxime to levels similar to the number of cells recovered on drug-free media, although the rate of recovery remained very low on agar supplemented with higher concentrations of the antibiotic. Furthermore, lowering the incubation temperature to 4 °C did not appear to negatively impact the CFU of EC18LG-0005-1 RifR pHYCTX14 recovered from the beads. It was concluded that incubating cells recovered from the biofilm conjugation model in LB w/o NaCl for 120 minutes at 4 °C would allow EC18LG-0005-1 RifR pHYCTX14 to grow on LB agar supplemented with 2 µg/mL cefotaxime.

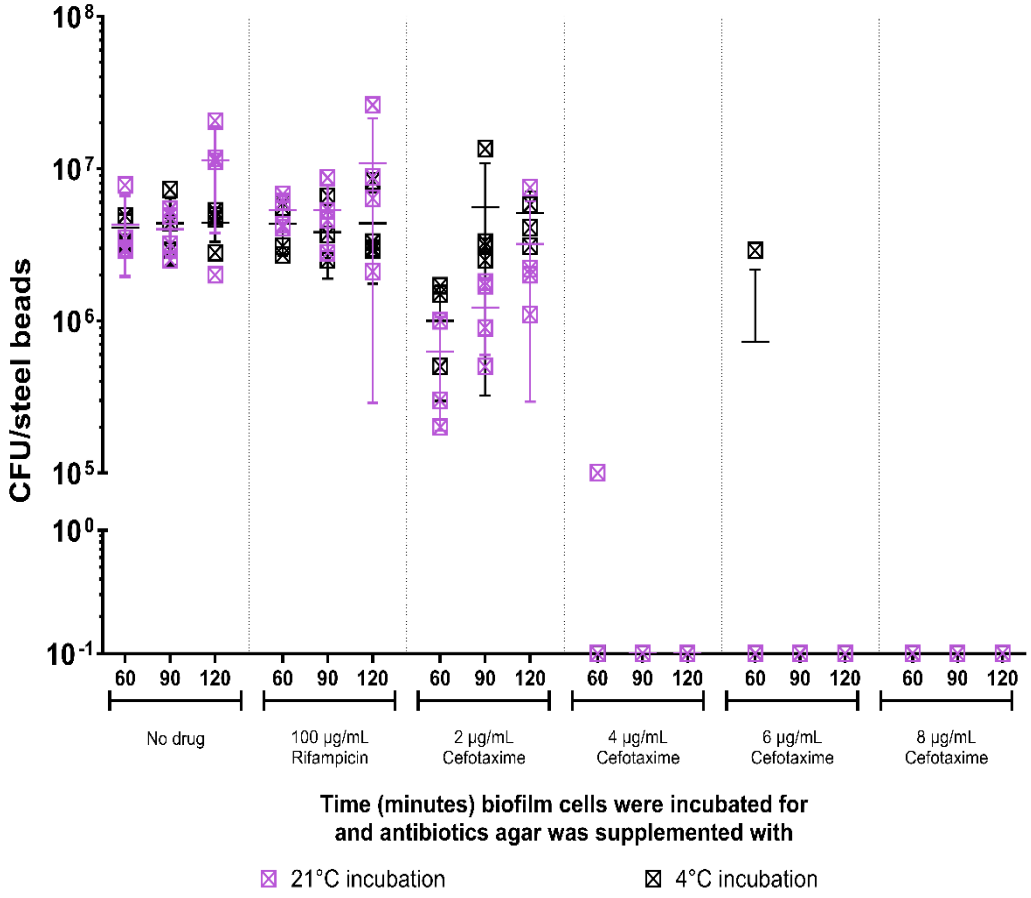

Figure 5.9 - CFU recovered from EC18LG-0005-1 RifR pHYCTX14 biofilms grown on ten steel beads on LB agar supplemented with no drug, LB agar supplemented with 100 µg/mL rifampicin and LB agar supplemented with 2, 4, 6, and 8 µg/mL cefotaxime after incubating in LB w/o NaCl at 21 °C and 4 °C, for 60, 90 and 120 minutes. Data points represent individual replicates. Horizontal lines show the mean, and error bars denote one standard deviation above and below the mean. For data points where zero was recorded, a pseudocount of 0.1 was plotted. The limit of detection was <1 CFU/ beads.

As there was concern that incubating the biofilm cells recovered from the multispecies biofilm at 21 °C for extended periods may lead to an excess outgrowth of transconjugants, as well as some background conjugation of pHYCTX14, which would impact the results in downstream experiments, incubating the cells at 4 °C alleviated this concern as the chances of successful conjugation and bacterial proliferation would be lower given the decreased rate of metabolism in bacterial cells at this temperature.

5.3.3 Optimised recovery of EC18LG-0005-1 RifR pHYCTX14 cells from the biofilm bead model

From the previous experiments, it was determined that recovering biofilm cells from the steel beads in LB w/o NaCl and introducing an incubation step at 4 °C for 120 minutes allowed EC18LG-0005-1 RifR pHYCTX14 to grow on LB agar supplemented with 2 µg/mL cefotaxime. However, it was unclear whether colonies could still be successfully grown on LB agar supplemented with both 100 µg/mL rifampicin and 2 µg/mL cefotaxime after recovery using the optimised method.

To test this, EC18LG-0005-1 RifR pHYCTX14 were grown on steel beads and recovered using the revised protocol before inoculating on LB agar supplemented with no drug, 100 µg/mL rifampicin, 2 µg/mL cefotaxime and both 100 µg/mL rifampicin and 2 µg/mL cefotaxime (**Figure 5.10**). The results indicated that although the average CFU of EC18LG-0005-1 RifR pHYCTX14 recovered on agar supplemented with both rifampicin and cefotaxime was slightly lower compared to when the strain was recovered on agar supplemented with either no drug or just one antibiotic, no significant difference was found between any of the conditions tested (**APPENDIX VI**).

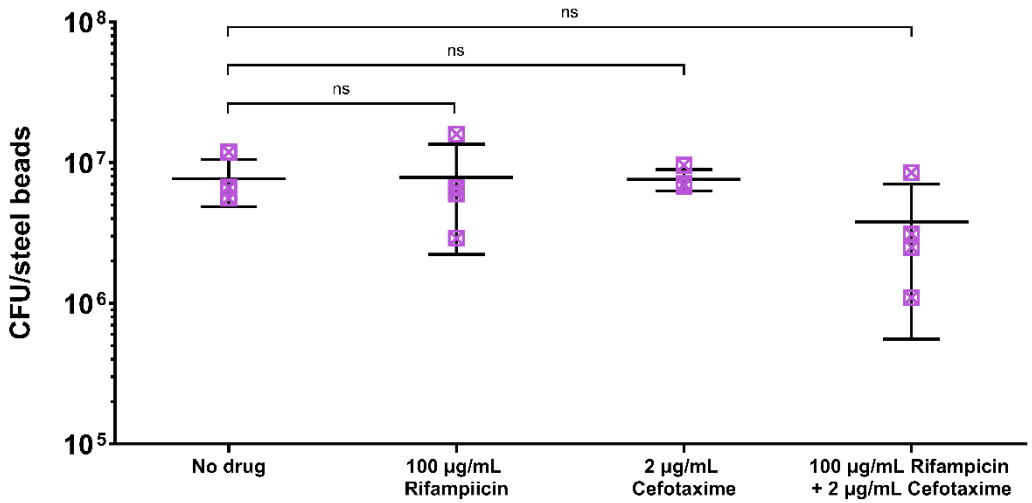

Figure 5.10 - CFU recovered from EC18LG-0005-1 RifR pHYCTX14 biofilms grown on ten steel beads on LB agar supplemented with no drug, LB agar supplemented with 100 µg/mL rifampicin, LB agar supplemented with 2 µg/mL cefotaxime and LB agar supplemented with 100 µg/mL rifampicin 2 µg/mL cefotaxime, after incubating in LB w/o NaCl at 4 °C, for 60, 90 and 120 minutes. Data points represent individual replicates. Horizontal lines show the mean, and error bars denote one standard deviation above and below the mean. No significant difference is represented by 'ns' (no significance). The limit of detection was <1 CFU/ beads.

5.3.3.1 Difficulty recovering strains carrying pHYCTX14 from the biofilm model only appeared to impact *E. coli*

As it was unclear whether the difficulty recovering bacterial isolates carrying pHYCTX14 from the biofilm model was strain specific, *S.* Typhimurium 14028S and EC18PK-0020-1 strains carrying pHYCTX14 (**Chapter 4**) were grown on steel beads and recovered without the 120-minute incubation step at 4 °C. Cells were inoculated onto LB agar plates with no drug as well as agar supplemented with 100 µg/mL of rifampicin or nalidixic acid (depending on the host marker). For plasmid selection, cells were inoculated on agar supplemented with 8 µg/mL cefotaxime, as well as 8 µg/mL cefotaxime with and without 100 µg/mL rifampicin or nalidixic acid as appropriate.

For *S.* Typhimurium 14028S, colonies from the rifampicin and nalidixic acid-resistant strains carrying pHYCTX14 were successfully recovered on all the agar plates (**Figure 5.11**).

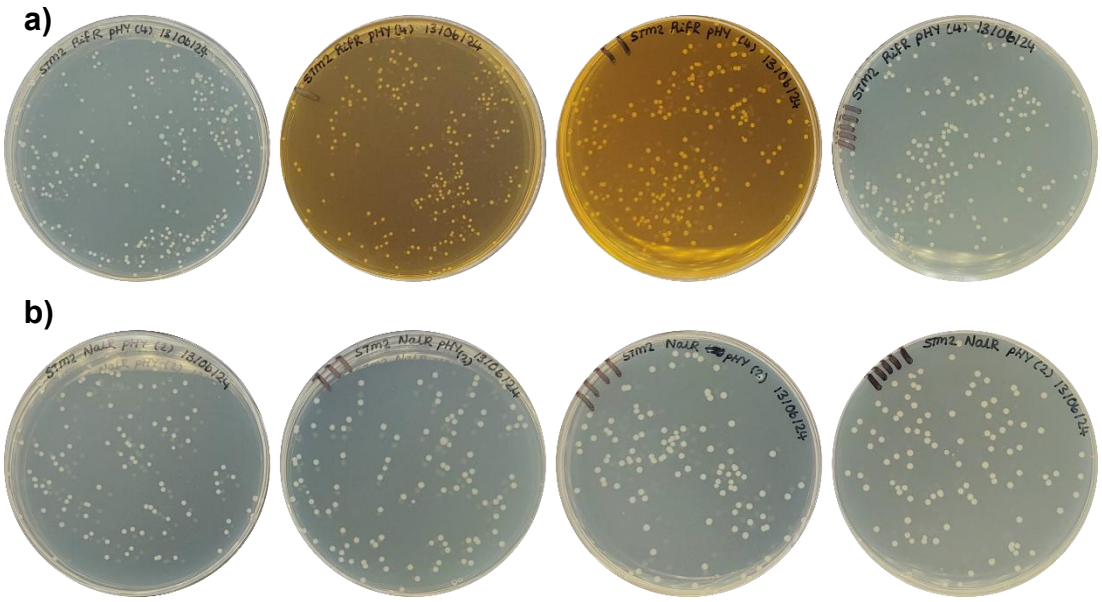

Figure 5.11 - Representative colonies of **a)** *S.* Typhimurium 14028S RifR pHYCTX14 recovered on LB agar supplemented with no drug, 100 µg/mL rifampicin, 100 µg/mL rifampicin and 8 µg/mL cefotaxime, and 8 µg/mL cefotaxime (in order from left to right), and **b)** *S.* Typhimurium 14028S NalR pHYCTX14 biofilms grown on steel beads recovered on LB agar supplemented with no drug, 100 µg/mL nalidixic acid, 100 µg/mL nalidixic acid and 8 µg/mL cefotaxime, and 8 µg/mL cefotaxime (in order from left to right).

For EC18PK-0020-1 strains carrying pHYCTX14, the results were identical to those obtained from EC18LG-0005-1 RifR pHYCTX14, and colonies could not be recovered on agar supplemented with 8 µg/mL cefotaxime, both with and without the addition of rifampicin or nalidixic acid (**Figure 5.12**). As described previously, the presence of the plasmid and *bla*$_{\text{CTX-M-14}}$ was confirmed by randomly selecting colonies from the no-drug plate and streaking onto LB agar supplemented with 8 µg/mL cefotaxime, as well as by PCR reactions, to verify that pHYCTX14, and therefore the *bla*$_{\text{CTX-M-14}}$ gene, had not been lost. The PCR reactions also verified that the *bla*$_{\text{CTX-M-14}}$ had not mobilised into the bacterial chromosome. These results suggested that the difficulties selecting for *bla*$_{\text{CTX-M-14}}$ and therefore pHYCTX14, in strains after recovery from the biofilm model, appeared only to impact *E. coli* in this study.

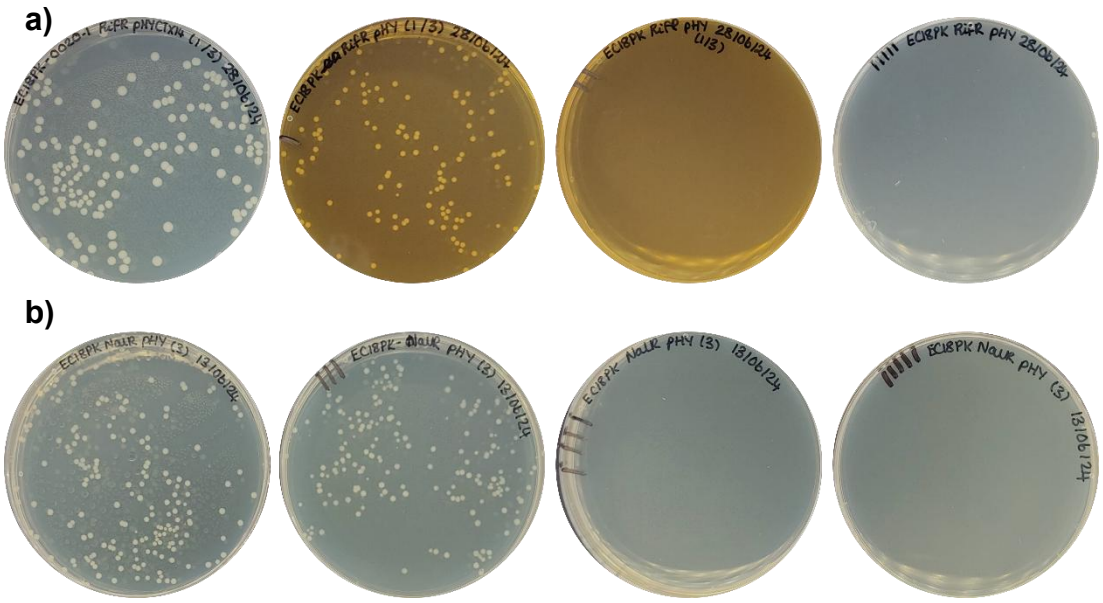

Figure 5.12 - Representative colonies of **a)** EC18PK-0020-1 RifR pHYCTX14 recovered on LB agar supplemented with no drug, 100 µg/mL rifampicin, 100 µg/mL rifampicin and 8 µg/mL cefotaxime, and 8 µg/mL cefotaxime (in order from left to right), and **b)** EC18PK-0020-1 NalR pHYCTX14 biofilms grown on steel beads recovered on LB agar supplemented with no drug, 100 µg/mL nalidixic acid, 100 µg/mL nalidixic acid and 8 µg/mL cefotaxime, and 8 µg/mL cefotaxime (in order from left to right).

5.3.4 Investigating the expression of *bla*$_{CTX-M-14}$ in biofilm and planktonic *E. coli* communities

To test the hypothesis that *bla*$_{CTX-M-14}$ was not actively expressed when *E. coli* cells were grown in a biofilm, primers were designed to measure the expression of pHYCTX14, *bla*$_{CTX-M-14}$ and *gyrB* in biofilm and planktonic EC18LG-0005-1 RifR pHYCTX14 cells using RTqPCR (**Table 5.2**)

Table 5.2 – List of primers for RTqPCR

Primers	Role
bla$_{CTX-M-14}$ (RTqPCR)	Amplification of *bla*$_{CTX-M-14}$ in pHYCTX14 to measure gene expression using RTqPCR
traM (RTqPCR)	Amplification of *traM* in pHYCTX14 to measure gene expression using RTqPCR
gyrB (RTqPCR)	Amplification of *gyrB* in *E. coli* to measure gene expression using RTqPCR

The primers were validated against the target genes of interest using isolated plasmid and genomic DNA. The average cycle threshold (CT) was plotted against $\log_{10}$ DNA copy number to obtain an R^2 value. Typically, an $R^2 > 0.98$ suggests a linear correlation between the experimental data and the regression line, indicating the primer's suitability for RTqPCR (Taylor et al., 2010).

For each reaction, the R^2 was determined (**Table 5.3**), and although not all primers returned $R^2 > 0.98$, they were found to be suitable to quantify gene expression of the required genes to answer the hypothesis. The presence of *gyrB* in the plasmid DNA template suggested that the plasmid DNA previously isolated was not completely free of chromosomal DNA. However, this was unlikely to impact downstream experiments.

Table 5.3 - R^2 value of each primer for plasmid DNA and genomic DNA, obtained by plotting average CT against log_{10} DNA copy number.

Primers	R^2 value	
	Plasmid DNA	Genomic DNA
bla$_{CTX-M-14}$	0.9926	0.8946
traM	0.9763	0.9877
gyrB	0.9866	0.9967

Due to time constraints during this study, no further experiments were undertaken after validation of the designed primers. Future work will aim to complete these experiments to investigate the expression of *bla*$_{CTX-M-14}$ in both biofilm and planktonic EC18LG-0005-1 RifR pHYCTX14 cells.

5.4 DISCUSSION

Of the three *E. coli* food isolates selected from the initial group of ten (**Chapter 4**), EC18LG-0005-1 was selected as the initial isolate used in the biofilm conjugation model, as it represented a common ST (ST10) found in the food survey (Janecko et al., 2023). This ST of *E. coli* has been found to inhabit the gut of various avian species as well as mammals (Zong et al., 2018), and in recent years, has been increasingly isolated from environmental samples (Cardenas-Arias et al., 2024). ST10 has been described as a high-risk lineage for the dissemination of MDR via MGEs, encoding resistance to a range of clinically relevant antibiotics such as cephalosporins, carbapenems and colistin (Fuga et al., 2022). Given that conjugation efficiency will be measured using a plasmid encoding *bla*$_{CTX-M-14,}$ conferring resistance to cephalosporins, in this study, the use of an ST10 *E. coli* in the model was of particular relevance to the real world.

Through initial attempts to conjugate pHYCTX14 between EC18LG-0005-1 RifR pHYCTX14 and *S.* Typhimurium 14028S NalR, it was identified that EC18LG-0005-1 RifR pHYCTX14 biofilm cells could not be directly recovered on LB agar supplemented with 100 µg/mL rifampicin and 8 µg/mL cefotaxime after growing on steel beads, both as a monospecies biofilm and as a mixed species biofilm with *S.* Typhimurium. It was confirmed that the *E. coli* strain was not outcompeted by *S*. Typhimurium in the biofilm, as blue and white

colonies, representing *E. coli* and *Salmonella*, respectively, were recovered at similar rates on agar plates used for blue/white screening. Subsequent investigations also verified that the *E. coli* cells recovered from the biofilm model still encoded *bla*$_{\text{CTX-M-14}}$ on pHYCTX14.

The recovery of EC18LG-0005-1 RifR pHYCTX14 from the biofilm model was optimised by introducing an incubation step at 4 °C for 120 minutes in LB w/o NaCl broth between the recovery of biofilm cells on the steel beads and inoculating onto agar plates supplemented with cefotaxime, as well as by lowering the concentration of cefotaxime from 8 µg/mL to 2 µg/mL. Although incubating the cells at both 4 °C and 21 °C increased the number of colonies recovered, 4 °C was chosen as the ideal temperature, as there would be a lower chance of the plasmid conjugating between cells during the incubation period, which would impact the number of transconjugants recorded in future experiments.

It was hypothesised that the difficulties growing *E. coli* carrying pHYCTX14 biofilm cells on LB agar supplemented with cefotaxime, even after growing the biofilms in media supplemented with a sub-inhibitory concentration of cefotaxime, were caused by a reduction in *bla*$_{\text{CTX-M-14}}$ expression when cells were grown in a biofilm, compared to when grown planktonically, and experiments were planned to investigate this further.

Studies have previously reported changes to bacterial gene expression in response to different environmental stimuli. In *E. coli,* for example, the expression of heat shock proteins via transcription factor σ32 increases when cells are under stress from elevated temperatures (Pérez-Morales et al., 2025). Additionally, changes in bacterial gene expression have also been observed when bacteria grow as a biofilm (Sauer et al., 2022). For instance, biofilm formation in bacteria is often promoted by an increase in intracellular c-di-GMP levels (Mhatre et al., 2020), which can be involved in the regulation of multiple stages in the biofilm lifecycle (Alotaibi and Bukhari, 2021). In *P. aeruginosa*, c-di-GMP can regulate initial attachment of cells by binding to the transcription regulator of flagellar gene expression, FleQ, which reduces cell motility. c-di-

GMP can also regulate biofilm maturation by increasing the production of EPS (Alotaibi and Bukhari, 2021).

It has been found that in the absence of selective pressure, expression of AMR genes can lead to a negative impact on bacterial fitness. In some cases, silencing of AMR genes has been found to benefit host fitness. For example, silencing of genes encoded on the RP1 plasmid has been found to benefit *E. coli* (Humphrey et al., 2012). Additionally, in an *in vivo* study investigating the expression of AMR genes encoded on plasmids, the silencing of *aadA1*, *bla*$_{\text{OXA-2}}$, *sul1*, and *tetA*, encoded on the IncN plasmid pVE46, was observed in a small sample of *E. coli* isolated from faecal samples of piglets that were orally inoculated with the bacteria. This suggests that AMR gene silencing is not unique to experiments conducted under laboratory conditions, and may occur in real-world environments (Enne et al., 2006). The impacts of biofilm formation on plasmid copy number and expression of AMR genes have also been studied previously in species such as *E. faecalis*, where an increase in plasmid copy number was observed in a subpopulation of biofilm cells (Cook and Dunny, 2013). However, the majority of research appears to focus on the impact of plasmid carriage on biofilm formation, and studies investigating the expression of genes, including AMR genes, encoded on plasmids within biofilm populations of bacteria appear to be limited.

The silencing of *bla*$_{\text{CTX-M-14}}$ raises interesting questions on the maintenance and detection of AMR genes, particularly those encoded on plasmids, where plasmids and their associated AMR genes may be maintained undetected in bacterial populations. This could lead to inaccurate susceptibility testing where resistance traits are hidden, potentially leading to the silent spread of AMR genes from seemingly non-problematic bacterial species and communities to those that are pathogenic, exacerbating the AMR crisis overall.

5.5 CONCLUSIONS

This chapter describes the optimisation of the biofilm conjugation model to allow the rate of pHYCTX14 conjugation between *E. coli* and *S.* Typhimurium within a biofilm community to be measured accurately.

Although it was not possible to complete the experiments designed to explore the expression of $bla_{CTX\text{-}M\text{-}14}$ in biofilm and planktonic *E. coli* cultures during this project, it would be useful to continue these experiments in the future, as they may provide new information regarding the impacts of biofilm formation on the expression of plasmid-encoded genes.

Furthermore, it was interesting that the difficulties encountered when selecting for $bla_{CTX\text{-}M\text{-}14}$ and therefore pHYCTX14, in strains after recovery from the biofilm model, were only observed in *E. coli*. Although the reason for this was unclear, additional investigations using other strains of *E. coli*, as well as other Gram-negative species of bacteria, would help to develop a clearer understanding of which bacterial strains and species exhibit this characteristic.

Although there were difficulties with determining conjugation phenotypically using the resistance marker encoded on pHYCTX14, alternative strategies, such as tagging the plasmid with either a fluorescent marker or another AMR gene, were not explored during this study. This was due to the desire to keep all factors of the experiments as close to the 'real-world' as possible, with minimal genetic manipulation that could have impacted the plasmid/ the plasmid host. Genetic manipulation of the plasmid would also have removed some of the 'real-world' relevance of the biofilm conjugation model.

Chapter 6 describes the use of the biofilm conjugation model to measure the impact of various stressors on the rate of pHYCTX14 conjugation between *E. coli* and *S.* Typhimurium.

CHAPTER 6:
INVESTIGATING THE RATE OF PLASMID MOVEMENT IN A MULTISPECIES BIOFILM UNDER STRESS

"If we knew what it was we were doing, it would not be called research, would it?"

< Albert Einstein >

6.1 INTRODUCTION

In **Chapter 5**, the multispecies biofilm conjugation model was optimised to allow plasmid movement between *E. coli* and *S.* Typhimurium to be measured.

The induction and impact of various chemicals on plasmid transfer between single species and communities of bacteria have been investigated in the past. These chemicals have included sub-inhibitory concentrations of antibiotics, such as meropenem and ciprofloxacin, that have been found to increase conjugation efficiency from *Klebsiella* to *E. coli* (Ding et al., 2022). Additionally, ciprofloxacin has also been found to increase plasmid movement from *Pseudomonas* (Shun-Mei et al., 2018) to *E. coli*. These studies have focused on using planktonic bacteria either in liquid or filter mating assays. The impact of regularly used non-antibiotic pharmaceuticals, such as ibuprofen and naproxen, on plasmid movement has also been studied previously, and these have been found to promote conjugation in microbial communities, such as those in activated sludge systems (Wang et al., 2022).

Aside from pharmaceutical related chemicals, it has previously been suggested that the HGT of plasmids encoding AMR genes can also be exacerbated by non-pharmaceutical related stresses present in the food processing environment (Zarzecka et al., 2022). Given that both *E. coli* and *S.* Typhimurium are commonly found in food products (He et al., 2023, Szmolka and Nagy, 2013), and the parent strain of the *E. coli* donor, EC18LG-0005-1 RifR pHYCTX14, used in the model, was also isolated from leafy greens in a food survey (Janecko et al., 2023), a number of food chain-related preservatives and supplements were selected to be used in the biofilm conjugation model to investigate the impact of various stressors on conjugation efficiency within a biofilm context. The use of food chain-related stressors was particularly relevant to the real world, especially given the role that biofilms play in the persistent contamination of environments related to the food industry (Van Houdt and Michiels, 2010, Rossi et al., 2014)

Preservatives that have previously been found to increase the rate of plasmid movement include artificial sweeteners (Alav and Buckner, 2024), sodium nitrite, sodium benzoate and triclocarban (Cen et al., 2020), as well as acidifiers such as phosphoric and citric acid (Zhang et al., 2025b).

For this study, sodium nitrite, sodium benzoate and sodium chloride, which are commonly used as additives in human food preparation, were chosen to be tested in the biofilm conjugation model. Sodium nitrite and sodium benzoate have been previously shown to affect the rate of conjugation in planktonic bacteria (Cen et al., 2020). Sodium chloride and sodium nitrite have also been recently investigated for their mechanisms of action and resistance in S. Typhimurium (Holden et al., 2025;. Aside from evidence on their impact on conjugation efficiency from previous research, these preservatives were also chosen for use in this study as they have been previously used by the group in biofilm experiments and were readily available.

Copper, which is often used both as an antimicrobial (Parra et al., 2018) and as a food supplement in food-producing animals (Espinosa and Stein, 2021), was also selected to be used in the biofilm conjugation model (as copper sulphate solution) as it has previously been found to decrease conjugation efficiency in bacteria (Palm et al., 2022).

Additionally, ciprofloxacin (cipro) and cefotaxime (cef) were also chosen to be used as stressors in the biofilm conjugation model. Ciprofloxacin has previously been suggested to significantly increase conjugation efficiency of pUCP24T between *E. coli* and *P. aeruginosa* (Shun-Mei et al., 2018), and as pHYCTX14 encodes $bla_{\text{CTX-M-14}}$, which confers resistance to cephalosporins such as cefotaxime, it was decided to investigate whether a subinhibitory concentration of cefotaxime would promote conjugation of the plasmid.

6.2 AIMS AND OBJECTIVES

- Select food chain-related preservatives and supplements previously found to impact conjugation rate.
- Determine the appropriate concentrations of chemicals to use in the biofilm conjugation model.
- Obtain a baseline rate of pHYCTX14 transfer from EC18LG-0005-1 RifR pHYCTX14 to *S.* Typhimurium 14028S NalR within a biofilm under no stress.
- Investigate the impact of different stressors on pHYCTX14 conjugation efficiency between EC18LG-0005-1 RifR pHYCTX14 and *S.* Typhimurium 14028S NalR within a multispecies biofilm community.

6.3 RESULTS

A range of food chain-related preservatives and supplements (**Table 6.1**), some previously found to affect the rate of plasmid movement, were selected alongside ciprofloxacin and cefotaxime to investigate the impact of environmental stressors on the conjugation efficiency of pHYCTX14 between EC18LG-0005-1 RifR pHYCTX14 and *S.* Typhimurium 14028S NalR within a biofilm context. Some of the preservatives selected have also recently been characterised for mechanisms of action and resistance in *S.* Typhimurium (Holden et al., 2025, Assaf et al., 2023).

Table 6.1 – Food chain-related chemicals previously found to affect the rate of plasmid movement.

Chemical	Impact on conjugation efficiency	Reference
Sodium nitrite ($NaNO_2$)	Increase	(Cen et al., 2020)
Sodium benzoate (C_6H_5COONa)	Increase	(Cen et al., 2020)
Sodium chloride (NaCl)	N/A	N/A
Copper sulphate (Cu)	Decrease	(Palm et al., 2022)

6.3.1 Determining the optimum concentrations of stressors to use in the biofilm conjugation model

To determine the optimum concentration of each chemical to use in the biofilm conjugation model, the fitness of EC18LG-0005-1 RifR pHYCTX14 and *S.* Typhimurium 14028S NalR was measured by growing the bacteria planktonically in LB w/o NaCl supplemented with the appropriate chemical at a range of concentrations (**Table 6.2**). Planktonic cultures were grown in 96-well plates, and absorbance at 600 nm was measured every 20 minutes for 18 hours to obtain growth curves. A bacterial control grown in LB w/o NaCl, without additional chemicals, and a broth sterility control were included in every 96-well plate. For bacterial growth under stress from ciprofloxacin and cefotaxime, growth curves were only obtained for the donor or recipient strain, respectively, as the donor strain is resistant to cefotaxime and the recipient strain is resistant to ciprofloxacin.

Table 6.2 – Concentrations of chemicals tested against EC18LG-0005-1 RifR pHYCTX14 and/or *S.* Typhimurium 14028S NalR in planktonic cultures. The corresponding figures of the growth curves obtained for each chemical and the concentration of the chemical selected to be used in the biofilm conjugation model are also provided.

Chemical	Concentrations tested	Corresponding figure	Concentration chosen for the biofilm conjugation model
Ciprofloxacin	0 - 0.006 µg/mL	6.1	0.006 µg/mL
Cefotaxime	0 – 0.5 µg/mL	6.2	0.125 µg/mL
Sodium nitrite	0 – 0.1%	6.3	0.06%
Sodium benzoate	0 – 0.8%	6.4	0.05%
Sodium chloride	0 – 15%	6.5	2.5%
Copper sulphate	0 – 3 mM	6.6	0.15 mM

Where growth curves were obtained for both the donor and recipient strain, the optimum concentration of chemicals chosen for the biofilm conjugation model was determined, where the growth curves indicated a reduction in EC18LG-0005-1 RifR pHYCTX14 growth where possible (**Figures 6.1 – 6.6**). The chemicals chosen for this study had an impact on the fitness of both

EC18LG-0005-1 RifR pHYCTX14 and S. Typhimurium 14028S NalR. However, due to time constraints, these experiments were limited to investigating the impact of these chemicals on conjugation efficiency within a biofilm, where the fitness of the donor strain was more strongly affected compared to the recipient strain.

For ciprofloxacin (**Figure 6.1**), an initial concentration of 0.06 µg/mL was selected for use in the biofilm model, as the results indicated that 0.006 µg/mL did not impact the fitness of EC18LG-0005-1 RifR pHYCTX14 in planktonic cultures. However, when LB w/o NaCl was supplemented with 0.06 µg/mL ciprofloxacin in the biofilm conjugation model, this concentration of the antibiotic completely restricted the growth of the donor strain. Therefore, the concentration of ciprofloxacin used in the biofilm conjugation model was lowered to 0.006 µg/mL.

For copper sulphate (**Figure 6.6**), the growth curve suggested that 1.5 mM would provide sufficient stress on the *E. coli* isolate. However, this concentration had a significant impact on the survival of both EC18LG-0005-1 RifR pHYCTX14 and *S.* Typhimurium 14028S NalR in a biofilm. Therefore, the final concentration selected to be used in the biofilm conjugation model was reduced to 0.15 mM.

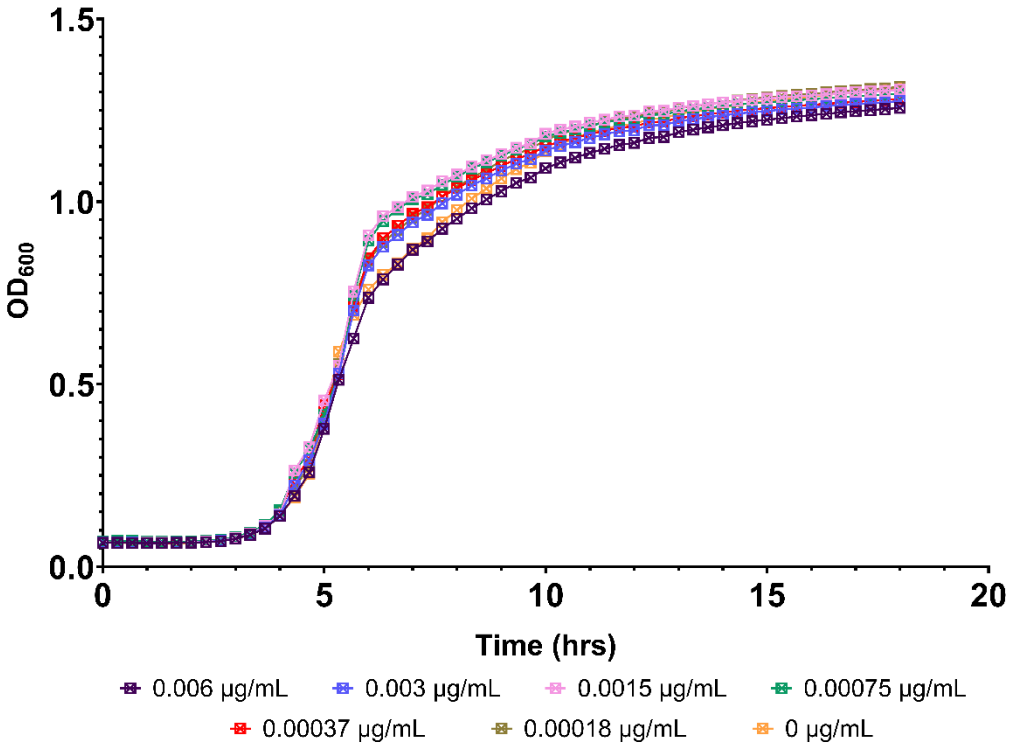

Figure 6.1 – Growth curves of EC18LG-0005-1 RifR pHYCTX14 grown in LB w/o NaCl broth supplemented with ciprofloxacin at a range of concentrations. Absorbance ($OD600_{nm}$) was measured every 20 minutes for 18 hours. Four biological replicates were included per concentration of antibiotic and data points represent the mean OD600nm.

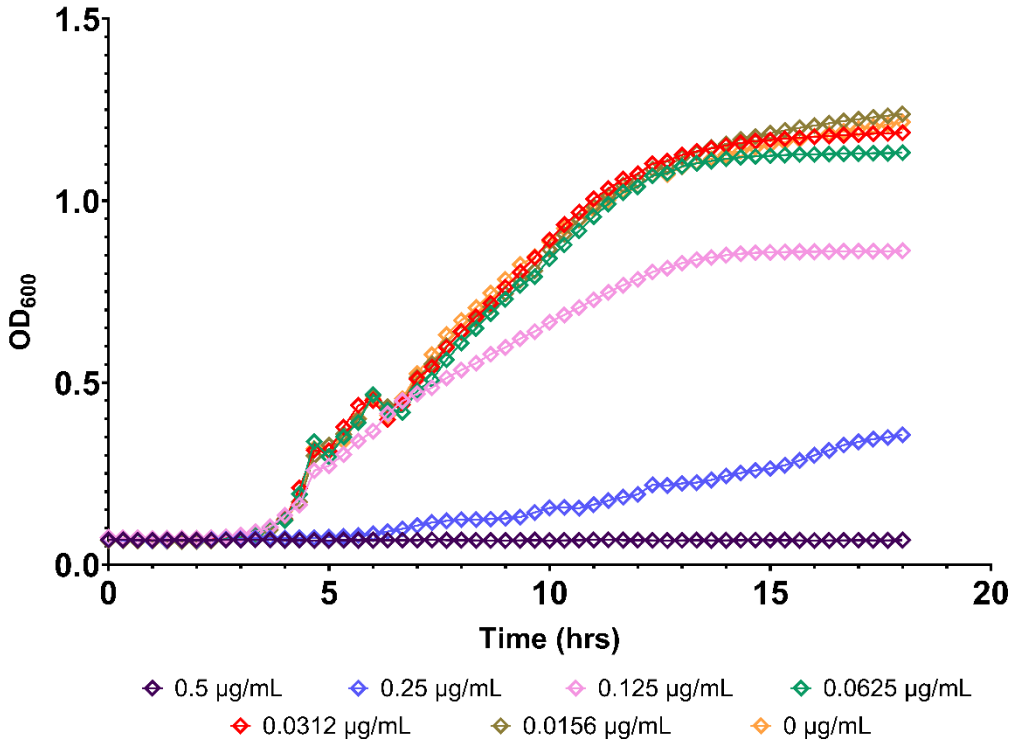

Figure 6.2 – Growth curves of *S.* Typhimurium 14028S NalR grown in LB w/o NaCl broth supplemented with cefotaxime at a range of concentrations. Absorbance ($OD600_{nm}$) was measured every 20 minutes for 18 hours. Four biological replicates were included per concentration of antibiotic and data points represent the mean OD600nm.

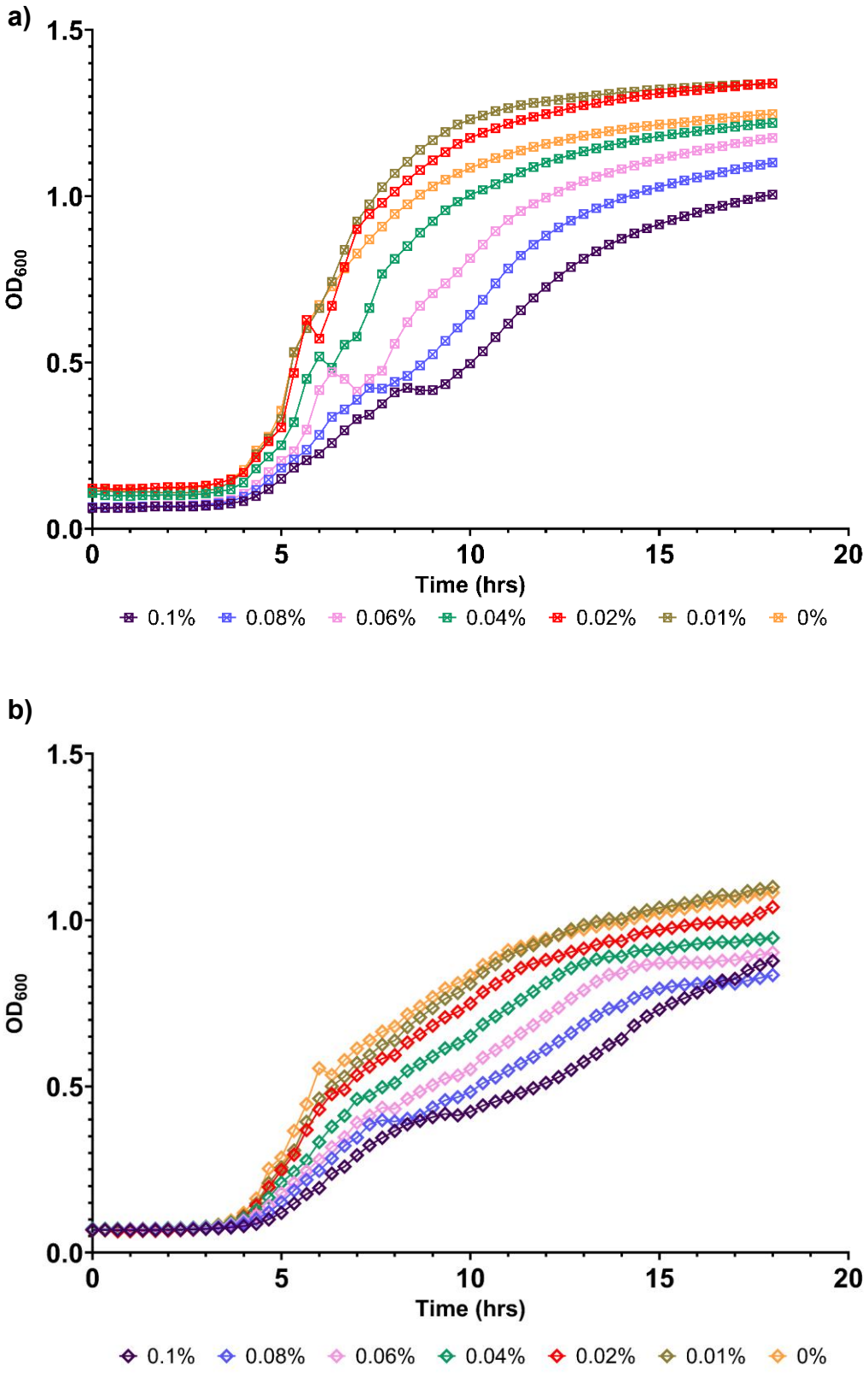

Figure 6.3 – Growth curves of **a)** EC18LG-0005-1 RifR pHYCTX14 and **b)** *S.* Typhimurium 14028S NalR grown in LB w/o NaCl broth supplemented with sodium nitrite at a range of concentrations. Absorbance ($OD600_{nm}$) was measured every 20 minutes for 18 hours. Four biological replicates were included per concentration of antibiotic and data points represent the mean OD600nm.

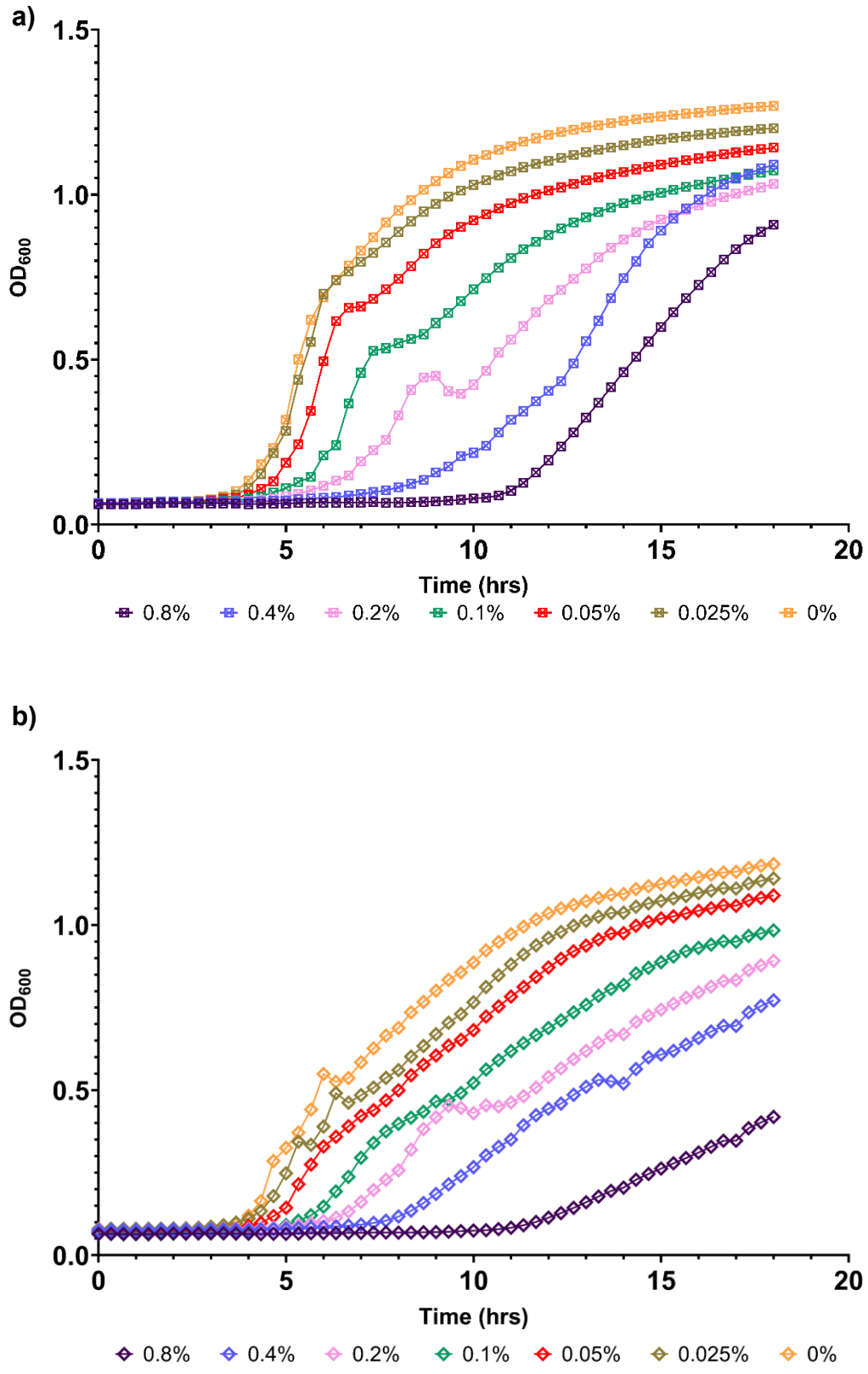

Figure 6.4 – Growth curves of **a)** EC18LG-0005-1 RifR pHYCTX14 and **b)** *S.* Typhimurium 14028S NalR grown in LB w/o NaCl broth supplemented with sodium benzoate at a range of concentrations. Absorbance ($OD600_{nm}$) was measured every 20 minutes for 18 hours. Four biological replicates were included per concentration of antibiotic and data points represent the mean OD600nm.

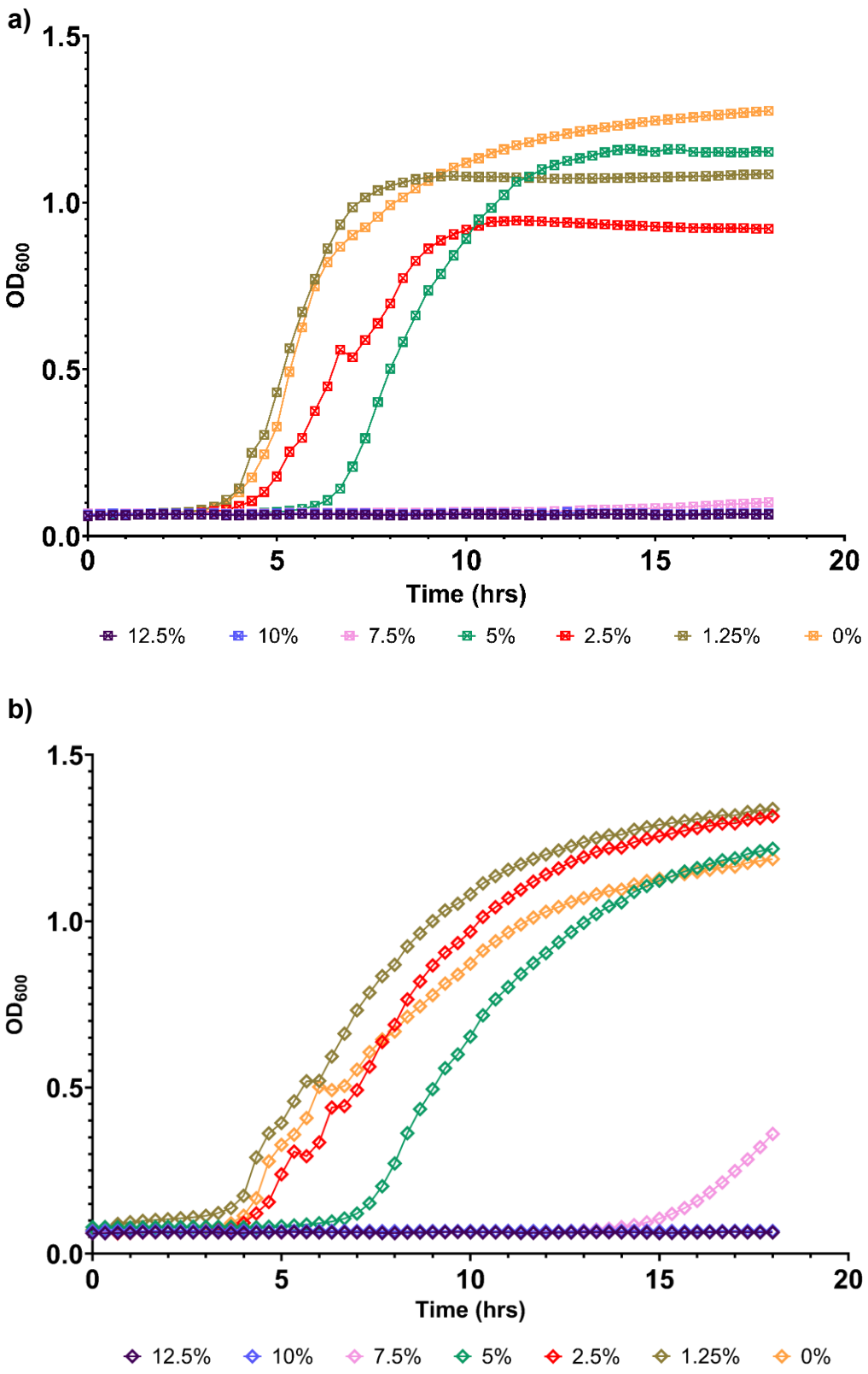

Figure 6.5 – Growth curves of **a)** EC18LG-0005-1 RifR pHYCTX14 and **b)** *S.* Typhimurium 14028S NalR grown in LB w/o NaCl broth supplemented with sodium chloride at a range of concentrations. Absorbance ($OD600_{nm}$) was measured every 20 minutes for 18 hours. Four biological replicates were included per concentration of antibiotic and data points represent the mean OD600nm.

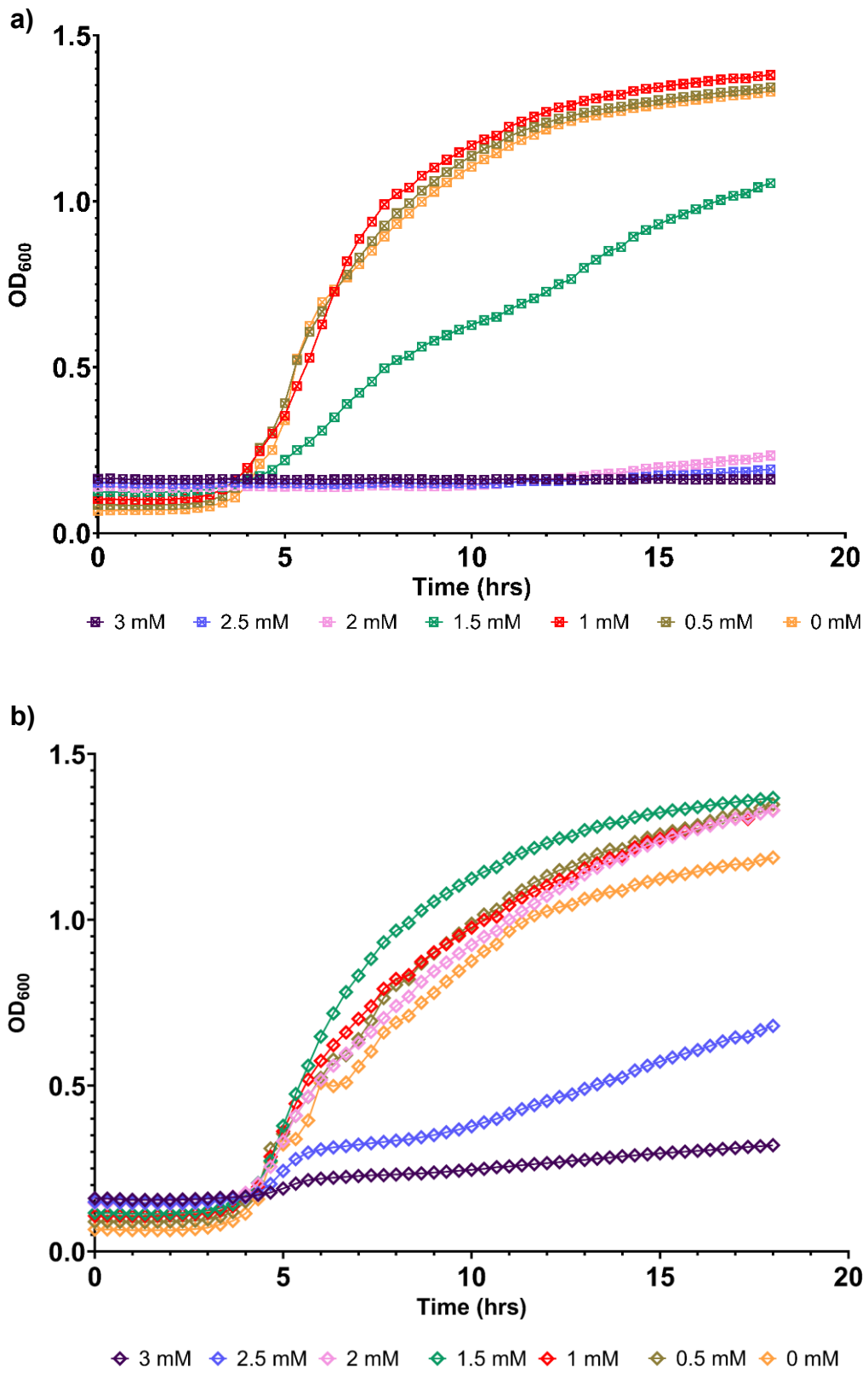

Figure 6.6 – Growth curves of **a)** EC18LG-0005-1 RifR pHYCTX14 and **b)** *S.* Typhimurium 14028S NalR grown in LB w/o NaCl broth supplemented with copper sulphate at a range of concentrations. Absorbance ($OD600_{nm}$) was measured every 20 minutes for 18 hours. Four biological replicates were included per concentration of antibiotic and data points represent the mean OD600nm.

6.3.2 Establishing a baseline rate of pHYCTX14 conjugation under no stress

After optimising the biofilm conjugation model to select for the donor cells after recovery from the steel beads (**Chapter 5**), conjugation of pHYCTX14 from EC18LG-0005-1 RifR pHYCTX14 to *S.* Typhimurium 14028S NalR, following the optimised protocol, was attempted to establish a baseline conjugation efficiency under no stress. As the number of transconjugants recovered from the model was expected to be low, cells recovered from the multispecies biofilm model were not diluted before inoculating onto LB agar supplemented with 100 µg/mL rifampicin and 2 µg/mL cefotaxime to select for transconjugants. Colonies recovered on LB agar supplemented with antibiotics for transconjugant selection were randomly selected to cross-check the species of the colonies recovered, as well as check for plasmid presence or absence, using PCR as detailed previously (**Chapter 4**). The recovered transconjugant colonies were also streaked onto XLD and Brilliance *Salmonella* agar to check their phenotype. The number of colonies recovered on the plates were recorded to calculate CFU, which was then used to calculate conjugation efficiency. The presence of transconjugants in the planktonic phase of the conjugation model was also investigated, and it was confirmed that no transconjugants were present in the planktonic population of bacterial cells. Hence, the results obtained were reflective of conjugation within the biofilm.

The results showed that pHYCTX14 could be successfully conjugated from EC18LG-0005-1 RifR pHYCTX14 to *S.* Typhimurium 14028S NalR (**Figure 6.7**). There was some variation in conjugation efficiency between the two experimental batches. However, no significance was found between the average conjugation efficiency obtained (Welch's *t*-test $p = 0.4151$).

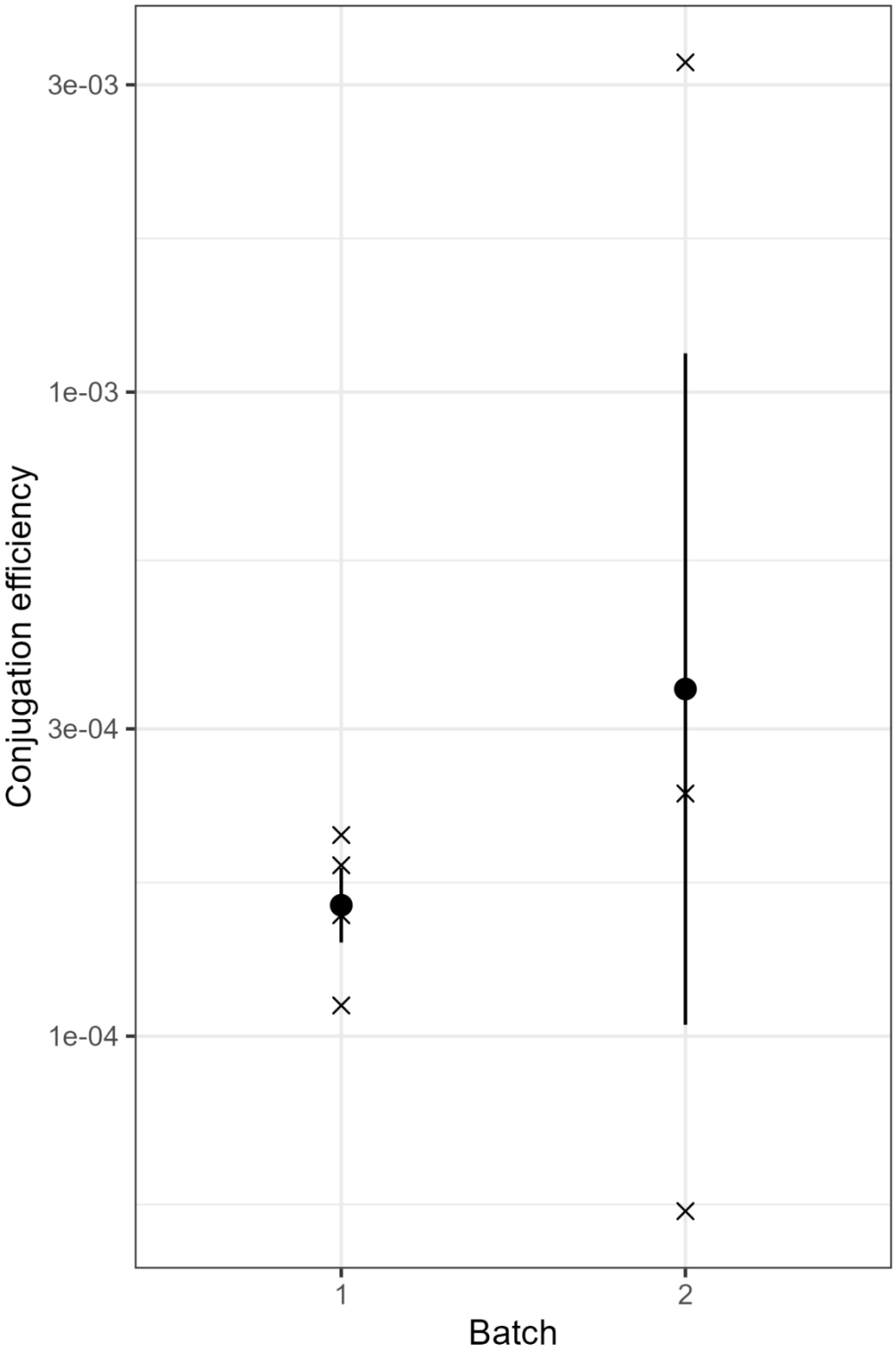

Figure 6.7 - Conjugation efficiency of pHYCTX14 from EC18LG-0005-1 RifR pHYCTX14 to *S.* Typhimurium 14028S NalR under no stress across experimental batches. Crosses represent individual replicates. Points show the mean, and errors bars denote one standard deviation above and below the mean.

6.3.3 Measuring conjugation efficiency under different conditions

After the baseline rate of conjugation under no stress was established, the conjugation efficiency of pHYCTX14 under the selected stressors was explored.

6.3.3.1 A strong batch effect was observed

Given the complexity of the experiments and the need for a very large number of plates in each run, different stressors were investigated in a series of repeated experiments constituting different 'batches'.

Initial analysis of the data showed variation between conditions, with the conjugation rate being higher in the no-stress controls and generally lower after stressors were introduced. Significantly fewer transconjugants were seen after ciprofloxacin exposure, in contrast to previous reports in *Pseudomonas*.

There was, however, a strong batch effect observed across experimental replicates with some stressors, for example, cefotaxime and sodium chloride, showing large variation between batches (**Figure 6.8**). Given these results, the in-house statistician was consulted to help analyse this data to account for batch effects.

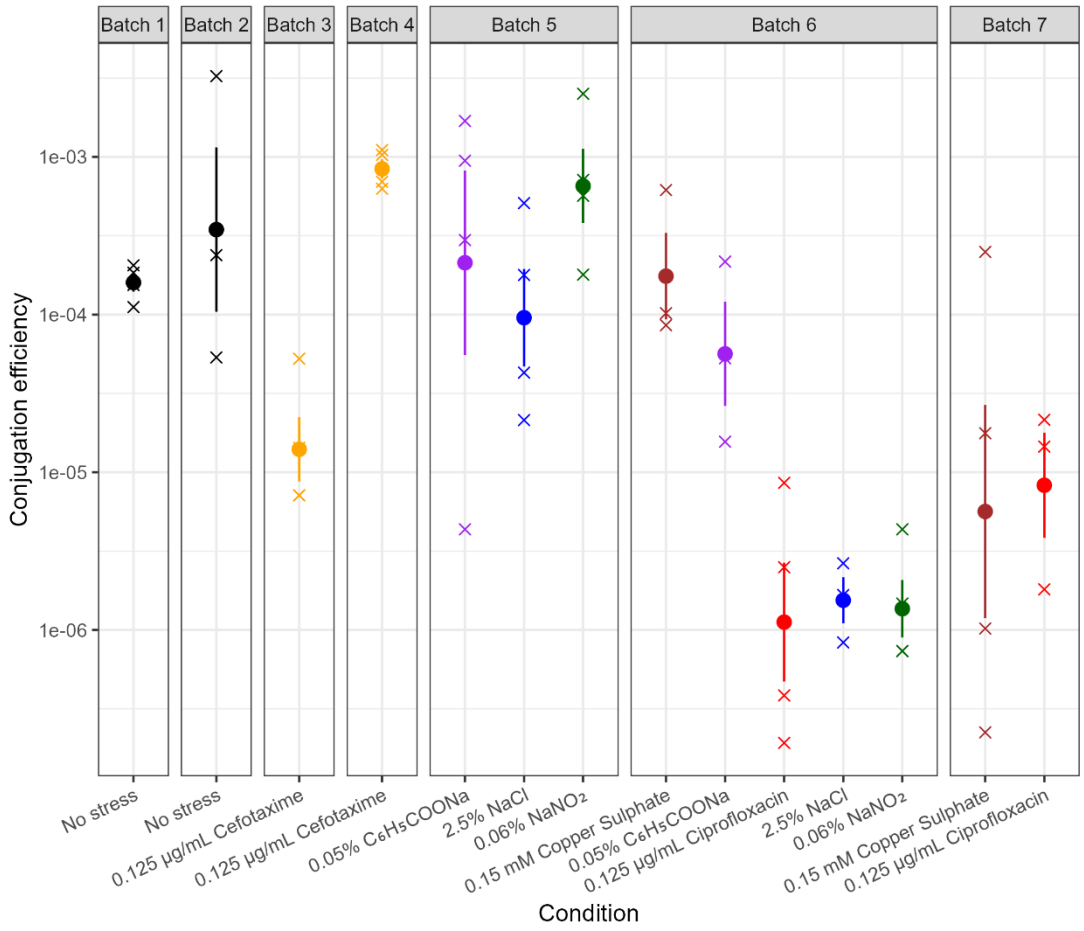

Figure 6.8 – Conjugation efficiency of pHYCTX14 from EC18LG-0005-1 RifR pHYCTX14 to *S.* Typhimurium 14028S NalR under different conditions across experimental batches. Crosses represent individual replicates. Points show the mean, and errors bars denote one standard error above and below the mean. For replicates where a zero was recorded, a pseudocount of half the smallest non-zero value in that condition/batch across replicates was plotted.

6.3.3.2 The starting concentrations of donors vs recipients differed between experimental batches

To investigate whether the ratio of donor and recipient cells at the beginning of the experiment was the cause of this batch effect, the CFU of EC18LG-0005-1 RifR pHYCTX14 and *S.* Typhimurium 14028S NalR at time zero was plotted (**Figure 6.9**).

The results showed that there was a very close correlation between the starting populations of donor to recipient inoculated into the biofilm conjugation model within each replicate. Though there was a strong difference between the starting populations of donor and recipient between experimental batches. However, there was no evidence that the starting concentrations of the donor or recipient impacted the number of transconjugants recovered at the end of the experiments.

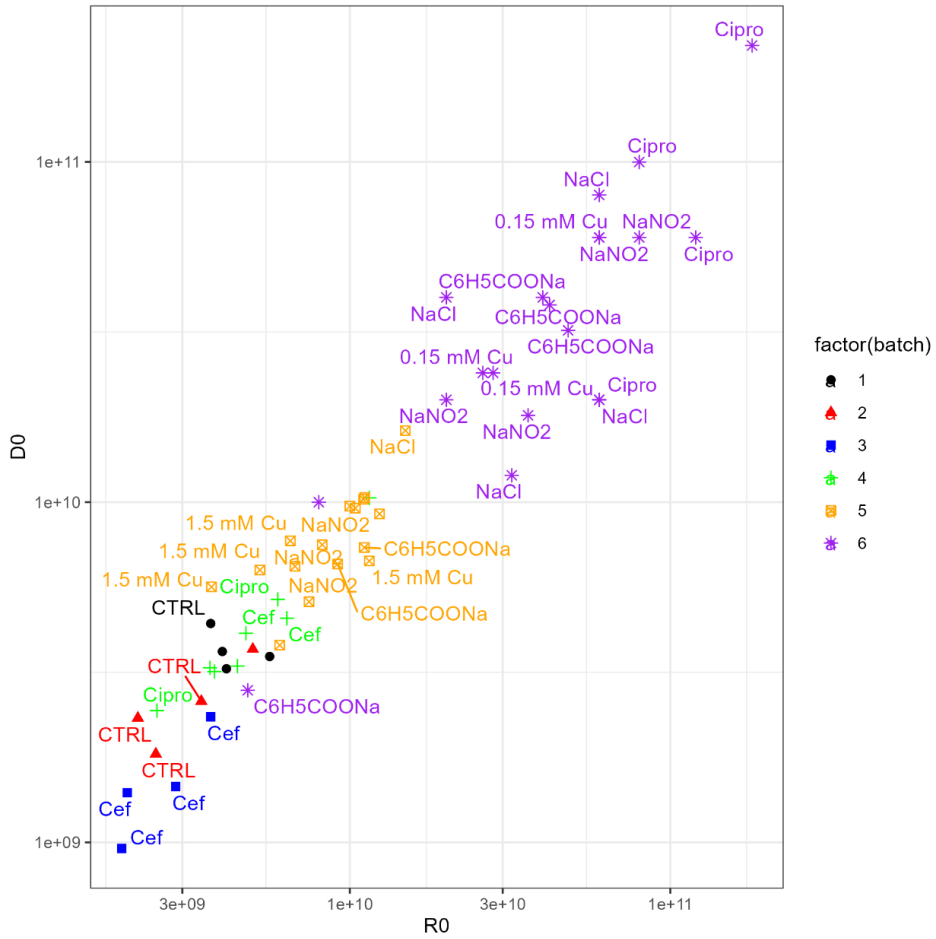

Figure 6.9 – Starting CFU of *S.* Typhimurium 14028S NalR (R0) and EC18LG-0005-1 RifR pHYCTX14 (D0) inoculated into the biofilm conjugation model for individual replicates across experimental batches and conditions. The limit of detection was <1 CFU/ beads.

6.3.3.3 The stressors tested had different impacts on conjugation efficiency

To statistically compare the differences in conjugation efficiency between experimental conditions, regression models of the data obtained were estimated, normalising for the batch effect. Data from experimental batches five to seven were used for this analysis, as these were the only batches with more than one condition. It was also not possible to compare the conjugation efficiency of pHYCTX14 obtained for the unstressed controls with the data obtained for the different stressors, limiting the comparison to a relative evaluation of the impact of different stresses on the rate of conjugation.

Regression analysis of the data showed that there were potentially large effects, of between 10 and 100-fold change in conjugation efficiency between some of the experimental conditions (**Figure 6.10**). Copper sulphate appeared to have the lowest impact on conjugation efficiency compared to the other conditions tested (**Figure 6.8 and Figure 6.10**), and the lowest conjugation efficiency was obtained for experiments supplemented with sodium chloride. However, whilst there was a 100-fold range between conjugation rates for the different stressors, the estimation of pairwise differences did not show any statistically significant changes between the stresses tested (**APPENDIX VII**).

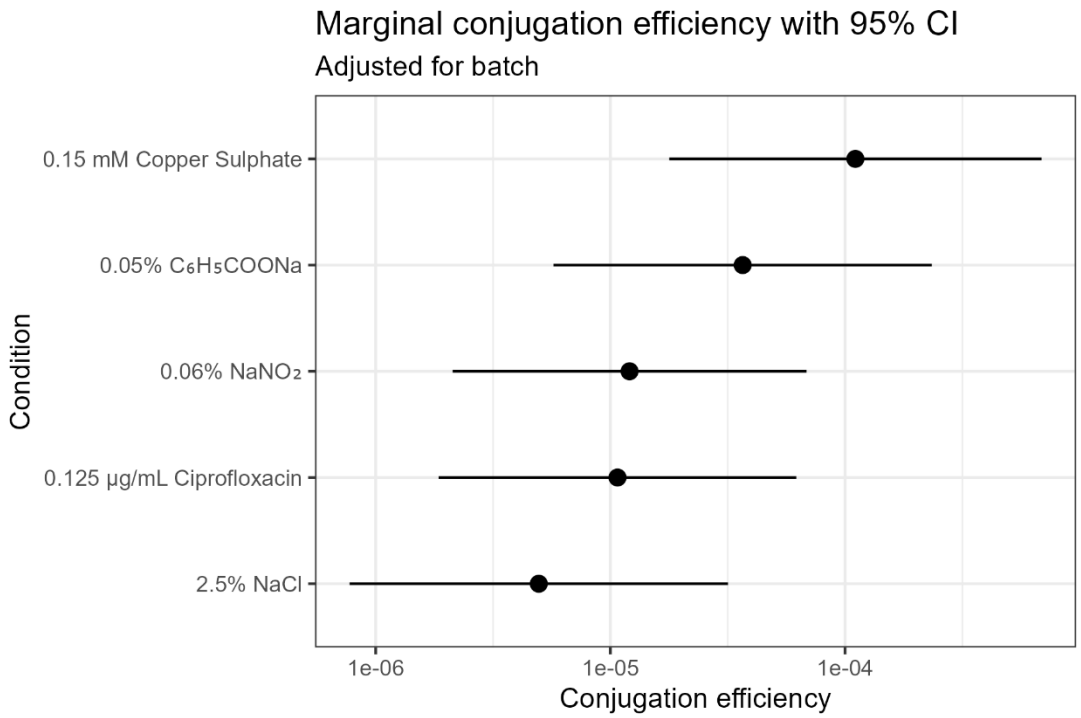

Figure 6.10 – Regression analysis of pHYCTX14 conjugation efficiency from EC18LG-0005-1 RifR pHYCTX14 to *S.* Typhimurium 14028S NalR adjusting for the batch effect. Points denote the mean conjugation efficiency and errors bars show the 95% confidence interval.

6.4 DISCUSSION

Using the biofilm conjugation model, the impact of a range of stressors on the rate of plasmid movement between *E. coli* and *S.* Typhimurium was investigated.

From the results obtained, there was evidence that the chemicals tested had an impact on the conjugation rate of pHYCTX14 between EC18LG-0005-1 RifR pHYCTX14 and *S.* Typhimurium 14028S NalR, with a spectrum between copper sulphate and sodium chloride when compared with the other experimental conditions. However, given the batch effect, there were no statistically significant differences between the rate of conjugation obtained for different experimental conditions when estimating pairwise differences.

It was particularly interesting that ciprofloxacin did not appear to increase the rate of pHYCTX14 movement between *E. coli* and *S*. Typhimurium, as recent research has suggested that this antibiotic can promote the movement of plasmids between bacteria such as *E. coli*, *Shigella sonnei* and *P. aeruginosa*

(Thanh Duy et al., 2020, Shun-Mei et al., 2018). Furthermore, the results also suggested that copper sulphate had the lowest impact on conjugation efficiency compared to other stressors tested, although copper sulphate was previously reported to significantly decrease the conjugation efficiency of an IncF plasmid by nearly 100-fold in *E. coli* (Palm et al., 2022). Sodium nitrite and sodium benzoate both led to lower rates of plasmid movement compared to the other experimental conditions, though subinhibitory concentrations of these food preservatives have formerly been found to increase plasmid transfer between two strains of *E. coli* in a study investigating the impact of preservatives on plasmid-mediated transfer of AMR genes (Cen et al., 2020).

These earlier studies have focused on measuring conjugation efficiency using liquid or filter conjugation assays, and it is possible that the chemicals may impact the rate of conjugation differently when bacteria are within a biofilm context. Additionally, some studies, such as those investigating the impact of ciprofloxacin (Shun-Mei et al., 2018), pre-grew the donor strain with a subinhibitory concentration of the drug, and the antibiotic was not used during the conjugation assays. It would be interesting to explore whether exposing the donor and/or recipient strains to the chemicals prior to conjugation would lead to different impacts on conjugation efficiency within biofilms in the future.

6.5 CONCLUSIONS

Overall, the stressors selected had different impacts on the rate of pHYCTX14 movement between EC18LG-0005-1 RifR pHYCTX14 and *S.* Typhimurium 14028S NalR within a biofilm. However, it was difficult to draw conclusions from these results as an unstressed control was not included in every experiment, and the results obtained could not be used to determine the impacts of the chemicals tested on conjugation efficiency in comparison to the unstressed condition. Going forward, repeating these experiments and including an unstressed control with every experimental condition, as well as testing chemicals against each other in some experiments, would allow these comparisons to be made. Obtaining additional data may also allow for more sophisticated statistical analyses. Furthermore, improving the experimental design, for example by increasing the number of samples taken from each

biological replicate, and standardising the inoculum at the beginning of the experiment across experimental batches, may reduce the variation in the CFU data collected. As whilst the inoculums were standardised by OD between batches, counting of the CFU showed that this worked well within batches, but there was still divergence between batches.

An additional limitation of this study was that the conjugation efficiency was not determined for the planktonic phase in the presence of chemicals. This was owing to the observation that there were no transconjugants recovered from the planktonic phase under no stress condition, suggesting that the planktonic phase would not be relevant given the high rate of transfer during conjugation experiments conducted on filters. However, it may be advantageous to also explore rate of plasmid movement in this context in the future.

Although this project explored plasmid conjugation within a simple multispecies biofilm community, it represents one of the first studies investigating the evolution of AMR within multispecies biofilms. It gives new information on how external stresses can influence the rate of HGT within these communities, and the data within experimental batches suggested that differences are likely between different stressors, although with the current experimental design and data obtained, it is not possible to reliably determine the impacts of these stressors on the conjugation efficiency of pHYCTX14.

In the future, this model can be adapted to use other clinically relevant plasmids as well as include additional species of bacteria to study the HGT of plasmids in more complex biofilms, including those that are relevant to the clinical environment, such as the CF lung. These experiments may provide new knowledge that can be used to help develop novel strategies to control the spread of AMR in biofilm populations.

CHAPTER 7: INVESTIGATING THE IMPORTANT GENES FOR PLASMID ACCEPTANCE IN *ESCHERICHIA COLI* AND *SALMONELLA ENTERICA* SEROVAR TYPHIMURIUM

"One sometimes finds what one is not looking for"

< Alexander Fleming >

7.1 INTRODUCTION

The role of MGEs in the dissemination of AMR has been well documented, and the conjugation of plasmids encoding AMR genes between bacterial cells has often been regarded as the most important mechanism for the spread of AMR both within and between species of pathogenic bacteria (Liu et al., 2024).

Whilst the general mechanism of plasmid conjugation, which involves the movement of genetic material from a donor to a recipient cell through structures such as pili (Von Wintersdorff et al., 2016, Burmeister, 2015), is well understood, and some studies have investigated the roles of restriction modification and CRISPR-Cas systems (Yang et al., 2024) as barriers to host plasmid acceptance, as well as the impact of flagella expression on plasmid uptake (Røder et al., 2024), genome-wide studies into the genes involved in plasmid acceptance within the host cell remain limited. Previously, the *E. coli* BW25113-derived Keio collection has been used to conduct a systematic investigation of plasmid acceptance in E. coli using an IncI2 plasmid. The study found that LPS played an essential role in plasmid uptake when conjugation experiments were completed using broth assays. However, one of the major drawbacks of this study was that the analysis was limited to non-essential genes (Allard et al., 2023) and could not be used to study the full complement of genes involved in plasmid acceptance. To address this gap in knowledge, a massively parallel transposon mutagenesis approach, TraDIS-*Xpress,* was used in this project to conduct high-throughput, genome-wide analyses of the genes involved in plasmid uptake in both *E. coli* and *S.* Typhimurium.

TraDIS-*Xpress* is a derivation of the original TraDIS method, in which transposon mutant libraries are created via the introduction (usually by transformation) of transposons (e.g. Tn5) into bacterial cells, where they randomly insert into the genome. The relative fitness impact of genes can then be assayed by growing these libraries in high-throughput screens and sequencing the input and output pools. Changes in mutant abundance within genes infer importance and identify non-essential or conditionally essential

genes for survival under any given condition (Barquist et al., 2016, Langridge et al., 2009).

TraDIS-*Xpress* combines an outwards-facing inducible promoter into the Tn5-derived transposon, allowing genes that are essential for survival in both control and experimental conditions, in addition to the non-essential genes, to be assayed. This addresses the limitation of TraDIS, which relies on insertional inactivation of genes and can only determine non-essential and conditionally essential genes (Yasir et al., 2020). TraDIS-*Xpress* can also identify fitness impacts resulting from the overexpression and repression of genes under different conditions (Yasir et al., 2020). This technique has previously been used to investigate the core genes involved in *S.* Typhimurium and *E. coli* biofilm formation (Holden et al., 2022), as well as the genes involved in susceptibility and resistance to a number of antibiotics, including triclosan, colistin, and meropenem in *E. coli* (Yasir et al., 2020, Yasir et al., 2022, Thomson et al., 2022).

This chapter describes the conjugation of pHYCTX14 into the previously generated *E. coli* BW25113 (Yasir et al., 2020) and *S.* Typhimurium 14028S (Holden et al., 2022) transposon mutant libraries to identify genes implicated in host plasmid acceptance, as well as the subsequent experiments to construct single gene deletion mutants in the EC18LG-0005-1 *E. coli* isolate to explore what roles the genes highlighted in the *E. coli* TraDIS-*Xpress* data may play in *E. coli* plasmid acceptance.

7.2 AIMS AND OBJECTIVES

- Conjugate pHYCTX14 into the *E. coli* BW25113 and *S.* Typhimurium 14028S transposon mutant libraries to investigate the genes involved in plasmid acceptance using TraDIS-*Xpress.*
- Expose the *E. coli* BW25113 and *S.* Typhimurium 14028S transposon mutant libraries to cefotaxime to help filter out genes that are only important for survival when exposed to beta-lactam antibiotics.
- Construct single gene deletion mutants in EC18LG-0005-1 to explore the roles the novel loci identified may play in plasmid acceptance.

7.3 RESULTS

To identify the genes implicated in plasmid acceptance, pHYCTX14 was conjugated into the *E. coli* BW25113 and *S.* Typhimurium 14028S transposon mutant libraries. As a control, the mutant libraries were also exposed to cefotaxime to help identify and filter out the genes that are only important for survival when exposed to beta-lactam antibiotics, rather than for plasmid acceptance.

Mutants recovered on LB agar supplemented with cefotaxime were sequenced, and reads were mapped to the appropriate reference genome using QuaTraDIS to generate plot files. These plots were then compared using the comparison pipeline in QuaTraDIS to determine significant differences between insertion frequencies between the control and test conditions for each gene. The differences in transposon insertion frequencies were also manually analysed in Artemis (version 18.2.0) (Carver et al., 2012). The results between the comparison pipeline and manual analyses were compared, and a list of genes was generated to take onto further experiments.

7.3.1 Pathway enrichment analysis

For both species, analysis of the TraDIS-*Xpress* data using the comparison pipeline found a large landscape of genes with diverse functions to have a role in plasmid acceptance, with 453 protected genes ($q < 0.01$ and -logFC) (genes with less insertions when compared with the control) and 183 disrupted genes ($q < 0.01$ and +logFC) (genes with more insertions when compared to the control) in *E. coli* (**APPENDIX VIII**), and 577 protected genes ($q < 0.01$ and -logFC) and 401 disrupted genes ($q < 0.01$ and +logFC) in *S.* Typhimurium (**APPENDIX IX**).

Given the large number of genes identified in the comparison pipeline, the list of protected genes from the pipeline was analysed using ShinyGo (version 0.82) (Ge et al., 2020), a pathway enrichment tool to identify over- and underrepresented pathways.

In *E. coli*, many of the enriched pathways were associated with metabolism (**Figure 7.1**), and the genes in these pathways were grouped into four major networks (**Figure 7.2**). These networks included: respiratory chain complexes, that are involved in adenosine triphosphate (ATP) synthesis (Price and Driessen, 2010); pyruvate metabolism, which produces acetyl-CoA, an important metabolic intermediate required for the first step of the tricarboxylic acid (TCA) cycle during aerobic respiration (Martínez-Reyes and Chandel, 2020); and succinyl-CoA, another metabolic intermediate of the TCA cycle (Martínez-Reyes and Chandel, 2020), suggesting that energy production played an important role in the acceptance of pHYCTX14.

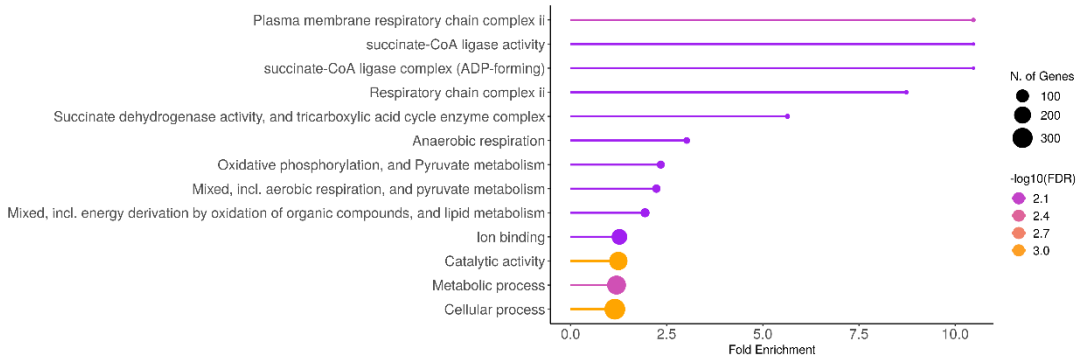

Figure 7.1 – Key enriched pathways associated with pHYCTX14 acceptance in *E. coli* BW25113

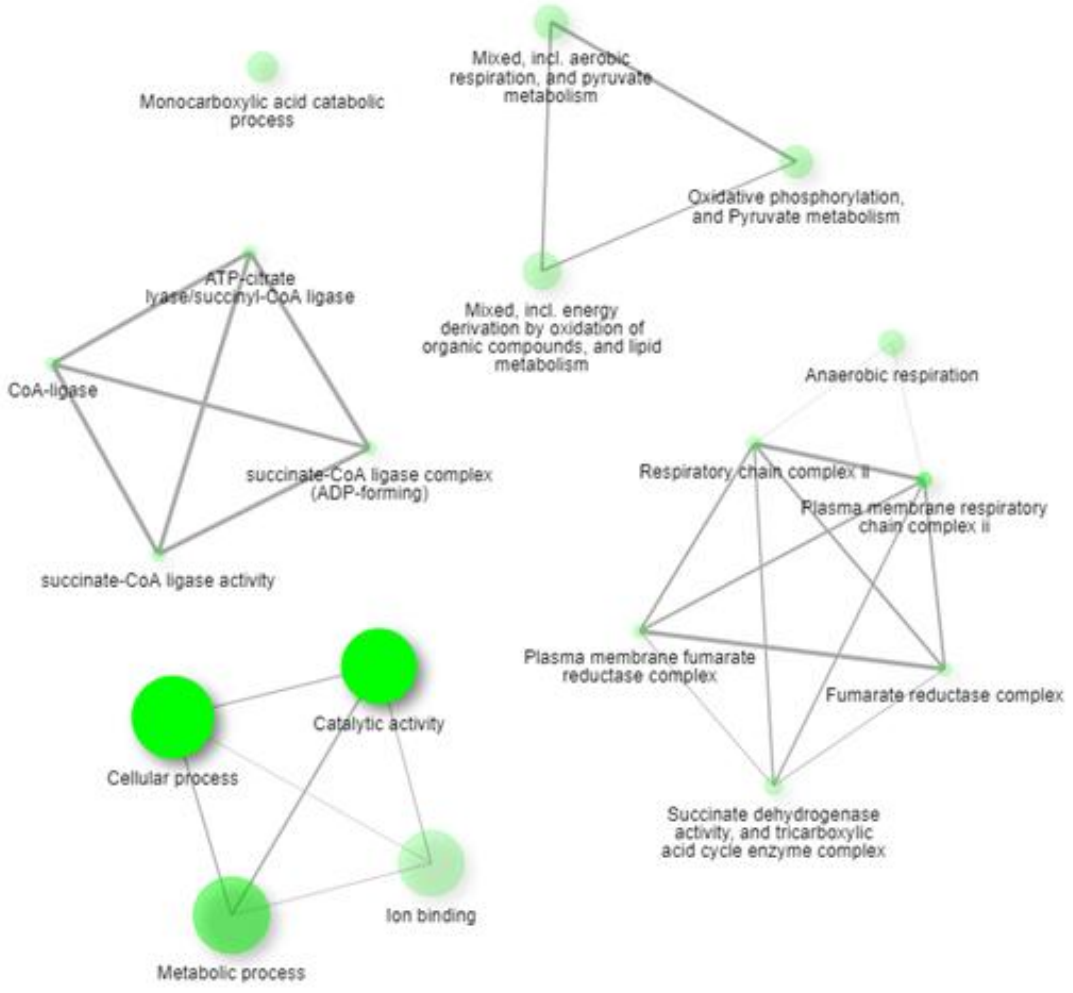

Figure 7.2 - Network of genes in the enriched pathways associated with pHYCTX14 acceptance in *E. coli* BW25113

In *Salmonella*, many of the enriched pathways, such as biosynthetic processes and small molecule binding, were again generally associated with fundamental biological processes of cells, although this analysis was limited to identifying processes at a relatively high level (**Figure 7.3**). Pathways associated with ATP-binding were also enriched, suggesting that energy production was important for the acceptance of pHYCTX14 in *S*. Typhimurium as well. In contrast to *E. coli*, most of the genes in these pathways were within one network (**Figure 7.4**), as opposed to four separate networks.

To determine specific operons and genes that may have a role in plasmid acceptance, a detailed analysis of the gene list from the comparison pipeline was also conducted, and the frequency of transposon insertions between the control libraries and the libraries that had accepted pHYCTX14 were also compared by manually analysing the plot files in Artemis. Key outcomes included genes involved in bacterial membrane structure, efflux, and RNA polymerase (RNAP) recycling.

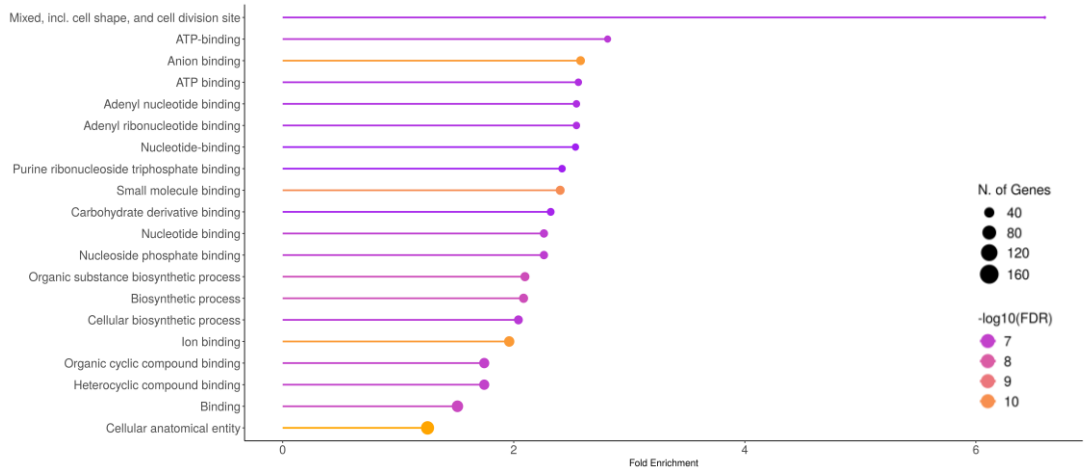

Figure 7.3 - Key enriched pathways associated with pHYCTX14 acceptance in *S.* Typhimurium 14028S

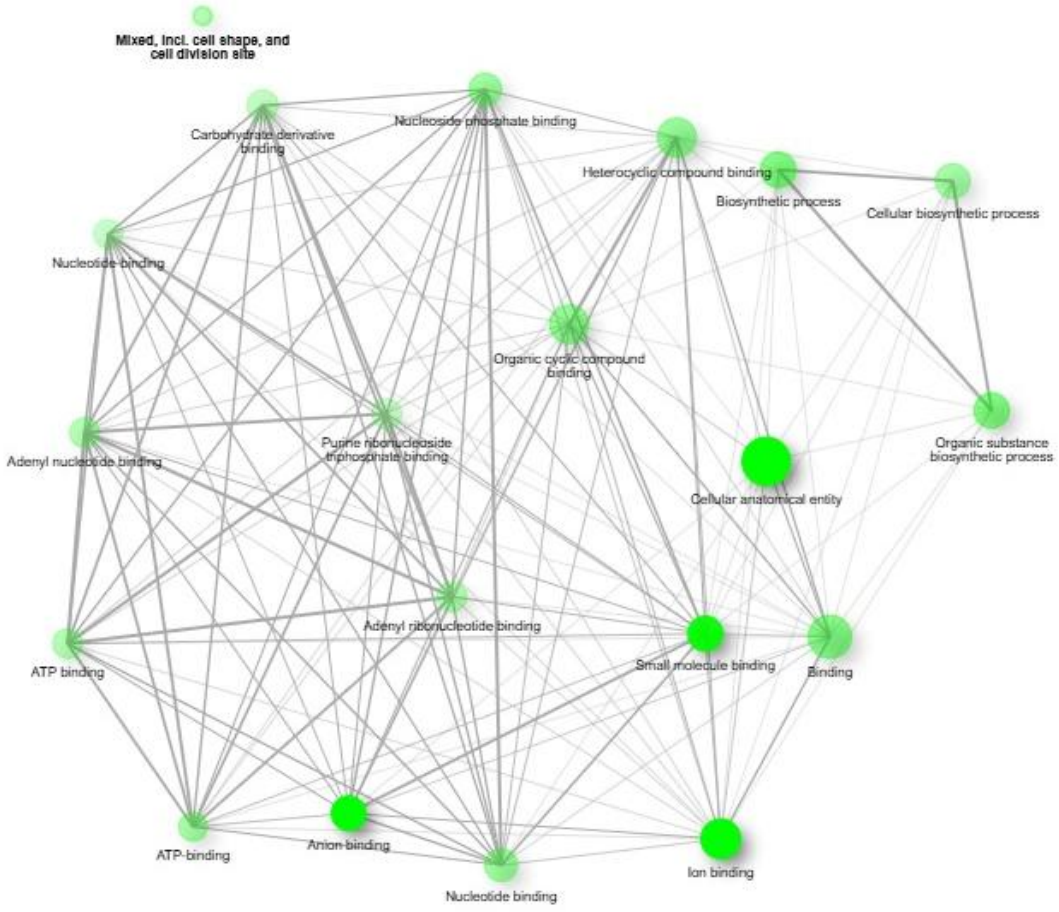

Figure 7.4 - Network of genes in the enriched pathways associated with pHYCTX14 acceptance in *S.* Typhimurium 14028S

7.3.2 Membrane structure

Analysis of the TraDIS-*Xpress* data found that membrane structure may have played a role in the acceptance of pHYCTX14 in both *E. coli* and *S.* Typhimurium. Significant differences in the frequency of transposon insertions were observed in many of the genes involved in lipopolysaccharide (LPS) synthesis in the mutants recovered on LB agar supplemented with cefotaxime after pHYCTX14 conjugation, when compared to the cefotaxime exposure controls.

LPS is a large glycolipid found in the outer membrane of most Gram-negative bacteria and plays a major role in preventing the entry of hydrophobic molecules into the cell (Zhang et al., 2013, Bertani and Ruiz, 2018). The structure of LPS consists of three main components: the core oligosaccharide, lipid-A core, and the O-antigen (Bertani and Ruiz, 2018). To help identify which stage of the LPS synthesis pathway the protected or disrupted genes may be involved in, an overview of the LPS synthesis pathway of *E. coli* K-12 (Moore et al., 2024, Karp et al., 2023) was mapped out (**Figure 7.5**).

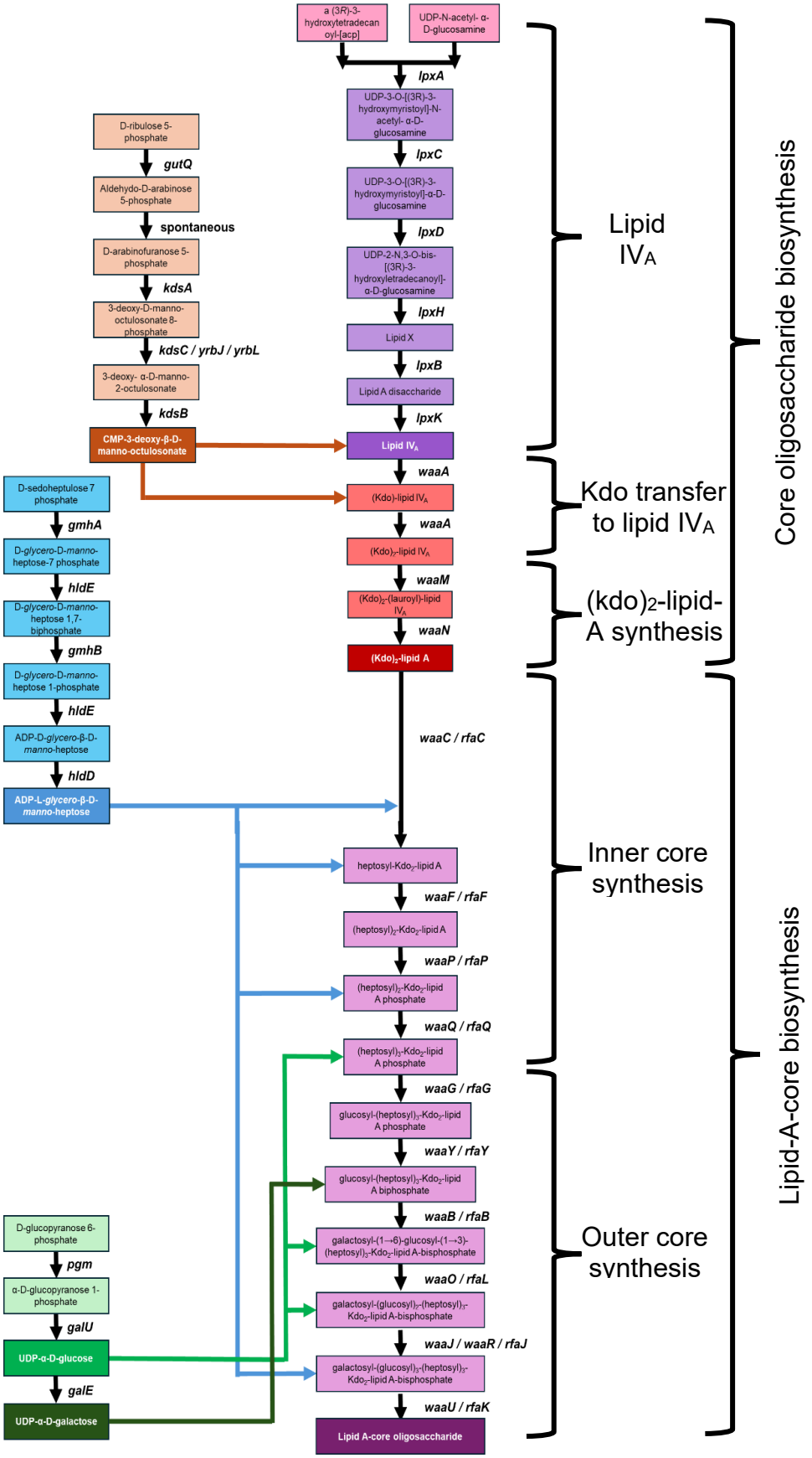

Figure 7.5 – Overview of the *E. coli* K-12 LPS synthesis pathway. The *S.* Typhimurium homologs of genes are shown where relevant (Moore et al., 2024, Karp et al., 2023, Bertani and Ruiz, 2018).

In *E. coli*, the protected genes, such as *galU*, *waaC* and *waaF*, are associated with the synthesis of the core oligosaccharide and inner lipid-A-core in LPS (Moore et al., 2024, Karp et al., 2023, Bertani and Ruiz, 2018), and the disrupted genes, such as *waaB*, *waaR* and *waaU*, are associated with the synthesis of the outer core (Bertani and Ruiz, 2018) (**Table 7.1, Figure 7.6**). This suggests that although the complete structure of the core oligosaccharide and inner lipid-A-core of the bacterial membrane may be important for plasmid acceptance in *E. coli* BW25113, disrupting the branching structure of the sugar residues in the outer core (Qian et al., 2014), may benefit plasmid uptake.

Table 7.1 – List of genes involved in LPS synthesis with significantly different transposon insertion frequencies in the *E. coli* BW25113 transposon mutant libraries that had accepted pHYCTX14, compared to the cefotaxime exposure control libraries.

Gene	Role	logFC	Protected/ disrupted
hldE	ADP-L-glycero-β-D-manno-heptose synthesis	-5.708995223	Protected
gmhB	ADP-L-glycero-β-D-manno-heptose synthesis	-4.720722341	Protected
hldD	ADP-L-glycero-β-D-manno-heptose synthesis	-5.091094484	Protected
pgm	UDP-α-D-galactose synthesis	-2.502332774	Protected
galU	UDP-α-D-galactose synthesis	-5.132544101	Protected
waaC	Lipid-A-core biosynthesis (inner core)	-4.846850794	Protected
waaF	Lipid-A-core biosynthesis (inner core)	-6.982926954	Protected
waaP	Lipid-A-core biosynthesis (inner core)	-4.146865687	Protected
waaQ	Lipid-A-core biosynthesis (inner core)	-0.885994467	Protected
waaG	Lipid-A-core biosynthesis (outer core)	-3.623628581	Protected
waaY	Lipid-A-core biosynthesis (outer core)	0.596017667	Disrupted
waaB	Lipid-A-core biosynthesis (outer core)	0.990346737	Disrupted
waaJ	Lipid-A-core biosynthesis (outer core)	0.669551686	Disrupted
waaR	Lipid-A-core biosynthesis (outer core)	0.930608705	Disrupted
waaU	Lipid-A-core biosynthesis (outer core)	1.032753646	Disrupted

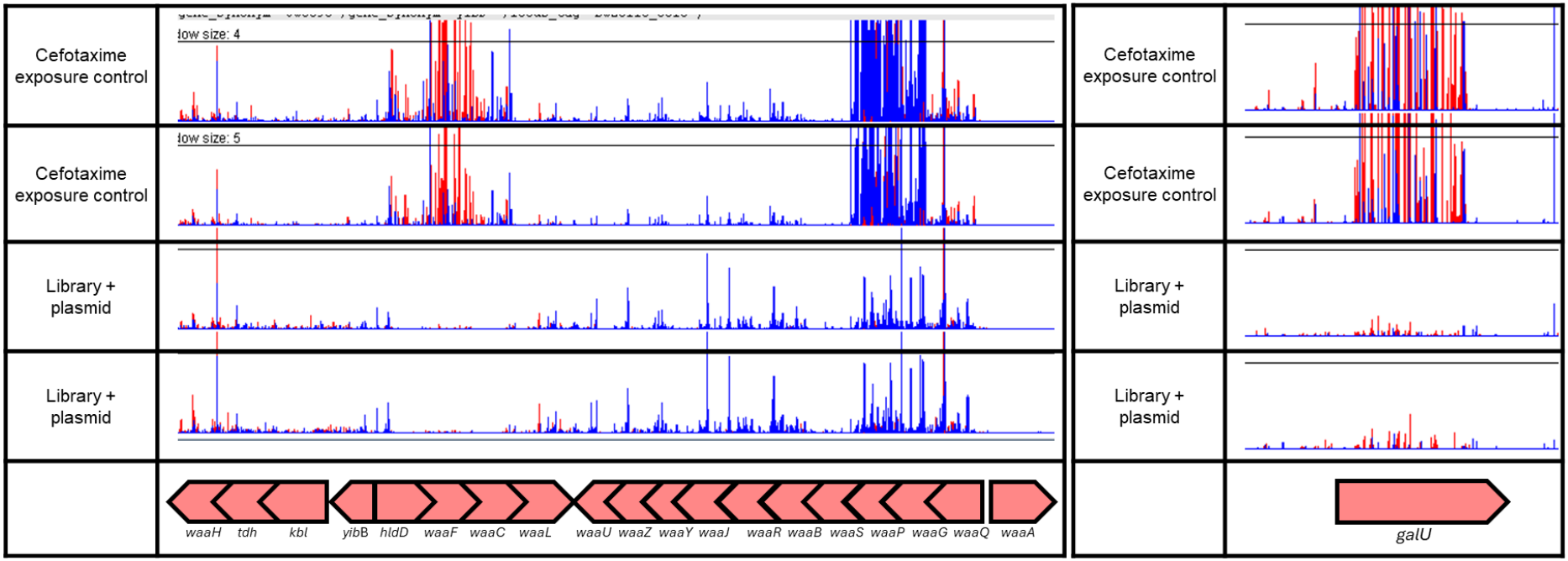

Figure 7.6 - Transposon insertion frequency in the genes involved in LPS synthesis of *E. coli* BW25113 mutants recovered on LB agar supplemented with cefotaxime after pHYCTX14 conjugation, relative to the cefotaxime exposure controls. Red peaks indicate transposon insertions in the forward (5' – 3') direction of DNA and blue peaks indicate transposon insertions in the reverse (3' – 5') direction. The height of the peaks represents the number of mutants with an insertion in that location.

In contrast to *E. coli*, the genes involved in LPS synthesis highlighted in the *S.* Typhimurium TraDIS-*Xpress* data were all protected (**Table 7.2**, **Figure 7.7**), suggesting that the structure of the LPS as a whole played a key role in the successful uptake of pHYCTX14 in *S*. Typhimurium.

Table 7.2 - List of genes involved in LPS synthesis with significantly different transposon insertion frequencies in the *S.* Typhimurium 14028S transposon mutant libraries that had accepted pHYCTX14, compared to the cefotaxime exposure control libraries.

Gene	Role	logFC	Protected/ disrupted
pgm	UDP-α-D-galactose synthesis	-4.67900318	Protected
galU	UDP-α-D-galactose synthesis	-6.396894362	Protected
galE	UDP-α-D-galactose synthesis	-5.089835283	Protected
rfaC	Lipid-A-core biosynthesis (inner core)	-1.5670041172	Protected
rfaF	Lipid-A-core biosynthesis (inner core)	-2.0993746899	Protected
rfaP	Lipid-A-core biosynthesis (inner core)	-5.0747994749	Protected
rfaQ	Lipid-A-core biosynthesis (inner core)	-3.2599072505	Protected
rfaG	Lipid-A-core biosynthesis (outer core)	-1.5601203219	Protected
rfaY	Lipid-A-core biosynthesis (outer core)	-3.3579407046	Protected
rfaB	Lipid-A-core biosynthesis (outer core)	-2.9276301924	Protected
rfaL	Lipid-A-core biosynthesis (outer core)	-6.0434072676	Protected
rfaJ	Lipid-A-core biosynthesis (outer core)	-6.82867812771	Protected
rfaK	Lipid-A-core biosynthesis (outer core)	-5.83683544772	Protected

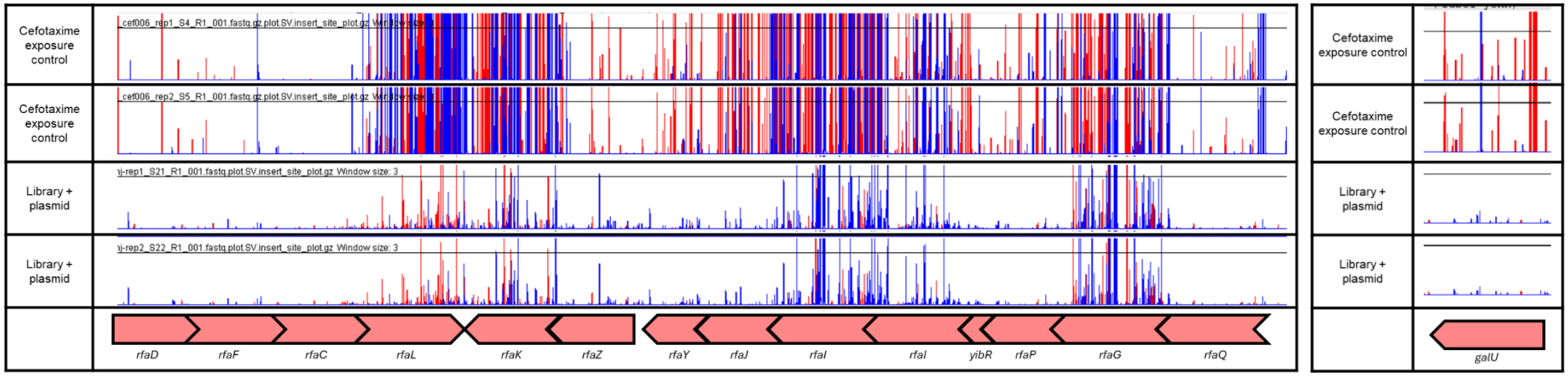

Figure 7.7 - Transposon insertion frequency in the genes involved in LPS synthesis of *S.* Typhimurium 14028S mutants recovered on LB agar supplemented with cefotaxime after pHYCTX14 conjugation, relative to the cefotaxime exposure controls. Red peaks indicate transposon insertions in the forward (5' – 3') direction of DNA and blue peaks indicate transposon insertions in the reverse (3' – 5') direction. The height of the peaks represents the number of mutants with an insertion in that location.

Protection of other membrane-associated genes, such as *mdo* genes (**Figure 7.8**), involved in membrane-derived oligosaccharide synthesis (Toguchi et al., 2000) and *mltC* (**Figure 7.9**), encoding a lytic transglycosylase involved in cell wall turnover (Monteiro et al., 2011), was also observed in *S.* Typhimurium 14028S.

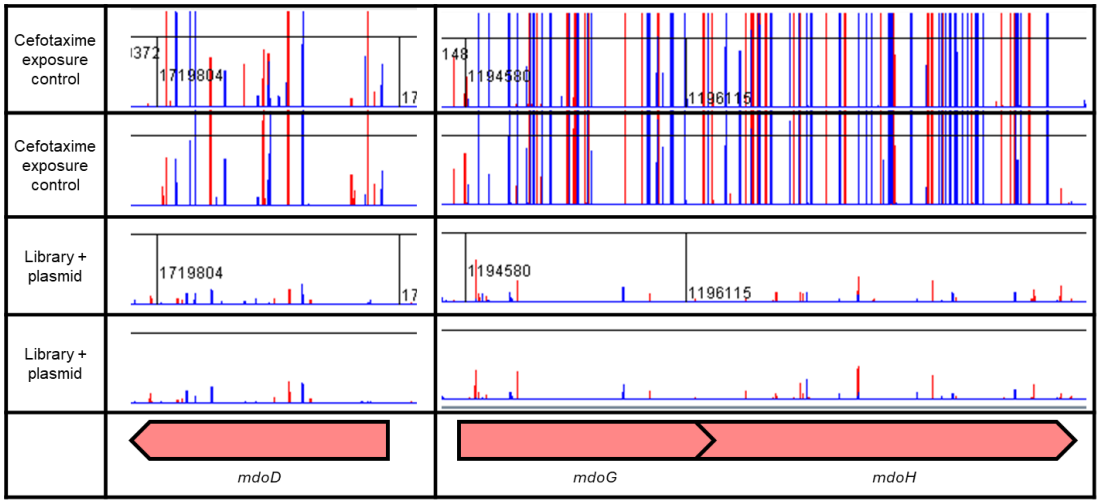

Figure 7.8 - Transposon insertion frequency in *mdoD*, *mdoG* and *mdoH* of *S.* Typhimurium 14028S mutants recovered on LB agar supplemented with cefotaxime after pHYCTX14 conjugation, relative to the cefotaxime exposure controls. Red peaks indicate transposon insertions in the forward (5' – 3') direction of DNA and blue peaks indicate transposon insertions in the reverse (3' – 5') direction. The height of the peaks represents the number of mutants with an insertion in that location.

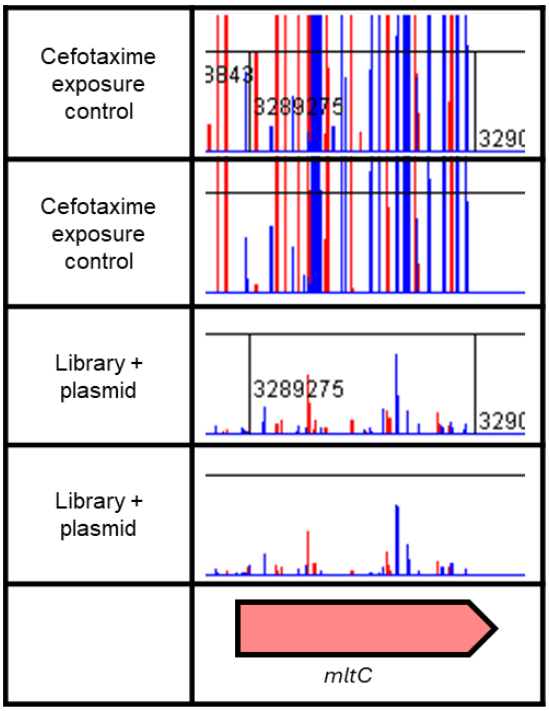

Figure 7.9 - Transposon insertion frequency in *mltC* of *S.* Typhimurium 14028S mutants recovered on LB agar supplemented with cefotaxime after pHYCTX14 conjugation, relative to the cefotaxime exposure controls. Red peaks indicate transposon insertions in the forward (5' – 3') direction of DNA and blue peaks indicate transposon insertions in the reverse (3' – 5') direction. The height of the peaks represents the number of mutants with an insertion in that location.

7.3.3 Efflux

Efflux pumps are bacterial membrane-embedded protein transporters involved in the transport of toxic substances, including antimicrobials, from inside the cell across the cytoplasmic membrane into the external environment (Gaurav et al., 2023, Webber and Piddock, 2003). These proteins can be found across both Gram-negative and -positive species of bacteria (Webber and Piddock, 2003), and play an important role in bacterial AMR, particularly in Gram-negative bacteria (Darby et al., 2023).

In *E. coli*, the data obtained using TraDIS-*Xpress* suggested that inactivation of AcrAB-TolC, a clinically important multidrug efflux pump belonging to the resistance-nodulation-division (RND) superfamily (Jang, 2023), would benefit acceptance of pHYCTX14, with an increased number of insertions observed in *acrA*, *acrB* and *tolC*, in the libraries that had accepted pHYCTX14, compared to the cefotaxime exposure controls (**Figure 7.10**). Protection of *acrR*, a transcriptional repressor which regulates the expression of AcrAB-TolC, was also observed.

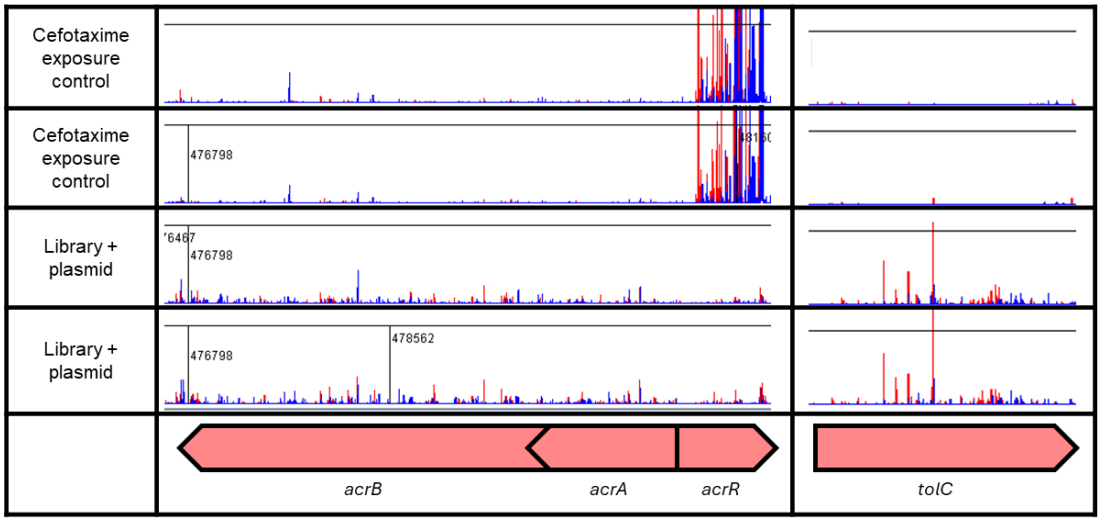

Figure 7.10 – Transposon insertion frequency in *acrB*, *acrA*, *acrR* and *tolC* of *E. coli* BW25113 mutants recovered on LB agar supplemented with cefotaxime after pHYCTX14 conjugation, relative to the cefotaxime exposure controls. Red peaks indicate transposon insertions in the forward (5' – 3') direction of DNA and blue peaks indicate transposon insertions in the reverse (3' – 5') direction. The height of the peaks represents the number of mutants with an insertion in that location.

In *S.* Typhimurium, however, no differences in transposon insertion frequencies were found in *acrA*, *acrB* and *tolC*, although protection of *acrR* was observed in the libraries that had accepted pHYCTX14 (**Figure 7.11**).

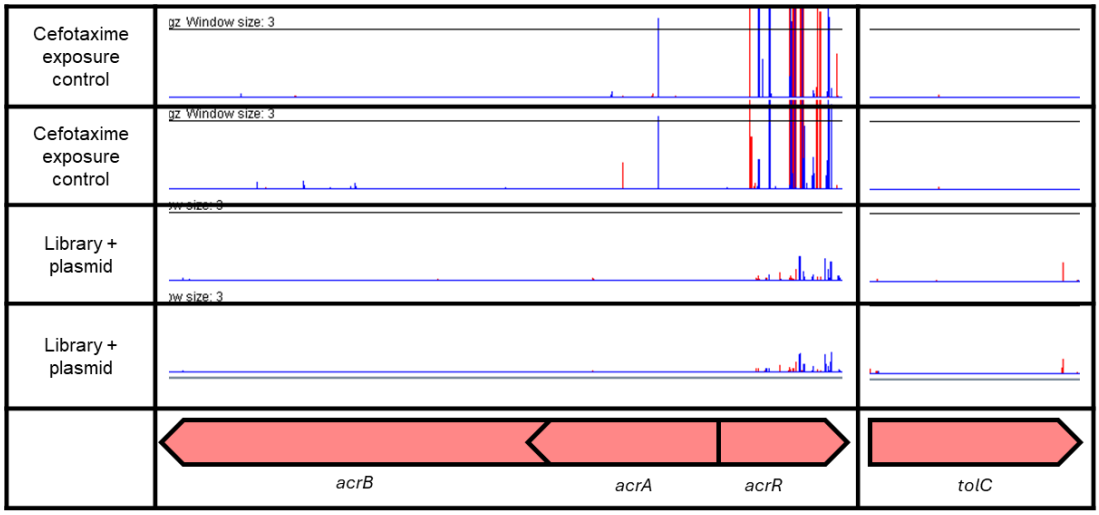

Figure 7.11 - Transposon insertion frequency in *acrB*, *acrA*, *acrR* and *tolC* of *S.* Typhimurium 14028S mutants recovered on LB agar supplemented with cefotaxime after pHYCTX14 conjugation, relative to the cefotaxime exposure controls. Red peaks indicate transposon insertions in the forward (5' – 3') direction of DNA and blue peaks indicate transposon insertions in the reverse (3' – 5') direction. The height of the peaks represents the number of mutants with an insertion in that location.

In EmrAB-TolC, an efflux pump belonging to the major facilitator superfamily (MFS) (Tanabe et al., 2009), protection of *emrA* and *emrB* was observed in both the *E. coli* (**Figure 7.12**) and *S.* Typhimurium (**Figure 7.13**) TraDIS-*Xpress* data, suggesting that disrupting the expression of this efflux pump would have a negative impact on pHYCTX14 acceptance in both species.

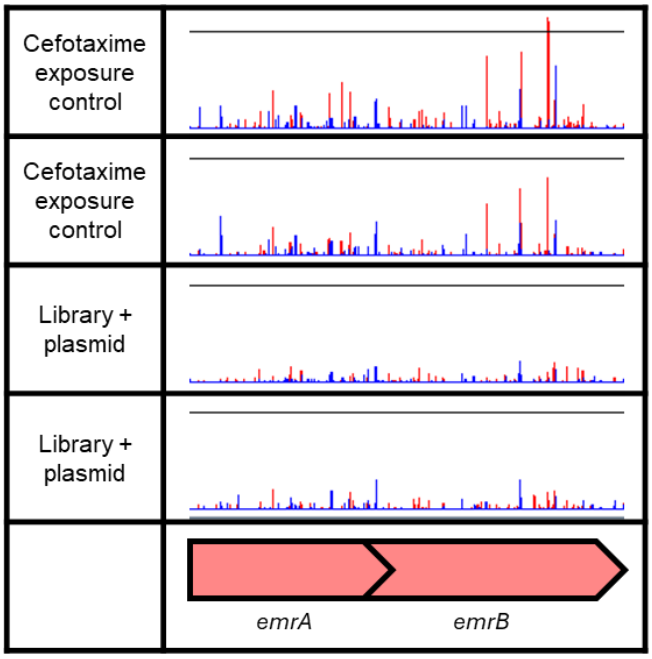

Figure 7.12 - Transposon insertion frequency in *emrA* and *emrB* of *E. coli* BW25113 mutants recovered on LB agar supplemented with cefotaxime after pHYCTX14 conjugation, relative to the cefotaxime exposure controls. Red peaks indicate transposon insertions in the forward (5' – 3') direction of DNA and blue peaks indicate transposon insertions in the reverse (3' – 5') direction. The height of the peaks represents the number of mutants with an insertion in that location.

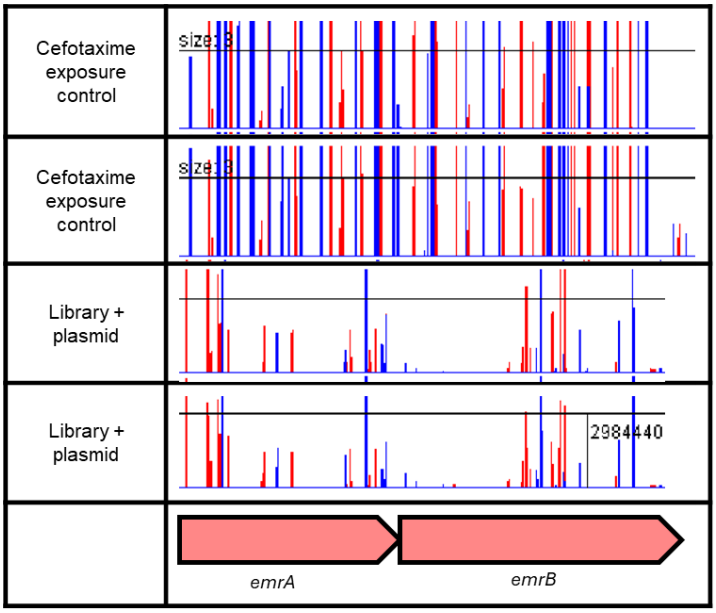

Figure 7.13 - Transposon insertion frequency in *emrA* and *emrB* of *S.* Typhimurium 14028S mutants recovered on LB agar supplemented with cefotaxime after pHYCTX14 conjugation, relative to the cefotaxime exposure controls. Red peaks indicate transposon insertions in the forward (5' – 3') direction of DNA and blue peaks indicate transposon insertions in the reverse (3' – 5') direction. The height of the peaks represents the number of mutants with an insertion in that location.

7.3.4 *rapA*

In *E. coli*, a large number of insertions were observed in *rapA* in the libraries that had accepted pHYCTX14 (**Figure 7.14**). *rapA* encodes RapA, an ATPase and RNAP–associated protein, which is a homolog of the switch/ sucrose non-fermentable (SWI/ SNF) helicase-like family of proteins found in eukaryotic cells (Jin et al., 2011, Cabrera and Jin, 2001, Lynch et al., 2007). It is involved in the release of RNAPs from DNA after transcription termination in a process called RNAP recycling (Qayyum et al., 2021), and mutations in *rapA* have been found to decrease resistance of UPEC to penicillin G, chloramphenicol and gentamicin by altering gene regulation in biofilms, although the structure of the biofilms formed was not impacted (Lynch et al., 2007).

The TraDIS-*Xpress* data suggested that disruption to the expression of *rapA* would benefit plasmid acquisition in *E. coli*. However, the underlying mechanism of how this gene may impact plasmid acceptance could not be concluded from the data currently available.

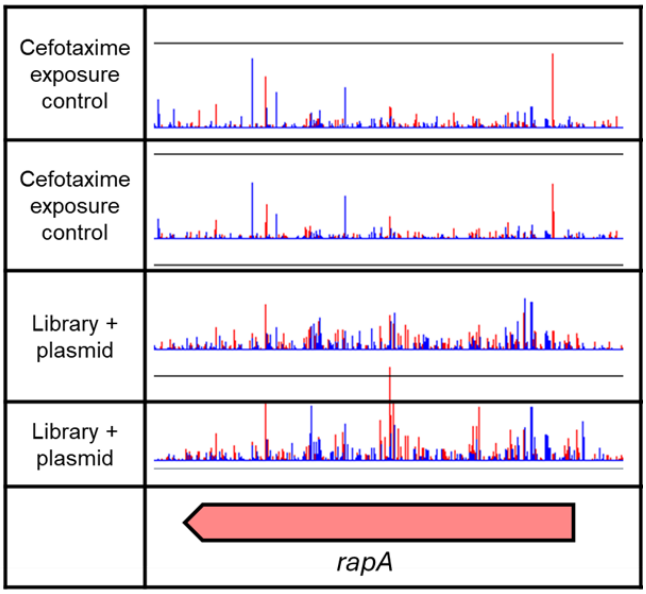

Figure 7.14 - Transposon insertion frequency in *rapA* of *E. coli* BW25113 mutants recovered on LB agar supplemented with cefotaxime after pHYCTX14 conjugation, relative to the cefotaxime exposure controls. Red peaks indicate transposon insertions in the forward (5' – 3') direction of DNA and blue peaks indicate transposon insertions in the reverse (3' – 5') direction. The height of the peaks represents the number of mutants with an insertion in that location.

7.3.5 Constructing single gene deletion mutants in *E. coli*

To investigate what roles some of the genes identified in *E. coli* may play in plasmid acceptance, the process of constructing single gene deletion mutants of the genes of interest in EC18LG-0005-1 (**Table 7.3**) using the G-DOC method (Lee et al., 2009) was started. The mutants created would be used in downstream conjugation experiments to measure the impact of gene deletion on pHYCTX14 conjugation efficiency.

Table 7.3 – Genes of interest identified in the *E. coli* TraDIS-*Xpress* data

Gene	Role	Hypothesised impact on plasmid acceptance
acrB	AcrAB-TolC efflux pump	Increase
tolC	AcrAB-TolC efflux pump	Increase
galU	UDP-α-D-galactose synthesis	Decrease
hldD	ADP-L-glycero-β-D-manno-heptose synthesis	Decrease
waaC	Lipid-A-core biosynthesis (inner core)	Decrease
waaB	Lipid-A-core biosynthesis (outer core)	Increase
waaJ	Lipid-A-core biosynthesis (outer core)	Increase
rapA	RNAP recycling factor	Increase

7.3.5.1 Cloning of homologous region one into pDOC-K

Homologous regions upstream and downstream of the target genes were designed and amplified via PCR (**Table 7.4**), before restriction digestion using the appropriate enzymes. pDOC-K was digested using the relevant restriction enzymes for homologous region one, and then the digested homologous regions were ligated into pDOC-K to construct vectors. Vectors consisting of the homologous regions were transformed into chemically competent NEB® 5-alpha Competent *E. coli* (High Efficiency) cells via heat shock, and cells were recovered on LB agar plates supplemented with 100 µg/mL kanamycin. A negative control of the digested vector with no inserts was also included.

Table 7.4 – List of primers for the amplification of homologous regions upstream and downstream of the target genes

Name	Role
acrB homologous region 1	Amplification of homologous regions adjacent to *acrB* in *E. coli* for insertion into pDOC-K to create the Δ*acrB* deletion mutant
acrB homologous region 2	
tolC homologous region 1	Amplification of homologous regions adjacent to *tolC* in *E. coli* for insertion into pDOC-K to create the Δ*tolC* deletion mutant
tolC homologous region 2	
galU homologous region 1	Amplification of homologous regions adjacent to *galU* in *E. coli* for insertion into pDOC-K to create the Δ*galU* deletion mutant
galU homologous region 2	
hldD homologous region 1	Amplification of homologous regions adjacent to *hldD* in *E. coli* for insertion into pDOC-K to create the Δ*hldD* deletion mutant
hldD homologous region 2	
waaC homologous region 1	Amplification of homologous regions adjacent to *waaC* in *E. coli* for insertion into pDOC-K to create the Δ*waaC* deletion mutant
waaC homologous region 2	
waaB homologous region 1	Amplification of homologous regions adjacent to *waaB* in *E. coli* for insertion into pDOC-K to create the Δ*waaB* deletion mutant
waaB homologous region 2	
waaJ homologous region 1	Amplification of homologous regions adjacent to *waaJ* in *E. coli* for insertion into pDOC-K to create the Δ*waaJ* deletion mutant
waaJ homologous region 2	
rapA homologous region 1	Amplification of homologous regions adjacent to *rapA* in *E. coli* for insertion into pDOC-K to create the Δ*rapA* deletion mutant
rapA homologous region 2	

7.3.5.2 Optimisation of pDOC-K restriction digestion

Initially, restriction digest of pDOC-K was performed sequentially with a one-hour incubation at 37 °C for each enzyme. However, this resulted in a large number of colonies recovered on agar plates supplemented with 100 µg/mL kanamycin for the negative control, suggesting that a large quantity of undigested pDOC-K was present.

To troubleshoot this, restriction digestion of pDOC-K was performed as a double digest with incubation at 37 °C overnight to explore whether a longer incubation period would increase the efficiency of pDOC-K digestion.

In parallel, 'outward' primers for homologous region one of each gene of interest were designed to amplify pDOC-K as a linear DNA fragment via inverse PCR (**Figure 7.15**). Primers were designed to include the appropriate endonucleases, and six random bases were added to the start of each primer. After amplification, agarose gel electrophoresis was used to confirm the presence of DNA fragments of the correct size and a PCR clean-up was carried out. Dpn-1 (R0176S, NEB) was added to the PCR products to remove any remaining template DNA (methylated pDOC-K), followed by a PCR clean-up before the linear pDOC-K fragments were digested sequentially using the appropriate restriction enzymes with a one-hour incubation at 37 °C for each enzyme. A PCR clean-up was carried out between each digestion step, and gel electrophoresis was used to confirm the size of the digested pDOC-K fragments. The digested vectors and inserts were then ligated and transformed into NEB® 5-alpha Competent *E. coli* (High Efficiency) cells as previously stated.

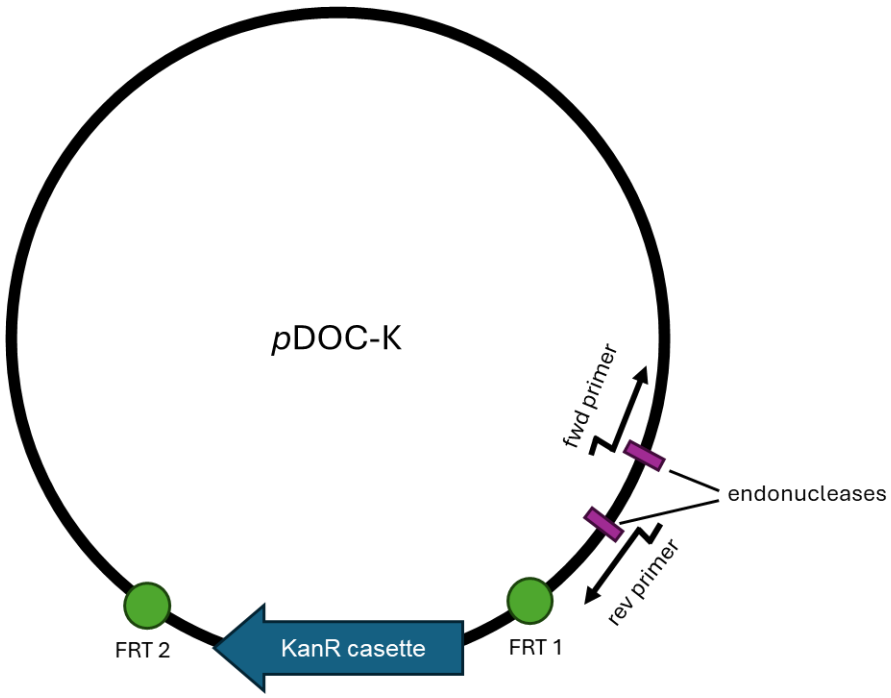

Figure 7.15 – The design of 'outward' primers for the amplification of pDOC-K as a linear DNA fragment.

Both the overnight double digest and inverse-PCR were successful, with bands of the appropriate size visualised via agarose gel electrophoresis. However, a significant amount of product loss appeared to occur during the PCR clean-up steps, as no bands were present on the agarose gel after the final clean-up step for both methods. Ligation of the homologous regions and transformation of the vectors into *E. coli* were still attempted, although no colonies were recovered on agar plates supplemented with 100 µg/mL kanamycin, suggesting that no vector was recovered after the final PCR clean-up, and therefore, the ligation and transformation steps were unsuccessful.

Due to time constraints, it was not possible to finish the optimisation of the protocol to construct the single gene deletion mutants in EC18LG-0005-1, and therefore, no further experiments were undertaken to investigate what roles the genes identified in *E. coli* may play in plasmid acceptance. The genes of interest identified in *S.* Typhimurium 14028S were also not explored further.

7.4 DISCUSSION

Using TraDIS-*Xpress* and pHYCTX14, a self-mobile, clinically relevant plasmid (**Chapter 3**), a large number of genes with a variety of functions were identified to play a role in plasmid acceptance in both *E. coli* and *S.* Typhimurium, and key results were found in genes associated with energy production, bacterial membrane structure, efflux, and RNAP recycling.

Many of the protected genes observed in the TraDIS-*Xpress* data appeared to be involved in metabolism, suggesting that energy production plays a crucial role in host plasmid acquisition. It is well known that the acceptance of a plasmid within a bacterial population can exert a metabolic burden, leading to a fitness cost in the host cell (Brockhurst and Harrison, 2022), and several reasons have been proposed for the fitness cost observed. These include the initial overexpression of plasmid-encoded genes in cells after plasmid acceptance, disruption to the overall stability of the host cell (Curtsinger et al., 2024), and activation of the SOS response, a bacterial stress response often induced by the conjugation of plasmids into the host cell (Curtsinger et al., 2024, Millan and MacLean, 2017).

The outcomes from the enrichment analysis supports the dogma that acquiring a plasmid is a metabolically costly process, and requires increased energy production from the bacterial cell. However, the specific pathways necessitating an increase in metabolism cannot be determined from the results obtained thus far.

Successful conjugation of a plasmid between bacterial cells is contact-dependent and requires the formation of a conjugative pilus (Virolle et al., 2020). The pilus extends from the membrane of the donor cell to make contact with the recipient, bringing the cells together to form a mating junction, facilitating plasmid transfer across the bacterial membrane (Low et al., 2022, Virolle et al., 2020, Waksman, 2025), and in both *E. coli* and *S.* Typhimurium, membrane structure appeared to play a strong role in plasmid acceptance.

In *E. coli*, protection of genes involved in the synthesis of the core oligosaccharide and inner lipid-A-core in LPS, and disruption of genes involved in the synthesis of the outer core was observed, suggesting that whilst the inner core is required for the cell to successfully transfer a plasmid into the cell, disrupting the structure of the outer core, which is typically made up of branching sugar residues (Qian et al., 2014), may increase plasmid acceptance. In *S.* Typhimurium, however, protection was observed in genes involved in the synthesis of both the inner and outer core of LPS, suggesting that in *Salmonella*, the complete structure of the outer core is required for plasmid uptake. Protection of other membrane-associated genes, such as *mdo* genes, encoding membrane-derived oligosaccharides found in the bacterial periplasmic space (Toguchi et al., 2000), and *mltC*, associated with peptidoglycan turnover in the cell wall (Monteiro et al., 2011), was also observed in the *S.* Typhimurium data. As plasmid conjugation requires two cells to come into contact with each other (Virolle et al., 2020), changes to the structure of the bacterial outer membrane may impact how efficiently the donor cell can make contact with the recipient, affecting host plasmid acceptance.

E. coli BW25113, which was used to generate the transposon mutant library used in this study (Yasir et al., 2020), is an *E. coli* K-12 derivative (Datsenko and Wanner, 2000), and due to an ancestral mutation, this strain does not

produce the O-antigen that attaches onto the outer core of LPS (Bertani and Ruiz, 2018). It is unclear how the absence or structure (given the diversity of this component (Bertani and Ruiz, 2018)) of the O-antigen may impact plasmid acquisition in the host cell. However, further investigations using a diverse panel of *E. coli* strains that encode this component of LPS may help to provide more information on how plasmid acceptance is affected by the structure of the outer membrane in Gram-negative bacteria. These experiments can also be extended to investigate a larger diversity of *S.* Typhimurium strains.

Overall, the data indicated that whilst bacterial membrane structure may play a key role in plasmid acceptance, different components of the membrane can impact this process in different ways, and these impacts may also be species or strain specific. This could be potentially exploited to block specific components needed for plasmid transfer in bacteria.

Furthermore, the results also suggested that efflux may play a role in host plasmid acceptance. In *E. coli*, the data indicated that disrupting the expression of the AcrAB-TolC efflux pump may benefit plasmid acceptance. In *S.* Typhimurium, disruption of *acrA*, *acrB* and *tolC* was not observed, although *acrR* was protected compared to the control libraries, suggesting that whilst AcrAB-TolC was not directly disrupted in *Salmonella*, the expression of the pump may have been repressed, and reduced expression of AcrAB-TolC may still benefit plasmid acceptance in this species. Protection of *emrA* and *emrB*, encoding the periplasmic adaptor protein and inner membrane transporter, respectively, of the EmrAB-TolC efflux pump (Yousefian et al., 2021) was also observed in both *E. coli* and *S*. Typhimurium, suggesting that expression of these proteins is important for plasmid acquisition in both species.

Although it was not possible to deduce the role that efflux plays in plasmid acceptance from these results, it was hypothesised that changes to the expression of these membrane-embedded proteins may alter membrane structure, leading to positive or negative impacts on plasmid acceptance within a new host. Previously, it was found that the deletion of AcrAB changed the expression of outer membrane porin proteins in various *Enterobacteriaceae,* leading to decreased susceptibility to cephalosporins (Saw et al., 2016).

There may also be an interplay between the acquisition of plasmid-encoded AMR and the expression of efflux.

In *E. coli*, *rapA* was also highlighted as a gene that may impact plasmid acceptance. An increased number of insertions was found in *rapA* in the mutants recovered from the libraries that had accepted the plasmid, suggesting that disruption to the expression of *rapA* would benefit plasmid acquisition in *E. coli.* Although it was not possible to conclude the underlying mechanism on how this gene may impact plasmid acceptance from these experiments, it was hypothesised that given the role *rapA* plays in RNAP recycling, inactivation of the gene may reduce the transcription of plasmid encoded genes after plasmid acceptance, alleviating the fitness cost caused by the initial overexpression of plasmid-encoded genes in cells uptake (Curtsinger et al., 2024). Further investigations to measure the location and abundance of RNAP during plasmid acquisition may be required to fully define the role of *rapA* in *E. coli* plasmid uptake.

7.5 CONCLUSIONS

This chapter describes the use of TraDIS-*Xpress* and pHYCTX14 to conduct whole-genome screening of the genes that may play a role in plasmid acquisition in *E. coli* BW25113 and *S.* Typhimurium 14028S.

A large landscape of genes with diverse functions was identified to have a role in plasmid acceptance in both species, and experiments to construct single gene deletion mutants in EC18LG-0005-1 of some of the genes highlighted in the *E. coli* TraDIS-*Xpress* data were started to investigate what roles they may have in plasmid acquisition.

The list of genes selected for downstream experiments (**Table 7.3**) included *rapA* and those involved in various stages of LPS synthesis, as well as *acrB* and *tolC,* to explore how changes to different components of the bacterial membrane may impact conjugation efficiency. However, due to the time constraints faced during this project, it was not possible to finish the planned experiments. It would be useful to complete the construction of these mutants

in the future, to establish how deletion of these genes would impact pHYCTX14 conjugation efficiency, first using nylon membrane filters, then also within a biofilm using the biofilm conjugation model to investigate changes to the rate of conjugation within a real-world context. The genes highlighted in the *S.* Typhimurium 14028S TraDIS-*Xpress* data should also be explored further.

Although the specific genes involved in plasmid acquisition may differ between bacterial species and strains, as well as the type of plasmid the host cell is gaining, and plasmid acceptance was only explored in one strain of *E. coli* and *S.* Typhimurium, using pHYCTX14 in this chapter, these experiments form the foundation to investigate the full complement of genes involved in plasmid acceptance. The results provide novel information on the host-plasmid interplay that can hopefully be explored further to help identify new approaches to reduce plasmid-mediated transfer of AMR in bacteria.

In the future, it may be possible to investigate the genes that impact plasmid acceptance in a wider range of bacterial strains and species, using a more diverse range of plasmids. In addition, transposon mutant libraries can also be generated in plasmids to investigate the importance of different plasmid-encoded genes in conjugation.

CHAPTER 8:
GENERAL DISCUSSION

“The most important step a man can take? The next one. Always the next one”

< Brandon Winn Sanderson >

8.1 EVOLUTION OF ANTIMICROBIAL RESISTANCE IN MULTISPECIES BIOFILMS

Despite the importance of biofilms in the context of bacterial AMR, most experiments are conducted using planktonic bacteria that are not representative of real-world bacterial communities (Trampari et al., 2021), and the impact of various stressors present in the environment on the movement of MGEs within multispecies biofilm communities remains unclear.

The overall aim of this study was to establish a better understanding of how external stress factors can influence the rate of plasmid movement within a multispecies biofilm community.

A multispecies biofilm conjugation model, consisting of the *E. coli* food isolate, EC18LG-0005-1 as the donor strain, and *S.* Typhimurium 14028S as the recipient strain, was developed to monitor the movement of pHYCTX14, a clinically relevant, self-mobile plasmid encoding *bla*$_{\text{CTX-M-14}}$, between the two species (**Figure 8.1**).

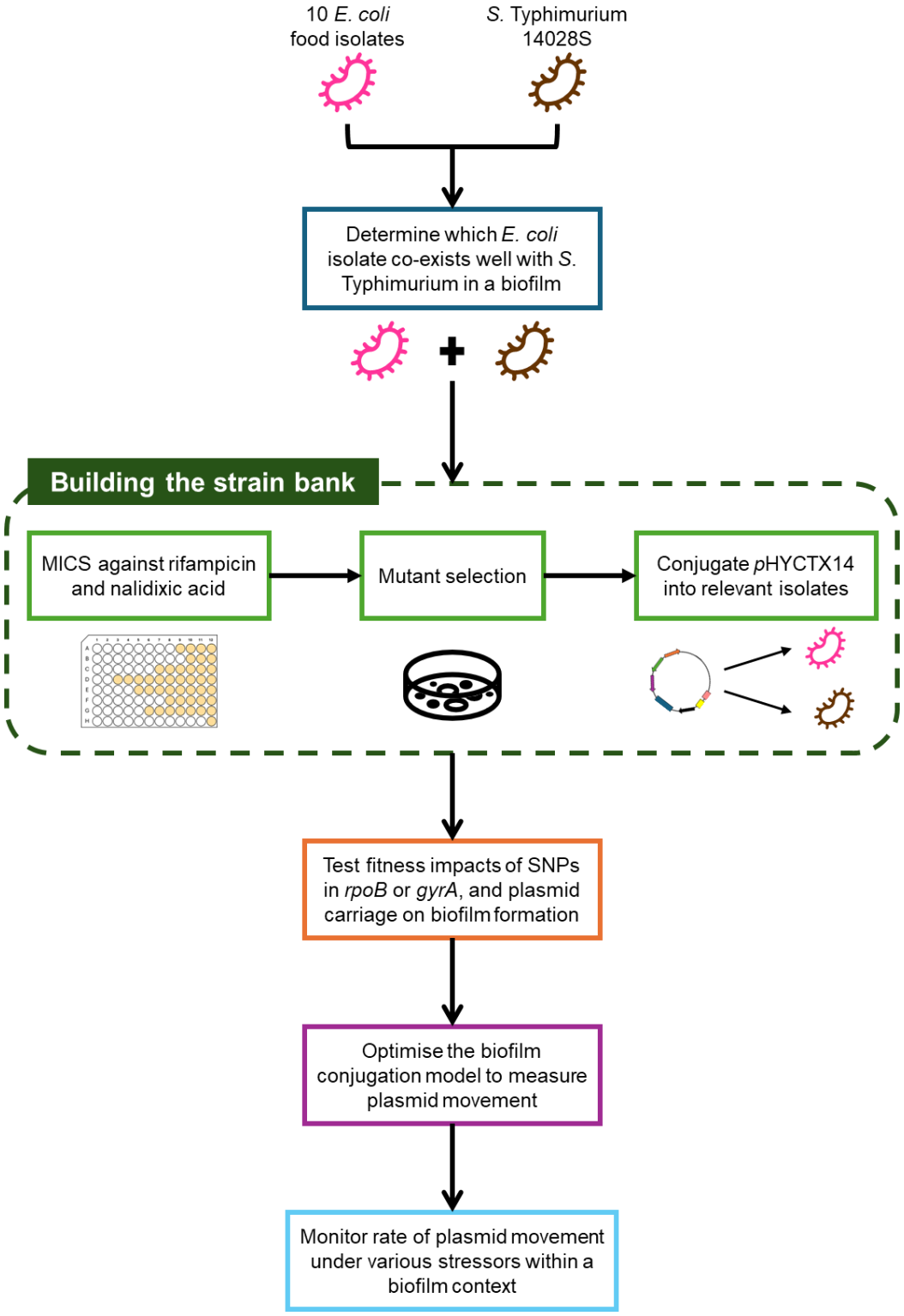

Figure 8.1 – Overview of the workflow used to develop the biofilm conjugation model used in this study to measure plasmid movement between *E. coli* and *S.* Typhimurium.

Using this model, the impact of a range of chemicals, including food preservatives and antimicrobials, on the rate of plasmid movement was investigated.

The results indicated that the chemicals tested had impacts on the conjugation efficiency of pHYCTX14 between EC18LG-0005-1 RifR pHYCTX14 and *S.* Typhimurium 14028S NalR, with the lowest rate of plasmid movement obtained for experiments conducted under stress from sodium nitrite, and the highest rate of plasmid movement obtained for experiments conducted under stress from copper sulphate overall. However, no statistically significant difference in conjugation efficiency was obtained, and it was difficult to draw definite conclusions from the results generated during these experiments due to technical limitations, such as the absence of an unstressed control in each experimental batch, this study represents one of the first models developed to explore the impact of environmental stress factors on the dissemination of AMR genes encoded on MGEs within multispecies biofilms. The data obtained suggested that the chemicals tested likely led to differences in conjugation efficiency. Repeating these experiments with adjustments to the experimental design may allow the differences in conjugation efficiency to be observed more clearly.

Although ciprofloxacin is often suggested to significantly increase the rate of conjugation, and this has been observed in some Gram-negative bacterial species in the past (Thanh Duy et al., 2020;, interestingly, this was not observed in the results obtained for this study. This demonstrates that the impacts of environmental stressors on conjugation efficiency may differ depending on experimental context (biofilm vs planktonic communities), as well as the bacterial species, the type of plasmid (for example, incompatibility type, resistance gene(s) encoded on the plasmid) and whether the stress is applied during the conjugation assay or if the bacteria is pre-grown under stress.

Previous examples of HGT within biofilms in the environment include the transfer of *bla*$_{\text{CTX-M-15}}$ through *Klebsiella pneumoniae* in France (Hennequin et al., 2012), as well as in multispecies bacterial populations where the HGT of

AMR genes have been demonstrated in oral biofilms comprising of *Streptococcus* spp (Chi et al., 2007), in addition to aquatic ecosystems where the conjugative plasmid pKJK5 was transferred between species of bacteria found within multispecies biofilms forming on microplastics in lake water (Arias-Andres et al., 2018).

Furthermore, during the initial attempts to conjugate pHYCTX14 from EC18LG-0005-1 RifR pHYCTX14 to *S.* Typhimurium 14028S, there were difficulties recovering the donor strain on LB agar supplemented with cefotaxime after growing on the steel beads. Additional investigations found that these difficulties were not due to loss of the plasmid and only appeared to impact *E. coli*. It was hypothesised that *bla*$_{\text{CTX-M-14}}$ was not actively expressed when cells were grown in a biofilm, and experiments were designed to explore the expression of *bla*$_{\text{CTX-M-14}}$ in biofilm and planktonic *E. coli* cells using RTqPCR. Previous studies have reported the silencing of AMR genes encoded on plasmids (Enne et al., 2006), and the expression of AMR genes in the absence of selective pressure may also negatively impact bacterial fitness (Humphrey et al., 2012). However, research on the expression of genes encoded on plasmids within biofilm populations is limited, and it would be useful to follow up on the unfinished RTqPCR experiments planned for this study in the future.

Combining a study of gene expression, population heterogeneity and plasmid transfer rates using the established model would be powerful in understanding how diversity of populations impacts AMR.

8.2 GENES IMPLICATED IN HOST PLASMID ACCEPTANCE

Although the HGT of MGEs, such as plasmids, encoding AMR genes via conjugation has often been considered as the key mechanism for the dissemination of resistance in bacteria (Liu et al., 2024), the understanding of the specific genes that play a role in host plasmid acceptance remains limited.

The overall aim of these experiments was to investigate the full complement of genes implicated in host plasmid acceptance.

To study this, a massively parallel transposon mutagenesis approach, TraDIS-*Xpress,* was used. pHYCTX14 was conjugated into the previously generated *E. coli* BW25113 and *S.* Typhimurium 14028S transposon mutant libraries. Using a combination of QuaTraDIS, a TraDIS analysis pipeline, and manual analyses of the transposon insertion frequencies in the libraries that had accepted a plasmid and the cefotaxime exposure control libraries, a list of genes implicated in *E. coli* and *S.* Typhimurium plasmid uptake was generated.

Analysis of the TraDIS-*Xpress* data found a large landscape of genes with diverse functions to have a role in plasmid acceptance in both *E. coli* and *S.* Typhimurium. Using a pathway enrichment tool, it was found that many of the genes were associated with metabolism, suggesting that energy production may have a key role in plasmid acceptance in both species. However, as the pathway analysis conducted using the TraDIS data obtained did not highlight any specific bacterial metabolic pathways, this analysis was limited to identifying processes at a relatively high level, and the specific pathways that required an increase in metabolism could not be determined from the results obtained. As the metabolic burden of host plasmid acceptance is well documented in research (Brockhurst and Harrison, 2022), these results support the principle that plasmid uptake is an energy-costly process, and there is an interplay between costs and benefits of plasmid acquisition, which involves lots of fundamental processes.

Other key outcomes from the TraDIS-*Xpress* data included identification of genes involved in bacterial membrane structure, efflux, and RNAP recycling.

In both *E. coli* and *S.* Typhimurium, significant differences were observed in the frequency of transposon insertions in many of the genes involved in LPS synthesis in the transposon mutant libraries that had accepted pHYCTX14, compared to the cefotaxime exposure control libraries. However, the specific components of LPS that were important for plasmid acceptance appear to differ between the two species. In *E. coli,* for example, protection of genes involved in the synthesis of components that make up the core oligosaccharide and inner lipid-A-core (for example, *galU*, *waaC* and *waaF*) of LPS was observed, whilst disruption of genes involved in the synthesis of the outer core

(for example, *waaB*, *waaR* and *waaU*) was also observed. In *S.* Typhimurium, the genes highlighted in the data were all protected. As cell-to-cell contact is important for plasmid conjugation, this data suggests that changes in the different components of the bacterial outer membrane may impact the process of plasmid uptake in different ways, and these impacts may be species or strain-specific.

Regarding efflux, the data suggested that efflux may play a role in plasmid acceptance. In both species, disrupted or reduced expression of the major AcrAB-TolC efflux pump appeared to benefit plasmid acceptance, although protection of other genes involved in the expression of other efflux pumps, such as *emrA* and *emrB* of EmrAB-TolC, was also observed. As deletion of efflux has previously been found to impact the structure of outer membrane proteins, including porins in *Enterobacteriaceae* (Saw et al., 2016), it was hypothesised that changes to the expression of efflux may alter membrane structure, leading to impacts on host plasmid acceptance. Given the role of efflux in bacterial AMR (Gaurav et al., 2023), there may also be an interplay between the acquisition of AMR genes and the expression of efflux, where elevated expression of efflux may no longer be required in cases where a gene encoding resistance has been acquired. Experiments investigating the role of efflux in plasmid uptake should be continued in the future to help better understand how these membrane-embedded proteins can influence plasmid acquisition.

In the *E. coli* transposon mutant libraries that had accepted pHYCTX14, an increased number of insertions was found in *rapA*, which encodes an RNAP-associated protein involved in RNAP recycling during transcription, and the results suggested that deletion of *rapA* would benefit plasmid uptake in this species. Whilst it was not possible to deduce the underlying mechanism of how this gene impacts plasmid acquisition from the results obtained, it was proposed that inactivation of *rapA* may reduce the fitness cost of plasmid acquisition by decreasing the transcription of plasmid-encoded genes, which are often overexpressed in the host cell after plasmid conjugation (Curtsinger et al., 2024). In *E. coli*, the expression of *rapA* has been found to be growth

rate dependent, with expression of the gene peaking during the early log phase of bacterial growth (Cabrera and Jin, 2001), and it has been found that *rapA* primarily interacts with RNAP bound to DNA post-transcription (known as a post-termination complex) to release RNAP from the DNA (Inlow et al., 2023). Studies investigating the impact of *rapA* deletion on bacterial fitness have found that, under normal laboratory conditions, where cells are grown in a nutrient-rich medium, growth is largely unaffected. However, when grown under stress, for example in high salt conditions (Sukhodolets et al., 2001), exposure to bile salts, and under osmotic stress (reference), the time for recovery of bacterial growth was increased, suggesting that *rapA* is important for the turnover of RNAP to maintain efficient levels of transcription (Fleurier et al., 2022), particularly under conditions where higher levels of transcription are required (Fleurier et al., 2022). Further investigations will be required to fully define the role of *rapA* in *E. coli* plasmid uptake.

8.3 CONCLUSIONS AND FUTURE WORK

In conclusion, this study describes the development of a multispecies biofilm conjugation model to establish a better understanding of how external stress factors can influence the rate of plasmid movement within a real-world context, as well as the use of TraDIS-*Xpress* to explore the full complement of genes implemented in plasmid acceptance. These experiments have laid the groundwork for further investigations into the evolution of AMR within multispecies biofilm communities and into developing a detailed insight into the host-plasmid interplay.

Whilst no statistically significant differences in the rate of plasmid movement between *E. coli* and *S.* Typhimurium within a biofilm under the chemicals tested, this was likely largely due to the batch effect, and the results of this study generally differed from those previously found in the literature. This may have been due to these studies using a different experimental set-up, for example, using liquid or filter conjugation assays to measure conjugation efficiency, and/ or pre-growing the donor strain with a subinhibitory concentration of the chemical tested (Cen et al., 2020, Shun-Mei et al., 2018, Palm et al., 2022).

Overall, this work describes a new method to monitor HGT within biofilms that allows for greater flexibility in the materials used as the substrate for biofilm formation in comparison to other closed biofilm models, such as those conducted in polystyrene plates. In the future, repeating the experiments conducted using the biofilm conjugation model, alongside improvements to the experimental design, such as the inclusion of an unstressed control with each stressor tested in the model, in addition to increasing the number of samples taken from each biological replicate, may allow for more sophisticated statistical analyses. This model could also be adapted to investigate plasmid movement in biofilm communities that are commonly found in clinically important infections, such as those that occur in the CF lung or chronic wounds, and it would be advantageous to develop a high-throughput method, such as flow cytometry, to investigate the impact of a broader range of environmental stressors on conjugation efficiency in biofilms. The movement of AMR genes between the bacterial chromosome and plasmids within and across species would also be interesting to explore

Furthermore, a high-throughput screen of the essential and non-essential genes required for host plasmid acceptance in *E. coli* and *S.* Typhimurium using an IncF plasmid was also conducted in this study, and the results obtained build on a previous investigation in plasmid uptake using the *E. coli* BW25113-derived Keio collection, where LPS was found to be important for plasmid uptake. The use of TraDIS-*Xpress* meant that both the non-essential and essential genes required for general bacterial survival could be assayed, addressing a key limitation of the previous study (Allard et al., 2023).

During this project, the process of constructing a number of single gene deletion mutants of some of the genes that were identified to be involved in *E. coli* plasmid acceptance were begun, to validate the TraDIS-*Xpress* data. Unfortunately, due to time constraints, it was not possible to complete these experiments. However, it would be useful to finish the construction of these mutants to establish how deleting these genes would impact the conjugation of pHYCTX14 into *E. coli* and use this information to help define the roles that these genes play in plasmid acquisition in this species. The genes identified to

play a role in plasmid acceptance in *S.* Typhimurium should also be explored further.

As the genes involved in plasmid acquisition may be host and/or plasmid-specific, investigating the genes implicated in plasmid uptake in a wider range of bacterial strains and species, using a more diverse range of plasmids, would be beneficial and may help to build a better understanding of host plasmid acceptance. Transposon mutant libraries should also be generated in plasmids to explore the roles of plasmid-encoded genes in conjugation, as this may also provide useful information on how specific components required for plasmid transfer in bacteria could be targeted to reduce the spread of AMR.

Finally, alongside conjugation, the roles of other mechanisms of HGT, such as OMVs (Johnston et al., 2023) and lateral transduction (Humphrey et al., 2021), in the dissemination of resistance in bacterial populations should also be studied.

REFERENCES

“Research is to see what everybody else has seen, and to think what nobody else has thought”

< Albert Szent-Györgyi >

ACMAN, M., WANG, R., VAN DORP, L., SHAW, L. P., WANG, Q., LUHMANN, N., YIN, Y., SUN, S., CHEN, H., WANG, H. & BALLOUX, F. 2022. Role of mobile genetic elements in the global dissemination of the carbapenem resistance gene blaNDM. *Nature Communications,* 13**,** 1131.

AFGAN, E., BAKER, D., BATUT, B., VAN DEN BEEK, M., BOUVIER, D., CECH, M., CHILTON, J., CLEMENTS, D., CORAOR, N., GRÜNING, B. A., GUERLER, A., HILLMAN-JACKSON, J., HILTEMANN, S., JALILI, V., RASCHE, H., SORANZO, N., GOECKS, J., TAYLOR, J., NEKRUTENKO, A. & BLANKENBERG, D. 2018. The Galaxy platform for accessible, reproducible and collaborative biomedical analyses: 2018 update.

ALAV, I. & BUCKNER, M. M. C. 2024. Non-antibiotic compounds associated with humans and the environment can promote horizontal transfer of antimicrobial resistance genes. *Critical reviews microbiology*.

ALHEDE, M., ALHEDE, M., QVORTRUP, K., KRAGH, K. N., JENSEN, P. Ø., STEWART, P. S. & BJARNSHOLT, T. 2020. The origin of extracellular DNA in bacterial biofilm infections in vivo. *Pathogens and disease,* 78**,** ftaa018.

ALIKHAN, N.-F., PETTY, N. K., BEN ZAKOUR, N. L. & BEATSON, S. A. 2011. BLAST Ring Image Generator (BRIG): simple prokaryote genome comparisons. *BMC genomics,* 12**,** 1-10.

ALLARD, N., COLLETTE, A., PAQUETTE, J., RODRIGUE, S. & CÔTÉ, J.-P. 2023. Systematic investigation of recipient cell genetic requirements reveals important surface receptors for conjugative transfer of IncI2 plasmids. *Communications Biology,* 6**,** 1172.

ALOTAIBI, G. F. & BUKHARI, M. A. 2021. Factors influencing bacterial biofilm formation and development. *Am. J. Biomed. Sci. Res,* 12**,** 617-626.

ALTSCHUL, S. F., MADDEN, T. L., SCHÄFFER, A. A., ZHANG, J., ZHANG, Z., MILLER, W. & LIPMAN, D. J. 1997. Gapped BLAST and PSI-BLAST: a new generation of protein database search programs. *Nucleic acids research,* 25**,** 3389-3402.

ANDREWS., S. 2024. FastQC A Quality Control tool for High Throughput Sequence Data. *Babraham Bioinformatics*.

ANGLES, M. L., MARSHALL KC FAU - GOODMAN, A. E. & GOODMAN, A. E. 1993. Plasmid Transfer between Marine Bacteria in the Aqueous Phase and Biofilms in Reactor Microcosms. *Applied and environmental microbiology*.

ARIAS-ANDRES, M., KLÜMPER, U., ROJAS-JIMENEZ, K. & GROSSART, H.-P. 2018. Microplastic pollution increases gene exchange in aquatic ecosystems. *Environmental Pollution,* 237**,** 253-261.

ASSAF, J. A., HOLDEN, E. R., TRAMPARI, E. & WEBBER, M. A. 2023. Common food preservatives impose distinct selective pressures on Salmonella Typhimurium planktonic and biofilm populations. *bioRxiv***,** 2023.09.28.559892.

AVILA-CALDERÓN, E. D., RUIZ-PALMA, M. D. S., AGUILERA-ARREOLA, M. G., VELÁZQUEZ-GUADARRAMA, N., RUIZ, E. A., GOMEZ-LUNAR, Z., WITONSKY, S. & CONTRERAS-RODRÍGUEZ, A. 2021. Outer Membrane Vesicles of Gram-Negative Bacteria: An Outlook on Biogenesis. *Frontiers in Microbiology,* 12.

AWAD, T. S., ASKER, D. & HATTON, B. D. 2018. Food-Safe Modification of Stainless Steel Food-Processing Surfaces to Reduce Bacterial Biofilms. *ACS Applied Materials & Interfaces,* 10**,** 22902-22912.

BAKER, K. S., DALLMAN, T. J., FIELD, N., CHILDS, T., MITCHELL, H., DAY, M., WEILL, F.-X., LEFÈVRE, S., TOURDJMAN, M., HUGHES, G., JENKINS, C. & THOMSON, N. 2018. Horizontal antimicrobial resistance transfer drives epidemics of multiple Shigella species. *Nature Communications,* 9**,** 1462.

BAKKEREN, E., HUISMAN, J. S., FATTINGER, S. A., HAUSMANN, A., FURTER, M., EGLI, A., SLACK, E., SELLIN, M. E., BONHOEFFER, S., REGOES, R. R., DIARD, M. & HARDT, W.-D. 2019. Salmonella persisters promote the spread of antibiotic resistance plasmids in the gut. *Nature,* 573**,** 276-280.

BALABAN, N. Q., HELAINE, S., LEWIS, K., ACKERMANN, M., ALDRIDGE, B., ANDERSSON, D. I., BRYNILDSEN, M. P., BUMANN, D., CAMILLI, A., COLLINS, J. J., DEHIO, C., FORTUNE, S., GHIGO, J.-M., HARDT, W.-D., HARMS, A., HEINEMANN, M., HUNG, D. T., JENAL, U., LEVIN, B. R., MICHIELS, J., STORZ, G., TAN, M.-W., TENSON, T., VAN MELDEREN, L. & ZINKERNAGEL, A. 2019. Definitions and guidelines for research on antibiotic persistence. *Nature Reviews Microbiology,* 17**,** 441-448.

BARQUIST, L., MAYHO, M., CUMMINS, C., CAIN, A. K., BOINETT, C. J., PAGE, A. J., LANGRIDGE, G. C., QUAIL, M. A., KEANE, J. A. & PARKHILL, J. 2016. The TraDIS toolkit: sequencing and analysis for dense transposon mutant libraries. *Bioinformatics,* 32**,** 1109-1111.

BAXTER, J. C. & FUNNELL, B. E. 2014. Plasmid Partition Mechanisms. *Microbiology Spectrum,* 2**,** 10.1128/microbiolspec.plas-0023-2014.

BERNE, C., ELLISON, C. K., DUCRET, A. & BRUN, Y. V. 2018. Bacterial adhesion at the single-cell level. *Nature Reviews Microbiology,* 16**,** 616-627.

BERTANI, B. & RUIZ, N. 2018. Function and Biogenesis of Lipopolysaccharides. LID - 10.1128/ecosalplus.ESP-0001-2018 [doi]. *EcoSal Plus*.

BEVAN, E. R., POWELL, M. J., TOLEMAN, M. A., THOMAS, C. M., PIDDOCK, L. J. V. & HAWKEY, P. M. 2021. Molecular characterization of plasmids encoding blaCTX-M from faecal Escherichia coli in travellers returning to the UK from South Asia. *Journal of Hospital Infection,* 114**,** 134-143.

BHUYAN, S., YADAV, M., GIRI, S. J., BEGUM, S., DAS, S., PHUKAN, A., PRIYADARSHANI, P., SARKAR, S., JAYSWAL, A., KABYASHREE, K., KUMAR, A., MANDAL, M. & RAY, S. K. 2023. Microliter spotting and micro-colony observation: A rapid and simple approach for counting bacterial colony forming units. *Journal of Microbiological Methods,* 207**,** 106707.

BJARNSHOLT, T. 2013. The role of bacterial biofilms in chronic infections. *Apmis,* 121**,** 1-58.

BOTTERY, M. J., MATTHEWS, J. L., WOOD, A. J., JOHANSEN, H. K., PITCHFORD, J. W. & FRIMAN, V.-P. 2022. Inter-species interactions alter antibiotic efficacy in bacterial communities. *The ISME Journal,* 16**,** 812-821.

BOWLER, P., MURPHY, C. & WOLCOTT, R. 2020. Biofilm exacerbates antibiotic resistance: Is this a current oversight in antimicrobial stewardship? *Antimicrobial Resistance & Infection Control,* 9**,** 162.
BOWRING, J. A.-O., SU, Y., ALSAADI, A., SVENNINGSEN, S. L., PARKHILL, J. A.-O. & INGMER, H. A.-O. 2022. Screening for Highly Transduced Genes in Staphylococcus aureus Revealed Both Lateral and Specialized Transduction.
BRACKMAN, G. & COENYE, T. 2015. Quorum sensing inhibitors as anti-biofilm agents. *Current pharmaceutical design,* 21**,** 5-11.
BRACKMAN, G., COS, P., MAES, L., NELIS, H. J. & COENYE, T. 2011. Quorum Sensing Inhibitors Increase the Susceptibility of Bacterial Biofilms to Antibiotics In Vitro and In Vivo. *Antimicrobial Agents and Chemotherapy,* 55**,** 2655-2661.
BRAUNER, A., FRIDMAN, O., GEFEN, O. & BALABAN, N. Q. 2016. Distinguishing between resistance, tolerance and persistence to antibiotic treatment. *Nature Reviews Microbiology,* 14**,** 320-330.
BROCKHURST, M. A. & HARRISON, E. 2022. Ecological and evolutionary solutions to the plasmid paradox. *Trends in Microbiology,* 30**,** 534-543.
BROEDERSZ, C. P., WANG, X., MEIR, Y., LOPARO, J. J., RUDNER, D. Z. & WINGREEN, N. S. 2014. Condensation and localization of the partitioning protein ParB on the bacterial chromosome. *Proceedings of the National Academy of Sciences,* 111**,** 8809-8814.
BROOK, I. 1989. Inoculum Effect. *Reviews of Infectious Diseases,* 11**,** 361-368.
BROWN, H. L., PURSLEY, I. G., HORTON, D. L. & LA RAGIONE, R. M. 2024. One health: a structured review and commentary on trends and themes. *One Health Outlook,* 6**,** 17.
BURMEISTER, A. R. 2015. Horizontal Gene Transfer. *Evolution, medicine, and public health,* 2015**,** 193-194.
BURMØLLE, M., REN, D., BJARNSHOLT, T. & SØRENSEN, S. J. 2014. Interactions in multispecies biofilms: do they actually matter? *Trends in microbiology,* 22**,** 84-91.
BURMØLLE, M., WEBB, J. S., RAO, D., HANSEN, L. H., SØRENSEN, S. J. & KJELLEBERG, S. 2006. Enhanced biofilm formation and increased resistance to antimicrobial agents and bacterial invasion are caused by synergistic interactions in multispecies biofilms. *Applied and environmental microbiology,* 72**,** 3916-3923.
CABRERA, J. E. & JIN, D. J. 2001. Growth phase and growth rate regulation of the rapA gene, encoding the RNA polymerase-associated protein RapA in Escherichia coli. *Journal of Bacteriology,* 183,20 : 6126-34.
CAMACHO, C., COULOURIS, G., AVAGYAN, V., MA, N., PAPADOPOULOS, J., BEALER, K. & MADDEN, T. L. 2009. BLAST+: architecture and applications. *BMC Bioinformatics,* 10**,** 421.
CÁMARA, M., GREEN, W., MACPHEE, C. E., RAKOWSKA, P. D., RAVAL, R., RICHARDSON, M. C., SLATER-JEFFERIES, J., STEVENTON, K. & WEBB, J. S. 2022. Economic significance of biofilms: a multidisciplinary and cross-sectoral challenge. *npj Biofilms and Microbiomes,* 8**,** 42.
CARATTOLI, A., ZANKARI, E., GARCÍA-FERNÁNDEZ, A., VOLDBY LARSEN, M., LUND, O., VILLA, L., MØLLER AARESTRUP, F. & HASMAN, H.

2014. In silico detection and typing of plasmids using PlasmidFinder and plasmid multilocus sequence typing.
CARDENAS-ARIAS, A. R., SANO, E., CARDOSO, B., FUGA, B., SELLERA, F. P., ESPOSITO, F., ARAVENA-RAMÍREZ, V., HUAMAN, D. C., GONZALES, C. D., ESPINOZA, L. L., HERNÁNDEZ, L. M. & LINCOPAN, N. 2024. Genomic data of global clones of CTX-M-65-producing Escherichia coli ST10 from South American llamas inhabiting the Andean Highlands of Peru. *Journal of Global Antimicrobial Resistance,* 36**,** 135-138.
CARVER, T., HARRIS, S. R., BERRIMAN, M., PARKHILL, J. & MCQUILLAN, J. A. 2012. Artemis: an integrated platform for visualization and analysis of high-throughput sequence-based experimental data. *Bioinformatics,* 28**,** 464-469.
CARVER, T. J., RUTHERFORD, K. M., BERRIMAN, M., RAJANDREAM, M.-A., BARRELL, B. G. & PARKHILL, J. 2005. ACT: the Artemis comparison tool. *Bioinformatics,* 21**,** 3422-3423.
CEN, T., ZHANG, X., XIE, S. & LI, D. 2020. Preservatives accelerate the horizontal transfer of plasmid-mediated antimicrobial resistance genes via differential mechanisms. *Environment International,* 138**,** 105544.
CHEE, M. S. J., SERRANO, E., CHIANG, Y. N., HARLING-LEE, J., MAN, R., BACIGALUPE, R., FITZGERALD, J. R., PENADÉS, J. R. & CHEN, J. 2023. Dual pathogenicity island transfer by piggybacking lateral transduction. *Cell,* 186**,** 3414-3426.e16.
CHEN, L., ZHENG, D., LIU, B., YANG, J. & JIN, Q. 2016. VFDB 2016: hierarchical and refined dataset for big data analysis--10 years on. *Nucleic Acids Res*.
CHEN, S., ZHOU, Y., CHEN, Y. & GU, J. 2018. fastp: an ultra-fast all-in-one FASTQ preprocessor. *bioRxiv***,** 274100.
CHI, F., NOLTE, O., BERGMANN, C., IP, M. & HAKENBECK, R. 2007. Crossing the barrier: Evolution and spread of a major class of mosaic pbp2x in Streptococcus pneumoniae, S. mitis and S. oralis. *International Journal of Medical Microbiology,* 297**,** 503-512.
CIOFU, O., MOSER, C., JENSEN, P. Ø. & HØIBY, N. 2022. Tolerance and resistance of microbial biofilms. *Nature Reviews Microbiology*.
COCK, P. J. A., CHILTON, J. M., GRÜNING, B., JOHNSON, J. E. & SORANZO, N. 2015. NCBI BLAST+ integrated into Galaxy. *GigaScience,* 4.
CONLON, B. P. 2014. Staphylococcus aureus chronic and relapsing infections: Evidence of a role for persister cells. *BioEssays,* 36**,** 991-996.
CONLON, B. P., ROWE, S. E. & LEWIS, K. 2015. Persister Cells in Biofilm Associated Infections. *In:* DONELLI, G. (ed.) *Biofilm-based Healthcare-associated Infections: Volume II.* Cham: Springer International Publishing.
CONSORTIUM, T. U. 2022. UniProt: the Universal Protein Knowledgebase in 2023. *Nucleic Acids Research,* 51**,** D523-D531.
COOK, L. C. & DUNNY, G. M. 2013. Effects of Biofilm Growth on Plasmid Copy Number and Expression of Antibiotic Resistance Genes in Enterococcus faecalis. *Antimicrobial Agents and Chemotherapy,* 57**,** 1850-1856.

COSTERTON, J. W., CHENG, K., GEESEY, G. G., LADD, T. I., NICKEL, J. C., DASGUPTA, M. & MARRIE, T. J. 1987. Bacterial biofilms in nature and disease. *Annual Reviews in Microbiology,* 41**,** 435-464.

CURTSINGER, H. D., MARTÍNEZ-ABSALÓN, S., LIU, Y. & LOPATKIN, A. J. 2024. The metabolic burden associated with plasmid acquisition: An assessment of the unrecognized benefits to host cells. *BioEssays,* 47**,** 2400164.

DARBY, E. M., TRAMPARI, E., SIASAT, P., GAYA, M. S., ALAV, I., WEBBER, M. A. & BLAIR, J. M. A. 2023. Molecular mechanisms of antibiotic resistance revisited. *Nature Reviews Microbiology,* 21**,** 280-295.

DAS, M., OJHA, A. K., DOLMA, K. G., MAJUMDAR, T., SARMAH, P., HAZARIKA, S., MODI, D., GOGOI, D., DAS, S. & RAMAMURTHY, T. 2025. Monitoring the potential dissemination of antimicrobial resistance in foods, environment, and clinical samples: a one health prospective. *Food Science and Biotechnology,* 34**,** 803-813.

DATSENKO, K. A. & WANNER, B. L. 2000. One-step inactivation of chromosomal genes in Escherichia coli K-12 using PCR products. *Proceedings of the National Academy of Sciences,* 97,12 (2000): 6640-5.

DE COSTER, W., D'HERT, S., SCHULTZ, D. T., CRUTS, M. & VAN BROECKHOVEN, C. 2018. NanoPack: visualizing and processing long-read sequencing data. *Bioinformatics,* 34**,** 2666-2669.

DEL POZO, J. L. & PATEL, R. 2007. The Challenge of Treating Biofilm-associated Bacterial Infections. *Clinical Pharmacology & Therapeutics,* 82**,** 204-209.

DIMITRIU, T. 2022. Evolution of horizontal transmission in antimicrobial resistance plasmids. *Microbiology,* 168.

DIMITRIU, T., SZCZELKUN, MARK D. & WESTRA, EDZE R. 2024. Various plasmid strategies limit the effect of bacterial restriction–modification systems against conjugation. *Nucleic Acids Research,* 52**,** 12976-12986.

DING, M., YE, Z., LIU, L., WANG, W., CHEN, Q., ZHANG, F., WANG, Y., SJÖLING, Å., MARTÍN-RODRÍGUEZ, A. J., HU, R., CHEN, W. & ZHOU, Y. 2022. Subinhibitory antibiotic concentrations promote the horizontal transfer of plasmid-borne resistance genes from Klebsiellae pneumoniae to Escherichia coli. *Frontiers in Microbiology,* Volume 13 - 2022.

DINGLE TANIS, C., GAMAGE, D., GOMEZ-VILLEGAS, S., HANSON BLAKE, M., REYES, J., ABBOTT, A., BURNHAM CAREY-ANN, D., DIEN BARD, J., FRITZ, S., MILLER WILLIAM, R., WESTBLADE LARS, F., ZIMMER, B., ARIAS CESAR, A. & BUTLER-WU, S. 2022. Prevalence and Characterization of the Cefazolin Inoculum Effect in North American Methicillin-Susceptible Staphylococcus aureus Isolates. *Journal of Clinical Microbiology,* 60**,** e02495-21.

DONLAN, R. M. 2001. Biofilm Formation: A Clinically Relevant Microbiological Process. *Clinical Infectious Diseases,* 33**,** 1387-1392.

DONLAN, R. M. 2002. Biofilms: microbial life on surfaces. *Emerging infectious diseases,* 8**,** 881-890.

DOSTER, E., LAKIN, S. M., DEAN, C. J., WOLFE, C., YOUNG, J. G., BOUCHER, C., BELK, K. E., NOYES, N. R. & MORLEY, P. S. 2019.

MEGARes 2.0: a database for classification of antimicrobial drug, biocide and metal resistance determinants in metagenomic sequence data. *Nucleic Acids Research,* 48**,** D561-D569.
ECKERT, C., GAUTIER, V. & ARLET, G. 2005. DNA sequence analysis of the genetic environment of various blaCTX-M genes. *Journal of Antimicrobial Chemotherapy,* 57**,** 14-23.
EHUWA, O., JAISWAL, A. A.-O. & JAISWAL, S. A.-O. 2021. Salmonella, Food Safety and Food Handling Practices. LID - 10.3390/foods10050907 [doi] LID - 907. *Foods*.
EL AILA, N. A., AL LAHAM, N. A. & AYESH, B. M. 2023. Prevalence of extended spectrum beta lactamase and molecular detection of blaTEM, blaSHV and blaCTX-M genotypes among Gram negative bacilli isolates from pediatric patient population in Gaza strip. *BMC Infectious Diseases,* 23**,** 99.
ELEMENT, S. J., MORAN, R. A., BEATTIE, E., HALL, R. J., SCHAIK, W. V. & BUCKNER, M. M. C. 2023. Growth in a biofilm promotes conjugation of a *bla*$_{\text{NDM-1}}$ bearing plasmid between *Klebsiella pneumoniae* strains. *mSphere,* 8**,** e00170-23.
ELIAS, S. & BANIN, E. 2012. Multi-species biofilms: living with friendly neighbors. *FEMS Microbiology Reviews,* 36**,** 990-1004.
ELLIS, C. N., TRAVERSE, C. C., MAYO-SMITH, L., BUSKIRK, S. W. & COOPER, V. S. 2015. Character displacement and the evolution of niche complementarity in a model biofilm community. *Evolution,* 69**,** 283-293.
ENNE, V. I., DELSOL AA FAU - ROE, J. M., ROE JM FAU - BENNETT, P. M. & BENNETT, P. M. 2006. Evidence of antibiotic resistance gene silencing in Escherichia coli. *Antimicrobial agents and chemotherapy*.
ESPINOSA, C. D. & STEIN, H. H. 2021. Digestibility and metabolism of copper in diets for pigs and influence of dietary copper on growth performance, intestinal health, and overall immune status: a review. *Journal of Animal Science and Biotechnology,* 12**,** 13.
EUCAST. 2022. *Antimicrobial susceptibility testing* [Online]. Available: **https://www.eucast.org/ast_of_bacteria** [Accessed 19th June 2025].
EZE, J., DUAN, Y., EZE, E., RAMANATHAN, R. & AJMAL, T. 2024. Machine learning-based optimal temperature management model for safety and quality control of perishable food supply chain. *Scientific Reports,* 14**,** 27228.
FAZLI, M., BJARNSHOLT, T., KIRKETERP-MØLLER, K., JØRGENSEN, B., ANDERSEN ANDERS, S., KROGFELT KAREN, A., GIVSKOV, M. & TOLKER-NIELSEN, T. 2009. Nonrandom Distribution of Pseudomonas aeruginosa and Staphylococcus aureus in Chronic Wounds. *Journal of Clinical Microbiology,* 47**,** 4084-4089.
FELDGARDEN, M., BROVER, V., HAFT, D. H., PRASAD, A. B., SLOTTA, D. J., TOLSTOY, I., TYSON, G. H., ZHAO, S., HSU, C. H., MCDERMOTT, P. F., TADESSE, D. A., MORALES, C., SIMMONS, M., TILLMAN, G., WASILENKO, J., FOLSTER, J. P. & KLIMKE, W. 2019. Validating the AMRFinder Tool and Resistance Gene Database by Using Antimicrobial Resistance Genotype-Phenotype Correlations in a Collection of Isolates. LID - 10.1128/AAC.00483-19 [doi] LID - e00483-19.

FENG, Y., LU, X., ZHAO, J., LI, H., XU, J., LI, Z., WANG, M., PENG, Y., TIAN, T., YUAN, G., ZHANG, Y., LIU, J., ZHANG, M., ZHU LA, A. L. T., QU, G., MU, Y., GUO, W., WU, Y., ZHANG, Y., WANG, D., HU, Y. & KAN, B. 2025. Regional antimicrobial resistance gene flow among the One Health sectors in China. *Microbiome,* 13**,** 3.

FISHER, R. A., GOLLAN, B. & HELAINE, S. 2017. Persistent bacterial infections and persister cells. *Nature Reviews Microbiology,* 15**,** 453-464.

FLEMING, D. & RUMBAUGH, K. P. 2017. Approaches to Dispersing Medical Biofilms. *Microorganisms,* 5**,** 15.

FLEMMING, H.-C., VAN HULLEBUSCH, E. D., NEU, T. R., NIELSEN, P. H., SEVIOUR, T., STOODLEY, P., WINGENDER, J. & WUERTZ, S. 2023. The biofilm matrix: multitasking in a shared space. *Nature Reviews Microbiology,* 21**,** 70-86.

FLEMMING, H.-C. & WINGENDER, J. 2010. The biofilm matrix. *Nature reviews microbiology,* 8**,** 623-633.

FLEMMING, H.-C., WINGENDER, J., SZEWZYK, U., STEINBERG, P., RICE, S. A. & KJELLEBERG, S. 2016. Biofilms: an emergent form of bacterial life. *Nature Reviews Microbiology,* 14**,** 563-575.

FLEURIER, S. A.-O., DAPA, T. A.-O. X., TENAILLON, O., CONDON, C. A.-O. & MATIC, I. A.-O. 2022. rRNA operon multiplicity as a bacterial genome stability insurance policy. *Nucleic Acids Res*.

FOSTER, J. S. & KOLENBRANDER, P. E. 2004. Development of a Multispecies Oral Bacterial Community in a Saliva-Conditioned Flow Cell. *Applied and Environmental Microbiology,* 70**,** 4340-4348.

FUGA, B., SELLERA, F. P., CERDEIRA, L., ESPOSITO, F., CARDOSO, B., FONTANA, H., MOURA, Q., CARDENAS-ARIAS, A., SANO, E., RIBAS, R. M., CARVALHO, A. C., TOGNIM, M. C. B., MORAIS, M. M. C. D., QUARESMA, A. J. P. G., SANTANA, Â. P., REIS, J. N., PILONETTO, M., VESPERO, E. C., BONELLI, R. R., CERQUEIRA, A. M. F., SINCERO, T. C. M. & LINCOPAN, N. 2022. WHO Critical Priority Escherichia coli as One Health Challenge for a Post-Pandemic Scenario: Genomic Surveillance and Analysis of Current Trends in Brazil. *Microbiology Spectrum,* 10**,** e01256-21.

FURSOVA, N. K., KISLICHKINA, A. A. & KHOKHLOVA, O. E. 2022. Plasmids Carrying Antimicrobial Resistance Genes in Gram-Negative Bacteria. *Microorganisms,* 10**,** 1678.

GALIÉ, S., GARCÍA-GUTIÉRREZ, C., MIGUÉLEZ, E. M., VILLAR, C. J. & LOMBÓ, F. 2018. Biofilms in the Food Industry: Health Aspects and Control Methods. *Frontiers in Microbiology,* 9.

GAMA, J. A., FREDHEIM, E. G. A., CLÉON, F., REIS, A. M., ZILHÃO, R. & DIONISIO, F. 2020. Dominance Between Plasmids Determines the Extent of Biofilm Formation. *Frontiers in Microbiology,* Volume 11 - 2020.

GARCÍA-BAYONA L AUID, S. N. F.-C., MICHAEL J., COYNE MJ FAU - FLORES, K., FLORES K FAU - ELMEKKI, N. M., ELMEKKI NM AUID-ORCID: ---487X FAU - SHEAHAN, M. L., SHEAHAN ML AUID- ORCID: --- FAU - CAMACHO, A. G., CAMACHO AG FAU - HUTT, K., HUTT K FAU - YILDIZ, F. H., YILDIZ FH AUID- ORCID: --- FAU - KOVÁCS, Á. T., KOVÁCS ÁT FAU - WALDOR, M. K., WALDOR MK AUID- ORCID: --- FAU - COMSTOCK, L. E. & COMSTOCK, L. E. 2024. A pervasive

large conjugative plasmid mediates multispecies biofilm formation in the intestinal microbiota increasing resilience to perturbations. LID - 2024.04.29.590671 [pii] LID - 10.1101/2024.04.29.590671 [doi]. *bioRxiv [Preprint]*.

GARCÍA-CONTRERAS, R., NUÑEZ-LÓPEZ, L., JASSO-CHÁVEZ, R., KWAN, B. W., BELMONT, J. A., RANGEL-VEGA, A., MAEDA, T. & WOOD, T. K. 2015. Quorum sensing enhancement of the stress response promotes resistance to quorum quenching and prevents social cheating. *The ISME Journal,* 9**,** 115-125.

GAURAV, A., BAKHT, P., SAINI, M., PANDEY, S. & PATHANIA, R. 2023. Role of bacterial efflux pumps in antibiotic resistance, virulence, and strategies to discover novel efflux pump inhibitors. LID - 10.1099/mic.0.001333 [doi] LID - 001333. *Microbiology,* 169,5.

GE, S. X., JUNG, D. & YAO, R. 2020. ShinyGO: a graphical gene-set enrichment tool for animals and plants. *Bioinformatics,* 36**,** 2628-2629.

GEISSMANN, Q. 2013. OpenCFU, a New Free and Open-Source Software to Count Cell Colonies and Other Circular Objects. *PLOS ONE,* 8**,** e54072.

GOEL, N., FATIMA, S. W., KUMAR, S., SINHA, R. & KHARE, S. K. 2021. Antimicrobial resistance in biofilms: Exploring marine actinobacteria as a potential source of antibiotics and biofilm inhibitors. *Biotechnology Reports,* 30**,** e00613.

GRENIER, F., MATTEAU, D., BABY, V. & RODRIGUE, S. 2014. Complete Genome Sequence of Escherichia coli BW25113. LID - 10.1128/genomeA.01038-14 [doi] LID - e01038-14.

GUILLAUME, O., BUTNARASU, C., VISENTIN, S. & REIMHULT, E. 2022. Interplay between biofilm microenvironment and pathogenicity of Pseudomonas aeruginosa in cystic fibrosis lung chronic infection. *Biofilm,* 4**,** 100089.

GUPTA, S. K., PADMANABHAN BR FAU - DIENE, S. M., DIENE SM FAU - LOPEZ-ROJAS, R., LOPEZ-ROJAS R FAU - KEMPF, M., KEMPF M FAU - LANDRAUD, L., LANDRAUD L FAU - ROLAIN, J.-M. & ROLAIN, J. M. 2014. ARG-ANNOT, a new bioinformatic tool to discover antibiotic resistance genes in bacterial genomes. *Antimicrob Agents Chemother*.

GUREVICH, A., SAVELIEV V FAU - VYAHHI, N., VYAHHI N FAU - TESLER, G. & TESLER, G. 2013. QUAST: quality assessment tool for genome assemblies. *Bioinformatics*.

GUYNET, C., CUEVAS A FAU - MONCALIÁN, G., MONCALIÁN G FAU - DE LA CRUZ, F. & DE LA CRUZ, F. 2011. The stb operon balances the requirements for vegetative stability and conjugative transfer of plasmid R388. *PLOS Genetics*.

HALAN, B., BUEHLER, K. & SCHMID, A. 2012. Biofilms as living catalysts in continuous chemical syntheses. *Trends in biotechnology,* 30**,** 453-465.

HE, Y., WANG, J., ZHANG, R., CHEN, L., ZHANG, H., QI, X. & CHEN, J. 2023. Epidemiology of foodborne diseases caused by Salmonella in Zhejiang Province, China, between 2010 and 2021. *Frontiers in Public Health,* Volume 11 - 2023.

HEMMATI, J., NAZARI, M., ABOLHASANI, F. S., AHMADI, A. & ASGHARI, B. 2024. In vitro investigation of relationship between quorum-sensing system genes, biofilm forming ability, and drug resistance in clinical isolates of Pseudomonas aeruginosa. *BMC Microbiology,* 24**,** 99.

HENGZHUANG, W., CIOFU O FAU - YANG, L., YANG L FAU - WU, H., WU H FAU - SONG, Z., SONG Z FAU - OLIVER, A., OLIVER A FAU - HØIBY, N. & HØIBY, N. 2013. High β-lactamase levels change the pharmacodynamics of β-lactam antibiotics in Pseudomonas aeruginosa biofilms.

HENNEQUIN, C., AUMERAN, C., ROBIN, F., TRAORE, O. & FORESTIER, C. 2012. Antibiotic resistance and plasmid transfer capacity in biofilm formed with a CTX-M-15-producing Klebsiella pneumoniae isolate. *Journal of Antimicrobial Chemotherapy,* 67**,** 2123-2130.

HENRIKSEN, N. N. S. E., HANSEN, M. F., KIESEWALTER, H. T., RUSSEL, J., NESME, J., FOSTER, K. R., SVENSSON, B., ØREGAARD, G., HERSCHEND, J. & BURMØLLE, M. 2022. Biofilm cultivation facilitates coexistence and adaptive evolution in an industrial bacterial community. *npj Biofilms and Microbiomes,* 8**,** 59.

HOBLEY, L., HARKINS, C., MACPHEE, C. E. & STANLEY-WALL, N. R. 2015. Giving structure to the biofilm matrix: an overview of individual strategies and emerging common themes. *FEMS Microbiology Reviews,* 39**,** 649-669.

HOGAN, S., O'GARA, J. P. & O'NEILL, E. 2018. Novel Treatment of Staphylococcus aureus Device-Related Infections Using Fibrinolytic Agents. *Antimicrobial Agents and Chemotherapy,* 62**,** 10.1128/aac.02008-17.

HØIBY, N., BJARNSHOLT, T., GIVSKOV, M., MOLIN, S. & CIOFU, O. 2010. Antibiotic resistance of bacterial biofilms. *International Journal of Antimicrobial Agents,* 35**,** 322-332.

HOLDEN, E. R., HORTON, J. C. I. & WEBBER, M. A. 2025. Common food preservatives induce an oxidative stress response in Salmonella enterica serovar Typhimurium. *Microbiology,* 171.

HOLDEN, E. R., YASIR, M., TURNER, A. K., CHARLES, I. G. & WEBBER, M. A. 2022. Comparison of the genetic basis of biofilm formation between Salmonella Typhimurium and Escherichia coli. *Microbial Genomics,* 8.

HUMPHREY, B., THOMSON, N. R., THOMAS, C. M., BROOKS, K., SANDERS, M., DELSOL, A. A., ROE, J. M., BENNETT, P. M. & ENNE, V. I. 2012. Fitness of Escherichia coli strains carrying expressed and partially silent IncN and IncP1 plasmids. *BMC Microbiology,* 12**,** 53.

HUMPHREY, S. A.-O., FILLOL-SALOM, A. A.-O. X., QUILES-PUCHALT, N. A.-O., IBARRA-CHÁVEZ, R. A.-O., HAAG, A. A.-O., CHEN, J. & PENADÉS, J. A.-O. 2021. Bacterial chromosomal mobility via lateral transduction exceeds that of classical mobile genetic elements.

HUSNA, A., RAHMAN, M. M., BADRUZZAMAN, A. T. M., SIKDER, M. H., ISLAM, M. R., RAHMAN, M. T., ALAM, J. & ASHOUR, H. M. 2023. Extended-Spectrum β-Lactamases (ESBL): Challenges and Opportunities. *Biomedicines,* 11**,** 2937.

HYNEN, A. L., LAZENBY, J. J., SAVVA, G. M., MCCAUGHEY, L. C., TURNBULL, L., NOLAN, L. M. & WHITCHURCH, C. B. 2021. Multiple holins contribute to extracellular DNA release in Pseudomonas aeruginosa biofilms. *Microbiology (Reading, England),* 167**,** 000990.

IDT. 2025. *OligoAnalyzer™ Tool* [Online]. Available: https://eu.idtdna.com/pages/tools/oligoanalyzer [Accessed 17th June 2025].

INGLE, D. J., VALCANIS, M., KUZEVSKI, A., TAUSCHEK, M., INOUYE, M., STINEAR, T., LEVINE, M. M., ROBINS-BROWNE, R. M. & HOLT, K. E. 2016. In silico serotyping of E. coli from short read data identifies limited novel O-loci but extensive diversity of O:H serotype combinations within and between pathogenic lineages. *Microbial Genomics*.

INLOW, K. A.-O., TENENBAUM, D., FRIEDMAN, L. A.-O., KONDEV, J. & GELLES, J. A.-O. 2023. Recycling of bacterial RNA polymerase by the Swi2/Snf2 ATPase RapA. *Proceedings of the National Academy of Sciences*.

JAKUBOVICS, N. S., SHIELDS, R. C., RAJARAJAN, N. & BURGESS, J. G. 2013. Life after death: the critical role of extracellular DNA in microbial biofilms. *Letters in Applied Microbiology,* 57**,** 467-475.

JAN, A. T. 2017. Outer Membrane Vesicles (OMVs) of Gram-negative Bacteria: A Perspective Update. *Frontiers in Microbiology,* 8.

JANECKO, N., ZAMUDIO, R., PALAU, R., BLOOMFIELD, S. J. & MATHER, A. E. 2023. Repeated cross-sectional study identifies differing risk factors associated with microbial contamination in common food products in the United Kingdom. *Food Microbiology,* 111**,** 104196.

JANG, S. 2023. AcrAB-TolC, a major efflux pump in Gram negative bacteria: toward understanding its operation mechanism. *BMB reports,* 56,6.

JARVIK, T., SMILLIE C FAU - GROISMAN, E. A., GROISMAN EA FAU - OCHMAN, H. & OCHMAN, H. 2010. Short-term signatures of evolutionary change in the Salmonella enterica serovar typhimurium 14028 genome.

JIA, B., RAPHENYA, A. R., ALCOCK, B., WAGLECHNER, N., GUO, P., TSANG, K. K., LAGO, B. A., DAVE, B. M., PEREIRA, S., SHARMA, A. N., DOSHI, S., COURTOT, M., LO, R., WILLIAMS, L. E., FRYE, J. G., ELSAYEGH, T., SARDAR, D., WESTMAN, E. L., PAWLOWSKI, A. C., JOHNSON, T. A., BRINKMAN, F. S., WRIGHT, G. D. & MCARTHUR, A. G. 2017. CARD 2017: expansion and model-centric curation of the comprehensive antibiotic resistance database. *Nucleic Acids Res*.

JIN, D. J., ZHOU, Y. N., SHAW, G. & JI, X. 2011. Structure and function of RapA: A bacterial Swi2/Snf2 protein required for RNA polymerase recycling in transcription. *Biochimica et Biophysica Acta (BBA) - Gene Regulatory Mechanisms,* 1809**,** 470-475.

JOHNSTON, E. A.-O., ZAVAN, L., BITTO, N. J., PETROVSKI, S., HILL, A. F. & KAPARAKIS-LIASKOS, M. A.-O. 2023. Planktonic and Biofilm-Derived Pseudomonas aeruginosa Outer Membrane Vesicles Facilitate Horizontal Gene Transfer of Plasmid DNA.

JOLLEY, K. A.-O., BRAY, J. A.-O. & MAIDEN, M. A.-O. 2018. Open-access bacterial population genomics: BIGSdb software, the PubMLST.org website and their applications.

KADEŘÁBKOVÁ, N., MAHMOOD, A. J. S. & MAVRIDOU, D. A. I. 2024. Antibiotic susceptibility testing using minimum inhibitory concentration (MIC) assays. *npj Antimicrobials and Resistance,* 2**,** 37.

KALLOVÁ, J., KETTNER, M., MAČIČKOVÁ, T., MILOŠOVIČ, P. & LANGŠÁDL, L. 1997. Aminoglycoside resistance. Enzymatic mechanisms in clinical bacterial strains in Slovakia during the last decade. *FEMS Immunology & Medical Microbiology,* 19**,** 89-94.

KAMALI, E., JAMALI, A., IZANLOO, A. & ARDEBILI, A. 2021. In vitro activities of cellulase and ceftazidime, alone and in combination against Pseudomonas aeruginosa biofilms. *BMC Microbiology,* 21**,** 347.
KAPLAN, J. B. 2010. Biofilm dispersal: mechanisms, clinical implications, and potential therapeutic uses. *Journal of dental research,* 89**,** 205-218.
KARCZMARCZYK, M., WANG, J., LEONARD, N. & FANNING, S. 2014. Complete nucleotide sequence of a conjugative IncF plasmid from an Escherichia coli isolate of equine origin containing blaCMY-2 within a novel genetic context. *FEMS Microbiology Letters,* 352**,** 123-127.
KARP, P. D., PALEY, S., CASPI, R., KOTHARI, A., KRUMMENACKER, M., MIDFORD, P. E., MOORE, L. R., SUBHRAVETI, P., GAMA-CASTRO, S., TIERRAFRIA, V. H., LARA, P., MUÑIZ-RASCADO, L., BONAVIDES-MARTINEZ, C., SANTOS-ZAVALETA, A., MACKIE, A., SUN, G., AHN-HORST, T. A., CHOI, H., COVERT, M. W., COLLADO-VIDES, J. & PAULSEN, I. 2023. The EcoCyc Database (2023). *EcoSal Plus,* 11**,** eesp-0002-2023.
KARYGIANNI, L., REN, Z., KOO, H. & THURNHEER, T. 2020. Biofilm Matrixome: Extracellular Components in Structured Microbial Communities. *Trends in Microbiology,* 28**,** 668-681.
KELVIN LEE, K. W., HOONG YAM, J. K., MUKHERJEE, M., PERIASAMY, S., STEINBERG, P. D., KJELLEBERG, S. & RICE, S. A. 2016. Interspecific diversity reduces and functionally substitutes for intraspecific variation in biofilm communities. *The ISME journal,* 10**,** 846-857.
KHATOON, Z., MCTIERNAN, C. D., SUURONEN, E. J., MAH, T.-F. & ALARCON, E. I. 2018. Bacterial biofilm formation on implantable devices and approaches to its treatment and prevention. *Heliyon,* 4**,** e01067-e01067.
KLAUSEN, M., HEYDORN A FAU - RAGAS, P., RAGAS P FAU - LAMBERTSEN, L., LAMBERTSEN L FAU - AAES-JØRGENSEN, A., AAES-JØRGENSEN A FAU - MOLIN, S., MOLIN S FAU - TOLKER-NIELSEN, T. & TOLKER-NIELSEN, T. 2003. Biofilm formation by Pseudomonas aeruginosa wild type, flagella and type IV pili mutants. *Mol Microbiol,* 48(6):1511-24.
KLAYMAN, B. J., VOLDEN, P. A., STEWART, P. S. & CAMPER, A. K. 2009. Escherichia coli O157: H7 requires colonizing partner to adhere and persist in a capillary flow cell. *Environmental science & technology,* 43**,** 2105-2111.
KOECHLER, S., FARASIN, J., CLEISS-ARNOLD, J. & ARSÈNE-PLOETZE, F. 2015. Toxic metal resistance in biofilms: diversity of microbial responses and their evolution. *Research in Microbiology,* 166**,** 764-773.
KOLÁŘ, M., URBÁNEK, K. & LÁTAL, T. 2001. Antibiotic selective pressure and development of bacterial resistance. *International Journal of Antimicrobial Agents,* 17**,** 357-363.
KOLMOGOROV, M., YUAN, J., LIN, Y. & PEVZNER, P. A. 2019. Assembly of long, error-prone reads using repeat graphs. *Nature Biotechnology,* 37**,** 540-546.
KÕRESSAAR, T., LEPAMETS, M., KAPLINSKI, L., RAIME, K., ANDRESON, R. & REMM, M. 2018. Primer3_masker: integrating masking of template sequence with primer design software. *Bioinformatics,* 34**,** 1937-1938.

KORESSAAR, T. & REMM, M. 2007. Enhancements and modifications of primer design program Primer3. *Bioinformatics,* 23**,** 1289-91.
KRAGH, K. N., HUTCHISON, J. B., MELAUGH, G., RODESNEY, C., ROBERTS, A. E., IRIE, Y., JENSEN, P., DIGGLE, S. P., ALLEN, R. J., GORDON, V. & BJARNSHOLT, T. 2016. Role of Multicellular Aggregates in Biofilm Formation.
KRAGH, K. N., TOLKER-NIELSEN, T. & LICHTENBERG, M. 2023. The non-attached biofilm aggregate. *Communications Biology,* 6**,** 898.
KWIECINSKI, J., PEETERMANS, M., LIESENBORGHS, L., NA, M., BJÖRNSDOTTIR, H., ZHU, X., JACOBSSON, G., JOHANSSON, B. R., GEOGHEGAN, J. A., FOSTER, T. J., JOSEFSSON, E., BYLUND, J., VERHAMME, P. & JIN, T. 2016. Staphylokinase Control of Staphylococcus aureus Biofilm Formation and Detachment Through Host Plasminogen Activation. *The Journal of Infectious Diseases,* 213**,** 139-148.
LANGMEAD, B. & SALZBERG, S. L. 2012. Fast gapped-read alignment with Bowtie 2. *Nature Methods,* 9**,** 357-359.
LANGMEAD, B., TRAPNELL, C., POP, M. & SALZBERG, S. L. 2009. Ultrafast and memory-efficient alignment of short DNA sequences to the human genome. *Genome Biology,* 10**,** R25.
LANGRIDGE, G. C., PHAN MD FAU - TURNER, D. J., TURNER DJ FAU - PERKINS, T. T., PERKINS TT FAU - PARTS, L., PARTS L FAU - HAASE, J., HAASE J FAU - CHARLES, I., CHARLES I FAU - MASKELL, D. J., MASKELL DJ FAU - PETERS, S. E., PETERS SE FAU - DOUGAN, G., DOUGAN G FAU - WAIN, J., WAIN J FAU - PARKHILL, J., PARKHILL J FAU - TURNER, A. K. & TURNER, A. K. 2009. Simultaneous assay of every Salmonella Typhi gene using one million transposon mutants. *Genome research,* 19,12.
LAWLEY, T. D., KLIMKE, W. A., GUBBINS, M. J. & FROST, L. S. 2003. F factor conjugation is a true type IV secretion system. *FEMS Microbiology Letters,* 224**,** 1-15.
LÉCUYER, F., BOURASSA, J.-S., GÉLINAS, M., CHARRON-LAMOUREUX, V., BURRUS, V. & BEAUREGARD, P. B. 2018. Biofilm Formation Drives Transfer of the Conjugative Element ICE*Bs1* in *Bacillus subtilis*. *mSphere,* 3**,** 10.1128/msphere.00473-18.
LEE, D. J., BINGLE, L. E. H., HEURLIER, K., PALLEN, M. J., PENN, C. W., BUSBY, S. J. W. & HOBMAN, J. L. 2009. Gene doctoring: a method for recombineering in laboratory and pathogenic Escherichia colistrains. *BMC Microbiology,* 9**,** 252.
LEE, J. J., LEE, J. H., KWON, D. B., JEON, J. H., PARK, K. S., LEE, C. R. & LEE, S. H. 2015. Fast and Accurate Large-Scale Detection of β-Lactamase Genes Conferring Antibiotic Resistance. *Antimicrobial agents and chemotherapy*.
LEVIN-REISMAN, I., RONIN, I., GEFEN, O., BRANISS, I., SHORESH, N. & BALABAN, N. Q. 2017. Antibiotic tolerance facilitates the evolution of resistance. *Science,* 355**,** 826-830.
LI, B., QIU, Y., ZHANG, J., HUANG, X., SHI, H. & YIN, H. 2018a. Real-Time Study of Rapid Spread of Antibiotic Resistance Plasmid in Biofilm Using Microfluidics. *Environmental Science & Technology,* 52**,** 11132-11141.

LI, H. 2018. Minimap2: pairwise alignment for nucleotide sequences. *Bioinformatics,* 34**,** 3094-3100.
LI, H. & DURBIN, R. 2009. Fast and accurate short read alignment with Burrows–Wheeler transform. *Bioinformatics,* 25**,** 1754-1760.
LI, H. & DURBIN, R. 2010. Fast and accurate long-read alignment with Burrows–Wheeler transform. *Bioinformatics,* 26**,** 589-595.
LI, J. J., SPYCHALA, C. N., HU, F., SHENG, J. F. & DOI, Y. 2015. Complete nucleotide sequences of bla(CTX-M)-harboring IncF plasmids from community-associated Escherichia coli strains in the United States. *Antimicrobial agents and chemotherapy*.
LI, P.-L., HWANG, I., MIYAGI, H., TRUE, H. & FARRAND, S. K. 1999. Essential components of the Ti plasmid trb system, a type IV macromolecular transporter. *Journal of bacteriology,* 181**,** 5033-5041.
LI, X., XIE, Y., LIU, M., TAI, C., SUN, J., DENG, Z. & OU, H.-Y. 2018b. oriTfinder: a web-based tool for the identification of origin of transfers in DNA sequences of bacterial mobile genetic elements. *Nucleic Acids Research,* 46**,** W229-W234.
LI, Y.-H. & TIAN, X. 2012. Quorum sensing and bacterial social interactions in biofilms. *Sensors (Basel, Switzerland),* 12**,** 2519-2538.
LIAO, X. P., XIA, J., YANG, L., LI, L., SUN, J., LIU, Y. H. & JIANG, H. X. 2015. Characterization of CTX-M-14-producing Escherichia coli from food-producing animals. *Frontiers in microbiology*.
LICHTENBERG, M., KVICH, L., LARSEN SARA LOUISE, B., JAKOBSEN TIM, H. & BJARNSHOLT, T. 2022. Inoculum Concentration Influences Pseudomonas aeruginosa Phenotype and Biofilm Architecture. *Microbiology Spectrum,* 10**,** e03131-22.
LIM, E. S., KOO, O. K., KIM, M.-J. & KIM, J.-S. 2019. Bio-enzymes for inhibition and elimination of Escherichia coli O157:H7 biofilm and their synergistic effect with sodium hypochlorite. *Scientific Reports,* 9**,** 9920.
LIN, Y., XU, X., MARÓTI, G., STRUBE, M. L. & KOVÁCS, Á. T. 2022a. Adaptation and phenotypic diversification of Bacillus thuringiensis biofilm are accompanied by fuzzy spreader morphotypes. *npj Biofilms and Microbiomes,* 8**,** 27.
LIN, Y., YUAN, J., KOLMOGOROV, M., SHEN, M. W., CHAISSON, M. & PEVZNER, P. A. 2016. Assembly of long error-prone reads using de Bruijn graphs. *Proceedings of the National Academy of Sciences,* 113**,** E8396-E8405.
LIN, Z., WANG, G., LI, S., ZHOU, L. & YANG, H. A.-O. 2022b. Dual-Species Biofilms Formed by Escherichia coli and Salmonella Enhance Chlorine Tolerance. *Applied and environmental microbiology*.
LISTER, J. L. & HORSWILL, A. R. 2014. Staphylococcus aureus biofilms: recent developments in biofilm dispersal. *Frontiers in cellular and infection microbiology,* 4**,** 178.
LIU, G., THOMSEN, L. E. & OLSEN, J. E. 2021. Antimicrobial-induced horizontal transfer of antimicrobial resistance genes in bacteria: a mini-review. *Journal of Antimicrobial Chemotherapy,* 77**,** 556-567.
LIU, H. Y., PRENTICE, E. L. & WEBBER, M. A. 2024. Mechanisms of antimicrobial resistance in biofilms. *npj Antimicrobials and Resistance,* 2**,** 27.

LOPES, S. P., CERI, H., AZEVEDO, N. F. & PEREIRA, M. O. 2012. Antibiotic resistance of mixed biofilms in cystic fibrosis: impact of emerging microorganisms on treatment of infection. *International journal of antimicrobial agents,* 40**,** 260-263.

LORIES, B., BELPAIRE, T. E. R., SMEETS, B. & STEENACKERS, H. P. 2024. Competition quenching strategies reduce antibiotic tolerance in polymicrobial biofilms. *npj Biofilms and Microbiomes,* 10**,** 23.

LORIES, B., ROBERFROID, S., DIELTJENS, L., DE COSTER, D., FOSTER, K. R. & STEENACKERS, H. P. 2020. Biofilm Bacteria Use Stress Responses to Detect and Respond to Competitors. *Current Biology,* 30**,** 1231-1244.e4.

LORUSSO, A. A.-O., CARRARA, J. A., BARROSO, C. D. N., TUON, F. F. & FAORO, H. A.-O. 2022. Role of Efflux Pumps on Antimicrobial Resistance in Pseudomonas aeruginosa. LID - 10.3390/ijms232415779 [doi] LID - 15779.

LOW, W. W., WONG, J. L. C., BELTRAN, L. C., SEDDON, C., DAVID, S., KWONG, H.-S., BIZEAU, T., WANG, F., PEÑA, A., COSTA, T. R. D., PHAM, B., CHEN, M., EGELMAN, E. H., BEIS, K. & FRANKEL, G. 2022. Mating pair stabilization mediates bacterial conjugation species specificity. *Nature Microbiology,* 7**,** 1016-1027.

LU, J., BREITWIESER, F. P., THIELEN, P. & SALZBERG, S. L. 2017. Bracken: estimating species abundance in metagenomics data. *PeerJ Comput Sci,* 3:e104.

LYNCH, S. V., DIXON, L., BENOIT, M. R., BRODIE, E. L., KEYHAN, M., HU, P., ACKERLEY, D. F., ANDERSEN, G. L. & MATIN, A. 2007. Role of the *rapA* Gene in Controlling Antibiotic Resistance of *Escherichia coli* Biofilms. *Antimicrobial Agents and Chemotherapy,* 51**,** 3650-3658.

MA, L., KONKEL, M. E. & LU, X. 2021. Antimicrobial Resistance Gene Transfer from Campylobacter jejuni in Mono- and Dual-Species Biofilms. *Applied and environmental microbiology*.

MADSEN, J. S., BURMØLLE, M., HANSEN, L. H. & SØRENSEN, S. J. 2012. The interconnection between biofilm formation and horizontal gene transfer. *FEMS Immunology & Medical Microbiology,* 65**,** 183-195.

MAJOWICZ, S. E., MUSTO, J., SCALLAN, E., ANGULO, F. J., KIRK, M., O'BRIEN, S. J., JONES, T. F., FAZIL, A., HOEKSTRA, R. M. & STUDIES, F. T. I. C. O. E. D. B. O. I. 2010. The Global Burden of Nontyphoidal Salmonella Gastroenteritis. *Clinical Infectious Diseases,* 50**,** 882-889.

MANEEWANNAKUL, K. & IPPEN-IHLER, K. 1993. Construction and analysis of F plasmid traR, trbJ, and trbH mutants. *Journal of Bacteriology,* 175**,** 1528-1531.

MANEEWANNAKUL, S., MANEEWANNAKUL, K. & IPPEN-IHLER, K. 1992. Characterization, localization, and sequence of F transfer region products: the pilus assembly gene product TraW and a new product, TrbI. *Journal of Bacteriology,* 174**,** 5567-5574.

MARSH, P. & ZAURA, E. 2017. Dental biofilm: ecological interactions in health and disease. *Journal of clinical periodontology,* 44**,** S12-S22.

MARTÍNEZ-REYES, I. & CHANDEL, N. S. 2020. Mitochondrial TCA cycle metabolites control physiology and disease. *Nature Communications,* 11**,** 102.

MATER, D. D., SAUCEDO JE FAU - TRUFFAUT, N., TRUFFAUT N FAU - BARBOTIN, J. N., BARBOTIN JN FAU - THOMAS, D. & THOMAS, D. 1999. Conjugative plasmid transfer between Pseudomonas strains within alginate bead microcosms: effect of the internal gel structure. *Biotechnol Bioeng*.

MATTHEWS, T. C., BRISTOW, F. R., GRIFFITHS, E. J., PETKAU, A., ADAM, J., DOOLEY, D., KRUCZKIEWICZ, P., CURATCHA, J., CABRAL, J., FORNIKA, D., WINSOR, G. L., COURTOT, M., BERTELLI, C., ROUDGAR, A., FEIJAO, P., MABON, P., ENNS, E., THIESSEN, J., KEDDY, A., ISAAC-RENTON, J., GARDY, J. L., TANG, P., JOÃO A CARRIÇO, T. I. C., CHINDELEVITCH, L., CHAUVE, C., GRAHAM, M. R., MCARTHUR, A. G., TABOADA, E. N., BEIKO, R. G., BRINKMAN, F. S. L., HSIAO, W. W. L. & DOMSELAAR, G. V. 2018. The Integrated Rapid Infectious Disease Analysis (IRIDA) Platform. *bioRxiv*, 381830.

MCVICKER, G. & TANG, C. M. 2016. Deletion of toxin–antitoxin systems in the evolution of Shigella sonnei as a host-adapted pathogen. *Nature Microbiology,* 2, 16204.

METZGER, G. A., RIDENHOUR, B. J., FRANCE, M., GLINIEWICZ, K., MILLSTEIN, J., SETTLES, M. L., FORNEY, L. J., STALDER, T. & TOP, E. M. 2022. Biofilms preserve the transmissibility of a multi-drug resistance plasmid. *npj Biofilms and Microbiomes,* 8, 95.

MHATRE, E., SNYDER, D. J., SILEO, E., TURNER, C. B., BUSKIRK, S. W., FERNANDEZ, N. L., NEIDITCH, M. B., WATERS, C. M. & COOPER, V. S. 2020. One gene, multiple ecological strategies: A biofilm regulator is a capacitor for sustainable diversity. *Proceedings of the National Academy of Sciences,* 117, 21647-21657.

MICHAELIS, C. & GROHMANN, E. 2023. Horizontal gene transfer of antibiotic resistance genes in biofilms. *Antibiotics,* 12, 328.

MILLAN, A. S. & MACLEAN, R. C. 2017. Fitness Costs of Plasmids: a Limit to Plasmid Transmission. *Microbiology Spectrum,* 5, 10.1128/microbiolspec.mtbp-0016-2017.

MISRA, T., TARE, M. & JHA, P. N. 2023. Characterization of functional amyloid curli in biofilm formation of an environmental isolate Enterobacter cloacae SBP-8. *Antonie van Leeuwenhoek,* 116, 829-843.

MONTEIRO, C., FANG, X., AHMAD, I., GOMELSKY, M. & RÖMLING, U. 2011. Regulation of Biofilm Components in Salmonella enterica Serovar Typhimurium by Lytic Transglycosylases Involved in Cell Wall Turnover. *Journal of Bacteriology,* 193, 6443-6451.

MOORE, LISA R., CASPI, R., BOYD, D., BERKMEN, M., MACKIE, A., PALEY, S. & KARP, PETER D. 2024. Revisiting the y-ome of Escherichia coli. *Nucleic Acids Research,* 52, 12201-12207.

MOREMI, N., SILAGO, V., MSELEWA, E. G., CHIFWAGUZI, A. P., MIRAMBO, M. M., MUSHI, M. F., MATEMBA, L., SENI, J. & MSHANA, S. E. 2021. Extended-spectrum β-lactamase blaCTX-M-1 group in gram-negative bacteria colonizing patients admitted at Mazimbu hospital and Morogoro Regional hospital in Morogoro, Tanzania. *BMC Research Notes,* 14, 77.

MUHAMMAD, M. H., IDRIS, A. L., FAN, X., GUO, Y., YU, Y., JIN, X., QIU, J., GUAN, X. & HUANG, T. 2020. Beyond risk: bacterial biofilms and their regulating approaches. *Frontiers in microbiology,* 11, 928.

MUSANNA, FARIDOON KHAN, U., HABIB, G., GUL, H., HAYAT, A. & UR REHMAN, M. 2024. Contribution of the gyrA and waaG mutants to fluoroquinolones resistance, biofilm development, and persister cells formation in Salmonella enterica serovar Typhi. *Gene,* 894**,** 147943.

MUTHUIRULANDI SETHUVEL, D. P., ANANDAN, S., DEVANGA RAGUPATHI, N. K., GAJENDIRAN, R., KURODA, M., SHIBAYAMA, K. & VEERARAGHAVAN, B. 2019. IncFII plasmid carrying antimicrobial resistance genes in Shigella flexneri: Vehicle for dissemination. *Journal of Global Antimicrobial Resistance,* 16**,** 215-219.

NADELL, C. D., DRESCHER, K. & FOSTER, K. R. 2016. Spatial structure, cooperation and competition in biofilms. *Nature Reviews Microbiology,* 14**,** 589-600.

NANOPORETECH. 2018. *Sequence correction provided by ONT Research* [Online]. Available: https://github.com/nanoporetech/medaka [Accessed].

OGBOLU, D. O., DAINI OA FAU - OGUNLEDUN, A., OGUNLEDUN A FAU - ALLI, A. O., ALLI AO FAU - WEBBER, M. A. & WEBBER, M. A. 2011. High levels of multidrug resistance in clinical isolates of Gram-negative pathogens from Nigeria. *International Journal of Antimicrobial Agents*.

OKSHEVSKY, M., REGINA, V. R. & MEYER, R. L. 2015. Extracellular DNA as a target for biofilm control. *Current Opinion in Biotechnology,* 33**,** 73-80.

OLSEN, I. 2015. Biofilm-specific antibiotic tolerance and resistance. *European Journal of Clinical Microbiology & Infectious Diseases,* 34**,** 877-886.

OTTO, M. 2013. Staphylococcal Infections: Mechanisms of Biofilm Maturation and Detachment as Critical Determinants of Pathogenicity. *Annual Review of Medicine,* 64**,** 175-188.

PAGE, A. J., BASTKOWSKI, S., YASIR, M., TURNER, A. K., LE VIET, T., SAVVA, G. M., WEBBER, M. A. & CHARLES, I. G. 2019. AlbaTraDIS: Comparative analysis of large datasets from parallel transposon mutagenesis experiments. *bioRxiv***,** 593624.

PAGE, A. J. & LANGRIDGE, G. C. 2019. Socru: Typing of genome level order and orientation in bacteria. *bioRxiv***,** 543702.

PALM, M. A.-O. X., FRANSSON, A., HULTÉN, J., BÚCARO STENMAN, K., ALLOUCHE, A., CHIANG, O. E., CONSTANDSE, M. L., VAN DIJK, K. J., ICLI, S., KLIMESOVA, B., KORHONEN, E., MARTÍNEZ-CRESPO, G. A.-O., MEGGERS, D., NAYDENOVA, M., POLYCHRONOPOULOU, M. A., SCHUNTERMANN, D. B., UNAL, H., WASYLKOWSKA, A. & FAREWELL, A. A.-O. 2022. The Effect of Heavy Metals on Conjugation Efficiency of an F-Plasmid in Escherichia coli. LID - 10.3390/antibiotics11081123 [doi] LID - 1123. *Antibiotics,* 19;11(8):1123.

PARIJS, I. & STEENACKERS, H. P. 2018. Competitive inter-species interactions underlie the increased antimicrobial tolerance in multispecies brewery biofilms.

PARKS, D. H., IMELFORT, M., SKENNERTON, C. T., HUGENHOLTZ, P. & TYSON, G. W. 2015. CheckM: assessing the quality of microbial genomes recovered from isolates, single cells, and metagenomes. *Genome research,* 25**,** 1043-1055.

PARRA, A., TORO, M., JACOB, R., NAVARRETE, P., TRONCOSO, M., FIGUEROA, G. & REYES-JARA, A. 2018. Antimicrobial effect of copper surfaces on bacteria isolated from poultry meat. *Braz J Microbiol*.

PENA, R. T., BLASCO, L., AMBROA, A., GONZÁLEZ-PEDRAJO, B., FERNÁNDEZ-GARCÍA, L., LÓPEZ, M., BLERIOT, I., BOU, G., GARCÍA-CONTRERAS, R. & WOOD, T. K. 2019. Relationship between quorum sensing and secretion systems. *Frontiers in Microbiology,* 10**,** 1100.

PERCIVAL, S. L., HILL, K. E., MALIC, S., THOMAS, D. W. & WILLIAMS, D. W. 2011. Antimicrobial tolerance and the significance of persister cells in recalcitrant chronic wound biofilms. *Wound Repair and Regeneration,* 19**,** 1-9.

PEREIRA, C. S., THOMPSON, J. A. & XAVIER, K. B. 2013. AI-2-mediated signalling in bacteria. *FEMS Microbiology Reviews,* 37**,** 156-181.

PÉREZ-MORALES, G., MARTÍNEZ-CONDE, K. V., CASPETA, L., MERINO, E., CEVALLOS, M. A., GOSSET, G. & MARTINEZ, A. 2025. Thermally adapted Escherichia coli keeps transcriptomic response during temperature upshift exposure. *Applied Microbiology and Biotechnology,* 109**,** 120.

PRICE, C. E. & DRIESSEN, A. J. M. 2010. Biogenesis of membrane bound respiratory complexes in Escherichia coli. *Biochimica et Biophysica Acta (BBA) - Molecular Cell Research,* 1803**,** 748-766.

QAYYUM, M. Z., MOLODTSOV, V., RENDA, A. & MURAKAMI, K. S. 2021. Structural basis of RNA polymerase recycling by the Swi2/Snf2 family of ATPase RapA in Escherichia coli. *Journal of Biological Chemistry,* 297(6):101404.

QIAN, J., GARRETT TA FAU - RAETZ, C. R. H. & RAETZ, C. R. 2014. In vitro assembly of the outer core of the lipopolysaccharide from Escherichia coli K-12 and Salmonella typhimurium. *Biochemistry,* 53,8 (2014): 1250-62.

QIU, Y., ZHANG, J., LI, B., WEN, X., LIANG, P. & HUANG, X. 2018. A novel microfluidic system enables visualization and analysis of antibiotic resistance gene transfer to activated sludge bacteria in biofilm. *Science of The Total Environment,* 642**,** 582-590.

QUÈBRE, V., DEL CAMPO, I., CUEVAS, A., SIGUIER, P., RECH, J., LE, P. T. N., TON-HOANG, B., CORNET, F., BOUET, J.-Y., MONCALIAN, G., DE LA CRUZ, F. & GUYNET, C. 2022. Characterization of the DNA Binding Domain of StbA, A Key Protein of A New Type of DNA Segregation System. *Journal of Molecular Biology,* 434**,** 167752.

RAWLINGS, D. E. 1999. Proteic toxin-antitoxin, bacterial plasmid addiction systems and their evolution with special reference to the pas system of pTF-FC2. *FEMS Microbiology Letters,* 176**,** 269-277.

REDMAN, W. K., WELCH, G. S. & RUMBAUGH, K. P. 2020. Differential Efficacy of Glycoside Hydrolases to Disperse Biofilms.

REDMAN, W. K., WELCH, G. S., WILLIAMS, A. C., DAMRON, A. J., NORTHCUT, W. O. & RUMBAUGH, K. P. 2021. Efficacy and safety of biofilm dispersal by glycoside hydrolases in wounds.

RENDUELES, O. & GHIGO, J.-M. 2012. Multi-species biofilms: how to avoid unfriendly neighbors. *FEMS microbiology reviews,* 36**,** 972-989.

RENDUELES, O., GHIGO, J.-M., GHANNOUM, M., PARSEK, M., WHITELEY, M. & MUKHERJEE, P. 2015. Mechanisms of Competition in Biofilm Communities. *Microbiology Spectrum,* 3**,** 3.3.28.

RICKARD, A. H., GILBERT, P., HIGH, N. J., KOLENBRANDER, P. E. & HANDLEY, P. S. 2003. Bacterial coaggregation: an integral process in the development of multi-species biofilms. *Trends in Microbiology,* 11**,** 94-100.

RØDER, H. A.-O., CHRISTIDI, E., AMADOR, C. A.-O. X., MUSIC, S., OLESEN, A. K., SVENSSON, B. A.-O., MADSEN, J. S., HERSCHEND, J., KREFT, J. U. A.-O. X. & BURMØLLE, M. A.-O. X. 2024. Flagellar interference with plasmid uptake in biofilms: a joint experimental and modeling study. *Applied and environmental microbiology*.

RØDER, H. L., TRIVEDI, U., RUSSEL, J., KRAGH, K. N., HERSCHEND, J., THALSØ-MADSEN, I., TOLKER-NIELSEN, T., BJARNSHOLT, T., BURMØLLE, M. & MADSEN, J. S. 2021. Biofilms can act as plasmid reserves in the absence of plasmid specific selection. *npj Biofilms and Microbiomes,* 7**,** 78.

RODIC, A., BLAGOJEVIC, B., ZDOBNOV, E., DJORDJEVIC, M. & DJORDJEVIC, M. 2017. Understanding key features of bacterial restriction-modification systems through quantitative modeling. *BMC systems biology*.

ROSSI, F., RIZZOTTI, L., FELIS, G. E. & TORRIANI, S. 2014. Horizontal gene transfer among microorganisms in food: Current knowledge and future perspectives. *Food Microbiology,* 42**,** 232-243.

ROZWANDOWICZ, M., BROUWER, M. S. M., FISCHER, J., WAGENAAR, J. A., GONZALEZ-ZORN, B., GUERRA, B., MEVIUS, D. J. & HORDIJK, J. 2018. Plasmids carrying antimicrobial resistance genes in Enterobacteriaceae. *Journal of Antimicrobial Chemotherapy,* 73**,** 1121-1137.

RUMBAUGH, K. P. & SAUER, K. A.-O. 2020. Biofilm dispersion.

RUSSEL, J., RØDER, H. L., MADSEN, J. S., BURMØLLE, M. & SØRENSEN, S. J. 2017. Antagonism correlates with metabolic similarity in diverse bacteria. *Proceedings of the National Academy of Sciences,* 114**,** 10684-10688.

SADIQ, F. A., DE REU, K., BURMØLLE, M., MAES, S. & HEYNDRICKX, M. 2023. Synergistic interactions in multispecies biofilm combinations of bacterial isolates recovered from diverse food processing industries. *Frontiers in Microbiology,* Volume 14 - 2023.

SADIQ, F. A., FLINT, S., LI, Y., LIU, T., LEI, Y., SAKANDAR, H. A. & HE, G. 2017. New mechanistic insights into the motile-to-sessile switch in various bacteria with particular emphasis on Bacillus subtilis and Pseudomonas aeruginosa: a review. *Biofouling,* 33**,** 306-326.

SAUER, K. A.-O., STOODLEY, P. A.-O. X., GOERES, D. A.-O., HALL-STOODLEY, L. A.-O., BURMØLLE, M. A.-O. X., STEWART, P. A.-O. & BJARNSHOLT, T. A.-O. 2022. The biofilm life cycle: expanding the conceptual model of biofilm formation.

SAW, H. T. H., WEBBER, M. A., MUSHTAQ, S., WOODFORD, N. & PIDDOCK, L. J. V. 2016. Inactivation or inhibition of AcrAB-TolC increases resistance of carbapenemase-producing Enterobacteriaceae to carbapenems. *Journal of Antimicrobial Chemotherapy,* 71**,** 1510-1519.

SAYERS, E. A.-O., BECK, J., BOLTON, E. E., BRISTER, J. R., CHAN, J., CONNOR, R., FELDGARDEN, M., FINE, A. M., FUNK, K., HOFFMAN, J., KANNAN, S., KELLY, C., KLIMKE, W., KIM, S. A.-O., LATHROP, S., MARCHLER-BAUER, A. A.-O., MURPHY, T. A.-O., O'SULLIVAN, C., SCHMIEDER, E., SKRIPCHENKO, Y., STINE, A., THIBAUD-NISSEN, F., WANG, J., YE, J., ZELLERS, E., SCHNEIDER, V. A. & PRUITT, K. D. 2024. Database resources of the National Center for Biotechnology Information in 2025. *Nucleic Acids Res*.

SCHWEIZER, H. P. 1991. Escherichia-Pseudomonas shuttle vectors derived from pUC18/19. *Gene,* 97**,** 109-112.

SCHWENGERS, O., JELONEK, L., DIECKMANN, M. A., BEYVERS, S., BLOM, J. & GOESMANN, A. 2021. Bakta: rapid and standardized annotation of bacterial genomes via alignment-free sequence identification. *Microbial Genomics,* 7.

SCHWERING, M., SONG, J., LOUIE, M., TURNER, R. J. & CERI, H. 2013. Multi-species biofilms defined from drinking water microorganisms provide increased protection against chlorine disinfection. *Biofouling,* 29**,** 917-928.

SEEMANN, T. 2015. *snippy: fast bacterial variant calling from NGS reads* [Online]. Available: https://github.com/tseemann/snippy [Accessed].

SEEMANN, T. 2016a. *ABRicate: mass screening of contigs for antiobiotic resistance genes* [Online]. Available: https://github.com/tseemann/abricate [Accessed].

SEEMANN, T. 2016b. *MLST: Scan contig files against PubMLST typing schemes* [Online]. Available: https://github.com/tseemann/mlst [Accessed].

SEEMANN, T. 2017. *Shovill: Faster SPAdes assembly of Illumina reads.* [Online]. Available: https://github.com/tseemann/shovill [Accessed].

SHAN, Y., BROWN GANDT, A., ROWE, S. E., DEISINGER, J. P., CONLON, B. P. & LEWIS, K. 2017. ATP-Dependent Persister Formation in Escherichia coli. *mBio,* 8**,** e02267-16.

SHUN-MEI, E., ZENG, J.-M., YUAN, H., LU, Y., CAI, R.-X. & CHEN, C. 2018. Sub-inhibitory concentrations of fluoroquinolones increase conjugation frequency. *Microbial Pathogenesis,* 114**,** 57-62.

SILVA, N., IGREJAS, G., GONÇALVES, A. & POETA, P. 2012. Commensal gut bacteria: distribution of Enterococcus species and prevalence of Escherichia coli phylogenetic groups in animals and humans in Portugal. *Annals of Microbiology,* 62**,** 449-459.

SINGH, S. S., SINGH N FAU - BONOCORA, R. P., BONOCORA RP FAU - FITZGERALD, D. M., FITZGERALD DM FAU - WADE, J. T., WADE JT FAU - GRAINGER, D. C. & GRAINGER, D. C. 2014. Widespread suppression of intragenic transcription initiation by H-NS. *Genes & development*.

SMITH, R. S. & IGLEWSKI, B. H. 2003. P. aeruginosa quorum-sensing systems and virulence. *Current Opinion in Microbiology,* 6**,** 56-60.

SNAPGENE. 2025. *SnapGene software version 8.0.3* [Online]. Available: www.snapgene.com [Accessed].

SOLHEIM, H. T., SEKSE, C., URDAHL, A. M., WASTESON, Y. & NESSE, L. L. 2013. Biofilm as an Environment for Dissemination of *stx* Genes by Transduction. *Applied and Environmental Microbiology,* 79**,** 896-900.

SOLOWIEJ-WEDDERBURN, J., PENTZ, J. T., LIZANA, L., SCHROEDER, B. O., LIND, P. A. & LIBBY, E. 2025. Competition and cooperation: The plasticity of bacterial interactions across environments. *PLOS Computational Biology,* 21**,** e1013213.

SØRUM, H. & SUNDE, M. 2001. Resistance to antibiotics in the normal flora of animals. *Veterinary research,* 32**,** 227-241.

STERN, A. L., VAN DER VERREN, S. E., NÄSVALL, J., GUTIÉRREZ-DE-TERÁN, H. & SELMER, M. 2018. Structural mechanism of AadA, a dual-specificity aminoglycoside adenylyltransferase from Salmonella enterica. *Journal of Biological Chemistry,* 293**,** 11481-11490.

SUKHODOLETS, M. V., CABRERA JE FAU - ZHI, H., ZHI H FAU - JIN, D. J. & JIN, D. J. 2001. RapA, a bacterial homolog of SWI2/SNF2, stimulates RNA polymerase recycling in transcription. *Genes and development*.

SULTAN, A. M., AMER, G. F. & NABIEL, Y. 2021. Quinolone-resistant uropathogenic E. coli: is there a relation between qnr genes, gyrA gene target site mutation and biofilm formation? *Journal of Medical Microbiology,* 70.

SZMOLKA, A. & NAGY, B. 2013. Multidrug resistant commensal Escherichia coli in animals and its impact for public health. *Frontiers in Microbiology,* Volume 4 - 2013.

TANABE, M., SZAKONYI, G., BROWN, K. A., HENDERSON, P. J. F., NIELD, J. & BYRNE, B. 2009. The multidrug resistance efflux complex, EmrAB from Escherichia coli forms a dimer in vitro. *Biochemical and Biophysical Research Communications,* 380**,** 338-342.

TAYLOR, S., WAKEM, M., DIJKMAN, G., ALSARRAJ, M. & NGUYEN, M. 2010. A practical approach to RT-qPCR—Publishing data that conform to the MIQE guidelines. *Methods,* 50**,** S1-S5.

THANABALASURIAR, A., SCOTT, B. N. V., PEISELER, M., WILLSON, M. E., ZENG, Z., WARRENER, P., KELLER, A. E., SUREWAARD, B. G. J., DOZIER, E. A. & KORHONEN, J. T. 2019. Neutrophil extracellular traps confine Pseudomonas aeruginosa ocular biofilms and restrict brain invasion. *Cell host & microbe,* 25**,** 526-536. e4.

THANH DUY, P., THI NGUYEN, T. N., VU THUY, D., CHUNG THE, H. A.-O., ALCOCK, F. A.-O., BOINETT, C., DAN THANH, H. N., THANH TUYEN, H., THWAITES, G. E., RABAA, M. A.-O. & BAKER, S. A.-O. 2020. Commensal Escherichia coli are a reservoir for the transfer of XDR plasmids into epidemic fluoroquinolone-resistant Shigella sonnei. *Nature Microbiology,* 5(2):256-264.

THOMSON, N. M., TURNER, A. K., YASIR, M., BASTKOWSKI, S., LOTT, M., WEBBER, M. A. & CHARLES, I. G. 2022. A whole-genome assay identifies four principal gene functions that confer tolerance of meropenem stress upon Escherichia coli. *Frontiers in Antibiotics,* Volume 1 - 2022.

TOGUCHI, A., SIANO M FAU - BURKART, M., BURKART M FAU - HARSHEY, R. M. & HARSHEY, R. M. 2000. Genetics of swarming motility in Salmonella enterica serovar typhimurium: critical role for lipopolysaccharide. *Journal of bacteriology,* 182,22 (2000): 6308-21.

TOKUDA, M. & SHINTANI, M. A.-O. 2024. Microbial evolution through horizontal gene transfer by mobile genetic elements. *Microbial Biotechnology*.

TOLKER-NIELSEN, T. 2015. Biofilm Development. *Microbiology Spectrum,* 3**,** 3.2.21.

TOUCHON, M. & ROCHA, E. P. C. 2007. Causes of Insertion Sequences Abundance in Prokaryotic Genomes. *Molecular Biology and Evolution,* 24**,** 969-981.

TRAMPARI, E., HOLDEN, E. R., WICKHAM, G. J., RAVI, A., MARTINS, L. D. O., SAVVA, G. M. & WEBBER, M. A. 2021. Exposure of Salmonella biofilms to antibiotic concentrations rapidly selects resistance with collateral tradeoffs. *npj Biofilms and Microbiomes,* 7**,** 3.

TRASTOY, R., MANSO, T., FERNÁNDEZ-GARCÍA, L., BLASCO, L., AMBROA, A., MOLINO, M. L. P. D., BOU, G., GARCÍA-CONTRERAS, R., WOOD, T. K. & TOMÁS, M. 2018. Mechanisms of Bacterial Tolerance and Persistence in the Gastrointestinal and Respiratory Environments. *Clinical Microbiology Reviews,* 31**,** 10.1128/cmr.00023-18.

TROXELL, B., PETRI, N., DARON, C., PEREIRA, R., MENDOZA, M., HASSAN, H. M. & KOCI, M. D. 2015. Poultry body temperature contributes to invasion control through reduced expression of Salmonella pathogenicity island 1 genes in Salmonella enterica serovars Typhimurium and Enteritidis. *Applied and environmental microbiology*.

TU, C. H., HOLT, M., RUAN, S. A. & BOURNE, C. 2020. Evaluating the Potential for Cross-Interactions of Antitoxins in Type II TA Systems. LID - 10.3390/toxins12060422 [doi] LID - 422. *Toxins*.

UNTERGASSER, A., CUTCUTACHE, I., KORESSAAR, T., YE, J., FAIRCLOTH, B. C., REMM, M. & ROZEN, S. G. 2012. Primer3--new capabilities and interfaces. *Nucleic Acids Res,* 40**,** e115.

UPRETI, C. A.-O., KUMAR, P., DURSO, L. A.-O. & PALMER, K. A.-O. 2024. CRISPR-Cas inhibits plasmid transfer and immunizes bacteria against antibiotic resistance acquisition in manure. *Applied and environmental microbiology*.

URUÉN, C., CHOPO-ESCUIN, G., TOMMASSEN, J., MAINAR-JAIME, R. C. & ARENAS, J. 2021. Biofilms as Promoters of Bacterial Antibiotic Resistance and Tolerance. *Antibiotics,* 10**,** 3.

VALVERDE, A., CANTÓN R FAU - GARCILLÁN-BARCIA, M. P., GARCILLÁN-BARCIA MP FAU - NOVAIS, A., NOVAIS A FAU - GALÁN, J. C., GALÁN JC FAU - ALVARADO, A., ALVARADO A FAU - DE LA CRUZ, F., DE LA CRUZ F FAU - BAQUERO, F., BAQUERO F FAU - COQUE, T. M. & COQUE, T. M. 2009. Spread of bla(CTX-M-14) is driven mainly by IncK plasmids disseminated among Escherichia coli phylogroups A, B1, and D in Spain. *Antimicrobial agents and chemotherapy*.

VAN DER VEEN, S. & ABEE, T. 2011. Mixed species biofilms of Listeria monocytogenes and Lactobacillus plantarum show enhanced resistance to benzalkonium chloride and peracetic acid. *International journal of food microbiology,* 144**,** 421-431.

VAN HOUDT, R. & MICHIELS, C. W. 2010. Biofilm formation and the food industry, a focus on the bacterial outer surface. *Journal of Applied Microbiology,* 109**,** 1117-1131.

VAN MELDEREN, L. 2010. Toxin–antitoxin systems: why so many, what for? *Current Opinion in Microbiology,* 13**,** 781-785.
VANASSCHE, T., PEETERMANS M FAU - VAN AELST, L. N. L., VAN AELST LN FAU - PEETERMANS, W. E., PEETERMANS WE FAU - VERHAEGEN, J., VERHAEGEN J FAU - MISSIAKAS, D. M., MISSIAKAS DM FAU - SCHNEEWIND, O., SCHNEEWIND O FAU - HOYLAERTS, M. F., HOYLAERTS MF FAU - VERHAMME, P. & VERHAMME, P. 2013. The role of staphylothrombin-mediated fibrin deposition in catheter-related Staphylococcus aureus infections.
VARPOSHTI, M., ENTEZARI, F. & FEIZABADI, M. M. 2014. Synergistic interactions in mixed-species biofilms of pathogenic bacteria from the respiratory tract. *Revista da Sociedade Brasileira de Medicina Tropical,* 47**,** 649-652.
VASER, R., SOVIĆ, I., NAGARAJAN, N. & ŠIKIĆ, M. 2017. Fast and accurate de novo genome assembly from long uncorrected reads. *Genome research,* 27**,** 737-746.
VESTBY, L. K., GRØNSETH, T., SIMM, R. & NESSE, L. L. 2020. Bacterial Biofilm and its Role in the Pathogenesis of Disease. *Antibiotics (Basel, Switzerland),* 9**,** 59.
VIGIL, P. D., WILES, T. J., ENGSTROM, M. D., PRASOV, L., MULVEY, M. A. & MOBLEY, H. L. 2012. The repeat-in-toxin family member TosA mediates adherence of uropathogenic Escherichia coli and survival during bacteremia. *Infection and immunity,* 80**,** 493-505.
VILLA, L., GARCÍA-FERNÁNDEZ, A., FORTINI, D. & CARATTOLI, A. 2010. Replicon sequence typing of IncF plasmids carrying virulence and resistance determinants. *Journal of Antimicrobial Chemotherapy,* 65**,** 2518-2529.
VIROLLE, C., GOLDLUST K, D. S., BIGOT, S, & C., L. 2020. Plasmid Transfer by Conjugation in Gram-Negative Bacteria: From the Cellular to the Community Level. LID - 10.3390/genes11111239 [doi] LID - 1239. *Genes (Basel)*.
VON WINTERSDORFF, C. J., PENDERS, J., VAN NIEKERK, J. M., MILLS, N. D., MAJUMDER, S., VAN ALPHEN, L. B., SAVELKOUL, P. H. & WOLFFS, P. F. 2016. Dissemination of antimicrobial resistance in microbial ecosystems through horizontal gene transfer. *Frontiers in microbiology***,** 173.
WAKSMAN, G. 2025. Molecular basis of conjugation-mediated DNA transfer by gram-negative bacteria. *Current Opinion in Structural Biology,* 90**,** 102978.
WANG, R., BONO, J. L., KALCHAYANAND, N., SHACKELFORD, S. & HARHAY, D. M. 2012. Biofilm formation by Shiga toxin–producing Escherichia coli O157: H7 and Non-O157 strains and their tolerance to sanitizers commonly used in the food processing environment. *Journal of food protection,* 75**,** 1418-1428.
WANG, R., KALCHAYANAND, N., SCHMIDT, J. W. & HARHAY, D. M. 2013. Mixed biofilm formation by Shiga toxin–producing Escherichia coli and Salmonella enterica serovar Typhimurium enhanced bacterial resistance to sanitization due to extracellular polymeric substances. *Journal of food protection,* 76**,** 1513-1522.

WANG, Y., YU, Z., DING, P., LU, J., KLÜMPER, U., MURRAY, A. K., GAZE, W. H. & GUO, J. 2022. Non-antibiotic pharmaceuticals promote conjugative plasmid transfer at a community-wide level. *Microbiome*.
WEBBER, M. A. & PIDDOCK, L. J. V. 2003. The importance of efflux pumps in bacterial antibiotic resistance. *Journal of Antimicrobial Chemotherapy,* 51**,** 9-11.
WEN, Y., BEHIELS, E. & DEVREESE, B. 2014. Toxin–Antitoxin systems: their role in persistence, biofilm formation, and pathogenicity. *Pathogens and Disease,* 70**,** 240-249.
WHITCHURCH, C. B., TOLKER-NIELSEN, T., RAGAS, P. C. & MATTICK, J. S. 2002. Extracellular DNA Required for Bacterial Biofilm Formation. *Science,* 295**,** 1487-1487.
WICAKSONO, W. A., ERSCHEN, S., KRAUSE, R., MÜLLER, H., CERNAVA, T. & BERG, G. 2022. Enhanced survival of multi-species biofilms under stress is promoted by low-abundant but antimicrobial-resistant keystone species. *Journal of Hazardous Materials,* 422**,** 126836.
WICK, R. 2017. *Filtlong. In GitHub repository. GitHub* [Online]. Available: https://github.com/rrwick/Filtlong [Accessed].
WICK, R. A.-O. & HOLT, K. A.-O. 2022. Polypolish: Short-read polishing of long-read bacterial genome assemblies. *PLoS Comput Biol*.
WINDELS, E. M., MICHIELS, J. E., FAUVART, M., WENSELEERS, T., VAN DEN BERGH, B. & MICHIELS, J. 2019. Bacterial persistence promotes the evolution of antibiotic resistance by increasing survival and mutation rates. *The ISME Journal,* 13**,** 1239-1251.
WINGENDER, J. & FLEMMING, H.-C. 2011. Biofilms in drinking water and their role as reservoir for pathogens. *International Journal of Hygiene and Environmental Health,* 214**,** 417-423.
WOOD, D. E. & SALZBERG, S. L. 2014. Kraken: ultrafast metagenomic sequence classification using exact alignments. *Genome Biology,* 15**,** R46.
WOOD, T. K., KNABEL, S. J. & KWAN, B. W. 2013. Bacterial persister cell formation and dormancy. *Applied and environmental microbiology,* 79**,** 7116-7121.
WOODFORD, N., TURTON, J. F. & LIVERMORE, D. M. 2011. Multiresistant Gram-negative bacteria: the role of high-risk clones in the dissemination of antibiotic resistance. *FEMS Microbiology Reviews,* 35**,** 736-755.
XICOHTENCATL-CORTES, J., CRUZ-CORDOVA, A., CAZARES-DOMINGUEZ, V., ESCALONA-VENEGAS, G., ZAVALA-VEGA, S., ARELLANO-GALINDO, J., ROMO-CASTILLO, M., HERNANDEZ-CASTRO, R., OCHOA, S. A. & LUNA-PINEDA, V. M. 2019. Uropathogenic Escherichia coli strains harboring tosA gene were associated to high virulence genes and a multidrug-resistant profile. *Microbial pathogenesis,* 134**,** 103593.
YANG, L., LIU, Y., WU, H., HØIBY, N., MOLIN, S. & SONG, Z. J. 2011. Current understanding of multi-species biofilms. *International Journal of Oral Science,* 3**,** 74-81.
YANG, Y., ZHOU, P., TIAN, D., WANG, W., ZHOU, Y. & JIANG, X. 2024. CRISPR-Cas3 and type I restriction-modification team up against bla(KPC)-IncF plasmid transfer in Klebsiella pneumoniae. *BMC microbiology*.

YAO, Y., MADDAMSETTI, R., WEISS, A., HA, Y., WANG, T., WANG, S. & YOU, L. 2022. Intra- and interpopulation transposition of mobile genetic elements driven by antibiotic selection. *Nature Ecology & Evolution,* 6**,** 555-564.

YASIR, M., TURNER, A. K., BASTKOWSKI, S., LOTT, M., HOLDEN, E. R., TELATIN, A., PAGE, A. J., WEBBER, M. A. & CHARLES, I. G. 2022. Genome-Wide Analysis of Innate Susceptibility Mechanisms of Escherichia coli to Colistin. *Antibiotics,* 11**,** 1668.

YASIR, M., TURNER, A. K., BASTKOWSKI, S. A.-O., BAKER, D., PAGE, A. J., TELATIN, A., PHAN, M. D., MONAHAN, L., SAVVA, G. M., DARLING, A., WEBBER, M. A. & CHARLES, I. G. 2020. TraDIS-Xpress: a high-resolution whole-genome assay identifies novel mechanisms of triclosan action and resistance. *Genome research*.

YOUSEFIAN, N., ORNIK-CHA, A., POUSSARD, S., DECOSSAS, M., BERBON, M., DAURY, L., TAVEAU, J.-C., DUPUY, J.-W., ĐORĐEVIĆ-MARQUARDT, S., LAMBERT, O. & POS, K. M. 2021. Structural characterization of the EmrAB-TolC efflux complex from E. coli. *Biochimica et Biophysica Acta (BBA) - Biomembranes,* 1863**,** 183488.

YUAN, L., WANG, H., LIU, W., SADIQ, F. A. & ZHAO, Y. 2022. Editorial: Multi-species biofilms in the food industry. *Frontiers in Microbiology,* 13.

ZANKARI, E., HASMAN H FAU - COSENTINO, S., COSENTINO S FAU - VESTERGAARD, M., VESTERGAARD M FAU - RASMUSSEN, S., RASMUSSEN S FAU - LUND, O., LUND O FAU - AARESTRUP, F. M., AARESTRUP FM FAU - LARSEN, M. V. & LARSEN, M. V. 2012. Identification of acquired antimicrobial resistance genes. *J Antimicrob Chemother*.

ZAPOTOCZNA, M., MCCARTHY, H., RUDKIN, J. K., O'GARA, J. P. & O'NEILL, E. 2015. An Essential Role for Coagulase in Staphylococcus aureus Biofilm Development Reveals New Therapeutic Possibilities for Device-Related Infections. *The Journal of Infectious Diseases,* 212**,** 1883-1893.

ZAPOTOCZNA, M., O'NEILL, E. & O'GARA, J. P. 2016. Untangling the diverse and redundant mechanisms of Staphylococcus aureus biofilm formation. *PLoS pathogens,* 12**,** e1005671.

ZARZECKA, U., CHAJĘCKA-WIERZCHOWSKA, W., ZAKRZEWSKI, A., ZADERNOWSKA, A. & FRAQUEZA, M. J. 2022. High pressure processing, acidic and osmotic stress increased resistance to aminoglycosides and tetracyclines and the frequency of gene transfer among strains from commercial starter and protective cultures. *Food Microbiology,* 107**,** 104090.

ZHANG, G., MEREDITH, T. C. & KAHNE, D. 2013. On the essentiality of lipopolysaccharide to Gram-negative bacteria. *Current Opinion in Microbiology,* 16**,** 779-785.

ZHANG, H., HE, S., PANG, X., HE, X., LIU, X., QIU, S., YANG, C. & SONG, H. 2025a. Regulatory role of ISEcp1 and spacer sequences in blaCTX-M–mediated cephalosporin resistance in Shigella. *Journal of Global Antimicrobial Resistance,* 44**,** 127-134.

ZHANG, Y., XUE, J., LUO, Y., MUHAMMAD, I., DONG, H., MA, H. & KONG, L. 2025b. Acidifiers promoted antibiotic resistance gene transfer via

plasmid conjugation. *Journal of Environmental Chemical Engineering,* 13**,** 117203.

ZHAO, Q.-Y., LI, W., CAI, R.-M., LU, Y.-W., ZHANG, Y., CAI, P., WEBBER, M. A. & JIANG, H.-X. 2021. Mobilization of Tn1721-like structure harboring blaCTX-M-27 between P1-like bacteriophage in Salmonella and plasmids in Escherichia coli in China. *Veterinary Microbiology,* 253**,** 108944.

ZHAO, Q. Y., CHEN, P. X., YANG, L., CAI, R. M., ZHU, J. H., FANG, L. X., WEBBER, M. A. & JIANG, H. X. 2020. Transmission of plasmid-borne and chromosomal blaCTX-M-64 among Escherichia coli and Salmonella isolates from food-producing animals via ISEcp1-mediated transposition. *Journal of Antimicrobial Chemotherapy*.

ZHAO, W. H. & HU, Z. Q. 2013. Epidemiology and genetics of CTX-M extended-spectrum β-lactamases in Gram-negative bacteria. *Critical reviews microbiology*.

ZHOU, L., ZHANG, Y., GE, Y., ZHU, X. & PAN, J. 2020. Regulatory mechanisms and promising applications of quorum sensing-inhibiting agents in control of bacterial biofilm formation. *Frontiers in microbiology***,** 2558.

ZHOU, Y., SMITH, D., LEONG, B. J., BRÄNNSTRÖM, K., ALMQVIST, F. & CHAPMAN, M. R. 2012. Promiscuous cross-seeding between bacterial amyloids promotes interspecies biofilms. *Journal of Biological Chemistry,* 287**,** 35092-35103.

ZIMIN, A. A.-O. & SALZBERG, S. A.-O. 2020. The genome polishing tool POLCA makes fast and accurate corrections in genome assemblies. *PLoS Comput Biol*.

ZONG, Z., FENN, S., CONNOR, C., FENG, Y. & MCNALLY, A. 2018. Complete genomic characterization of two Escherichia coli lineages responsible for a cluster of carbapenem-resistant infections in a Chinese hospital. *Journal of Antimicrobial Chemotherapy,* 73**,** 2340-2346.

ZWEIFEL, C. & STEPHAN, R. 2012. Spices and herbs as source of Salmonella-related foodborne diseases. *Food Research International,* 45**,** 765-769.

APPENDICES

“Sometimes a scream is better than a thesis”

< Ralph Waldo Emerson >

APPENDIX I: List of *E. coli* food isolates initially chosen to grow in competition with *S.* Typhimurium 14028S

Table A.1 – List of *E. coli* food isolates initially chosen to grow in competition with *S.* Typhimurium 14028S

Name	ST	Plasmids	
		Quantity	Incompatibility type
EC18LG-0005-1	10	0	-
EC18PR-0174-1	155	0	-
EC18PR-0008-3	216	0	-
EC18PK-0020-1	399	1	Col156
EC18CH-0012-4	607	0	-
EC18LG-0011-1	939	0	-
EC18PK-0012-1	1429	1	IncY
EC18PK-0002-3	1434	2	Col156, p0111
EC18PK-0011-1	2531	3	FIA pBK30683+, IncR, IncY
EC18SM-0013-1	5474	1	ColRNAI

APPENDIX II: List of additional bacterial isolates used or arising from this study

Table A.2 - List of additional bacterial isolates used or arising from this study

Name	Source	Genomic mutations conferring AMR			Plasmid(s)		Antibiotic selection
		Animo acid substitution	Gene of substitution	AMR	Incompatibility type	Resistance gene(s)	
S. Typhimurium 14028S RifR	Made in house	His526Tyr	*rpoB*	Rifampicin	IncFIB(S)	-	100 µg/mL rifampicin
S. Typhimurium 14028S RifR pHYCTX14	Made in house	His526Tyr	*rpoB*	Rifampicin	IncFIB(S)	-	100 µg/mL rifampicin 8 µg/mL cefotaxime
S. Typhimurium 14028S NalR pHYCTX14	Made in house	Ser83Phe	*gyrA*	Nalidixic acid	IncFIB(S)	-	100 µg/mL nalidixic acid 8 µg/mL cefotaxime
E. coli EC18LG-0005-1 RifR	Made in house	Glu513Leu	*rpoB*	Rifampicin	-	-	100 µg/mL rifampicin
E. coli EC18LG-0005-1 NalR	Made in house	Asp87Asn	*gyrA*	Nalidixic acid	-	-	100 µg/mL nalidixic acid
E. coli EC18LG-0005-1 NalR pHYCTX14	Made in house	Asp87Asn	*gyrA*	Nalidixic acid	IncFII	$bla_{CTX\text{-}M\text{-}14}$	100 µg/mL nalidixic acid 8 µg/mL cefotaxime

E. coli EC18PK-0020-1	(Janecko et al., 2023)	-	-	-	-	IncY	-	-
E. coli EC18PK-0020-1 RifR	Made in house	-	Asp596Tyr	*rpoB*	Rifampicin	IncY	-	100 µg/mL rifampicin
E. coli EC18PK-0020-1 RifR pHYCTX14	Made in house	-	Asp596Tyr	*rpoB*	Rifampicin	IncFII	$bla_{\text{CTX-M-14}}$	100 µg/mL nalidixic acid 8 µg/mL cefotaxime
E. coli EC18PK-0020-1 NalR	Made in house	-	Ser83Leu	*gyrA*	Nalidixic acid	IncY	-	100 µg/mL nalidixic acid
E. coli EC18PK-0020-1 NalR pHYCTX14	Made in house	-	Ser83Leu	*gyrA*	Nalidixic acid	IncFII	$bla_{\text{CTX-M-14}}$	100 µg/mL nalidixic acid 8 µg/mL cefotaxime
E. coli EC18PR-0008-3	(Janecko et al., 2023)	-	-	-	-	IncY	-	-

APPENDIX III: Illumina NextSeq short-read sequencing

NextSeq500 protocol:

A tagmentation master mix consisting of 0.5 µL of Tagmentation Buffer (TB1) was mixed with 0.5 µL Bead Linked Transposomes (BLT) (20018704, Illumina), and 4 µl molecular grade water was prepared per sample, and 5 µL was added to a 96-well plate. 2 µl of DNA (a total of 10 ng DNA when samples are normalised to 5 ng/µL) was mixed with the 5 µl of the tagmentation mix using a pipette and heated to 55 ºC for 15 minutes in a PCR block. A PCR master mix consisting of 10 µl KAPA 2G Fast Hot Start Ready Mix (KK5601, Merck) and 2 µl molecular-grade water was prepared per sample, and 12 µL was added to each well to be used in a 96-well plate. 1 µl 10µM primer mix containing both P7 and P5 Illumina 9 bp barcodes (An accessible, efficient and global approach for the large-scale sequencing of bacterial genomes | Genome Biology | Full Text (biomedcentral.com)) was added to each well, and 7 µL of the DNA/ tagmentation master mix was added to the wells. The PCR was run with 72ºC for 3 minutes, 95ºC for 1 minute, 14 cycles of 95ºC for 10 seconds, 55ºC for 20 seconds and 72ºC for 3 minutes. The libraries were quantified using the Promega QuantiFluor® dsDNA System (E2670, Promega) and run on a GloMax® Discover Microplate Reader. Libraries were pooled following quantification in equal quantities. The final pool was double-SPRI size selected between 0.5 and 0.7X bead volumes using sample purification beads (Illumina® DNA Prep, (M) Tagmentation (96 Samples, IPB), 20060059). The final pool was quantified on a Qubit 3.0 instrument and run on a D5000 ScreenTape (5067-5579, Agilent) using the Agilent Tapestation 4200 to calculate the final library pool molarity. The pool was run at a final concentration of 1.5 pM on an Illumina Nextseq500 instrument using a Mid Output Flowcell (NSQ® 500 Mid Output KT v2 (300 cycle) FC-404-2003, Illumina) following the Illumina recommended denaturation and loading recommendations, which included a 1% PhiX spike in (PhiX Control v3 FC-110-3001, Illumina).

NextSeq2000 protocol:

A tagmentation master mix consisting of 0.5 µL of Tagmentation Buffer (TB1) was mixed with 0.5 µL Bead Linked Transposomes (BLT) (20018704, Illumina), and 4 µl molecular grade water was prepared per sample and 5 µL added to a 96-well plate. 2 µl of DNA (a total of 10 ng DNA when samples are normalised to 5 ng/µL) was mixed with the 5 µl of the tagmentation mix using a pipette and heated to 55 ºC for 15 minutes in a PCR block. A PCR master mix consisting of 10 µl KAPA 2G Fast Hot Start Ready Mix (KK5601, Merck) and 2 µl molecular-grade water was prepared per sample, and 12 µL was added to each well to be used in a 96-well plate. 1 µl 10µM primer mix containing both P7 and P5 Illumina UDT UDI (Unique Dual Index) 10mer indexed primers were added to each well, and 7 µL of the DNA/ tagmentation master mix was added to the wells. The PCR was run with 72ºC for 3 minutes, 95ºC for 1 minute, 14 cycles of 95ºC for 10 seconds, 55ºC for 20 seconds and 72ºC for 3 minutes. The libraries were quantified using the Promega QuantiFluor® dsDNA System (E2670, Promega) and run on a GloMax® Discover Microplate Reader. The final pool was double-SPRI size selected between 0.5 and 0.7X bead volumes using sample purification beads (Illumina® DNA Prep, (M) Tagmentation (96 Samples, IPB), 20060059). The final pool was quantified on a Qubit 3.0 instrument and run on a D5000 ScreenTape (5067-5579, Agilent) using the Agilent Tapestation 4200 to calculate the final library pool molarity. The pool was run at a final concentration of 750 pM on an Illumina Nextseq2000 instrument.

APPENDIX IV: Oxford Nanopore Technology long-read DNA sequencing

Native barcoding low-cost method:

For long read sequencing, up to 400 ng of DNA (in 10 µl) was incubated with 0.875 µl Ultra II End-prep reaction buffer (E7546L, NEB), 0.375 µl Ultra II End-prep enzyme mix (E7546L, NEB). Samples were incubated at RT for 5 minutes, then at 65 °C for 5 minutes. 1.25 µl of a unique native barcode (EXP-NBD196) and 12.5µl Blunt/TA Ligase Master Mix (M0367L, NEB) was added to each well, mixed and incubated for a minimum of 20 minutes at RT. Following native barcoding, a 1 × SPRI bead clean-up on all libraries using sample purification beads (Illumina® DNA Prep, (M) Tagmentation (96 Samples, IPB), 20060059), with a single 80% ethanol wash. Barcoded libraries were resuspended in 10 µl of water. All samples were pooled together, followed by another 0.6X SPRI bead clean-up using sample purification beads. The pooled library was eluted in 30 µl nuclease-free water. To the 30 µl pooled library, 5 µl Adapter Mix II (AMX II), 10 µl NEBNext Quick Ligation Reaction Buffer (5X) (E6056S, NEB) and 5 µl Quick T4 DNA Ligase (E6056S, NEB) were added and flick mixed in this order. The ligation reaction was left for a minimum of 10 minutes at RT. The pool was cleaned with a 0.5X SPRI bead clean-up using Short Fragment Buffer (SFB). The library was eluted and loaded onto a primed MinION/promethION flow cell in accordance with Oxford Nanopore Technologies protocol (SQK-LSK-109). Base calling was carried out using Guppy [v6.06] (Oxford Nanopore Technologies).

APPENDIX V: Testing the impact of mutations in *rpoB* and *gyrA*, as well as carriage pHYCTX14, on biofilm formation

Table A.3 – *p*-values obtained from Welch's *t*-test of *S.* Typhimurium 14028S CFU recovered from steel beads compared to the CFU of mutant strains derived from the wildtype.

Strain	*p*-value
S. Typhimurium 14028S RifR	0.391
S. Typhimurium 14028S RifR pHYCTX14	0.643
S. Typhimurium 14028S NalR	0.364
S. Typhimurium 14028S NalR pHYCTX14	0.641

Table A.4 - *p*-values obtained from Welch's *t*-test of EC18PK-0020-1 CFU recovered from steel beads compared to the CFU of mutant strains derived from the wildtype.

Strain	*p*-value
EC18PK-0020-1 RifR	0.893
EC18PK-0020-1 RifR pHYCTX14	0.981
EC18PK-0020-1 NalR	0.608
EC18PK-0020-1 NalR pHYCTX14	0.635

Table A.5 - *p*-values obtained from Welch's *t*-test of EC18LG-0005-1 CFU recovered from steel beads compared to the CFU of mutant strains derived from the wildtype. A significant difference ($p \leq 0.05$) is represented by an asterisk (*).

Strain	*p*-value
EC18LG-0005-1 RifR	0.941
EC18LG-0005-1 RifR pHYCTX14	0.106
EC18LG-0005-1 NalR	0.029*
EC18LG-0005-1 NalR pHYCTX14	0.034*

APPENDIX VI: Comparing the CFU of EC18LG-0005-1 RifR pHYCTX14 biofilm cells recovered on agar supplemented with different antibiotics

Table A.6 - *p*-values obtained from Welch's *t*-test of EC18LG-0005-1 RifR pHYCTX14 biofilm CFU recovered on LB agar supplemented with no drug, compared to the CFU of cells recovered on LB agar supplemented with 100 µg/mL rifampicin, 2 µg/mL cefotaxime and 100 µg/mL rifampicin and 2 µg/mL rifampicin.

Antibiotic colonies were recovered on	*p*-value
100 µg/mL rifampicin	0.958
2 µg/mL cefotaxime	0.964
100 µg/mL rifampicin and 2 µg/mL rifampicin	0.121

APPENDIX VII: Pairwise comparisons of pHYCTX14 conjugation efficiency obtained for different experimental conditions using the biofilm conjugation model

Table A.7 – Estimated pairwise differences between pHYCTX14 conjugation efficiency obtained for different experimental conditions using the biofilm conjugation model

Contrast	ratio	SE	df	null	t.ratio	p.value
0.15 mM Cu vs C_6H_5COONa	3.0214573	4.2251608	29	1	0.7907259	0.9312418
0.15 mM Cu vs Cipro	10.3166204	11.7310731	29	1	2.0523678	0.2676199
0.15 mM Cu vs NaCl	22.3306189	31.2268041	29	1	2.2211041	0.2005210
0.15 mM Cu vs NaNO2	9.1679672	12.3472457	29	1	1.6451934	0.4820197
C6H5COONa vs Cipro	3.4144518	4.5436151	29	1	0.9228345	0.8857370
C6H5COONa vs NaCl	7.3906782	8.3177750	29	1	1.7772756	0.4054577
C6H5COONa vs NaNO2	3.0342865	3.3122696	29	1	1.0168213	0.8455455
Cipro vs NaCl	2.1645285	2.8803406	29	1	0.5802975	0.9769516
Cipro vs NaNO2	0.8886599	1.1342533	29	1	-0.0924820	0.9999824
NaCl vs NaNO2	0.4105559	0.4481686	29	1	-0.8155293	0.9237092

APPENDIX VIII: Genes determined by TraDIS-*Xpress* to be implicated in *E. coli* plasmid acceptance

Table A.8 - List of protected genes in the *E. coli* BW25113 transposon mutant libraries that had accepted pHYCTX14 from the QuaTraDIS comparison pipeline.

Gene	Function	logFC
crr	glucose-specific enzyme IIA component of PTS	-9.891750079
pal	peptidoglycan-associated outer membrane lipoprotein	-9.162091056
atpE	F0 sector of membrane-bound ATP synthase and subunit c	-8.684747643
tyrT	tRNA-Tyr	-8.325454823
1536890_1536919		-7.673308104
2859837_2859855		-7.640888694
murG	N-acetylglucosaminyl transferase	-7.135881566
ydfA	Qin prophage; uncharacterized protein	-7.089917002
waaF	ADP-heptose:LPS heptosyltransferase II	-6.982926954
3275060_3275142		-6.93679782
marR	transcriptional repressor of multiple antibiotic resistance	-6.927432329
lon		-6.383212315
hldE	fused heptose 7-phosphate kinase/heptose 1-phosphate adenyltransferase	-5.708995223
acrR	transcriptional repressor	-5.283143077
galU	glucose-1-phosphate uridylyltransferase	-5.132544101
hldD	ADP-L-glycero-D-mannoheptose-6-epimerase and NAD(P)-binding	-5.091094484
waaC	ADP-heptose:LPS heptosyl transferase I	-4.846850794
gmhB	D and D-heptose 1 and 7-bisphosphate phosphatase	-4.720722341
ompR	response regulator in two-component regulatory system with EnvZ	-4.50441891

nrdH	hydrogen donor for NrdEF electron transport system; glutaredoxin-like protein	-4.35670045
nuoN	NADH:ubiquinone oxidoreductase and membrane subunit N	-4.255081501
dacA	D-alanyl-D-alanine carboxypeptidase (penicillin-binding protein 5)	-4.19493097
3227996_3228082		-4.158901817
waaP	kinase that phosphorylates core heptose of lipopolysaccharide	-4.146865687
dsbA	periplasmic protein disulfide isomerase I	-3.766787279
rfaH	transcription antitermination protein	-3.694330421
atpG	F1 sector of membrane-bound ATP synthase and gamma subunit	-3.686381588
marC	UPF0056 family inner membrane protein	-3.666199556
atpB	F0 sector of membrane-bound ATP synthase and subunit a	-3.664499715
envZ	sensory histidine kinase in two-component regulatory system with OmpR	-3.624054178
waaG	glucosyltransferase I	-3.623628581
yrbN	uncharacterized protein	-3.600430416
650007_650030		-3.511368136
lrhA	transcriptional repressor of flagellar and motility and chemotaxis genes	-3.493409983
crp	cAMP-activated global transcription factor and mediator of catabolite repression	-3.454412075
lon	DNA-binding ATP-dependent protease La	-3.427312
cyaA	adenylate cyclase	-3.266886821
lpxC	UDP-3-O-acyl N-acetylglucosamine deacetylase	-3.235598702
soxR	redox-sensitive transcriptional activator of soxS; autorepressor	-3.170699806
4478321_4478357		-3.11779043
rseA	anti-sigma factor	-3.014663989

ycbC	DUF218 superfamily protein	-2.976264077
ompW	outer membrane protein W	-2.949063903
sdhA	succinate dehydrogenase and flavoprotein subunit	-2.852758823
ryjA	novel sRNA and function unknown	-2.83638198
greA	transcript cleavage factor	-2.818056787
sucD	succinyl-CoA synthetase and NAD(P)-binding and alpha subunit	-2.68142812
ymfL	e14 prophage; putative DNA-binding transcriptional regulator	-2.628867023
gmhA	D-sedoheptulose 7-phosphate isomerase	-2.599409766
modA	molybdate transporter subunit	-2.593784315
atpD	F1 sector of membrane-bound ATP synthase and beta subunit	-2.56267503
mgrB	regulatory peptide for PhoPQ and feedback inhibition	-2.506790581
pgm	phosphoglucomutase	-2.502332774
pdxJ	'pyridoxine 5"-phosphate synthase'	-2.461736103
surA	peptidyl-prolyl cis-trans isomerase (PPIase)	-2.46133287
4539599_4539635		-2.458687846
yifK	putative APC family amino acid transporter	-2.418612545
sucC	succinyl-CoA synthetase and beta subunit	-2.363559908
cpxA	sensory histidine kinase in two-component regulatory system with CpxR	-2.348173185
uof	ryhB-regulated fur leader peptide	-2.331318507
slt	lytic murein transglycosylase and soluble	-2.293402945
sra	stationary-phase-induced ribosome-associated protein	-2.290136551
yjcC	putative membrane-anchored cyclic-di-GMP phosphodiesterase	-2.280225212
deaD	ATP-dependent RNA helicase	-2.270207812
envC	activator of AmiB and C murein hydrolases and septal ring factor	-2.222671359

4219303_4219373		-2.211025852
frdD	fumarate reductase (anaerobic) and membrane anchor subunit	-2.200436296
3196502_3196627		-2.174417529
argP	transcriptional regulator for arginine transport and DNA replication genes; replication initiation inhibitor	-2.117914873
4117879_4117976		-2.109073898
yijF	DUF1287 family protein	-2.095263589
folP	7 and 8-dihydropteroate synthase	-2.078804039
dam	DNA adenine methyltransferase	-2.063086879
clpP	proteolytic subunit of ClpA-ClpP and ClpX-ClpP ATP-dependent serine proteases	-2.055137244
3591756_3591855		-1.988269212
ychN	putative sulfur relay protein	-1.966401718
ytjC	phosphatase	-1.955943408
narY	nitrate reductase 2 (NRZ) and beta subunit	-1.950638533
ptsN	sugar-specific enzyme IIA component of PTS	-1.94562687
rssB	PcnB-degradosome interaction factor; response regulator	-1.941320351
ybjD	putative OLD family ATP-dependent endonuclease; DUF2813 family protein	-1.919691645
htpX	putative endopeptidase	-1.910434024
sgcA	putative phosphotransferase enzyme IIA component	-1.90923461
ompF	outer membrane porin 1a (Ia;b;F)	-1.906529792
dsbB	oxidoreductase that catalyzes reoxidation of DsbA protein disulfide isomerase I	-1.880187358
frvB	putative PTS enzyme and IIB component/IIC component	-1.8755091
clpX	ATPase and specificity subunit of ClpX-ClpP ATP-dependent serine protease	-1.856161597
cbpM	modulator of CbpA co-chaperone	-1.844408589
ybgL	UPF0271 family protein	-1.817532701

tatC	TatABCE protein translocation system subunit	-1.816141507
dadX	alanine racemase and catabolic and PLP-binding	-1.80844821
upp	uracil phosphoribosyltransferase	-1.80664063
gcvA	glycine cleavage system transcriptional activator; autorepressor	-1.796259847
rbsB	D-ribose transporter subunit	-1.792673122
baeR	response regulator in two-component regulatory system with BaeS	-1.791940741
yecA	UPF0149 family protein	-1.776682921
usg	putative semialdehyde dehydrogenase	-1.765801253
gshA	glutamate-cysteine ligase	-1.738659568
grxC	glutaredoxin 3	-1.733167227
ubiX	3-octaprenyl-4-hydroxybenzoate carboxy-lyase	-1.705945649
iscR	isc operon transcriptional repressor; suf operon transcriptional activator; oxidative stress-and iron starvation-inducible; autorepressor	-1.690646605
nuoC	NADH:ubiquinone oxidoreductase and fused CD subunit	-1.68475463
pyrG	CTP synthetase	-1.662213348
ygbE	DUF3561 family inner membrane protein	-1.66146849
hemA	glutamyl tRNA reductase	-1.628042896
ypfH	palmitoyl-CoA esterase activity and uncertain physiological substrate	-1.610590008
rsmH	16S rRNA m(4)C1402 methyltransferase and SAM-dependent	-1.606716264
artQ	arginine transporter subunit	-1.601838121
yeeT	CP4-44 prophage; uncharacterized protein	-1.601819659
sodA	superoxide dismutase and Mn	-1.598575031

ftsP	septal ring component that protects the divisome from stress; multicopy suppressor of ftsI(Ts)	-1.588791724
1049777_1050545		-1.583100109
fecB	iron-dicitrate transporter subunit	-1.578405292
speB	agmatinase	-1.57222727
psuG	'pseudouridine 5"-phosphate glycosidase'	-1.564714477
yhbJ	adaptor protein RapZ for GlmZ/GlmY sRNA decay; glucosamine-6-phosphate regulated; NTPase	-1.55892785
beeE		-1.558770393
uvrD	DNA-dependent ATPase I and helicase II	-1.558571798
ftsN	essential cell division protein	-1.557958645
ydgH	DUF1471 family periplasmic protein	-1.555363119
emrD	multidrug efflux system protein	-1.514751315
yggW	HemN family putative oxidoreductase	-1.514092402
yidQ	DUF1375 family outer membrane protein	-1.508399398
thiD	bifunctional hydroxy-methylpyrimidine kinase/ hydroxy-phosphomethylpyrimidine kinase	-1.498126994
cpxR	response regulator in two-component regulatory system with CpxA	-1.495069522
thiF	adenylyltransferase and modifies ThiS C-terminus	-1.487985105
ybaM	DUF2496 family protein	-1.486896945
pepA	multifunctional aminopeptidase A: a cyteinylglycinase and transcription regulator and site-specific recombination factor	-1.475957878
yibH	putative membrane fusion protein (MFP) component of efflux pump	-1.459808666
yceG	septation protein and ampicillin sensitivity	-1.442913299
fliO	flagellar biosynthesis protein	-1.441868363

ptrA	protease III	-1.432249322
yjjV	putative DNase	-1.42961363
dgkA	diacylglycerol kinase	-1.426512482
oppB	oligopeptide transporter subunit	-1.404433219
rhtB	homoserine and homoserine lactone and S-methyl-methionine efflux pump	-1.397436039
ybhB	kinase inhibitor homolog and UPF0098 family	-1.384552987
ada	fused DNA-binding transcriptional dual regulator/O6-methylguanine-DNA methyltransferase	-1.377695044
amiB	N-acetylmuramoyl-l-alanine amidase II	-1.375710441
thrC	L-threonine synthase	-1.364122292
emrB	multidrug efflux system protein	-1.341022345
glnL	sensory histidine kinase in two-component regulatory system with GlnG	-1.339455775
rihC	ribonucleoside hydrolase 3	-1.338423235
tsaA	tRNA-Thr(GGU) m(6)t(6)A37 methyltransferase and SAM-dependent	-1.320259743
aer	fused signal transducer for aerotaxis sensory component/methyl accepting chemotaxis component	-1.316080022
citG	'2-(5""-triphosphoribosyl)-3''-dephosphocoenzyme-A synthase'	-1.313771777
napG	ferredoxin-type protein essential for electron transfer from ubiquinol to periplasmic nitrate reductase (NapAB)	-1.313443998
fixB	putative electron transfer flavoprotein and NAD/FAD-binding domain and ETFP adenine nucleotide-binding domain-like protein	-1.311121447
prc	carboxy-terminal protease for penicillin-binding protein 3	-1.294208912
yigZ	UPF0029 family protein	-1.288270705
yqeF	short chain acyltransferase	-1.287236212

frlR	putative DNA-binding transcriptional regulator	-1.286241802
lrp	leucine-responsive global transcriptional regulator	-1.285860776
recG	ATP-dependent DNA helicase	-1.274249847
frlC	fructoselysine 3-epimerase	-1.262614678
metL	Bifunctional aspartokinase/homoserine dehydrogenase 2	-1.258523017
yeeP		-1.254339077
mnmE	tRNA U34 5-methylaminomethyl-2-thiouridine modification GTPase	-1.254245463
phnP	5-phospho-alpha-D-ribosyl 1 and 2-cyclic phosphate phosphodiesterase	-1.246589928
luxS	S-ribosylhomocysteine lyase	-1.236310936
emrA	multidrug efflux system	-1.234636726
pdxA	4-hydroxy-L-threonine phosphate dehydrogenase and NAD-dependent	-1.231388792
yccU	putative CoA-binding protein	-1.230404942
ttcA	tRNA 2-thiocytidine biosynthesis protein	-1.22831247
glcF	glycolate oxidase 4Fe-4S iron-sulfur cluster subunit	-1.221175537
xylA	D-xylose isomerase	-1.211494257
fucR	l-fucose operon activator	-1.2055592
nikD	nickel transporter subunit	-1.203686266
wecG	UDP-N-acetyl-D-mannosaminuronic acid transferase	-1.195280402
arfB	alternative stalled-ribosome rescue factor B; peptidyl-tRNA hydrolase and ribosome-attached	-1.194451583
ycfQ	repressor for bhsA(ycfR)	-1.188590216
ahr	aldehyde reductase and NADPH-dependent and Zn-containing and broad specificity	-1.187823269
cpsG	phosphomannomutase	-1.186848632
napC	quinol dehydrogenase and electron source for NapAB	-1.183504567
mdtP	outer membrane factor of efflux pump	-1.183268838

cutC	copper homeostasis protein	-1.171740104
phnF	putative DNA-binding transcriptional regulator of phosphonate uptake and biodegradation	-1.169638397
dgoT	D-galactonate transporter	-1.149675747
gstA	glutathionine S-transferase	-1.148252725
335467_335825		-1.146581006
mrcA	fused penicillin-binding protein 1a: murein transglycosylase/murein transpeptidase	-1.136265974
rbsC	D-ribose transporter subunit	-1.129582759
rsxG	SoxR iron-sulfur cluster reduction factor component; putative membrane protein of electron transport complex	-1.128811602
kgtP	alpha-ketoglutarate transporter	-1.127250583
frwD	putative enzyme IIB component of PTS	-1.126371197
nagB	glucosamine-6-phosphate deaminase	-1.123116549
ilvA	L-threonine dehydratase and biosynthetic; also known as threonine deaminase	-1.123038613
thiH	tyrosine lyase and involved in thiamine-thiazole moiety synthesis	-1.12018233
frdA	fumarate reductase (anaerobic) catalytic and NAD/flavoprotein subunit	-1.117411842
rne	fused ribonucleaseE: endoribonuclease/RNA-binding protein/RNA degradosome binding protein	-1.115225713
yggI	Zn-dependent metalloprotease-related protein	-1.103817279
fliH	negative regulator of FliI ATPase activity	-1.103258833
ysaC		-1.099816739
glpX	fructose 1 and 6-bisphosphatase II	-1.092551414
pgrR	murein peptide degradation regulator	-1.090069054

mnmC	fused 5-methylaminomethyl-2-thiouridine-forming enzyme methyltransferase and FAD-dependent demodification enzyme	-1.082901714
ygeX	2 and 3-diaminopropionate ammonia lyase and PLP-dependent	-1.080062305
yifE	UPF0438 family protein	-1.077152448
phnI	ribophosphonate triphosphate synthase complex putative catalytic subunit	-1.075548068
aaeR	transcriptional regulator for aaeXAB operon	-1.072499782
fadD	acyl-CoA synthetase (long-chain-fatty-acid--CoA ligase)	-1.066043725
csrB	CsrA-binding sRNA and antagonizing CsrA regulation	-1.06511912
dgoR	putative DNA-binding transcriptional regulator	-1.063109127
znuB	zinc transporter subunit: membrane component of ABC superfamily	-1.063079403
hslO	heat shock protein Hsp33	-1.051184182
mnmG	5-methylaminomethyl-2-thiouridine modification at tRNA U34	-1.04883016
ycfJ	uncharacterized protein	-1.045943072
yeiB	DUF418 family putative inner membrane protein	-1.042699442
pcnB	poly(A) polymerase	-1.034676536
gshB	glutathione synthetase	-1.033107765
apaH	diadenosine tetraphosphatase	-1.031176467
yjcO	Sel1 family TPR-like repeat protein	-1.028245567
uspC	universal stress protein	-1.026312759
yegL	VMA domain protein	-1.021107586
rlpA	septal ring protein and suppressor of prc and minor lipoprotein	-1.020378989
ycgJ	uncharacterized protein	-1.008207185
yheT	UPF0017 family putative hydrolase	-1.007910593
ampG	muropeptide transporter	-1.006234852

basR	response regulator in two-component regulatory system with BasS	-0.998839305
dgoK	2-oxo-3-deoxygalactonate kinase	-0.998033549
hybG	hydrogenase 2 accessory protein	-0.99784485
uxaA	altronate hydrolase	-0.995967381
gcvP	glycine decarboxylase and PLP-dependent and subunit (protein P) of glycine cleavage complex	-0.992182684
creA	putative periplasmic protein	-0.990270919
ynfH	oxidoreductase and membrane subunit	-0.986832632
sgbU	putative L-xylulose 5-phosphate 3-epimerase	-0.983974546
dppC	dipeptide/heme transporter	-0.983415259
citA	sensory histidine kinase in two-component regulatory system with CitB	-0.982100009
ysgA	putative carboxymethylenebutenolidase	-0.973898106
yhiI	putative membrane fusion protein (MFP) of efflux pump	-0.973430956
rdgC	nucleoid-associated ssDNA and dsDNA binding protein; competitive inhibitor of RecA function	-0.972502236
metE	5-methyltetrahydropteroyltriglutamate-homocysteine S-methyltransferase	-0.972327804
mprA	transcriptional repressor of microcin B17 synthesis and multidrug efflux	-0.969838654
rimI	ribosomal-protein-S18-alanine N-acetyltransferase	-0.96786236
yegQ	putative peptidase	-0.964892122
wzzE	Entobacterial Common Antigen (ECA) polysaccharide chain length modulation protein	-0.962160379
kdgK	2-dehydro-3-deoxygluconokinase	-0.961390516
amyA	cytoplasmic alpha-amylase	-0.959121558
360066_360651		-0.95361242

yahO	periplasmic protein and function unknown and YhcN family	-0.950027304
glnG	fused DNA-binding response regulator in two-component regulatory system with GlnL: response regulator/sigma54 interaction protein	-0.941751984
cheA	fused chemotactic sensory histidine kinase in two-component regulatory system with CheB and CheY: sensory histidine kinase/signal sensing protein	-0.939076166
entE	2 and 3-dihydroxybenzoate-AMP ligase component of enterobactin synthase multienzyme complex	-0.939008693
yidR	DUF3748 family protein	-0.93761718
phnG	ribophosphonate triphosphate synthase subunit	-0.9358605
moaC	molybdopterin biosynthesis and protein C	-0.93513976
yghR	putative ATP-binding protein	-0.934048711
yhbV	U32 peptidase family protein	-0.933833821
proX	glycine betaine transporter subunit	-0.924739711
speA	biosynthetic arginine decarboxylase and PLP-binding	-0.921926955
metB	cystathionine gamma-synthase and PLP-dependent	-0.917268312
yjhQ	putative acetyltransferase	-0.91612226
yphD	inner membrane putative ABC superfamily sugar transporter permease	-0.910257761
plsY	putative glycerol-3-phosphate acyltransferase	-0.906544452
hybF	protein involved with the maturation of hydrogenases 1 and 2	-0.905367892
aspC	aspartate aminotransferase and PLP-dependent	-0.902979466
trpR	transcriptional repressor and tryptophan-binding	-0.901292095
intD	DLP12 prophage; putative phage integrase	-0.898455624

rseC	SoxR iron-sulfur cluster reduction factor component; with RsxABCDEG	-0.8957278
etk	tyrosine-protein kinase and role in O-antigen capsule formation	-0.894440996
uvrA	ATPase and DNA damage recognition protein of nucleotide excision repair excinuclease UvrABC	-0.890684106
2282397_2283592		-0.89008896
yhjC	LysR family putative transcriptional regulator	-0.888777092
waaQ	lipopolysaccharide core biosynthesis protein	-0.885994467
aroG	3-deoxy-D-arabino-heptulosonate-7-phosphate synthase and phenylalanine repressible	-0.884664558
mepM	murein DD-endopeptidase and space-maker hydrolase and septation protein	-0.882025016
paoD	moco insertion factor for PaoABC aldehyde oxidoreductase	-0.879019569
yfeD	DUF1323 family putative DNA-binding protein	-0.87469618
alaC	valine-pyruvate aminotransferase 3	-0.874635119
gadW	transcriptional activator of gadA and gadBC; repressor of gadX	-0.872937957
xisD		-0.872169015
yabI	DedA family inner membrane protein	-0.872033173
cdh	CDP-diacylglycerol phosphotidylhydrolase	-0.87115374
glsB	glutaminase 2	-0.866226064
bcsG	DUF3260 family inner membrane protein associated with cellulose production	-0.861972516
sspA	stringent starvation protein A and phage P1 late gene activator and RNAP-associated acid-resistance protein and inactive glutathione S-transferase homolog	-0.860271258

idi	isopentenyl diphosphate isomerase	-0.859086855
bioC	malonyl-ACP O-methyltransferase and SAM-dependent	-0.856254667
damX	cell division protein that binds to the septal ring	-0.854261635
livF	leucine/isoleucine/valine transporter subunit	-0.851105511
ygiM	SH3 domain protein	-0.846091006
yicI	putative alpha-glucosidase	-0.842867268
mtlA	fused mannitol-specific PTS enzymes: IIA components/IIB components/IIC components	-0.838278631
clsA	cardiolipin synthase 1	-0.837059047
rbsK	ribokinase	-0.833163293
exoD		-0.831736165
mazG	nucleoside triphosphate pyrophosphohydrolase	-0.83044463
trkH	potassium transporter	-0.822834027
yoaD	putative membrane-anchored cyclic-di-GMP phosphodiesterase and regulator of cellulose production	-0.822831793
yhcM	putative AFG1-like family P-loop ATPase	-0.819536802
nagZ	beta N-acetyl-glucosaminidase	-0.811175494
typA	GTP-binding protein	-0.808597088
mltB	membrane-bound lytic murein transglycosylase B	-0.805098011
yhdP	DUF3971-AsmA2 domains protein	-0.802262178
sthA	pyridine nucleotide transhydrogenase and soluble	-0.796583858
aegA	putative oxidoreductase and FeS binding subunit/NAD/FAD-binding subunit	-0.796397836
ecpA	ECP pilin	-0.795844645
rsxC	SoxR iron-sulfur cluster reduction factor component; putative membrane-associated NADH oxidoreductase of electron transport complex	-0.795304554

gadY	sRNA antisense regulator of gadAB transcriptional activator GadX mRNA and Hfq-dependent	-0.791177181
yphA	DoxX family inner membrane protein	-0.78727418
ppc	phosphoenolpyruvate carboxylase	-0.786835641
fryA	putative PTS enzyme and Hpr component/enzyme I component/enzyme IIA component	-0.785907363
yagF	CP4-6 prophage; dehydratase family protein	-0.782198978
lpoA	OM lipoprotein stimulator of MrcA transpeptidase	-0.779779219
fiu	catecholate siderophore receptor Fiu	-0.778320697
recQ	ATP-dependent DNA helicase	-0.77701107
dgoA	2-oxo-3-deoxygalactonate 6-phosphate aldolase	-0.775139773
rbbA	ribosome-associated ATPase: ATP-binding protein/ATP-binding membrane protein	-0.774235906
kup	potassium transporter	-0.773684192
curA	curcumin/dihydrocurcumin reductase and NADPH-dependent	-0.773072883
ompX	outer membrane protein X	-0.771488387
leuB	3-isopropylmalate dehydrogenase and NAD(+)-dependent	-0.770276794
yagE	2-keto-3-deoxy gluconate (KDG) aldolase; CP4-6 prophage	-0.766210228
allR	transcriptional repressor of all and gcl operons; glyoxylate-induced	-0.765458453
eutJ	ethanolamine utilization protein and HSP70/actin superfamily protein	-0.763678029
rbsA	fused D-ribose transporter subunits of ABC superfamily: ATP-binding components	-0.762939268
rffH	glucose-1-phosphate thymidylyltransferase	-0.760062552
yfaD	transposase_31 family protein	-0.759815127

feaB	phenylacetaldehyde dehydrogenase	-0.758739485
rseB	anti-sigma E factor and binds RseA	-0.758275403
pitA	phosphate transporter and low-affinity; tellurite importer	-0.757593974
ybjO	DUF2593 family inner membrane protein	-0.756973654
uxuA	mannonate hydrolase	-0.75434083
yidA	sugar phosphate phosphatase; substrates include erythrose 4-P and mannose 1-P phosphatase	-0.752291489
paoB	PaoABC aldehyde oxidoreductase and FAD-containing subunit	-0.750805118
yjbB	putative Na+/Pi-cotransporter	-0.749569786
mhpR	mhp operon transcriptional activator	-0.747270126
ygdH	UPF0717 family protein	-0.744389086
menA	1 and 4-dihydroxy-2-naphthoate octaprenyltransferase	-0.74191275
yjfC	ATP-Grasp family ATPase	-0.738687696
phnK	carbon-phosphorus lyase complex subunit and putative ATP transporter ATP-binding protein	-0.736701237
ydcI	putative DNA-binding transcriptional regulator	-0.735007112
hdfR	flhDC operon transcriptional repressor	-0.732838309
ygeY	putative peptidase	-0.732385434
menC	O-succinylbenzoyl-CoA synthase	-0.729305158
yhjY	autotransporter beta-domain protein	-0.728622965
paaZ	fused oxepin-CoA hydrolase/3-oxo-5 and 6-dehydrosuberyl-CoA semialdehyde dehydrogenase	-0.727421777
caiB	crotonobetainyl CoA:carnitine CoA transferase	-0.726789967
frlA	putative fructoselysine transporter	-0.726413993
srlQ	D-arabinose 5-phosphate isomerase	-0.725651311
342165_342797		-0.725070578

yihU	gamma-hydroxybutyrate dehydrogenase and NADH-dependent	-0.724867696
fabR	transcriptional repressor of fabA and fabB	-0.72225912
wzxE	O-antigen translocase	-0.721400103
yigA	DUF484 family protein	-0.720441091
yghD	putative membrane-anchored secretion pathway M-type protein	-0.718591293
phnE		-0.718544978
gspG	pseudopilin and cryptic and general secretion pathway	-0.716254769
hypE	carbamoyl dehydratase and hydrogenases 1 and 2 and 3 maturation protein	-0.715798814
ytfK	DUF1107 family protein	-0.715418324
uhpA	response regulator in two-component regulatory system wtih UhpB	-0.713770576
yegD	Hsp70 chaperone family protein	-0.711376563
arnD	undecaprenyl phosphate-alpha-L-ara4FN deformylase	-0.709039717
bacA	undecaprenyl pyrophosphate phosphatase	-0.701395236
mtgA	biosynthetic peptidoglycan transglycosylase	-0.694454554
glpA	sn-glycerol-3-phosphate dehydrogenase (anaerobic) and large subunit and FAD/NAD(P)-binding	-0.691403406
paoC	PaoABC aldehyde oxidoreductase and Moco-containing subunit	-0.69089078
gabD	succinate-semialdehyde dehydrogenase I and NADP-dependent	-0.689687279
yghO		-0.685612255
gltB	glutamate synthase and large subunit	-0.68160471
lysC	lysine-sensitive aspartokinase 3	-0.680500558
dppB	dipeptide/heme transporter	-0.680086554

paoA	PaoABC aldehyde oxidoreductase and 2Fe-2S subunit	-0.680017248
yjhP	putative methyltransferase	-0.67945996
ydiU	UPF0061 family protein	-0.678015956
fhuB	fused iron-hydroxamate transporter subunits of ABC superfamily: membrane components	-0.677904446
yihV	putative sugar kinase	-0.674999427
fhuC	iron-hydroxamate transporter subunit	-0.674949595
aldA	aldehyde dehydrogenase A and NAD-linked	-0.674029398
wecC	UDP-N-acetyl-D-mannosaminuronic acid dehydrogenase	-0.673872798
wecB	UDP-N-acetyl glucosamine-2-epimerase	-0.672752993
yfcP	putative fimbrial-like adhesin protein	-0.671501883
poxB	pyruvate dehydrogenase (pyruvate oxidase) and thiamine triphosphate-binding and FAD-binding	-0.66822769
yahJ	putative metallo-dependent hydrolase domain deaminase	-0.668023178
fdoG	formate dehydrogenase-O and large subunit	-0.665805912
ggt	gamma-glutamyltranspeptidase	-0.659400904
fpr	ferredoxin-NADP reductase	-0.655343758
avtA	valine-pyruvate aminotransferase 1	-0.652865955
cof	thiamine pyrimidine pyrophosphate hydrolase; HMP-PP phosphatase	-0.650626757
ybbN	DnaK co-chaperone and thioredoxin-like protein	-0.649027776
2297895_2298550		-0.647003966
mdtL	multidrug efflux system protein	-0.645020901
rimJ	ribosomal-protein-S5-alanine N-acetyltransferase	-0.643235848
frlB	fructoselysine-6-P-deglycase	-0.642935194
yrdA	bacterial transferase hexapeptide domain protein	-0.637636056

yigB	5-amino-6-(5-phospho-D-ribitylamino) uracil phosphatase; pyrimidine phosphatase; riboflavin synthesis	-0.633069094
ilvC	ketol-acid reductoisomerase and NAD(P)-binding	-0.627367215
yijO	AraC family putative transcriptional activator	-0.623151593
lysU	lysine tRNA synthetase and inducible	-0.622996017
bax	putative glucosaminidase	-0.620605336
melR	melibiose operon transcriptional regulator; autoregulator	-0.620087939
nrfE	heme lyase (NrfEFG) for insertion of heme into c552 and subunit NrfE	-0.619962374
clpA	ATPase and specificity subunit of ClpA-ClpP ATP-dependent serine protease and chaperone activity	-0.619673222
yhjJ	putative periplasmic M16 family chaperone	-0.619158192
yjbH	DUF940 family extracellular polysaccharide protein	-0.618818473
cysN	sulfate adenylyltransferase and subunit 1	-0.60752353
cdaR	carbohydrate diacid regulon transcriptional regulator; autoregulator	-0.607130003
pgaC	biofilm PGA synthase PgaCD and catalytic subunit; poly-beta-1 and 6-N-acetyl-D-glucosamine synthase; c-di-GMP-stimulated activity and dimerization	-0.605679286
mdtB	multidrug efflux system and subunit B	-0.602488314
frdB	fumarate reductase (anaerobic) and Fe-S subunit	-0.599615196
pflC	putative [formate-C-acetyltransferase 2]-activating enzyme; pyruvate formate-lyase 1-activating enzyme	-0.597506447
yaaJ	putative transporter	-0.595072021

alsB	D-allose transporter subunit	-0.59111934
fucI	L-fucose isomerase	-0.590145289
malQ	4-alpha-glucanotransferase (amylomaltase)	-0.588034634
nagE	fused N-acetyl glucosamine specific PTS enzyme: IIC and IIB and and IIA components	-0.587288018
dsbD	fused thiol:disulfide interchange protein: activator of DsbC/conserved protein	-0.584783407
mutL	methyl-directed mismatch repair protein	-0.584199426
caiE	stimulator of CaiD and CaiB enzyme activities	-0.582971471
tamB	translocation and assembly module for autotransporter export and inner membrane subunit	-0.581795286
gadB	glutamate decarboxylase B and PLP-dependent	-0.581735201
yjiR	putative DNA-binding transcriptional regulator/putative aminotransferase	-0.580569655
qorA	quinone oxidoreductase and NADPH-dependent	-0.578258835
nikA	nickel-binding and heme-binding periplasmic protein	-0.575934065
malT	mal regulon transcriptional activator	-0.574843722
yeeE	UPF0394 family inner membrane protein	-0.569069311
leuC	3-isopropylmalate dehydratase large subunit	-0.567318697
yjcD	inner membrane putative guanine permease	-0.565192011
bcsC	cellulose synthase subunit	-0.564174317
yjiA	GTP-binding protein and putative GTPase	-0.562559714
iadA	isoaspartyl dipeptidase	-0.562043524
bcsA	cellulose synthase and catalytic subunit	-0.561158907
norR	anaerobic nitric oxide reductase DNA-binding transcriptional activator	-0.55943049

copA	copper transporter	-0.553434155
tldD	putative peptidase	-0.553264551
yicJ	putative transporter	-0.55223458
kefC	potassium:proton antiporter	-0.550819473
djlC	J domain-containing HscC co-chaperone; Hsc56	-0.550481133
uxuB	D-mannonate oxidoreductase and NAD-dependent	-0.549376785
lyxK	L-xylulose kinase	-0.547968394
cstA	carbon starvation protein involved in peptide utilization; APC peptide transporter family protein	-0.547100013
gntT	gluconate transporter and high-affinity GNT I system	-0.545809443
yhgF	putative transcriptional accessory protein	-0.538330443
yhcG	DUF1016 family protein in the PD-(D/E)XK nuclease superfamily	-0.534837778
prpC	2-methylcitrate synthase	-0.53468474
argH	argininosuccinate lyase	-0.528637132
fadA	3-ketoacyl-CoA thiolase (thiolase I)	-0.523368854
idnO	5-keto-D-gluconate-5-reductase	-0.520840524
gadX	acid resistance regulon transcriptional activator; autoactivator	-0.518842191
yjgR	DUF853 family protein with NTPase fold	-0.514405932
glsA	glutaminase 1	-0.512365526
yjiY	putative transporter	-0.510023076
malZ	maltodextrin glucosidase	-0.508431113
gpp	guanosine pentaphosphatase/exopolyphosphatase	-0.491567654
hycC	hydrogenase 3 and membrane subunit	-0.491050937
yahF	putative NAD(P)-binding succinyl-CoA synthase	-0.481892373
rcsD	phosphotransfer intermediate protein in two-component regulatory system with RcsBC	-0.472088771

ilvB	acetolactate synthase 2 large subunit	-0.462665877
treF	cytoplasmic trehalase	-0.459501173
metH	homocysteine-N5-methyltetrahydrofolate transmethylase and B12-dependent	-0.459409724
nlpD	activator of AmiC murein hydrolase activity and lipoprotein	-0.456548649
ygcB	R-loop helicase-annealase Cas3 needed for Cascade anti-viral activity	-0.452761238

Table A.9 - List of disrupted genes in the *E. coli* BW25113 transposon mutant libraries that had accepted pHYCTX14 from the QuaTraDIS comparison pipeline.

Gene	Function	logFC
2707641_2707739		8.632626042
ubiG	bifunctional 3-demethylubiquinone-93-methyltransferase/ 2-octaprenyl-6-hydroxy phenol methylase	8.451714322
leuV	tRNA-Leu	8.436679791
ftsL	membrane bound cell division protein at septum containing leucine zipper motif	8.062615517
metG	methionyl-tRNA synthetase	7.662185619
rimP	ribosome maturation factor for 30S subunits	7.60985379
cyaR	sRNA antisense regulator of ompX mRNA instability and Hfq-dependent and cAMP-induced	7.555797651
3478730_3478752		7.4106828
orn	oligoribonuclease	7.348428919
metY	tRNA-Met	7.348419926
valS	valyl-tRNA synthetase	7.283244947
1933355_1933385		6.946908055
895151_895249		6.904071835
3808456_3808478		6.860142666
2145154_2145182		6.719429474
gltU	tRNA-Glu	6.617269659
tolC	transport channel	4.244323506
1924179_1924263		3.658882518
3271177_3271206		3.20036149
pth	peptidyl-tRNA hydrolase	2.768268362
msyB	multicopy suppressor of secY and secA	2.434180676
yhbY	RNA binding protein associated with pre-50S ribosomal subunits	2.397969581
nsrR	nitric oxide-sensitive repressor for NO regulon	2.383834727
guaA	GMP synthetase (glutamine aminotransferase)	2.331106349
obgE	GTPase involved in cell partioning and DNA repair	2.323787202
lysS	lysine tRNA synthetase and constitutive	2.320031834

pfkA	6-phosphofructokinase I	2.21297383
yafN	antitoxin of the YafO-YafN toxin-antitoxin system	2.199122577
cspE	constitutive cold shock family transcription antitermination protein; negative regulator of cspA transcription; RNA melting protein; ssDNA-binding protein	2.186979797
acrA	multidrug efflux system	2.17238817
yceD	DUF177 family protein	1.979260175
rnhA	ribonuclease HI and degrades RNA of DNA-RNA hybrids	1.902902622
fliN	flagellar motor switching and energizing component	1.876255394
cspA	RNA chaperone and antiterminator and cold-inducible	1.875510889
acrB	multidrug efflux system protein	1.838286263
fis	global DNA-binding transcriptional dual regulator	1.829873795
kdsC	3-deoxy-D-manno-octulosonate 8-phosphate phosphatase	1.803686858
pstB	phosphate transporter subunit	1.775357568
yehR	lipoprotein and DUF1307 family	1.696028421
yjjY	uncharacterized protein	1.689199339
ndh	respiratory NADH dehydrogenase 2/cupric reductase	1.681093512
glpD	sn-glycerol-3-phosphate dehydrogenase and aerobic and FAD/NAD(P)-binding	1.671591584
ychQ	SIRB family inner membrane protein	1.657894091
cnu	nucleoid-associated oriC-binding protein; H-NS and StpA stabilizing factor	1.567720875
dnaK	chaperone Hsp70 and with co-chaperone DnaJ	1.547306996
ycgY	uncharacterized protein	1.520310969
pta	phosphate acetyltransferase	1.467941415
dusB	tRNA-dihydrouridine synthase B	1.430793236
sokA		1.416040134
gcvB	sRNA antisense regulator represses oppA and dppA and gltI and livJ expression and Hfq-dependent	1.387637087
yjdK	uncharacterized protein	1.385216063

ydfK	cold shock protein and function unknown and Qin prophage	1.362036
pyrF	'orotidine-5''-phosphate decarboxylase'	1.299089656
dksA	transcriptional regulator of rRNA transcription and DnaK suppressor protein	1.288221319
intG		1.281178905
lepA	back-translocating elongation factor EF4 and GTPase	1.271760566
eamA	cysteine and O-acetyl-L-serine efflux system	1.251882837
yfiR	putative periplasmic inhibitor of YfiN activity	1.240759119
gcvR	transcriptional repressor and regulatory protein accessory to GcvA	1.217340085
ppk	polyphosphate kinase and component of RNA degradosome	1.20846946
guaB	IMP dehydrogenase	1.204790917
waaZ	lipopolysaccharide core biosynthesis protein	1.196749787
prfC	peptide chain release factor RF-3	1.180085263
pyrC	dihydro-orotase	1.155650766
tfaX	578408_578591	1.152777216
slyA	global transcriptional regulator	1.134047163
yncI		1.09478351
ydeM	putative YdeN-specific sulfatase-maturating enzyme	1.093535619
ybcM	DLP12 prophage; putative DNA-binding transcriptional regulator	1.091521476
cedA	cell division modulator	1.074382783
corA	magnesium/nickel/cobalt transporter	1.061575743
purR	transcriptional repressor and hypoxanthine-binding	1.037952549
rnd	ribonuclease D	1.034424156
waaU	lipopolysaccharide core biosynthesis	1.032753646
ykgH	putative inner membrane protein	1.031585858
wbbK	lipopolysaccharide biosynthesis protein	1.031408636
ybfE	LexA-regulated protein and CopB family	1.025756786

aroA	5-enolpyruvylshikimate-3-phosphate synthetase	1.012750075
mcrA	putative 5-methylcytosine/5-hydroxymethylcytosine-specific restriction nuclease; 5-methylcytosine DNA binding protein; e14 prophage gene	1.001582413
rapA	RNA polymerase remodeling/recycling factor ATPase; RNA polymerase-associated and ATP-dependent RNA translocase	0.995643326
waaB	UDP-D-galactose:(glucosyl)lipopolysaccharide-1 and 6-D-galactosyltransferase	0.990346737
hfq	global sRNA chaperone; HF-I and host factor for RNA phage Q beta replication	0.980484215
yehA	putative fimbrial-like adhesin protein	0.970562682
mrp	antiporter inner membrane protein	0.970024043
ychE	UPF0056 family inner membrane protein	0.963672186
narL	response regulator in two-component regulatory system with NarX (or NarQ)	0.962277339
yagM	CP4-6 prophage; uncharacterized protein	0.962191729
yfcQ	putative fimbrial-like adhesin protein	0.957536371
flhD	flagellar class II regulon transcriptional activator and with FlhC	0.946372888
yebO	putative inner membrane protein	0.943207367
mtlD	mannitol-1-phosphate dehydrogenase and NAD-dependent	0.935798361
waaR	UDP-D-galactose:(glucosyl)lipopolysaccharide-alpha-1 and 3-D-galactosyltransferase	0.930608705
rcsB	response regulator in two-component regulatory system with RcsC and YojN	0.928198025
yigG	PRK11371 family inner membrane protein	0.918061975

pyrD	dihydro-orotate oxidase and FMN-linked	0.914804333
mcrC	5-methylcytosine-specific restriction enzyme McrBC and subunit McrC	0.88332714
agaR	transcriptional repressor of the aga regulon	0.875317054
lit	e14 prophage; cell death peptidase and inhibitor of T4 late gene expression	0.874878189
yiiE	CopG family putative transcriptional regulator	0.874083323
rzpR		0.868477118
3354046_3354145		0.867652788
ygcG	uncharacterized protein	0.865178142
pgi	glucosephosphate isomerase	0.863906399
yqgE	uncharacterized protein	0.855621036
ahpC	alkyl hydroperoxide reductase and C22 subunit	0.846150638
wbbH	O-antigen polymerase	0.834556255
yceJ	putative cytochrome b561	0.82872964
ycfZ	inner membrane protein	0.822689885
ibpB	heat shock chaperone	0.82182213
arcB	aerobic respiration control sensor histidine protein kinase and cognate to two-component response regulators ArcA and RssB	0.818332229
ygdI	DUF903 family verified lipoprotein	0.816407029
sfmZ	response regulator family protein	0.807645383
ydiP	putative DNA-binding transcriptional regulator	0.793416674
tdh	L-threonine 3-dehydrogenase and NAD(P)-binding	0.790724018
ribB	3 and 4-dihydroxy-2-butanone-4-phosphate synthase	0.786958443
rzoR	Rac prophage; putative lipoprotein	0.782328779
yfjI	CP4-57 prophage; uncharacterized protein	0.767424947
pstS	periplasmic phosphate binding protein and high-affinity	0.763802513
kbl	glycine C-acetyltransferase	0.759362979
yggN	DUF2884 family putative periplasmic protein	0.755068469

wbbI	d-Galf:alpha-d-Glc beta-1 and 6-galactofuranosyltransferase	0.749593507
ydeT		0.749072857
yeaG	protein kinase and endogenous substrate unidentified; autokinase	0.74643588
astE	succinylglutamate desuccinylase	0.74370816
tgt	tRNA-guanine transglycosylase	0.743329727
ygjQ	DUF218 superfamily protein	0.735326298
alpA	CP4-57 prophage; DNA-binding transcriptional activator	0.707732276
yiaB	YiaAB family inner membrane protein	0.703163709
yjgN	DUF898 family inner membrane protein	0.700426177
ugd	UDP-glucose 6-dehydrogenase	0.695050938
yjhB	putative transporter	0.693883636
wzxB	putative polisoprenol-linked O-antigen transporter	0.690435739
ybhM	UPF0005 family inner membrane protein	0.688546252
yjgL	uncharacterized protein	0.681341858
yfjJ	CP4-57 prophage; uncharacterized protein	0.680037728
566776_568034		0.678254426
purF	amidophosphoribosyltransferase	0.674611563
tdcA	tdc operon transcriptional activator	0.674548561
emrY	putative multidrug efflux system	0.674504914
ftnA	ferritin iron storage protein (cytoplasmic)	0.671173511
waaJ	UDP-D-glucose:(galactosyl)lipopolysaccharide glucosyltransferase	0.669551686
yahL	uncharacterized protein	0.664828623
yodB	cytochrome b561 homolog	0.6640285
brnQ	branched-chain amino acid transport system 2 carrier protein; LIV-II transport system for Ile and Leu and and Val	0.659583915
yddA	putative multidrug transporter subunit of ABC superfamily and membrane component/ATP-binding component	0.658507582
yedV	putative sensory kinase in two-component regulatory system with YedW	0.653905513

glpQ	periplasmic glycerophosphodiester phosphodiesterase	0.653465513
ybeU	DUF1266 family protein	0.648356616
arpB		0.63332134
yobF	DUF2527 family heat-induced protein	0.629952071
yddW	liprotein and glycosyl hydrolase homolog	0.624653855
yegI	protein kinase-related putative non-specific DNA-binding protein	0.622712612
yaeF	putative lipoprotein	0.62138164
nupC	nucleoside (except guanosine) transporter	0.621045997
fimA	major type 1 subunit fimbrin (pilin)	0.615565277
yafT	lipoprotein	0.610369869
ygiL	putative fimbrial-like adhesin protein	0.608873833
ycjM	alpha amylase catalytic domain family protein	0.607766079
yhiL		0.596173102
waaY	lipopolysaccharide core biosynthesis protein	0.596017667
yfbK	Von Willebrand factor domain putative lipoprotein	0.591247307
yehB	putative outer membrane protein	0.577542203
rclC	reactive chlorine species (RCS) stress resistance inner membrane protein	0.577044634
dnaJ	chaperone Hsp40 and DnaK co-chaperone	0.575788417
ycaN	LysR family putative transcriptional regulator	0.566095996
mqsR	GCU-specific mRNA interferase toxin of the MqsR-MqsA toxin-antitoxin system; biofilm/motility regulator; anti-repressor	0.565200038
fimB	tyrosine recombinase/inversion of on/off regulator of fimA	0.563298737
fucP	L-fucose transporter	0.562835784
rhsH		0.558244741
ybfD	H repeat-associated putative transposase	0.5449451

bluF	anti-repressor for YcgE and blue light-responsive; FAD-binding; has c-di-GMP phosphodiesterase-like EAL domain and but does not degrade c-di-GMP	0.536309725
mfd	transcription-repair coupling factor	0.530692504
lysP	lysine transporter	0.530668722
yfiN	putative membrane-anchored diguanylate cyclase with an N-terminal periplasmic domain	0.524606796
ynaI	mechanosensitive channel protein and very small conductance	0.517432881
ydeN	putative Ser-type periplasmic non-aryl sulfatase	0.501051523
mcrB	5-methylcytosine-specific restriction enzyme McrBC and subunit McrB	0.499959701
ybfL		0.490221066
yhiJ	DUF4049 family protein	0.486452366
gtrB	CPS-53 (KpLE1) prophage; bactoprenol glucosyl transferase	0.479195517
yhhI	putative transposase	0.473861813
ygeQ		0.458527183

APPENDIX IX: Genes determined by TraDIS-*Xpress* to be implicated in *S.* Typhimurium plasmid acceptance

Table A.10 – List of protected genes in the *S.* Typhimurium 14028S transposon mutant libraries that had accepted pHYCTX14 from the QuaTraDIS comparison pipeline.

Gene	Function	logFC
glyS	glycyl-tRNA synthetase subunit beta	-19.01703114
murF	UDP-N-acetylmuramoyl-tripeptide--D-alanyl-D-alani ne ligase	-17.72560728
3663869_3663983	hypothetical protein	-17.29235408
rplD	50S ribosomal protein L4	-17.27993551
rplR	50S ribosomal protein L18	-14.87355293
proS	prolyl-tRNA synthetase	-14.59883214
prsA	ribose-phosphate pyrophosphokinase	-14.34454948
cydC	cysteine/glutathione ABC transporter membrane/ATP-binding component	-14.18345252
folE	GTP cyclohydrolase I	-13.90316186
rpoD	RNA polymerase sigma factor RpoD	-13.8101669
argS	arginyl-tRNA synthetase	-13.79107935
thrS	threonyl-tRNA synthetase	-13.60325887
ycfW	outer membrane-specific lipoprotein transporter subunit LolE	-13.55496069
lpdA	dihydrolipoamide dehydrogenase	-13.36914614
2824016_2824139	Gifsy-1 prophage protein	-13.35187613
crr	glucose-specific PTS system component	-12.86196458
alaS	alanyl-tRNA synthetase	-12.78190064
ribH	riboflavin synthase subunit beta	-12.71602375
ppnK	inorganic polyphosphate/ATP-NAD kinase	-12.7086332
nrdA	ribonucleotide-diphosphate reductase subunit alpha	-12.6994984
infA	translation initiation factor IF-1	-12.58946722
ftsB	cell division protein FtsB	-12.4452945
glyQ	glycyl-tRNA synthetase subunit alpha	-12.24028635
gpsA	NAD(P)H-dependent glycerol-3-phosphate dehydrogenase	-12.17142917
orf70	hypothetical protein	-12.1581222
2083024_2083243	putative cytoplasmic protein	-12.02405801
tyrU	tRNA-Tyr	-11.98324249

pheT	phenylalanyl-tRNA synthetase subunit beta	-11.84578728
pheS	phenylalanyl-tRNA synthetase subunit alpha	-11.7595211
ileS	isoleucyl-tRNA synthetase	-11.6841382
gltX	glutamyl-tRNA synthetase	-11.66981284
dfp	bifunctional phosphopantothenoylcysteine decarboxylase/phosphopantothenate synthase	-11.6602842
sucB	dihydrolipoamide acetyltransferase	-11.61049355
secB	preprotein translocase subunit SecB	-11.59024791
2446154_2446358	hypothetical protein	-11.34238738
secD	preprotein translocase subunit SecD	-11.3110266
942901_943027	hypothetical protein	-11.25150284
rpsB	30S ribosomal protein S2	-11.24958319
clpX	ATP-dependent protease ATP-binding subunit	-11.22901959
1565233_1565359	hypothetical protein	-11.2281525
rrmJ	23S rRNA methyltransferase J	-11.22522299
flgB	flagellar basal body rod protein FlgB	-11.15233995
fabI	enoyl-(acyl carrier protein) reductase	-11.06354718
3832814_3832976	conserved hypothetical protein	-11.04494271
3832780_3832954	hypothetical protein	-11.0449427
mviN	putative virulence protein	-10.96563866
rpoB	DNA-directed RNA polymerase subunit beta	-10.96475492
trxC	thioredoxin 2	-10.95105784
ftsY	cell division protein FtsY	-10.91784092
1755684_1755894	hypothetical protein	-10.91687371
trmE	tRNA modification GTPase TrmE	-10.85951127
fabH	3-oxoacyl-(acyl carrier protein) synthase III	-10.8591717
mrdA	penicillin-binding protein 2	-10.84758985
rpsA	30S ribosomal protein S1	-10.8332411
mukE	condesin subunit E	-10.7991821
dnaK	molecular chaperone DnaK	-10.77233604
adk	adenylate kinase	-10.7444215
926969_927134	hypothetical protein	-10.71762017
ispA	geranyltranstransferase	-10.65482626
folC	bifunctional folylpolyglutamate synthase/ dihydrofolate synthase	-10.64147329
dnaN	DNA polymerase III subunit beta	-10.61167303
1996366_1996594	hypothetical protein	-10.58865911
dnaE	DNA polymerase III subunit alpha	-10.58496671

399119_399233	hypothetical protein	-10.53025968
ipk	4-diphosphocytidyl-2-C-methyl-D-erythritol kinase	-10.46737195
ygfZ	putative global regulator	-10.42165225
1696702_1696807	hypothetical protein	-10.41031301
cydD	cysteine/glutathione ABC transporter membrane/ATP-binding component	-10.40756563
trmU	tRNA (5-methylaminomethyl-2-thiouridylate)-methyltransferase	-10.36988731
1299672_1299867	conserved hypothetical protein	-10.35400075
2397714_2397861	hypothetical protein	-10.34931354
lgt	prolipoprotein diacylglyceryl transferase	-10.33134311
1083563_1083962	minor tail protein	-10.3221518
kdtA	3-deoxy-D-manno-octulosonic-acid transferase	-10.31558938
folB	'bifunctional dihydroneopterin aldolase/dihydroneopterin triphosphate 2''-epimerase'	-10.28620143
accD	acetyl-CoA carboxylase subunit beta	-10.24762779
2125757_2125982	DNA binding protein	-10.22211637
rplA	50S ribosomal protein L1	-10.20992121
1639902_1640112	hypothetical protein	-10.1650785
1304043_1304181	putative bacteriophage protein	-10.13131342
hisS	histidyl-tRNA synthetase	-10.08535673
dapE	succinyl-diaminopimelate desuccinylase	-10.04289826
1335445_1335610	isocitrate dehydrogenase and NADP-dependent	-10.01644819
nusB	transcription antitermination protein NusB	-9.954767744
yebA	hypothetical protein	-9.939133192
ynbE	putative outer membrane lipoprotein	-9.937864715
rplM	50S ribosomal protein L13	-9.930461728
yfiO	outer membrane protein assembly complex subunit YfiO	-9.883768193
3361048_3361165	hypothetical protein	-9.873424611
accB	acetyl-CoA carboxylase biotin carboxyl carrier protein subunit	-9.785927022
accC	acetyl-CoA carboxylase biotin carboxylase subunit	-9.771428543
700127_700277	hypothetical protein	-9.765506961
cca	'multifunctional tRNA nucleotidyl transferase/2''3''-cyclic phosphodiesterase/2''nucleotidase/phosphatase'	-9.688023438

2373809_2374100	bicyclomycin/multidrug efflux system	-9.597373185
cspA	major cold shock protein	-9.579092234
2308711_2308819	hypothetical protein	-9.53772999
coaD	phosphopantetheine adenylyltransferase	-9.522740979
nadE	NAD synthetase	-9.518958148
gyrA	DNA gyrase subunit A	-9.490140037
791381_792215	putative glycosyltransferase	-9.456492371
mreC	cell wall structural complex MreBCD transmembrane component MreC	-9.454149422
rpoC	'DNA-directed RNA polymerase subunit beta'"	-9.415104932
aspS	aspartyl-tRNA synthetase	-9.402153794
sirC	putative transcriptional regulator	-9.352144862
msbA	lipid transporter ATP-binding/permease protein	-9.32967186
2033683_2033827	hypothetical protein	-9.235419307
topA	DNA topoisomerase I	-9.211124663
733101_733251	conserved hypothetical protein	-9.158466601
lpxK	'tetraacyldisaccharide 4'"-kinase'	-9.09138908
cysB	transcriptional regulator CysB	-9.071087826
ybgC	acyl-CoA thioester hydrolase YbgC	-9.070350725
ftsI	division specific transpeptidase	-9.053802853
mraY	phospho-N-acetylmuramoyl-pentapeptide-transferase	-9.048418699
lipA	lipoyl synthase	-9.028103908
2136008_2136482	putative endoprotease	-8.983772465
flgG	flagellar basal body rod protein FlgG	-8.916302553
ftsA	cell division protein FtsA	-8.915732254
ispD	2-C-methyl-D-erythritol 4-phosphate cytidylyltransferase	-8.913342665
yfgE	DNA replication initiation factor	-8.864839643
3213533_3213719	conserved hypothetical protein	-8.793945373
mukF	condesin subunit F	-8.674996036
314632_315175	putative cytoplasmic protein	-8.34624418
sitB	putative ATP-binding protein	-8.248011808
678227_678434	hypothetical protein	-8.247973253
thiI	thiamine biosynthesis protein ThiI	-8.108873063
glmM	phosphoglucosamine mutase	-7.97361005
yidC	putative inner membrane protein translocase component YidC	-7.943233004
tsf	elongation factor Ts	-7.854631787
ftsK	DNA translocase FtsK	-7.84909843
lon	DNA-binding ATP-dependent protease La	-7.70131012
sapC	peptide transport protein	-7.55777215

pps	phosphoenolpyruvate synthase	-7.541985917
2342648_2342762	hypothetical protein	-7.506186825
dapF	diaminopimelate epimerase	-7.485055377
cueR	DNA-binding transcriptional regulator CueR	-7.479815903
mdoH	glucosyltransferase MdoH	-7.389862798
yhgI	putative DNA uptake protein	-7.383653376
fusA	elongation factor G	-7.340376885
nifS	cysteine desulfurase	-7.334968551
hflB	ATP-dependent metalloprotease	-7.331448031
asrC	anaerobic sulfide reductase	-7.315925953
1188558_1188696	hypothetical protein	-7.279907219
glyT	tRNA-Gly	-7.228308992
aceF	dihydrolipoamide acetyltransferase	-7.114557026
dnaB	replicative DNA helicase	-7.110409694
tolQ	colicin uptake protein TolQ	-7.105446053
1730127_1730844	putative inner membrane protein	-7.07028903
1398233_1398449	hypothetical protein	-7.054931308
2846370_2846505	hypothetical protein	-7.041310795
fmt	methionyl-tRNA formyltransferase	-7.038446126
secA	preprotein translocase subunit SecA	-7.001176964
rne	ribonuclease E	-6.920558354
glmU	bifunctional N-acetylglucosamine-1-phosphate uridyltransferase/glucosamine-1-phosphate acetyltransferase	-6.909849349
yqhC	putative transcriptional regulator	-6.905476594
hcp	hydroxylamine reductase	-6.898998153
2265632_2265749	hypothetical protein	-6.869455851
rfaJ	lipopolysaccharide glucosyltransferase	-6.828678128
4583350_4583683	putative regulatory protein	-6.827023049
mdoG	glucan biosynthesis protein G	-6.797515599
yieE	putative cytoplasmic protein	-6.77920997
glmS	D-fructose-6-phosphate amidotransferase	-6.714790306
seqA	replication initiation regulator SeqA	-6.708486862
yfgM	putative inner membrane protein	-6.707144767
arcB	aerobic respiration control sensor protein ArcB	-6.661383437
flhB	flagellar biosynthesis protein FlhB	-6.611754745
metZ	tRNA-Met	-6.592651435
3525085_3525205	hypothetical protein	-6.552183984
fliS	flagellar protein FliS	-6.493145042
nmpC	putative outer membrane porin precursor	-6.434619883
1977498_1977786	hypothetical protein	-6.420494426

galU	UTP--glucose-1-phosphate uridylyltransferase subunit GalU	-6.396894363
ybdQ	putative universal stress protein	-6.323065565
narG	nitrate reductase 1 alpha subunit	-6.318787367
ilvN	acetolactate synthase 1 regulatory subunit	-6.285292245
proC	pyrroline-5-carboxylate reductase	-6.258243145
1053675_1055112	putative transcriptional regulator	-6.240873025
mukB	cell division protein MukB	-6.218868535
marR	DNA-binding transcriptional repressor MarR	-6.215469809
cspB	putative cold-shock protein	-6.185042188
guaA	bifunctional GMP synthase/glutamine amidotransferase protein	-6.172559337
fruK	1-phosphofructokinase	-6.149090387
yjgP	putative permease	-6.146909885
mrcB	penicillin-binding protein 1b	-6.098236206
cysE	serine acetyltransferase	-6.076520985
sdhA	succinate dehydrogenase flavoprotein subunit	-6.066503578
rfaL	O-antigen ligase	-6.043407268
254798_255083	30S ribosomal protein S2	-6.024707755
833678_834377	putative cytoplasmic protein	-5.972921911
aceK	bifunctional isocitrate dehydrogenase kinase/phosphatase protein	-5.953551753
cyoB	cytochrome o ubiquinol oxidase subunit I	-5.93948391
murB	UDP-N-acetylenolpyruvoylglucosamine reductase	-5.936187569
prc	carboxy-terminal protease	-5.933385553
dxs	1-deoxy-D-xylulose-5-phosphate synthase	-5.899232023
zwf	glucose-6-phosphate 1-dehydrogenase	-5.892898957
rfaK	putative hexose transferase	-5.836835448
fldA	flavodoxin FldA	-5.809487206
1668390_1668969	putative transcriptional regulator	-5.798777921
glnD	PII uridylyl-transferase	-5.790021853
ssaE	secretion system effector	-5.763802663
dnaX	DNA polymerase III subunits gamma and tau	-5.759564873
cspC	cold shock-like protein CspC	-5.753505046
tuf_2	elongation factor Tu	-5.751510272
ycaJ	recombination factor protein RarA	-5.736598464
yjeQ	ribosome-associated GTPase	-5.716335417

mppA	periplasmic murein tripeptide transport protein	-5.712350319
4014491_4015577	putative periplasmic protein	-5.67494743
ppa	inorganic pyrophosphatase	-5.651619574
dnaQ	DNA polymerase III subunit epsilon	-5.614220618
dsbA	periplasmic protein disulfide isomerase I	-5.613974328
ftsQ	cell division protein FtsQ	-5.601989463
hslJ	heat-inducible protein	-5.589085671
ycfJ	hypothetical protein	-5.585003211
yhdG	tRNA-dihydrouridine synthase B	-5.577225527
2509959_2510514	putative NTP pyrophosphohydrolase	-5.533948144
cobC	'alpha ribazole-5''-P phosphatase'	-5.524810578
1063098_1063359	hypothetical protein	-5.524698134
ygiN	putative cytoplasmic protein	-5.477791155
basS	sensor protein BasS/PmrB	-5.456977226
polA	DNA polymerase I	-5.437069838
cobU	adenosylcobinamide kinase/adenosylcobinamide-phosphate guanylyltransferase	-5.406845293
proB	gamma-glutamyl kinase	-5.398494338
438081_438243	hypothetical protein	-5.393387145
ychK	hypothetical protein	-5.382624641
garD	galactarate dehydrogenase	-5.347328791
3932730_3932850	hypothetical protein	-5.339390835
apaG	ApaG	-5.274853481
fdnG	formate dehydorgenase-N alpha subunit	-5.267991027
acrR	DNA-binding transcriptional repressor AcrR	-5.265612698
fliH	flagellar assembly protein H	-5.24951005
yrfF	putative inner membrane protein	-5.235091621
95982_96177	putative inner membrane protein	-5.222725206
fadD	long-chain-fatty-acid--CoA ligase	-5.205019035
phoL	putative phosphate starvation-inducible protein	-5.194868514
acrA	acridine efflux pump	-5.185530425
nagB	glucosamine-6-phosphate deaminase	-5.184356716
flgA	flagellar basal body P-ring biosynthesis protein FlgA	-5.182436238
rfaI	lipopolysaccharide-alpha-1 and 3-D-galactosyltransferase	-5.141274137
yohJ	hypothetical protein	-5.126378428
torA	trimethylamine N-oxide reductase subunit	-5.099760546
galE	UDP-galactose-4-epimerase	-5.089835283
thiC	thiamine biosynthesis protein ThiC	-5.087396218

rfaP	lipopolysaccharide core biosynthetic protein	-5.074799475
ptsH	phosphohistidinoprotein-hexose phosphotransferase component of PTS system (Hpr)	-5.070983581
bglA	6-phospho-beta-glucosidase A	-5.046215655
trxB	thioredoxin reductase	-5.044758661
fruA	fructose-specific PTS system IIBC component	-5.03838571
1904219_1905545	putative glutamic dehyrogenase-like protein	-5.037447533
1686849_1686969	hypothetical protein	-5.011647916
2802005_2802370		-5.009528734
rfaH	transcriptional activator RfaH	-4.993306105
2981059_2981167	hypothetical protein	-4.943650678
1312759_1313124		-4.938234378
hmpA	nitric oxide dioxygenase	-4.919693823
1680341_1680476	hypothetical protein	-4.911319492
1680334_1680472	hypothetical protein	-4.911319452
2144827_2145214	hypothetical protein	-4.88506781
1964822_1965218	putative cytoplasmic protein	-4.857924708
plsX	putative glycerol-3-phosphate acyltransferase PlsX	-4.856695249
pduC	propanediol dehydratase large subunit	-4.844630726
ligA	NAD-dependent DNA ligase LigA	-4.825161058
hybD	hydrogenase 2 maturation endopeptidase	-4.786420903
ygdP	dinucleoside polyphosphate hydrolase	-4.737684867
2017847_2018987	putative cytoplasmic protein	-4.737583498
ompC	outer membrane porin protein C	-4.711094973
trkH	potassium transporter	-4.69272029
pgm	phosphoglucomutase	-4.679003188
nusA	transcription elongation factor NusA	-4.678112427
yecP	putative enzyme	-4.666536695
cyaA	adenylate cyclase	-4.652062762
helD	DNA helicase IV	-4.646089158
3788229_3788949	putative regulatory protein	-4.645817151
ilvA	threonine dehydratase	-4.639924513
3289137_3289263	hypothetical protein	-4.626682847
ydiD	short chain acyl-CoA synthetase	-4.60346551
2788680_2788917	conserved hypothetical protein	-4.598274992
btuC	vtamin B12-transporter permease	-4.566161039
proA	gamma-glutamyl phosphate reductase	-4.559609015
yjjK	putative ABC transporter ATP-binding protein	-4.543009928

1895516_1896635	hydrogenase-1 small subunit	-4.542208269
yfaW	putative galactonate dehydratase	-4.535807719
mltC	murein transglycosylase C	-4.535544578
mrcA	peptidoglycan synthetase	-4.518215288
fixX	putative ferredoxin	-4.500353159
2954824_2955802	tricarboxylic transport	-4.496521194
sapF	peptide transport protein	-4.490180851
rho	transcription termination factor Rho	-4.489984668
1621972_1623775	putative hydrogenase-1 large subunit	-4.48268972
tyrP	tyrosine-specific transport protein	-4.472121524
1715446_1715884	putative sugar-specific PTS enzyme II	-4.463194745
wcaE	glycosyl transferase	-4.452819094
ydiQ	putative electron transfer flavoprotein YdiQ	-4.448526679
fis	DNA-binding protein Fis	-4.427731473
cysJ	sulfite reductase subunit alpha	-4.421517457
nuoC	bifunctional NADH:ubiquinone oxidoreductase subunit C/D	-4.420542244
kgd	alpha-ketoglutarate decarboxylase	-4.419085938
yaiU	flagellar protein	-4.416881847
1344741_1344867	putative lipoprotein	-4.414750359
yaoF	putative hemolysin	-4.381016301
1091135_1094486	host specificity protein J	-4.361606007
rspA	putative dehydratase	-4.356041203
2091088_2091208	hypothetical protein	-4.322214454
anmK	anhydro-N-acetylmuramic acid kinase	-4.313131613
crp	cAMP-regulatory protein	-4.312643365
ruvB	Holliday junction DNA helicase B	-4.308069067
pgi	glucose-6-phosphate isomerase	-4.296880107
sapA	peptide transport protein	-4.268660756
sufB	cysteine desulfurase activator complex subunit SufB	-4.242441668
3516973_3518254	cytosine deaminase	-4.215443364
yggX	hypothetical protein	-4.186955375
pcnB	poly(A) polymerase I	-4.185134851
prfC	peptide chain release factor 3	-4.169285342
rfbP	undecaprenol-phosphate galactosephosphotransferase/O-antigen transferase	-4.159607056
1286587_1286920	conserved hypothetical protein	-4.150598514
yebK	DNA-binding transcriptional regulator HexR	-4.139949656
466391_467084	putative regulatory protein	-4.139221213
slyA	transcriptional regulator SlyA	-4.069827978
fruR	DNA-binding transcriptional regulator FruR	-4.063976997

1362920_1363106	hypothetical protein	-4.063309104
trxA	thioredoxin	-4.041410256
sdhB	succinate dehydrogenase iron-sulfur subunit	-4.040614203
artQ	arginine transporter permease subunit ArtQ	-4.025612203
yraM	putative transglycosylase	-3.98769929
cobB	NAD-dependent deacetylase	-3.986798139
ung	uracil-DNA glycosylase	-3.977643581
cvpA	colicin V production protein	-3.961282889
2538049_2538298	putative regulatory protein	-3.952479017
iciA	chromosome replication initiation inhibitor protein	-3.937046601
aceE	pyruvate dehydrogenase subunit E1	-3.926916696
artP	arginine transporter ATP-binding subunit	-3.920819034
rfbD	dTDP-4-dehydrorhamnose reductase	-3.903790459
1896631_1898425	hydrogenase 1 large subunit	-3.894131763
narI	nitrate reductase 1 gamma subunit	-3.883105592
2611246_2611807	putative acetyltransferase	-3.863559917
rseA	anti-RNA polymerase sigma factor SigE	-3.860466208
2002454_2003404		-3.847838565
3010871_3011006	conserved hypothetical protein	-3.826733092
infB	translation initiation factor IF-2	-3.811511334
dniR	membrane-bound lytic murein transglycosylase D	-3.794438329
ydgH	putative periplasmic protein	-3.780587917
tuf_1	elongation factor Tu	-3.759621464
proQ	putative solute/DNA competence effector	-3.75136683
yncB	putative NADP-dependent oxidoreductase	-3.750563034
ybiT	putative ABC transporter ATPase component	-3.74627621
surA	peptidyl-prolyl cis-trans isomerase SurA	-3.737876944
ycbY	23S rRNA m(2)G2445 methyltransferase	-3.729970191
3807399_3807591	hypothetical protein	-3.718424539
1640381_1641848	putative coiled-coil protein	-3.708313021
737793_738369	putative inner membrane protein	-3.696467508
yhbJ	hypothetical protein	-3.6955229
sapB	peptide transport protein	-3.684210597
rfbC	dTDP-4 and deoxyrhamnose 3 and 5 epimerase	-3.681844297
2849613_2850069	putative cytoplasmic protein	-3.679851858

nuoE	NADH dehydrogenase subunit E	-3.666340278
aadA	aminoglycoside resistance protein	-3.622312728
4164428_4164533	hypothetical protein	-3.596350724
2098339_2099441	2098339_2099441	-3.591704759
ygiR	hypothetical protein	-3.572524901
asmA	putative assembly protein	-3.571478052
pgpA	phosphatidylglycerophosphatase A	-3.567213688
rfbN	rhamnosyl transferase	-3.563247883
eutQ	putative ethanolamine utilization protein	-3.549925328
ydcI	putative transcriptional regulator	-3.543322593
pitA	low-affinity phosphate transporter	-3.543231803
2459624_2460524	putative cytoplasmic protein	-3.538979657
ycfH	putative metallodependent hydrolase	-3.509895979
mdoD	glucan biosynthesis protein D	-3.501210362
638839_639421	putative regulatory protein	-3.495258158
2573771_2574770	putative oxidoreductase	-3.454603678
speG	spermidine N1-acetyltransferase	-3.44559993
2803870_2805367	head-tail preconnector-like protein	-3.441624308
tbpA	thiamine transporter substrate binding subunit	-3.439472477
2498695_2499151	hypothetical protein	-3.434845431
yceA	hypothetical protein	-3.433415904
ychJ	hypothetical protein	-3.402855818
333235_337330	putative RHS-like protein	-3.400490794
yojN	phosphotransfer intermediate protein in two-component regulatory system with RcsBC	-3.399575063
yniC	2-deoxyglucose-6-phosphatase	-3.389951062
yajF	fructokinase	-3.389348909
1309762_1311259	prophage head-tail preconnector	-3.379980835
kdsB	3-deoxy-manno-octulosonate cytidylyltransferase	-3.376066001
emrB	putative multidrug transport protein	-3.362328197
rfaY	lipopolysaccharide core biosynthesis protein	-3.357940705
4059857_4060115	hypothetical protein	-3.356561409
sapD	peptide transport protein	-3.336215262
yobG	hypothetical protein	-3.303458447
2418130_2418256	hypothetical protein	-3.290477471
1332050_1334153	SspH1	-3.282866555
sixA	phosphohistidine phosphatase	-3.269904644
rfaQ	lipopolysaccharide core biosynthesis protein	-3.259907251
eutL	putative carboxysome structural protein	-3.240584754
4201618_4201744	hypothetical protein	-3.238880861

flgL	flagellar hook-associated protein FlgL	-3.236662495
rnhB	ribonuclease HII	-3.225199195
hisD	histidinol dehydrogenase	-3.223186826
apbA	2-dehydropantoate 2-reductase	-3.216794931
cypD	peptidyl-prolyl cis-trans isomerase (rotamase D)	-3.204900867
hydN	electron transport protein HydN	-3.2037027
ydeA	sugar efflux transporter	-3.203574404
flgC	flagellar basal body rod protein FlgC	-3.189884983
1329625_1329826	PagJ	-3.18400876
ybeA	SPOUT methyltransferase superfamily protein	-3.17479041
phnS	2-aminoethylphosphonate transporter	-3.167827285
nuoL	NADH dehydrogenase subunit L	-3.162586008
aroE_3	shikimate 5-dehydrogenase	-3.161408895
1642106_1643114	putative transcriptional regulator	-3.154366469
emrR	transcriptional repressor MprA	-3.145219604
narX	nitrate/nitrite sensor protein NarX	-3.140288409
ycfQ	putative transcriptional repressor	-3.137466985
fliI	flagellum-specific ATP synthase	-3.121147453
engA	GTP-binding protein EngA	-3.116791633
bolA	transcriptional regulator BolA	-3.109784152
rnb	exoribonuclease II	-3.108282831
1399092_1400001	nucleotide excision repair endonuclease	-3.074142011
2555314_2556166	hypothetical protein	-3.046355223
caiA	crotonobetainyl-CoA dehydrogenase	-3.039480926
aceB	malate synthase	-3.03617515
yrbB	hypothetical protein	-3.026448947
btuE	putative glutathione peroxidase	-3.023065758
fumA	fumarase A	-3.001276251
1586929_1589371	putative dimethyl sulphoxide reductase chain A1	-3.000987174
galP	galactose/proton symporter	-2.994323638
gor	glutathione reductase	-2.966125971
gshA	glutamate--cysteine ligase	-2.96449708
miaA	tRNA delta(2)-isopentenylpyrophosphate transferase	-2.964463501
rseB	periplasmic negative regulator of sigmaE	-2.963818141
ydhB	putative DNA-binding transcriptional regulator	-2.962666631
1350731_1351706	putative ABC transporter protein	-2.934736613
2809855_2810257	hypothetical protein	-2.933029705

rfaB	UDP-D-galactose:(glucosyl)lipopolysaccharide-1 and 6-D-galactosyltransferase	-2.927630192
2520199_2521303	putative cytoplasmic protein	-2.925393062
sseC	translocation machinery component	-2.909614098
pdhR	transcriptional regulator PdhR	-2.907592096
uvrA	excinuclease ABC subunit A	-2.893114265
1857496_1857622	hypothetical protein	-2.876245802
ilvB	acetolactate synthase catalytic subunit	-2.865125306
504669_504774	hypothetical protein	-2.847809019
pduG	propanediol dehydratase reactivation protein	-2.843049689
yehU	putative sensor kinase	-2.843048438
3202331_3203561	putative transport protein	-2.829828759
ypfG	putative periplasmic protein	-2.8236093
hpaX	4-hydroxyphenylacetate catabolism	-2.806816614
nrfB	cytochrome c-type protein NrfB	-2.799105499
tig	trigger factor	-2.798779453
987673_988585	putative transcriptional regulator	-2.797307101
yecN	putative inner membrane protein	-2.791442172
172522_173929	Na+/galactoside symporter	-2.784481918
cls	cardiolipin synthetase	-2.781175152
1288091_1290446	exodeoxyribonuclease 8	-2.752282641
yebS	putative inner membrane protein	-2.722417108
yfiD	autonomous glycyl radical cofactor GrcA	-2.712799124
yejK	nucleoid-associated protein NdpA	-2.712617721
ybbJ	hypothetical protein	-2.708463058
yncA	putative acyltransferase	-2.700499152
2741862_2742501	hypothetical protein	-2.69924991
rlpA	rare lipoprotein A	-2.684553224
zntB	zinc transporter	-2.673204064
sun	16S rRNA methyltransferase B	-2.655594113
cueO	multicopper oxidase	-2.639655454
srfC	putative virulence protein	-2.631865557
4706053_4706794	4-hydroxy-2-oxoglutarate aldolase	-2.630504141
535084_535210	hypothetical protein	-2.608274172
lplA	lipoate-protein ligase A	-2.579293943
gshB	glutathione synthetase	-2.566995728
yihS	putative isomerase	-2.565742685
ydgA	putative periplasmic protein	-2.553184992
lonH	putative protease	-2.548495342
rfc	O-antigen polymerase	-2.521780645
yrbH	D-arabinose 5-phosphate isomerase	-2.519795458

pipC	pathogenicity island-encoded protein C	-2.518362026
aroD	3-dehydroquinate dehydratase	-2.517563754
ychM	putative sulfate transporter YchM	-2.511845592
fbp	fructose-1 and 6-bisphosphatase	-2.511428431
narZ	nitrate reductase 2 alpha subunit	-2.499674609
hypA_2	hydrogenase nickel incorporation protein HybF	-2.482441747
pfkB	6-phosphofructokinase 2	-2.480931199
aroK	shikimate kinase I	-2.458635475
nadC	quinolinate phosphoribosyltransferase	-2.457247746
csgD	DNA-binding transcriptional regulator CsgD	-2.45633825
yliB	putative ABC transporter periplasmic binding protein	-2.4433228
cpxA	two-component sensor protein	-2.4426402
1359827_1360373	chorismate mutase	-2.431377898
yigN	DNA recombination protein RmuC	-2.426900708
soxR	redox-sensing transcriptional activator	-2.415131232
yeeZ	putative dehydratase	-2.410344373
984415_985099	putative integrase	-2.404997517
slrP	leucine-rich repeat-containing protein	-2.39629941
1711774_1712893	putative cellulase protein	-2.395951707
nirB	nitrite reductase large subunit	-2.386340067
1682561_1683623	putative periplasmic protein	-2.3689147
ybdL	putative aminotransferase	-2.353737896
sfbB	putative ABC-type transport system ATPase component	-2.336057686
3832942_3833950	putative regulatory protein	-2.331138023
pstS	phosphate transporter subunit	-2.316872931
yebU	rRNA (cytosine-C(5)-)-methyltransferase RsmF	-2.30081871
1375201_1376398	arylsulfatase regulator	-2.300790549
yqjA	hypothetical protein	-2.274532365
wzzB	lipopolysaccharide O-antigen chain length regulator	-2.245819396
acnB	bifunctional aconitate hydratase 2/2-methylisocitrate dehydratase	-2.245553312
emrA	multidrug resistance secretion protein	-2.242976955
serC	phosphoserine aminotransferase	-2.239220583
hisP	histidine/lysine/arginine/ornithine transporter subunit	-2.236929064
yigQ	putative periplasmic protein	-2.225297567
ytfL	putative hemolysin-like protein	-2.22311383
2110376_2111063	pro-head protease	-2.203551944

rpoN	RNA polymerase factor sigma-54	-2.186402916
mdlB	putative multidrug transporter membrane\ATP-binding component	-2.180416132
3943101_3943983	putative Zn-dependent hydrolase	-2.178084299
phoB	transcriptional regulator PhoB	-2.167805717
adiY	transcriptional activator	-2.146556223
aroE_2	shikimate 5-dehydrogenase	-2.146327281
wecD	TDP-fucosamine acetyltransferase	-2.143286764
mfd	transcription-repair coupling factor	-2.140488167
515791_516847	putative cysteine synthase/cystathionine beta-synthase	-2.132229829
speA	arginine decarboxylase	-2.129729867
311893_314533	putative chaperone ATPase	-2.128472118
nlpC	lipoprotein	-2.107683628
bioB	biotin synthetase	-2.102878679
3704538_3706098	putative periplasmic phosphate-binding protein	-2.101708052
rfaF	ADP-heptose:LPS heptosyltransferase II	-2.09937469
entF	enterobactin synthase subunit F	-2.079140572
rfbI	CDP-6-deoxy-delta-3 and 4-glucoseen reductase	-2.076880406
rfbU	mannosyl transferase	-2.068128762
fadJ	multifunctional fatty acid oxidation complex subunit alpha	-2.050571521
3851426_3851912	putative acetyltransferase	-2.026303611
2265836_2267078	multidrug efflux system subunit MdtA	-2.006636414
3629161_3629344	hypothetical protein	-1.971150779
rbsB	D-ribose transporter subunit RbsB	-1.956497517
yibK	putative tRNA/rRNA methyltransferase YibK	-1.953638546
lysC	aspartate kinase III	-1.952855592
2101418_2102759	hypothetical protein	-1.940502626
corE	hypothetical protein	-1.927599553
rluD	23S rRNA pseudouridine synthase D	-1.903962241
hemF	coproporphyrinogen III oxidase	-1.903540559
aroB	3-dehydroquinate synthase	-1.890864852
phnW	2-aminoethylphosphonate--pyruvate transaminase	-1.890064176
nlpD	lipoprotein NlpD	-1.888231601
956950_957271	putative inner membrane protein	-1.860636295
yhhF	16S rRNA m(2)G966-methyltransferase	-1.857649039
yrbC	putative transport protein	-1.843053907
58945_60148	putative nitrite reductase	-1.822238345

ycbB	hypothetical protein	-1.820690156
mutS	DNA mismatch repair protein	-1.804899062
1349097_1350732	putative ABC transporter periplasmic binding protein	-1.783895311
1097258_1097840	tail fiber assembly like-protein	-1.783467526
ygiC	putative glutathionylspermidine synthase	-1.757020451
rrsH	16S ribosomal RNA	-1.755864938
pduX	propanediol utilization protein	-1.749604258
thrA	bifunctional aspartokinase I/homeserine dehydrogenase I	-1.722073492
avtA	valine--pyruvate transaminase	-1.715107814
nadR	nicotinamide-nucleotide adenylyltransferase	-1.697559037
gph	phosphoglycolate phosphatase	-1.681028431
mdlA	putative multidrug transporter membrane\ATP-binding component	-1.662697834
dcuB	anaerobic C4-dicarboxylate transporter	-1.648046476
1317319_1320415	phage tail component H-like protein	-1.631551179
ilvG	acetolactate synthase 2 catalytic subunit	-1.627750001
yjjW	pyruvate formate lyase-activating enzyme	-1.610281288
ssaQ	type III secretion system protein	-1.587188716
rfaC	ADP-heptose:LPS heptosyl transferase I	-1.567004117
celF	phospho-beta-glucosidase/cellobiose-6-phosphate hydrolase	-1.562304215
rfaG	glucosyltransferase I	-1.560120322
2794714_2797810	phage tail component H-like protein	-1.55794072
2981899_2982022	hypothetical protein	-1.555733508
frdA	fumarate reductase flavoprotein subunit	-1.526625981
greA	transcription elongation factor GreA	-1.518553585
iroD	enterochelin esterase=-like protein	-1.507408018
3733080_3734115	putative phosphotriesterase	-1.491235244
oafA	O-antigen acetylase	-1.489206133
2911325_2912339	putative dehydrogenase	-1.478713837
purG	phosphoribosylformylglycinamidine synthase	-1.448647819
allC	allantoate amidohydrolase	-1.42474503
wza	putative outer membrane polysaccharide export protein	-1.414144999

rbsA	D-ribose transporter ATP binding protein	-1.402455671
sipB	translocation machinery component	-1.374862517
ybfM	putative outer membrane protein	-1.364707168
gltS	glutamate transport protein	-1.343841244
glpR	DNA-binding transcriptional repressor GlpR	-1.341841368

Table A.11 – List of disrupted genes in the *S.* Typhimurium 14028S transposon mutant libraries that had accepted pHYCTX14 from the QuaTraDIS comparison pipeline.

Gene	Function	logFC
2710093_2710216	type IV pilus biogenesis/stability protein PilW	12.34856798
psd	phosphatidylserine decarboxylase	12.1652138
yhbP	hypothetical protein	12.08146599
hslV	ATP-dependent protease peptidase subunit	12.00401973
3941018_3941198	hypothetical protein	11.89637779
4315067_4315187	hypothetical protein	11.87090285
hupA	transcriptional regulator HU subunit alpha	11.84217902
yifA	transcriptional regulator HdfR	11.81052219
4680456_4681266	putative inner membrane protein	11.76445688
3690392_3690500	hypothetical protein	11.75235199
391080_391605	putative outer membrane protein	11.74846888
1549051_1549171	hypothetical protein	11.66858998
yhbT	putative lipid carrier protein	11.41718748
1303054_1303357	phage-holin analog protein	11.39526541
moeB	molybdopterin biosynthesis protein MoeB	11.35127876
134688_134793	hypothetical protein	11.29330709
17664_17787	hypothetical protein	11.26299299
ycfS	putative periplasmic protein	11.24166314
ansA	cytoplasmic asparaginase I	11.1222847
3335173_3335281	hypothetical protein	11.11701819
2508680_2508854	hypothetical protein	11.10012706
98643_98802	hypothetical protein	11.02378465
stfF	putative minor fimbrial subunit	11.01967028
3770552_3770684	hypothetical protein	11.01266441
2905914_2906040	hypothetical protein	11.0017561
900253_900415	hypothetical protein	10.99444264
thrL	thr operon leader peptide	10.93715393
3852192_3852324	hypothetical protein	10.90371601
926621_926762	hypothetical protein	10.87760031
3794139_3794265	hypothetical protein	10.85976518
2388218_2388737	hypothetical protein	10.80547068
argW	tRNA-Arg	10.7915088
4298125_4298257	putative cytoplasmic protein	10.763388
409240_409342	putative cytoplasmic protein	10.72262801
4087149_4087183		10.69650397
4353223_4353331	hypothetical protein	10.69131922
3377872_3378022	hypothetical protein	10.68432936
183432_183717	putative outer membrane protein	10.65644502
sopE2	type III-secreted effector protein	10.62615511
4647441_4647549	hypothetical protein	10.58116527

4175964_4176150	hypothetical protein	10.56105438
nirD	nitrite reductase small subunit	10.52884917
2339343_2339451	hypothetical protein	10.41028551
yifL	putative outer membrane lipoprotein	10.3927635
4675397_4675658	hypothetical protein	10.38497955
spr	putative outer membrane lipoprotein	10.38314602
4066032_4066968	putative reverse transcriptase	10.35704027
srlR	DNA-binding transcriptional repressor SrlR	10.35243566
ybiI	hypothetical protein	10.34390967
dps	DNA starvation/stationary phase protection protein Dps	10.32705345
3073138_3073519	putative cytoplasmic protein	10.3199666
2971816_2971993	hypothetical protein	10.30157412
2569136_2569283	hypothetical protein	10.21865784
ygdD	hypothetical protein	10.20285589
4626223_4626454	hypothetical protein	10.19654414
3999763_3999871	hypothetical protein	10.18555288
2813181_2813258	tRNA-Arg	10.18522927
4310315_4310483	hypothetical protein	10.12846363
3881550_3881694	conserved hypothetical protein	10.12546465
955377_955569	conserved hypothetical protein	10.11795687
1559384_1559690	outer membrane protein	10.06223606
dinI	DNA damage-inducible protein I	10.05272428
1809301_1809514	conserved domain protein	10.00856212
4219597_4219954	conserved hypothetical protein	9.949465645
2822704_2823013	hypothetical protein	9.915651263
cbiN	cobalt transport protein CbiN	9.911510219
1980070_1980946	putative inner membrane protein	9.876342583
slrB	glucitol/sorbitol-specific PTS system component IIA	9.857091362
17042_17486	hypothetical protein	9.851556367
znuB	high-affinity zinc transporter membrane component	9.835520647
lysY	tRNA-Lys	9.83428392
2927300_2927567	putative transposase	9.814587902
ppiC	peptidyl-prolyl cis-trans isomerase C	9.811696993
3568594_3568738	hypothetical protein	9.804592777
1143229_1143337	hypothetical protein	9.784779547
3302109_3302214	hypothetical protein	9.772600282
yecH	putative cytoplasmic protein	9.766035371
1341059_1341188	hypothetical protein	9.741378403
3436647_3436776	hypothetical protein	9.727489862
2928019_2928658	putative cytoplasmic protein	9.723122421
1419533_1419740	hypothetical protein	9.721652116
3314215_3314410	hypothetical protein	9.717182464
3182640_3182757	hypothetical protein	9.712519513
1341717_1341825	conserved hypothetical protein	9.703057873

4297945_4298110	putative periplasmic protein	9.690616352
folA	dihydrofolate reductase	9.674525232
4392708_4393053	putative cytoplasmic protein	9.673050961
1337336_1337585	hypothetical protein	9.640940102
4833960_4834140	hypothetical protein	9.633745026
2919625_2919739	hypothetical protein	9.622367079
dnaC	DNA replication protein DnaC	9.564323741
4126681_4126867	hypothetical protein	9.558041544
4479419_4479533	putative cytoplasmic protein	9.548059595
2829158_2829443	excisionase-like protein	9.543168608
4011518_4011680	hypothetical protein	9.523497672
2361471_2361576	hypothetical protein	9.496253831
1390428_1390845	pyrimidine (deoxy)nucleoside triphosphate pyrophosphohydrolase	9.490086222
pheV	tRNA-Phe	9.478620227
3892839_3893049	putative cytoplasmic protein	9.463752885
stfE	putative minor fimbrial subunit	9.436550172
2090430_2090643	putative cold-shock protein	9.430938635
618677_618750	tRNA-OTHER	9.374155658
2814159_2814285	hypothetical protein	9.367613355
1729597_1729999	putative dipicolinate reductase	9.354036919
639709_640051	putative regulatory protein	9.345538799
4377954_4378128	putative cytoplasmic protein	9.317049413
3904877_3905129	hypothetical protein	9.308881313
316754_316865	invasol SirA	9.254394899
138754_138877	hypothetical protein	9.228751417
glyX	tRNA-Gly	9.217522943
2553682_2553823	hypothetical protein	9.178064716
hfq	RNA-binding protein Hfq	9.176639204
fabZ	(3R)-hydroxymyristoyl-ACP dehydratase	9.176315028
213057_213171	hypothetical protein	9.170763932
cedA	cell division modulator	9.138229516
ssaR	type III secretion system protein	9.108242574
ychH	hypothetical protein	9.101808206
nuoJ	NADH dehydrogenase subunit J	9.101739957
2060567_2060705	hypothetical protein	9.087888282
2499319_2499454	hypothetical protein	9.087819383
402094_402289	putative copper chaperone	9.061885083
34375_34816	putative transcriptional regulator	9.032615308
4233380_4233560	hypothetical protein	9.011810744
yrbA	putative transcriptional regulator	9.003031787
2034144_2034261	hypothetical protein	8.963359617
2590332_2590560	putative cytoplasmic protein	8.959106925
678398_678539	hypothetical protein	8.946588233
1188893_1189040	hypothetical protein	8.94167548
1920254_1920428	putative cytoplasmic protein	8.941370763
3183984_3184095	hypothetical protein	8.940532507

ycdC	putative transcriptional repressor	8.931308932
3019237_3019342	hypothetical protein	8.927574925
ydhI	putative inner membrane protein	8.861400338
4577948_4578236	putative regulatory protein	8.851980025
4548709_4548805	hypothetical protein	8.835167223
994688_994946	hypothetical protein	8.819978686
3482354_3482456	hypothetical protein	8.819564671
4083980_4083997		8.810866718
grxC	glutaredoxin 3	8.81053347
leuZ	tRNA-Leu	8.792299885
4219569_4219752	hypothetical protein	8.758153511
nuoA	NADH dehydrogenase subunit A	8.757980767
1762418_1762580	conserved hypothetical protein	8.757807996
2015792_2015897	hypothetical protein	8.715390978
eutN	putative detox protein	8.712185643
1409398_1409647	hypothetical protein	8.705054635
rof	Rho-binding antiterminator	8.669026875
2107694_2108207	hypothetical protein	8.658074957
766192_766318	hypothetical protein	8.63901496
3199027_3199198	hypothetical protein	8.619414946
934779_934917	hypothetical protein	8.609800979
dacB	D-alanyl-D-alanine carboxypeptidase/endopeptidase	7.360507219
yegH	putative inner membrane protein	6.999398842
cdaR	carbohydrate diacid transcriptional activator CdaR	6.709102579
rph	ribonuclease PH	6.279507896
3336302_3336707	putative cytoplasmic protein	6.142188373
yfgJ	putative cytoplasmic protein	6.12114018
sseB	enhanced serine sensitivity protein SseB	6.012623033
3210548_3210968	hypothetical protein	5.994554672
hycH	hydrogenase 3 large subunit processing protein	5.968681705
solA	N-methyltryptophan oxidase	5.776693448
yjfP	esterase	5.576269679
smpB	SsrA-binding protein	5.553817221
ybiB	hypothetical protein	5.515133938
4169525_4170048		5.47175357
95262_95379	hypothetical protein	5.438442728
yhhY	putative acetyltransferase YhhY	5.372980107
2816703_2816883	putative bacteriophage protein	5.338916091
yjiS	putative cytoplasmic protein	5.278421659
rtcA	'RNA 3''-terminal-phosphate cyclase'	5.225635744
4824881_4825340	putative cytoplasmic protein	5.075240613
yrbG	putative calcium/sodium:proton antiporter	4.853438354
bcfC	fimbrial usher	4.762942833

pflF	putative pyruvate formate lyase	4.524295444
318837_319221	putative periplasmic protein	4.507176028
dgoK	2-oxo-3-deoxygalactonate kinase	4.494286939
hycD	hydrogenase 3 membrane subunit	4.481077813
hofC	type IV pilin biogenesis protein	4.443597486
yfhB	hypothetical protein	4.322013586
iadA	isoaspartyl dipeptidase	4.297908626
435407_436121	putative inner membrane protein	4.194163106
3378033_3378654	putative inner membrane protein	4.120540581
yifK	putative transport protein YifK	4.002030277
bcfA	fimbrial subunit	3.976920698
allB	allantoinase	3.895024011
focA	formate transporter	3.884615585
ygjQ	putative integral membrane protein	3.771379427
4496548_4497937	putative methyl-accepting chemotaxis protein	3.761098482
32115_32445	hypothetical protein	3.696354462
mazG	nucleoside triphosphate pyrophosphohydrolase	3.68177769
4573793_4574447	putative anaerobic dehydrogenase component	3.652064527
zntR	zinc-responsive transcriptional regulator	3.563304139
rhuM	putative cytoplasmic protein	3.560287759
oadG	oxaloacetate decarboxylase subunit gamma	3.556870539
3962471_3962597	hypothetical protein	3.446952608
4154253_4155333	4-alpha-L-fucosyltransferase	3.439710306
yjcE	Na/H transport protein	3.426731394
yjfL	putative inner membrane protein	3.386617565
argB	acetylglutamate kinase	3.369886911
3335905_3336316	putative cytoplasmic protein	3.317751417
lrhA	NADH dehydrogenase transcriptional repressor	3.292722438
3981505_3982249	putative cytoplasmic protein	3.290589393
citX2	putative cytoplasmic protein	3.244133557
ydiP	putative transcriptional regulator	3.192034741
wecB	UDP-N-acetyl glucosamine-2-epimerase	3.151390039
2968559_2969009	putative inner membrane protein	3.135666011
825819_826665	fumarate hydratase	3.120990415
mod	DNA methylase	3.118449915
fdhD	formate dehydrogenase accessory protein	3.100720318
1203593_1204166	putative inner membrane protein	3.079368962
stfA	putative fimbrial subunit	3.037158873
3850515_3851055	hypothetical protein	3.029523322
yjiJ	putative sugar transporter	3.013111895
4280041_4280173	hypothetical protein	3.008371472

copR	transcriptional regulatory protein YedW	2.970125767
4293708_4295043	putative Na+/galactoside symporter	2.966614794
yjbG	putative periplasmic protein	2.953092135
csiE	stationary phase inducible protein CsiE	2.92952913
2386386_2386914	putative phage tail fiber assembly protein	2.866613903
thiH	thiamine biosynthesis protein ThiH	2.807978039
polB	DNA polymerase II	2.795277173
envR	DNA-binding transcriptional regulator EnvR	2.792464391
23334_24039	putative cytoplasmic protein	2.773198829
nrfD	putative formate-dependent nitrate reductase	2.757519676
uspB	universal stress protein UspB	2.7506482
sugE	quaternary ammonium compound-resistance protein SugE	2.715873529
4237366_4238101	putative hydrolase	2.711844342
94842_95259	putative secreted protein	2.680812822
yjfR	putative L-ascorbate 6-phosphate lactonase	2.659105957
3375255_3375933	putative disulfide oxidoreductase	2.646474172
rimI	ribosomal-protein-alanine N-acetyltransferase	2.64610994
yhbW	hypothetical protein	2.623280333
rhaB	rhamnulokinase	2.612422666
4435977_4436706	putative cytoplasmic protein	2.579116139
mutM	formamidopyrimidine-DNA glycosylase	2.578222908
corA	magnesium/nickel/cobalt transporter CorA	2.548894999
2770966_2772163	putative permease	2.541951805
gcd	glucose dehydrogenase	2.525473422
pduQ	propanol dehydrogenase	2.520046202
mtlD	mannitol-1-phosphate 5-dehydrogenase	2.519743829
4281497_4282805	putative C4-dicarboxylate transport system	2.505645605
tdcC	threonine/serine transporter TdcC	2.504373183
nudC	NADH pyrophosphatase	2.502917549
3267172_3267904	putative outer membrane lipoprotein	2.498072971
4759524_4760616	putative ABC-type sugar/spermidine/putrescine transport system ATPase component	2.490397569
yhjD	putative tRNA-processing ribonuclease	2.485138418
pepE	peptidase E	2.435513975

yhjH	EAL domain-containing protein	2.4310572
4280656_4281340	putative outer membrane protein	2.416902485
ecnR	putative regulatory protein	2.415926899
4447640_4448594	putative methyl-accepting chemotaxis protein	2.37969247
htrA	serine endoprotease	2.357569427
feoB	ferrous iron transport protein B	2.345920497
idnR	L-idonate regulator	2.329498438
sopA	secreted effector protein	2.315253676
1346296_1347340	putative cytoplasmic protein	2.298481385
dipZ	thiol:disulfide interchange protein precursor	2.277505116
citC	citrate lyase synthetase	2.264798465
nanA	N-acetylneuraminate lyase	2.264571971
yifB	putative ATP-dependent protease	2.263047457
yhdP	hypothetical protein	2.26209566
3818230_3818344	hypothetical protein	2.251426111
gsp	bifunctional glutathionylspermidine amidase/glutathionylspermidine synthetase	2.250961215
dinP	DNA polymerase IV	2.247334262
eutS	putative carboxysome structural protein	2.244867322
yhfA	hypothetical protein	2.23585121
4454251_4454566	putative inner membrane protein	2.228221718
tas	putative aldo-keto reductase	2.222553289
38772_39534	putative outer membrane/exported protein	2.204250556
yijP	hypothetical protein	2.202843996
res	DNA restriction enzyme	2.202504022
idnT	L-idonate transport protein	2.185569174
yneA	putative sugar transport protein	2.182066111
ppdB	hypothetical protein	2.180472097
hybB	putative hydrogenase 2 b cytochrome subunit	2.180445957
4813211_4813991	putative PTS permease	2.166794867
3680835_3681750	putative cytoplasmic protein	2.166473156
potB	spermidine/putrescine ABC transporter membrane protein	2.139002067
malM	maltose regulon periplasmic protein	2.118968224
116188_116941	putative secreted protein	2.107062766
ushA	'bifunctional UDP-sugar hydrolase/5''-nucleotidase periplasmic precursor'	2.106767159
sopB	secreted effector protein	2.090455797
uhpB	sensory histidine kinase UhpB	2.078805374
yjbB	putative transport protein	2.078173564
4437893_4438499	putative cytoplasmic protein	2.077082278
yjiW	endoribonuclease SymE	2.072501

4694242_4695265	myo-inositol 2-dehydrogenase	2.04984514
stbA	putative fimbrial major subunit	2.046635658
yijD	hypothetical protein	2.044991784
15013_15961	putative transcriptional regulator	2.04453576
4527448_4528336	putative transcriptional regulator	2.034967841
sbcC	exonuclease subunit SbcC	2.030898605
fimI	fimbrial protein	2.028073994
pgtA	activator	2.025623115
fimC	periplasmic chaperone	1.994445783
yjfJ	putative phage shock protein A	1.994423839
371988_373326	putative permease	1.98029835
4437441_4437897	putative cytoplasmic protein	1.972205291
4669313_4670522	putative permease	1.96009963
gntT	high-affinity gluconate permease	1.935295919
yjjQ	putative transcriptional regulator	1.933789708
metL	bifunctional aspartate kinase II/homoserine dehydrogenase II	1.926440978
recQ	ATP-dependent DNA helicase RecQ	1.909864658
yhdH	putative oxidoreductase	1.905695288
stiC	putative fimbrial usher	1.900002427
sipD	translocation machinery component	1.893116984
3296427_3296955	putative monoamine oxidase	1.891951694
3349848_3350832	putative periplasmic dicarboxylate-binding protein	1.880640533
invB	secretion chaperone	1.853056123
yjeP	hypothetical protein	1.843317121
yiiD	putative acetyltransferase	1.842168097
sopD	secreted effector protein	1.829151219
4826399_4827464	hypothetical protein	1.825712407
yjcB	putative inner membrane protein	1.819483261
3212273_3212906	hypothetical protein	1.817806997
idnO	gluconate 5-dehydrogenase	1.815301155
1179985_1181266	putative sialic acid transporter	1.81380785
dcuR	DNA-binding transcriptional activator DcuR	1.800886415
490948_492460	putative periplasmic protein	1.790304744
3786167_3787013	putative sugar kinase	1.789447945
4454578_4455184	putative soluble lytic murein transglycosylase	1.788093891
ybbY	putative purine permease YbbY	1.779800338
318367_318853	putative cytoplasmic protein	1.779472437
yfdH	putative glycosyltransferase	1.778636992
xylA	xylose isomerase	1.778611365
ydeY	putative sugar transport protein	1.777619038
4269880_4270204	putative inner membrane protein	1.775658729
4843251_4843824	putative outer membrane protein	1.770421387
632880_633867	putative phosphosugar isomerase	1.764034406
hilD	invasion protein regulatory protein	1.757361132

rarD	chloramphenicol resistance	1.755694401
dcuS	sensory histidine kinase DcuS	1.75484764
yadI	putative PTS enzyme	1.742551663
yggB	mechanosensitive channel MscS	1.737247582
fidL	putative inner membrane protein	1.734271263
yheS	putative ABC transporter ATP-binding protein	1.730048416
bglJ	DNA-binding transcriptional activator BglJ	1.72938918
4331529_4332387	putative inner membrane protein	1.728092778
3374569_3375241	putative disulfide bond formation protein	1.725897374
fdoG	formate dehydrogenase alpha subunit	1.713521409
3335298_3335814	putative ATP-dependent RNA helicase-like protein	1.707718827
yjdE	arginine:agmatin antiporter	1.707703185
4726678_4727899	arginine deiminase	1.705383273
2670136_2672350	putative diguanylate cyclase	1.697810165
cycA	D-alanine/D-serine/glycine permease	1.682557123
metC	cystathionine beta-lyase	1.664351606
prgK	needle complex inner membrane lipoprotein	1.656417116
gatY_1	tagatose-bisphosphate aldolase	1.656083628
4324989_4326780	putative arylsulfate sulfotransferase	1.648761046
tldD	protease TldD	1.644717196
sthA	putative fimbrial chaparone	1.627240968
3350873_3351356	putative inner membrane protein	1.626416007
3792806_3793163	putative phage endolysin	1.622695134
ycaM	putative amino-acid transporter	1.615909901
2332945_2334187	putative oxidoreductase	1.611839771
4333622_4334747	putative cytoplasmic protein	1.600996578
3879590_3881546	putative cytoplasmic protein	1.595440446
ybdN	'putative 3''-phosphoadenosine 5''-phosphosulfate sulfotransferase'	1.591435772
ybeQ	TPR repeat-containing protein	1.590297845
3372753_3374550	putative arylsulfate sulfotransferase	1.586964956
4007282_4008203	putative sugar kinase	1.578436408
katG	hydroperoxidase	1.574027675
spaR	needle complex export protein	1.571906236
stjC	putative periplasmic chaperone protein	1.569130868
42931_44185	putative cytoplasmic protein	1.568806344
4168325_4168688	putative cytoplasmic protein	1.565289716
4749316_4752832	putative DNA helicase	1.548784114
yibD	glycosyl transferase	1.536398352
4577710_4577926	putative cytoplasmic protein	1.531844301
yiaH	putative inner membrane protein	1.527840718

ygiK	putative transporter	1.496197056
wcaK	putative pyruvyl transferase	1.483608647
invC	ATP synthase SpaL	1.474869698
4442505_4444053	putative inner membrane protein	1.473904817
4242109_4242958	putative cytoplasmic protein	1.466991617
4813980_4814817	putative PTS permease	1.460522184
ptsA	PEP-protein phosphotransferase	1.459054243
yjgN	putative inner membrane protein	1.444651986
3870827_3871760	putative chemotaxis protein	1.442190613
yiaB	putative inner membrane protein	1.438657053
yiiG	putative cytoplasmic protein	1.424664872
stjB	putative fimbrial usher protein	1.376646889
4670518_4671682	putative metallo-dependent hydrolase	1.373705762
lpfD		1.361089189
2096200_2097763	hypothetical protein	1.350988425
xylR	xylose operon regulatory protein	1.348824922
3318869_3319928	putative methyl-accepting chemotaxis protein	1.33834901
lpfA	long polar fimbrial protein A precursor	1.329330506
3784794_3786114	anaerobic C4-dicarboxylate transporter	1.329237043
sipA	secreted effector protein	1.326823899
3311397_3312274		1.319234492
4495919_4496552	hypothetical protein	1.3087593
2538834_2539353	putative periplasmic protein	1.304289552
yicL	putative permease	1.303309107
61793_63413	putative transcriptional regulator	1.28891078
invA	needle complex export protein	1.283334993
3536145_3536763	L(+)-tartrate dehydratase subunit beta	1.282227872
4049048_4050311	putative permease	1.265740202
4240203_4241067	putative membrane-associated metal-dependent hydrolase	1.260272909
35338_37057	putative arylsulfatase	1.235656173